

A PARAMETRIC STUDY ON THREE DIMENSIONAL MODELING OF
PARALLEL TUNNEL INTERACTIONS

A THESIS SUBMITTED TO
THE GRADUATE SCHOOL OF NATURAL AND APPLIED SCIENCES
OF
MIDDLE EAST TECHNICAL UNIVERSITY

BY

SALAHADDİN MİRAC KARADEMİR

IN PARTIAL FULFILLMENT OF THE REQUIREMENTS
FOR
THE DEGREE OF MASTER OF SCIENCE
IN
CIVIL ENGINEERING

SEPTEMBER 2010

Approval of the thesis:

**A PARAMETRIC STUDY ON THREE DIMENSIONAL
MODELING OF PARALLEL TUNNEL INTERACTIONS**

submitted by **SALAHADDİN MİRAC KARADEMİR** in partial fulfillment
of the requirements for the degree of **Master of Science in Civil Engineering**
Department, Middle East Technical University by,

Prof. Dr. Canan Özgen _____
Dean, Graduate School of **Natural and Applied Sciences**

Prof. Dr. Güney Özcebe _____
Head of Department, **Civil Engineering**

Prof Dr. Orhan Erol _____
Supervisor, **Civil Engineering Dept., METU**

Examining Committee Members:

Prof. Dr. Kemal Önder Çetin _____
Civil Engineering Dept., METU

Prof. Dr. Orhan Erol _____
Civil Engineering Dept., METU

Asst. Prof. Dr. Nejan Huvaj Sarihan _____
Civil Engineering Dept., METU

Prof. Dr. Vedat Doyuran _____
Geological Engineering Dept., METU

Dr. Özgür Kuruoğlu _____
Yüksel Proje A.Ş.

Date: _____ 17.09.2010

I hereby declare that all information in this document has been obtained and presented in accordance with academic rules and ethical conduct. I also declare that, as required by these rules and conduct, I have fully cited and referenced all material and results that are not original to this work.

Name, Last Name : SALAHADDİN MİRAC KARADEMİR

Signature :

ABSTRACT

A PARAMETRIC STUDY ON THREE DIMENSIONAL MODELING OF PARALLEL TUNNEL INTERACTIONS

Karademir, Salahaddin Miraç

M.S., Department of Civil Engineering

Supervisor: Prof. Dr. Orhan Erol

September 2010, 199 pages

A parametric study is performed to investigate the parallel tunnel interaction. Three dimensional finite element analyses were performed to determine the effects of soil stiffness, pillar width and advancement level of the second tunnel on the behaviour of displacement, bending moment and shear force of the previously constructed tunnel. In the analysis PLAXIS 3D Tunnel geotechnical finite element package was used. This program allows the user to define the actual construction stages of a NATM tunnel construction. In the analysis, construction stages are defined in such a way that firstly one of the tunnels is constructed and the construction of the second tunnel starts after the construction of the first tunnel. The mid-length section of the first tunnel is investigated in six different locations and at seven different advancement levels in terms of displacement, bending moment and shear forces. It is found that, displacement and bending moment behaviour are more related with soil stiffness and pillar width than the behaviour of shear forces. While the level of advancement of the second tunnel causes different type of responses on the shear force behaviour, level of advancement does not affect the type of behaviour of displacements and bending moments. Another finding of the

research is that pillar width has an evident influence on the behaviour of displacements and bending moment than the soil stiffness. It is also found that the interaction effect may be eliminated by increasing the pillar width equal or larger than an approximate value of 2.5 – 3.0 D (diameter) for an average soil stiffness value.

Keywords: NATM; Parallel Tunnel Interaction; Pillar Width; Finite Element

ÖZ

PARALEL TÜNEL ETKİLEŞİMİ ÜZERİNE ÜÇ BOYUTLU PARAMETRİK ÇALIŞMA

Karademir, Salahaddin Miraç

Yüksek Lisans, İnşaat Mühendisliği Bölümü

Tez Yöneticisi: Prof. Dr. Orhan Erol

Eylül 2010, 199 sayfa

Paralel tünel etkileşimini incelemek üzere bir parametrik çalışma gerçekleştirilmiştir. Zeminin elastisite modülünün, paralel tüneller arasındaki mesafenin ve sonradan inşaatı yapılacak olan tünelin ilerleme seviyesinin önceden inşaatı tamamlanmış bir tünelin üzerinde oluşturacağı deformasyon, moment ve kesme kuvveti davranışlarını belirlemek amacıyla üç boyutlu sonlu elemanlar analizleri gerçekleştirilmiştir. Analizlerde PLAXIS 3D Tunnel sonlu elemanlar bilgisayar programı kullanılmıştır. Bu program ile kullanıcı tarafından bir NATM tünelinin inşaat aşamaları tanımlanabilmektedir. Analizlerde öncelikli olarak bir tünelin inşaatı tamamlanmış olup, ikinci paralel tünel birinci tünelin inşaatının tamamlanmasından sonra modellenmiştir. Önceden inşaatı tamamlanmış tünelin tam ortasından alınan bir kesit altı farklı noktasında ve ikinci tünel inşaatının yedi farklı aşamasında deformasyonlar, moment ve kesme kuvvetleri açısından incelenmiştir. Analizler sonucunda deformasyon ve moment davranışlarının daha çok zeminin elastisite modülüne ve tüneller arası bırakılan mesafeye göre etkilendiği saptanmıştır. İkinci tünelin inşaatı sırasındaki farklı inşaat aşamalarında kesme kuvvetleri değişken bir davranış özelliği gösterirken, deformasyon ve moment üzerinde bu durumun

bir etki oluřturduęu gözlenmemiřtir. Analizler sonucu saptanan dięer bir bulgu ise, deformasyon ve moment davranıřı üzerinde tüneller arası bırakılan mesafe, zeminin elastisite modülüne göre daha etkin rol oynamaktadır. Ayrıca analizlere göre ortalama bir zemin elastisite modülü için tüneller arasındaki mesafenin yaklaşık olarak $2.5 - 3.0 D$ (tünel çapı) kadar mesafede olması etkileřimi elimine etmektedir.

Anahtar Kelimeler: NATM; Paralel Tünel Etkileřimi; Tüneller Arası Mesafe; Sonlu Elemanlar

To My Family...

ACKNOWLEDGEMENTS

I would like to express my special thanks to my dear supervisor, Prof. Dr. Orhan Erol, for his brilliant ideas, endless support and guidance throughout this study. I am grateful that, he did not only provide support about this study but also shared his invaluable experience about life.

I also express my deepest gratefulness to Prof. Dr. Kemal Önder Çetin for his guidance, support and kindness.

It is with pleasure to express my gratefulness to Yüksel Proje managers especially to my bosses Mr. Atilla Horoz and Dr. Özgür Kuruoğlu for their endless patience and tolerance throughout the research.

I wish to present my special thanks to my mother Marziye Karademir and my father Mustafa Karademir and my ingenious sisters Ebru and Tuba for their unlimited patience and support during my whole life.

Sincere thanks to my friends for their precious friendship and continuous support. Especially, the friends who look after me in bad times are invaluable.

TABLE OF CONTENTS

ABSTRACT.....	iv
ÖZ.....	vi
ACKNOWLEDGEMENTS.....	ix
TABLE OF CONTENTS.....	x
LIST OF FIGURES.....	xiii
LIST OF TABLES.....	xxii
CHAPTERS	
1. INTRODUCTION.....	1
1.1 General Information	1
1.2 Chronology of Tunnelling	2
1.3 Types of Tunnels	3
1.3.1 Based on Service	3
1.3.2 Based on Construction Technique.....	3
1.4 Numerical Methods in Geotechnical Engineering	5
1.4.1 Finite Element Method.....	5
1.5 Research Objective.....	6
1.6 Scope of the Study.....	6
2. LITERATURE REVIEW.....	8
2.1 Introduction	8
2.2 Analytical Solutions	8
2.3 Numerical Solutions on 2D	13
2.4 Numerical Solutions on 3D	36
2.5 Experimental Studies.....	38
2.6 Case Studies	45
3. NUMERICAL MODELING.....	50
3.1 Introduction	50

3.2	Geometry and Definition.....	55
3.3	Modeling Parameters.....	60
3.3.1	Soil Parameters.....	60
3.3.2	Lining Parameters.....	61
3.4	Construction Procedure.....	62
3.5	Analysis Details.....	63
4.	DISCUSSION OF THE RESULTS	67
4.1	Behaviour of Displacements	67
4.1.1	Behaviour of Displacement at 1	67
4.1.2	Behaviour of Displacement at 2	71
4.1.3	Behaviour of Displacement at 3	74
4.1.4	Behaviour of Displacement at 4	77
4.1.5	Behaviour of Displacement at 5	80
4.1.6	Behaviour of Displacement at 6	83
4.2	Behaviour of Bending Moments	85
4.2.1	Behaviour of Bending Moment at 1	86
4.2.2	Behaviour of Bending Moment at 2	89
4.2.3	Behaviour of Bending Moment at 3	91
4.2.4	Behaviour of Bending Moment at 4.....	95
4.2.5	Behaviour of Bending Moment at 5	98
4.2.6	Behaviour of Bending Moment at 6.....	102
4.3	Behaviour of Shear Forces	105
4.3.1	Behaviour of Shear Force at 1	106
4.3.2	Behaviour of Shear Force at 2	111
4.3.3	Behaviour of Shear Force at 3	113
4.3.4	Behaviour of Shear Force at 4	118
4.3.5	Behaviour of Shear Force at 5	121
4.3.6	Behaviour of Shear Force at 6.....	123
5.	CONCLUSION	126

REFERENCES.....	130
APPENDICES	
A.DISPLACEMENTS.....	133
B.BENDING MOMENTS.....	152
C.SHEAR FORCES.....	172

LIST OF FIGURES

FIGURES

Figure 2.1 Diagram of the additional tangential stresses of the lining (Fotieva and Sheinin, 1966)	9
Figure 2.2 Diagram illustrating calculation of the tunnels (Dunaevskii, 1986).....	10
Figure 2.3 The variation of tangential stresses of specific points on tunnels with the distance between parallel tunnels (Gerçek, 1988)	12
Figure 2.4 The variation of second order stresses at the mid-height of the pillar with the pillar width (Gerçek, 1988).....	13
Figure 2.5 Pillar stresses vs. pillar width (Ghaboussi & Ranken, 1976)	15
Figure 2.6 Unlined tunnel displacements $H/D=5.5$ (Ghaboussi & Ranken, 1976).....	16
Figure 2.7 Lined tunnel displacements $H/D=5.5$ (Ghaboussi & Ranken, 1976).....	17
Figure 2.8 Distribution of liner bending moments for the deep tunnels (Ghaboussi & Ranken, 1976)	17
Figure 2.9 Additional surface settlement arising from two tunnel interaction (Ghaboussi & Ranken, 1976).....	18
Figure 2.10 Settlement graphs for shallow ($H/D=1.5$) tunnels (Ghaboussi & Ranken, 1976)	19
Figure 2.11 Settlement graphs for deep ($H/D=5.5$) tunnels (Ghaboussi & Ranken, 1976).....	20
Figure 2.12 Settlement above 2 nd tunnel for horizontally aligned tunnels (Addenbroke & Potts, 1996)	22

Figure 2.13 Eccentricity of S_{\max} with pillar width (Addenbroke & Potts, 1996).....	22
Figure 2.14 Settlement above the 2 nd of two piggy back excavations (Addenbroke & Potts, 1996)	23
Figure 2.15 Position of inflection point with pillar depth (Addenbroke & Potts, 1996).....	24
Figure 2.16 Response of 1 st lining to passage of 2 nd tunnel (Addenbroke & Potts, 1996).....	24
Figure 2.17 Results compared with FLAC 2D and PLAXIS (Kooi & Verruijt, 2001)	25
Figure 2.18 Scaled displacements for $d/a=4$ and $y=d$ (Kooi & Verruijt, 2001).....	26
Figure 2.19 Comparison of ground settlements of twin tunnels (Yu and Akagi, 2003).....	27
Figure 2.20 Interaction factor with depth (Yu and Akagi, 2003).....	28
Figure 2.21 Geometrical parameters and in-situ stress field in the numerical analyses (Gerçek, 2005)	29
Figure 2.22 Effect of pillar width on the degree of interaction (Gerçek, 2005).....	29
Figure 2.23 The effect of position of openings (Gerçek, 2005).....	30
Figure 2.24 Configurations considered in the analyses of the interaction between twin tunnels (Chehade & Shahrour 2007)	31
Figure 2.25 Mesh used in the analysis of tunnels with horizontal alignment (Chehade & Shahrour 2007).....	32
Figure 2.26 Horizontally aligned tunnels: settlement, bending moment and thrust in the right tunnel (Chehade & Shahrour 2007)	33
Figure 2.27 Vertically aligned tunnels: settlement, bending moment and thrust in the tunnel (Chehade & Shahrour 2007)	34

Figure 2.28 Inclined aligned tunnels: settlement, bending moment and thrust in the tunnel (Chehade & Shahrour 2007)	35
Figure 2.29 The 3D model used in the analyses (Ng, Lee and Tang, 2004).....	36
Figure 2.30 Plain Strain Test Tank Configuration (Kim, Burd & Milligan, 1998).....	39
Figure 2.31 Total and incremental bending moments (Kim, Burd & Milligan, 1998).....	39
Figure 2.32 Variation of pillar springline incremental bending moment with W/D (Kim, Burd & Milligan, 1998)	40
Figure 2.33 Deformed cross-sections for W/D=0.4 (Kim, Burd & Milligan, 1998).....	41
Figure 2.34 Variation of incremental diameter change with W/D (Kim, Burd & Milligan, 1998).....	41
Figure 2.35 Schematic plot of the model test of twin tunnels in two and three layered formations (Chu, Hsu, Chang and Lin, 2006)	42
Figure 2.36 Distribution of radial strains with time, (a) homogeneous material, (b) two-layered formations, (c) three layered formations (Chu, Hsu, Chang and Lin, 2006)	44
Figure 2.37 Measured strains at the crowns for different stiffness ratios (Chu, Hsu, Chang and Lin, 2006)	45
Figure 2.38 Proposed criterion to delineate the interactive effect (Chern and Hsiao, 2005).....	46
Figure 2.39 Assessment of tunnel interaction in Hsuehshan Tunnels (Chern and Hsiao, 2005)	47
Figure 2.40 The cross section layout of the Hsuehshan Tunnels (Lee, Lu and Lee, 2005).....	47

Figure 2.41 Finite element mesh used in the analyses (Karakus, Ozsan and Basarir, 2005)	48
Figure 2.42 Construction sequences adopted in the FEM analyses (Karakus, Ozsan and Basarir, 2005).....	49
Figure 3.1 Position of the nodes and stress points (Plaxis 3D Tunnel User’s Manual, 2001)	53
Figure 3.2 Creating a 3D model and finite element mesh (Plaxis 3D Tunnel User’s Manual, 2001).....	53
Figure 3.3 Geometry of the problem (Pillar width = 0.5D)	55
Figure 3.4 Geometry of the problem (Pillar width = 1.0D)	56
Figure 3.5 Geometry of the problem (Pillar width = 1.5D)	56
Figure 3.6 Geometry of the problem (Pillar width = 2.0D)	57
Figure 3.7 Cross-section of the NATM Tunnel	58
Figure 3.8 Generated mesh on 2D.....	59
Figure 3.9 Generated mesh on 3D.....	59
Figure 3.10 Typical construction stage procedure	63
Figure 3.11 Typical displacement diagram	65
Figure 3.12 Typical bending moment diagram	65
Figure 3.13 Typical shear force diagram.....	66
Figure 3.14 Construction stages at which data is collected.....	66
Figure 4.1 Displacement values at the top side of the tunnel.....	68
Figure 4.2 Percent change in displacement at the top side of the tunnel	68
Figure 4.3 Displacement values at the top side of the tunnel.....	69
Figure 4.4 Percent change in displacement at the top side of the tunnel	69
Figure 4.5 Change in percent increase for different pillar width values.	70
Figure 4.6 Displacement values at the right-top side of the tunnel.....	71
Figure 4.7 Percent change in displacement at the right-top side of the tunnel	72

Figure 4.8 Displacement values at the right-top side of the tunnel.....	72
Figure 4.9 Percent change in displacement at the right-top side of the tunnel	73
Figure 4.10 Change in percent increase for different pillar width values	74
Figure 4.11 Displacement values at the right-bottom side of the tunnel	75
Figure 4.12 Percent change in displacement at the right-bottom side of the tunnel	75
Figure 4.13 Displacement values at the right-bottom side of the tunnel	76
Figure 4.14 Percent change in displacement at the right-bottom side of the tunnel	76
Figure 4.15 Displacement values at the bottom side of the tunnel	78
Figure 4.16 Percent change in displacement at the bottom side of the tunnel	78
Figure 4.17 Displacement values at the bottom side of the tunnel	79
Figure 4.18 Percent change in displacement at the bottom side of the tunnel	79
Figure 4.19 Change in percent increase for different pillar width values	80
Figure 4.20 Displacement values at the left-bottom side of the tunnel...	81
Figure 4.21 Percent change in displacement at the left-bottom side of the tunnel	81
Figure 4.22 Displacement values at the left-bottom side of the tunnel...	82
Figure 4.23 Percent change in displacement at the left-bottom side of the tunnel	82
Figure 4.24 Displacement values at the left-top side of the tunnel	84
Figure 4.25 Percent change in displacement at the left-top side of the tunnel	84

Figure 4.26 Displacement values at the left-top side of the tunnel	85
Figure 4.27 Percent change in displacement at the left-top side of the tunnel	85
Figure 4.28 Bending moment values at the top side of the tunnel	86
Figure 4.29 Percent change in bending moment at the top side of the tunnel	87
Figure 4.30 Bending moment values at the top side of the tunnel	88
Figure 4.31 Percent change in bending moment at the top side of the tunnel	89
Figure 4.32 Change in percent increase for different pillar width values	89
Figure 4.33 Bending moment values at the right-top side of the tunnel	90
Figure 4.34 Percent change in bending moment at the right-top side of the tunnel	90
Figure 4.35 Change in percent increase for different pillar width values	91
Figure 4.36 Bending moment values at the right-bottom side of the tunnel	92
Figure 4.37 Percent change in bending moment at the right-bottom side of the tunnel	92
Figure 4.38 Bending moment values at the right-bottom side of the tunnel	94
Figure 4.39 Percent change in bending moment at the right-bottom side of the tunnel	94
Figure 4.40 Change in percent increase for different pillar width values	95
Figure 4.41 Bending moment values at the bottom side of the tunnel	96

Figure 4.42 Percent change in bending moment at the bottom side of the tunnel	96
Figure 4.43 Bending moment values at the bottom side of the tunnel....	97
Figure 4.44 Percent change in bending moment at the bottom side of the tunnel	97
Figure 4.45 Change in percent increase for different pillar width values	98
Figure 4.46 Bending moment values at the left-bottom side of the tunnel	99
Figure 4.47 Percent change in bending moment at the left-bottom side of the tunnel	99
Figure 4.48 Bending moment values at the left-bottom side of the tunnel	100
Figure 4.49 Percent change in bending moment at the left-bottom side of the tunnel	101
Figure 4.50 Change in percent increase for different pillar width values	102
Figure 4.51 Bending moment values at the left-top side of the tunnel .	103
Figure 4.52 Percent change in bending moment at the left-top side of the tunnel	103
Figure 4.53 Bending moment values at the left-top side of the tunnel .	104
Figure 4.54 Percent change in bending moment at the left-top side of the tunnel	104
Figure 4.55 Change in percent increase for different pillar width values	105
Figure 4.56 Shear force values at the top side of the tunnel	107
Figure 4.57 Shear force values at the top side of the tunnel	107
Figure 4.58 Percent change in shear force at the top side of the tunnel	108

Figure 4.59 Percent change in shear force at the top side of the tunnel	108
Figure 4.60 Shear force values at the top side of the tunnel	109
Figure 4.61 Shear force values at the top side of the tunnel	109
Figure 4.62 Percent change in shear force at the top side of the tunnel	110
Figure 4.63 Percent change in shear force at the top side of the tunnel	110
Figure 4.64 Shear force values at the right-top side of the tunnel	111
Figure 4.65 Percent change in shear force at the right-top side of the tunnel	112
Figure 4.66 Shear force values at the right-top side of the tunnel	113
Figure 4.67 Percent change in shear force at the right-top side of the tunnel	113
Figure 4.68 Shear force values at the right-bottom side of the tunnel ..	114
Figure 4.69 Shear force values at the right-bottom side of the tunnel ..	115
Figure 4.70 Percent change in shear force at the right-bottom side of the tunnel	115
Figure 4.71 Percent change in shear force at the right-bottom side of the tunnel	116
Figure 4.72 Shear force values at the right-bottom side of the tunnel ..	116
Figure 4.73 Shear force values at the right-bottom side of the tunnel ..	117
Figure 4.74 Percent change in shear force at the right-bottom side of the tunnel	117
Figure 4.75 Percent change in shear force at the right-bottom side of the tunnel	118
Figure 4.76 Shear force values at the bottom side of the tunnel	119
Figure 4.77 Percent change in shear force at the bottom side of the tunnel	119
Figure 4.78 Shear force values at the bottom side of the tunnel	120

Figure 4.79 Percent change in shear force at the bottom side of the tunnel	120
Figure 4.80 Shear force values at the left-bottom side of the tunnel	121
Figure 4.81 Shear force values at the left-bottom side of the tunnel	121
Figure 4.82 Percent change in shear force at the left-bottom side of the tunnel	122
Figure 4.83 Percent change in shear force at the left-bottom side of the tunnel	122
Figure 4.84 Shear force values at the left-top side of the tunnel.....	123
Figure 4.85 Percent change in shear force at the left-top side of the tunnel	124
Figure 4.86 Shear force values at the left-top side of the tunnel.....	124
Figure 4.87 Percent change in shear force at the left-top side of the tunnel	125

LIST OF TABLES

TABLES

Table 3.1 Parameters of hardening soil model	52
Table 3.2 Geometrical properties of tunnel cross-section	57
Table 3.3 Material properties of soil	60
Table 3.4 Material properties of shotcrete	61
Table 3.5 Variables of the parametric study	64

CHAPTER 1

INTRODUCTION

1.1 General Information

Tunnels are important for both in geotechnical engineering and every day life of the people. Tunnels are constructed for different purposes such as transportation of people and materials, water conveyance and storage. The type of the tunnel depends on both the purpose of the construction and the properties of the surrounding soil. The task of a geotechnical engineer is to design tunnels which meet the needs in a safe and economic manner.

Tunnels are constructed for hundreds of years but in engineering point of view the design of tunnels has improved greatly with analytical solutions proposed by engineers and with the development of computer technology.

Tunnels are constructed in order to meet the demands for long term conditions as all other constructed facilities. However, existing tunnels may not meet the demands in some cases. The factors that affect the change of demand may be increase in population in cities, industrial development of a region or political investments. Increase in demand may lead to the construction of new tunnels next to existing ones. In these cases the interaction between previously constructed tunnel and new one becomes an important subject.

The use of the underground area, especially in large cities, became a must with the development of cities in many countries. In some cities, the geotechnical and underground conditions impose the construction of new tunnels close to existing ones. In other cases the solution of twin tunnels presents major advantages, such as the reduction of the both the tunnel diameter and the soil movement due to tunnel construction (Chehade and Shahrour, 2007).

Also, Addenbroke & Potts (1996) states that, excavation of new tunnels close to existing tunnels may be needed for construction activities like metro construction in crowded cities. New tunnels adjacent to existing tunnels may be excavated not only for the metro construction but also for an improvement of a network. For this reason, Addenbroke & Potts (1996) suggested to investigate the interaction between the tunnels and ground response.

1.2 Chronology of Tunnelling

First underground constructions were for defense and mining purposes. The primitive examples of tunnels are the salt mine in Hallstat(B.C. 2500) and flint mines in France and Portugal(B.C. 2000) (Megaw and Barlett, 1981).

Water supplying is another use of tunnels in history. Greeks and Romans were the first builders of canals. According to Sinha(1989), the Greeks used advanced surveying techniques about 500 B.C. to excavate tunnels from both portals toward the middle of the tunnel in order to decrease the time needed for the construction of the tunnel.

In modern era, with the development of technology, tunnelling operations improved greatly since new construction techniques were available such as, TBM, NATM or shield tunnelling. Also, the availability of computer based solution techniques for tunnelling has an important effect on the development of tunnel construction.

1.3 Types of Tunnels

Tunnels can be classified in several ways. Basically, tunnels can be categorized according to their function and according to the construction technique.

1.3.1 Based on Service

The constructed tunnel can be used for a railway tunnel, metro tunnel, highway tunnel or water conveyance tunnel. Design criteria such as cross-section of the tunnel, gradient and applicability of the construction technique to the surrounding soil media all depends on the function of the tunnel.

1.3.2 Based on Construction Technique

Cut and cover and earth boring&pipe jacking are the main construction techniques of tunnelling. A cut and cover construction technique refers simply, the excavation of a trench with a support system such as piles, and the construction of the tunnels in the trench. The construction technique depends on soil conditions and surrounding environment, especially. For instance, Megaw and Barlett (1981) states that, cut and cover method may be preferred for a metro tunnel where it is possible to construct the tunnel in a shallow depth

without considerable disturbance of streets and urban activities. They also suggest that when a city is a heavily crowded, deeper tunnelling is applicable.

Earth boring is a method in which the soil is generally removed by an auger and small diameter pipes are installed. In pipe jacking, during the excavation process the pipe is jacked at the same time. TBM(Tunnel Boring Machine) is a common example of it. When the excavation is in progress, pre-fabricated segments of the tunnel lining is placed by using TBM.

The NATM (New Austrian Tunnelling Method) is another construction technique which is widely used. It is important to explain the NATM philosophy since a NATM type of a tunnel is examined in the content of the study.

The New Austrian Tunnelling Method (NATM) emerged in the years 1957 to 1965 and was entitled in this way to be distinguished from the Old Austrian Tunnelling Method. The NATM is developed by Austrian Tunnelling specialists (Von Rabcewicz, Pacher, Müller-Salzburg). Its main idea is to head the tunnel conventionally, to apply support (mainly shotcrete) sparingly and to follow the principles of the observational method. The NATM requires the distortion of the ground to be kept to a minimum. But at the same time sufficient ground deformation should be allowed in order to mobilise the strength of the ground (Kolymbas, 2005).

Kolymbas (2005), states that the best definition of NATM belongs to H. Lauffer and it is as follows:

“NATM is a tunnelling method in which excavation and support procedures, as well as measures to improve the ground depend on observation of deformation and are continuously adjusted to the encountered conditions.”

1.4 Numerical Methods in Geotechnical Engineering

Numerical methods are widely used in geomechanics as the computer technology is developed. Beam element method (coefficient of subgrade reaction method), finite element method, finite difference method, boundary element method, discrete element method and hybrid & complementary methods are the main types of numerical methods which are used in geotechnical engineering. In this part, only finite element method will be described briefly, since it is more widely used. Also, the computer program (PLAXIS 3D Tunnel) which is used in the analyses is based on finite element modeling.

1.4.1 Finite Element Method

Finite element method, is one of the most widely used numerical methods in geotechniques and also in tunnel engineering. In this method, the soil is modelled as a continuum but discontinuities can be also modelled individually (Gnilsen, 1989).

In the finite element method (FEM), the ground is discretized into a limited number of smaller elements which are connected at nodal points. Each element is geometrically defined and limited in size. Any change in subsurface conditions such as excavation or loading affects these elements. The stress, strain and deformation induced in one element affects the behaviour of

neighbouring elements, and so forth. Complicated conditions, stage construction, time effect and non-homogenities can be simulated by finite element method more easily as compared to analytical solutions. Gnilsen (1989), also states that, the output of the analysis is typically complex and it makes the assessment of results difficult. A post-processor may be utilized in order to eliminate this problem. A graphical display capability should be needed (Gnilsen, 1989).

1.5 Research Objective

The purpose of this study is to investigate the effect of pillar width and soil stiffness on the behavior of displacements and sectional forces (bending moment and shear force) of an existing tunnel, when a new tunnel is excavated parallel to it. A parametric study has been performed in order to explore the behavior of two parallel NATM tunnels.

1.6 Scope of the Study

Following this introduction,

Chapter 2 presents an extensive literature review on the parallel tunnel interactions. Analytical solutions, numerical solutions, experimental solutions and case studies in the literature are discussed.

Chapter 3 gives details of the numerical modeling. It defines the geometry of the problem and geometry of the tunnel section. Also, soil profile and soil

parameters are defined. Then, details regarding finite element model are given. The chapter is concluded by presenting the material properties and construction stages used in the analysis.

Chapter 4 includes the discussion of the results. To determine the parallel tunnel interaction, effect of soil stiffness, pillar width and the advancement level on the behaviour of displacement, bending moment and shear force are discussed and FEM results are illustrated graphically.

Chapter 5 presents major research findings and conclusions.

CHAPTER 2

LITERATURE REVIEW

2.1 Introduction

In the literature, there are number of studies which deal with the interaction of parallel tunnels. These studies will be classified under the titles of: analytical solutions, numerical solutions in 2D, numerical solutions in 3D, experimental solutions and case studies. In this chapter, results of available research studies will be discussed and summarized.

2.2 Analytical Solutions

A study was carried out by Fotieva and Sheinin (1966), in order to determine the distribution of stresses in the lining of a circular tunnel when driving a parallel tunnel. In their study, two plane problems of theory of elasticity is solved to determine the state of stress of an elastic medium weakened by two circular holes, one of which is reinforced and state of stress of a medium weakened by one reinforced hole. It was planned to determine the additional field of stresses by subtracting the stresses of two circular holes from one circular hole (Fotieva & Sheinin, 1966).

To illustrate the solution, a numerical example is done with initial data of: $R=3$ m, $r=2.8$ m, $a=8$ m, $E_0=50000$ kg/cm², $E_1=300000$ kg/cm², $\nu_0=0.4$, $\nu_1=0.2$, $\gamma=2.2$ t/m³, where, R is the outer diameter of tunnel, r is the inner diameter of

the tunnel, a is the center to center distance between tunnels, E_0 is the modulus of elasticity of the rock mass, E_1 is the modulus of elasticity of the lining material, ν_0 is the Poisson's ratio of the rock mass, ν_1 is the Poisson's ratio of the lining material and γ is the unit weight of the soil. The values of obtained additional stresses are shown in Figure 2.1.

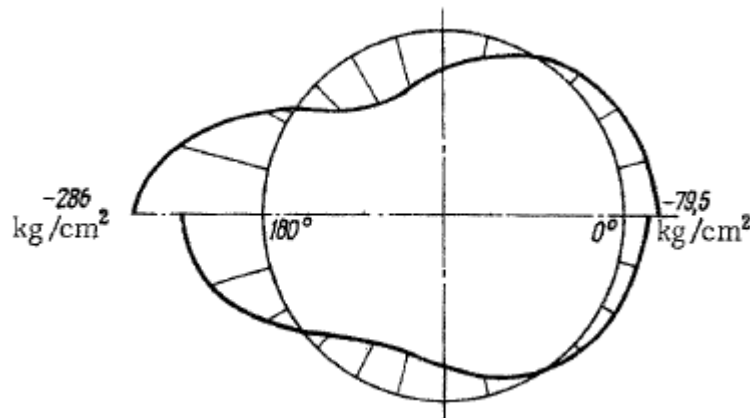


Figure 2.1 Diagram of the additional tangential stresses of the lining
(Fotieva and Sheinin, 1966)

Fotieva and Sheinin (1966), concluded that the additional stresses reach to a maximum value in the section $\theta = 180^\circ$ when a parallel tunnel is driven. Additional stress values due to second tunnel depend upon the ratio G_0/G_1 (moduli of shear for the rock and lining material) and the relative distance between the tunnels R/a . In the example, it was observed that the driving of the second tunnel results in overloading on the tunnel lining and this overloading may be important. The author suggested taking into account this situation during the calculation of the lining stresses (Fotieva & Sheinin, 1966).

Another study was conducted by Dunaevskii (1986) to determine the stresses and forces in linings of two non-circular parallel tunnels. He used a method which was based on analytical methods and Schwartz algorithm. By using this method the author compiled a program in FORTRAN language.

In this study variable parameters are changed in order to determine the behavior of the linings of two identical parallel tunnels. The values of d/B , which is the relative distance between tunnels are, assumed to be equal to 1.5, 2.0, 2.5 and 3.0. On the other hand, the relative average thickness δ (the ratio of the difference of the average radii of the outside and inside contours of the lining section to the average radius of the outside contour) was assigned equal to 0.22, 0.19 and 0.16, which corresponds to the radii of $R_1 = 2.5, 2.6$ and 2.7 meters, respectively. For all these values of relative distance between tunnels and relative average thickness, the ratio of the modulus of elasticity of the lining material and rock mass, E_1 / E_z , was assumed to be equal to 0.33, 3.3, 20 and 50 (Dunaevskii, 1986). The diagram illustrating the geometry of the tunnels is shown in Figure 2.2.

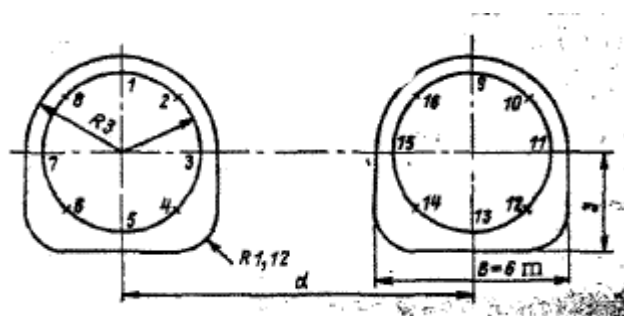


Figure 2.2 Diagram illustrating geometry of the tunnels (Dunaevskii, 1986)

The results of the calculations showed that the stresses and internal forces change monotonically with the increase of the ratio d/B . The mutual effects of the tunnels on stresses and forces in the lining of the left tunnel can be neglected when $\delta = 0.22$ and $d/B > 2.5$, when $\delta = 0.19$ and $d/B > 4$ and when $\delta = 0.16$ and $d/B > 5$ (Dunaevskii, 1986).

Gerçek (1988), conducted another study to investigate the interaction of parallel tunnels or roadways. In his study, some useful approaches have been presented which can be used by design engineers and the distribution of generated stresses have been considered. Also, information about previous studies on this subject in the literature has been given in his study.

According to U.S. Army Corps of Engineers the necessary pillar width between tunnels should be 1-1.3 D for good quality rock and at least 3 D for poor quality rock conditions where D is the diameter of the tunnel. (Gerçek, 1988)

Also, in his study Gerçek (1988) stated that the determination of the zone of influence of an underground opening may be used in order to estimate the interaction degree between parallel tunnels and he suggested using Kirsh's solution for circular openings and Ingliss's solution for ellipse openings.

Roark and Young (1975) offered a practical solution to determine the stresses on infinite number of parallel tunnels. In his study, Gerçek used this approach in order to determine the variation of tangential stresses of specific points on tunnels with the distance between parallel tunnels. The results are presented in

Figure 2.3 and as it seen from the figure, the interaction between parallel tunnels becomes practically negligible when the center to center distance between tunnels exceeds 3D where D is the tunnel diameter (Gerçek, 1988).

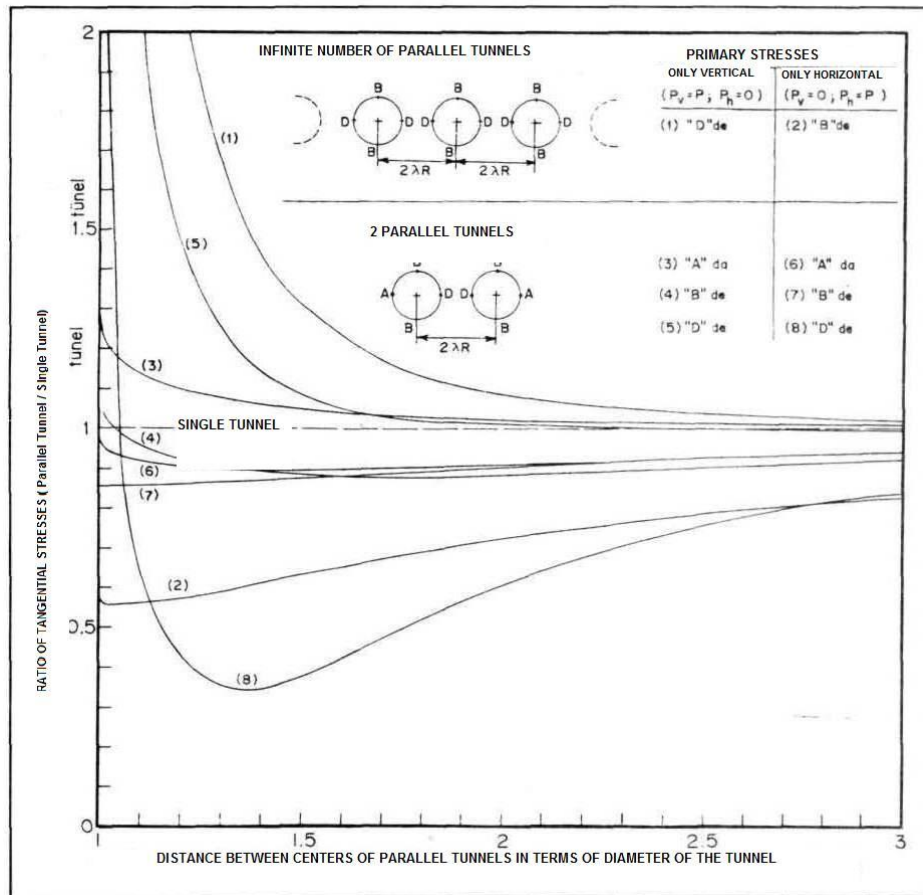


Figure 2.3 The variation of tangential stresses of specific points on tunnels with the distance between parallel tunnels (Gerçek, 1988)

Scwaigerer(1970) offered a solution to determine the second order stresses at the mid-height of the pillar between circular parallel tunnels. The variation of

the vertical stresses at the mid-height of the pillar with pillar width is given in Figure 2.4. The figure showed that, as the pillar width decreases vertical second order stresses increases sharply (Gerçek, 1988).

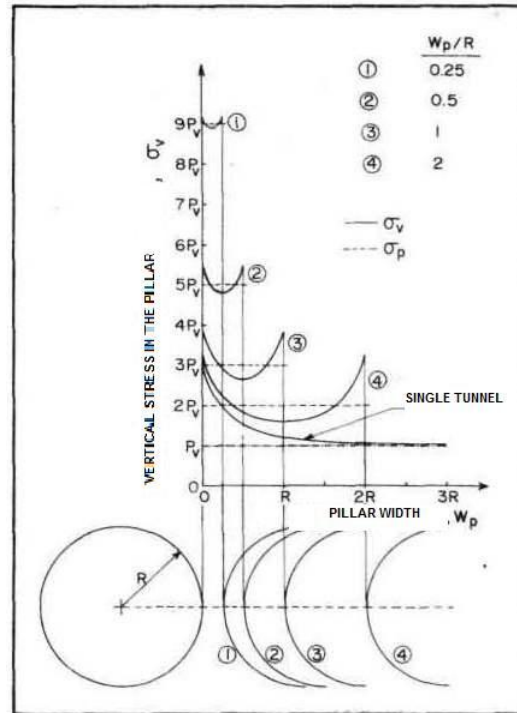


Figure 2.4 The variation of second order stresses at the mid-height of the pillar with the pillar width (Gerçek, 1988)

2.3 Numerical Solutions on 2D

One of the earliest numerical studies about interaction between parallel tunnels was conducted by Ghaboussi and Ranken in 1976. A series of parametric finite element analyses were performed in order to investigate the behavior of two parallel tunnels which are close to each other. The variable parameters selected

in the study are: the width of the pillar separating the two tunnels; the tunnel depth; support condition; and sequence of excavation (Ghaboussi & Ranken, 1976).

In order to determine the influence of pillar width, three values of pillar width to diameter ratios, W/D , were considered as $W/D = 1.0, 0.5$ and 0.25 and two tunnel depth to diameter ratios, H/D , were considered as $H/D = 1.5$ for the shallow depth and $H/D = 5.5$ for the moderately deep tunnel. In this part of the study the sequence of excavation was modeled such that the two tunnels are being advanced together at or near the same rate. Also, both tunnels were assumed to be either lined or unlined which means that in the lined tunnel analyses excavation of the tunnel and the installation of the liner are done simultaneously, on the other hand, in the unlined tunnel analyses it is assumed that there exists a certain time gap between the excavation of the tunnel and the installation of the liner. From the analyses performed it was found that interaction is most severe for the unlined tunnel case. As the spacing between two such tunnels is reduced, the vertical stress in the pillar increases rapidly while the horizontal confining stress approaches zero. Interaction between two lined tunnels was also observed from the analyses. For the lined tunnel analyses, the pillar stresses were controlled by the deformation of the tunnel liners, and the changes in the medium stresses were small since, the liner displacements were also small. Another finding of the study is that the depth of the tunnel is not a significant factor which effects the normalized pillar stresses. Figure 2.5 illustrates the variation of pillar stresses with pillar width (Ghaboussi & Ranken, 1976).

Tunnel displacements also change with the change of the pillar width between the parallel tunnels. Two sets of analyses were performed as lined and unlined

analyses for different pillar width values of a deep tunnel ($H/D=5.5$). For the unlined case, the downward displacement of two tunnel case is greater around the upper half of the perimeter than the single tunnel case because of the vertical compression and resultant shortening of the pillar and the difference increases as the pillar width decreases. On the other hand, interaction between the two tunnels prevents the outward displacement of the pillar which resulted in less inward displacement at the crown and invert and more outward displacement at the abutment than in single tunnel, for the lined tunnel analyses case. Also in this case, the effect of the pillar width can be observed. Figure 2.6 and 2.7 shows the unlined and lined tunnel displacement patterns, respectively (Ghaboussi & Ranken, 1976).

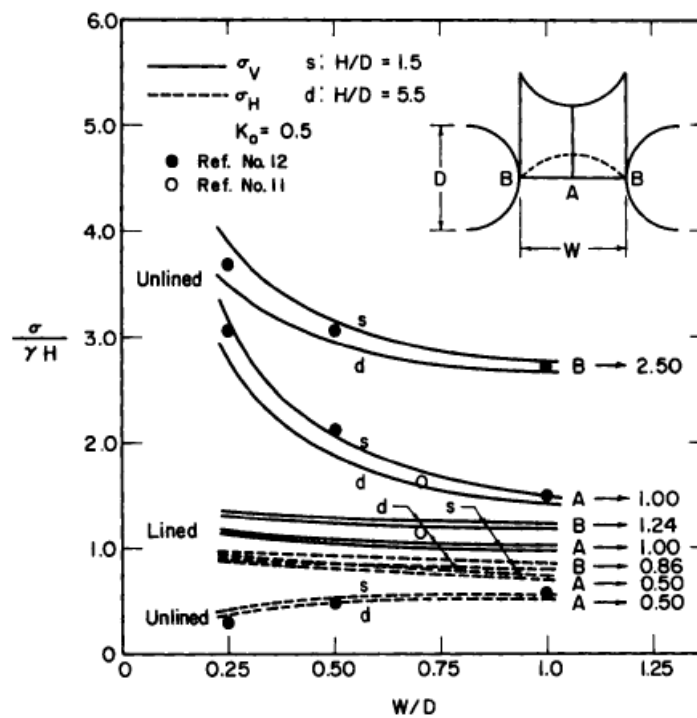


Figure 2.5 Pillar stresses vs. pillar width (Ghaboussi & Ranken, 1976)

Generally, the distribution of the liner forces and bending moments do not differ greatly from the distribution for a single excavated tunnel under the assumption that the construction stages of two parallel lined tunnels are simultaneously occurred. Figure 2.8 shows the distribution of the liner moments for deep ($H/D = 5.5$) tunnels. From the Figure 2.8 it is observed that, generally the bending moments values are smaller than single tunnel case due to interaction. The effect of interaction on bending moments are more evident at the pillar location because of the reduction in displacements which results in reduction in bending moments, also. Moreover, it is observed that the interaction becomes more effective as the pillar width between the parallel tunnels reduces (Ghaboussi & Ranken, 1976).

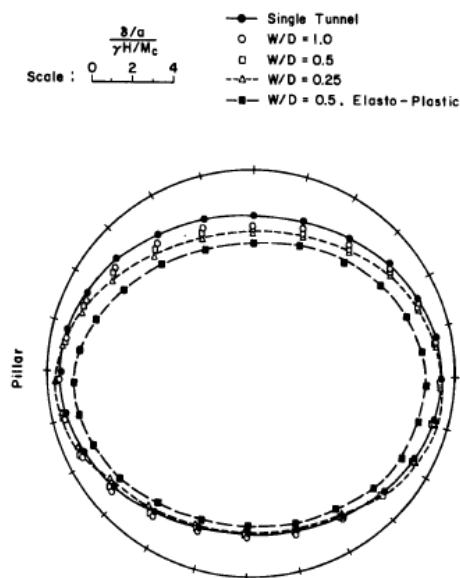


Figure 2.6 Unlined tunnel displacements $H/D=5.5$
(Ghaboussi & Ranken, 1976)

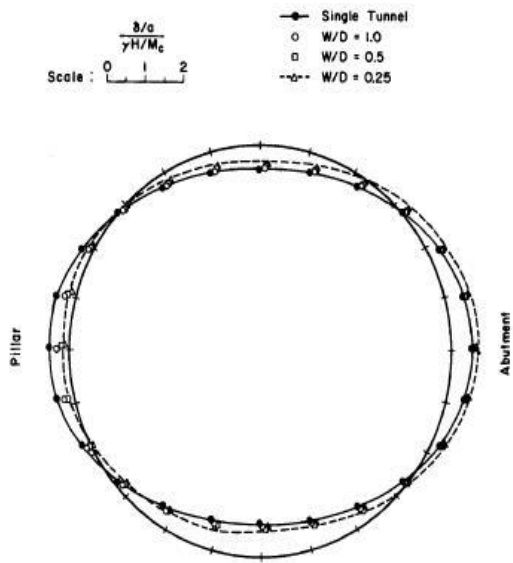


Figure 2.7 Lined tunnel displacements $H/D=5.5$
(Ghaboussi & Ranken, 1976)

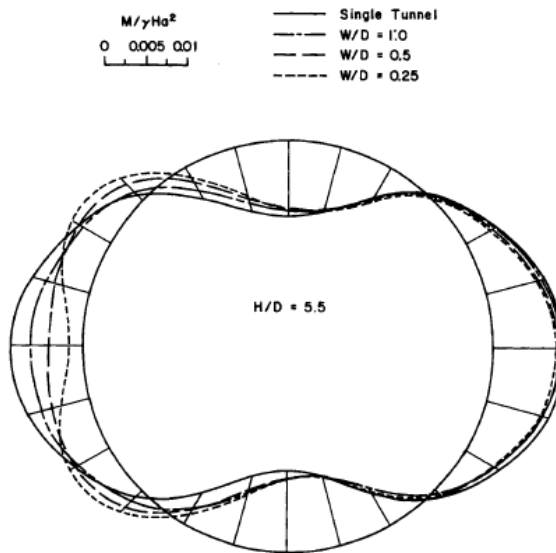


Figure 2.8 Distribution of liner bending moments for the deep tunnels
(Ghaboussi & Ranken, 1976)

Surface settlement due to parallel tunnel interaction is another subject which was investigated by Ghaboussi & Ranken. The total amount of surface settlement is divided into two parts as combined settlements of two single tunnels and additional settlement due to the interaction of parallel tunnels as shown in Figure 2.9 (Ghaboussi & Ranken, 1976).

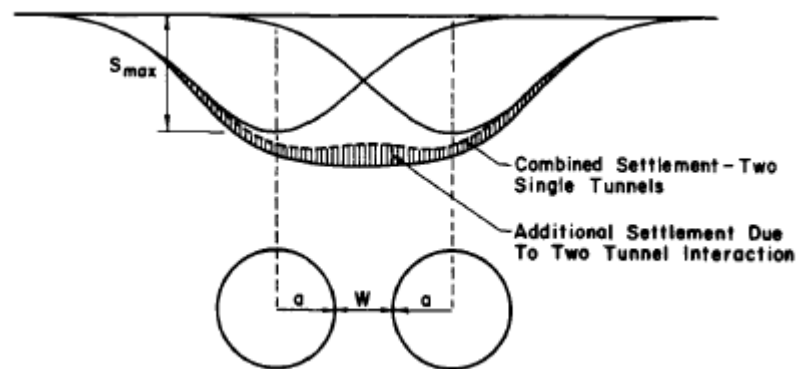


Figure 2.9 Additional surface settlement arising from two tunnel interaction (Ghaboussi & Ranken, 1976)

A series of finite element analyses were performed for unlined two parallel tunnels in order to determine the effect of interaction on surface settlements. From the analyses it was observed that the additional surface settlement due to interaction of two parallel unlined tunnels increases as the pillar width decreases for shallow ($H/D = 1.5$) tunnels. On the other hand, the additional surface settlement due to interaction of two parallel unlined tunnels increases as the pillar width decreases for deep ($H/D = 5.5$) tunnels, but the amount of increase is smaller when it is compared with the shallow one. Also, the additional settlement is quite large for the greatest pillar width ($W/D = 1.0$) which is used in the analyses. The results of the analyses are shown in Figure 2.10 and Figure 2.11 for shallow and deep tunnel, respectively. The analyses

performed in this study showed that the additional surface settlements due to parallel tunnel interaction may be eliminated by increasing the pillar width between the tunnels. The width of the pillar which has to be left between the parallel tunnels depends on the depth of the tunnel. Approximately, a pillar width in terms of tunnel diameter of “2” ($W/D=2$) may be sufficient for shallow tunnels for this purpose. On the other hand, it was observed that much greater pillar width is needed for deep tunnels (Ghaboussi & Ranken, 1976).

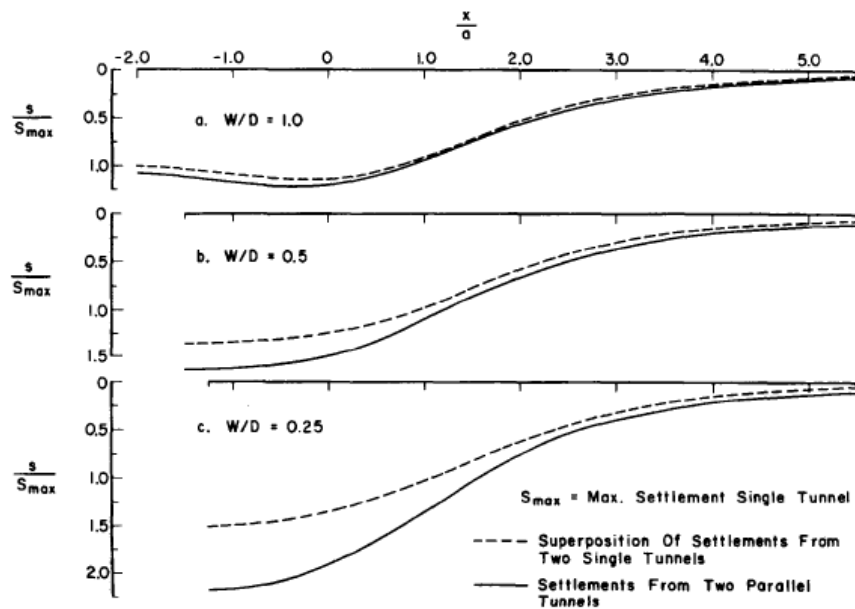


Figure 2.10 Settlement graphs for shallow ($H/D=1.5$) tunnels (Ghaboussi & Ranken, 1976)

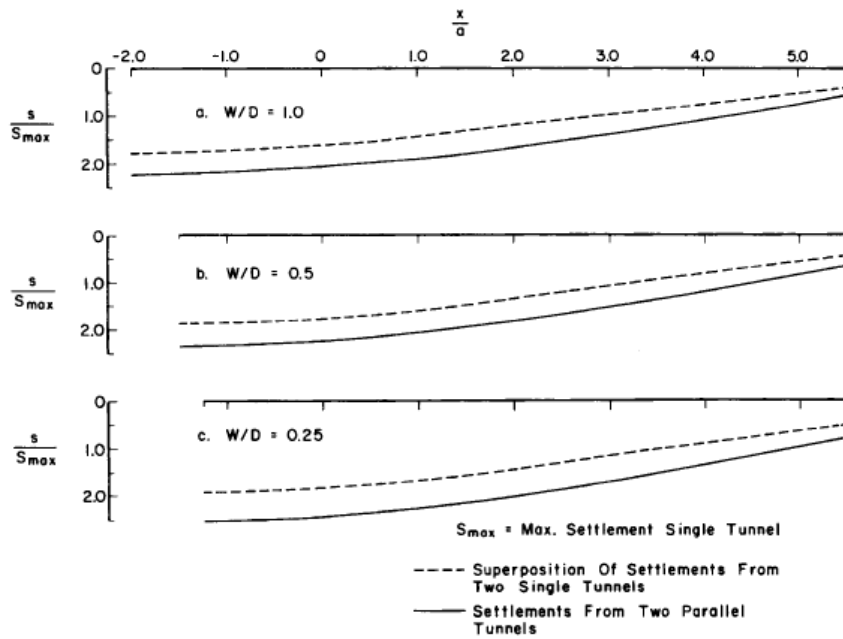


Figure 2.11 Settlement graphs for deep ($H/D=5.5$) tunnels
(Ghaboussi & Ranken, 1976)

In order to determine the interaction effects of sequence of construction on parallel tunnels a number of finite element analyses were performed. The results reveal that the excavation of a tunnel parallel and adjacent to a previously constructed tunnel causes additional displacements and liners forces in the previously constructed tunnel. The intensity of the interaction strongly depends on displacements, which are permitted during the construction of the new tunnel. Two extremely different conditions were analyzed; in one condition the new tunnel was lined right after the excavation; on the other hand, the new tunnel was left unlined in the second condition. When the new constructed tunnel was lined right after the excavation the increase of displacements and liner forces because of the new tunnel resulted in a more acceptable condition in the previously constructed tunnel if it is compared with the analyses of unlined condition. For the unlined condition, especially at the

location of the pillar the amount of increase of displacements and liner forces are greater than the lined case (Ghaboussi & Ranken, 1976).

A numerical parametric study was conducted by Addenbroke & Potts (1996), to investigate twin tunnel behaviour. Two different conditions are analyzed, as vertically aligned parallel tunnel and horizontally aligned parallel tunnel. The spacing between the two parallel tunnel is a variable. The reactions of both the ground surface and the tunnel linings are analyzed for these cases. (Addenbroke & Potts, 1996)

Figure 2.12 illustrates the settlement graph under the effect of the second tunnel excavation of a horizontally aligned parallel tunnel. It is observed that the shape of the settlement profiles above each of the second tunnel is very similar to the greenfield profile which is simply the predicted settlement of a single tunnel. On the other hand, the lateral position of the maximum settlement is shifted with respect to the tunnel center line, towards previously constructed tunnel. Figure 2.13 shows the variation of eccentricity of S_{\max} with pillar width for horizontally aligned parallel tunnel. The eccentricity is accepted as zero when there is no interaction between tunnels. As shown in the figure, the eccentricity of S_{\max} is nearly 2 times of pillar width when the pillar width is less than 1 diameter. As the spacing increases, eccentricity decreases and the eccentricity is less than 0.25 of pillar width when pillar width is greater than 7 diameters (Addenbroke & Potts, 1996).

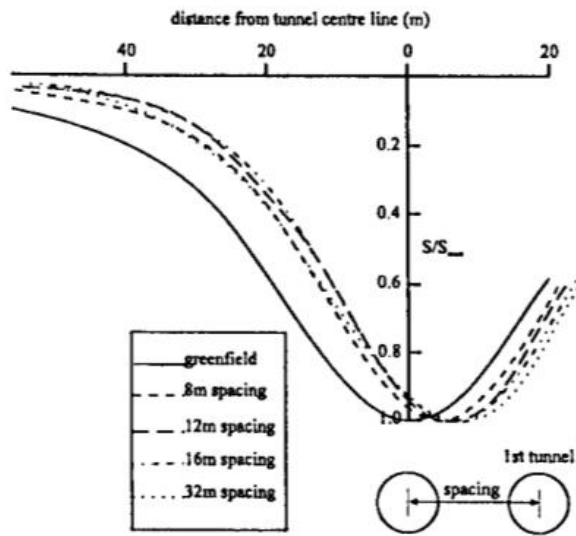


Figure 2.12 Settlement above 2nd tunnel for horizontally aligned tunnels (Addenbroke & Potts, 1996)

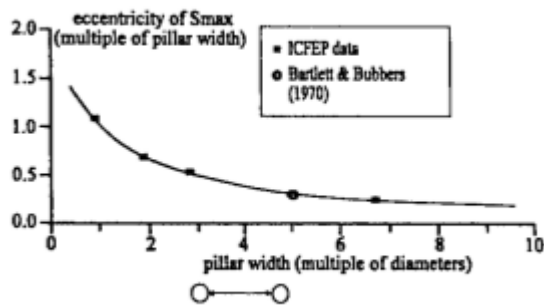


Figure 2.13 Eccentricity of S_{max} with pillar width (Addenbroke & Potts, 1996)

For vertically aligned parallel tunnel, analyses performed with different spacings show the settlement profile wider than the single tunnel case profile. As shown in Figure 2.14, as the spacing between piggy back tunnels reduces,

the bottom part of the settlement profile gets more flattened. Figure 2.15 shows that, the closer the pillar depth, the normalised position of the inflection point gets larger. The settlement profile can be twice as wide as the single tunnel's settlement profile for a pillar depth of less than 1 diameter and this result is in accordance with the assumed settlement profile by superposition (Addenbroke & Potts, 1996).

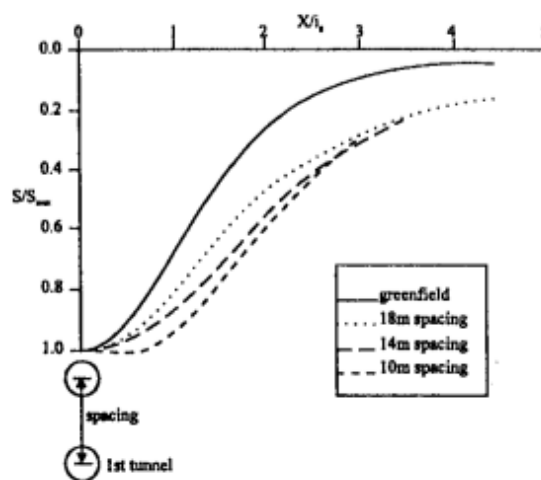


Figure 2.14 Settlement above the 2nd of two piggy back excavations
(Addenbroke & Potts, 1996)

Addenbroke & Potts(1996), investigated the influence of the excavation of the second tunnel on the lining to the first tunnel. The results showed that the horizontal diameter of the previously excavated tunnel increases, and the vertical diameter decreases as the second tunnel passes. The magnitude of this induced distortion reduces with increasing pillar width, and is negligible for pillar widths greater than 7 tunnel diameters for side by side (horizontally aligned) tunnels. In piggy back (vertically aligned) tunnels, the horizontal diameter of the previously excavated tunnel decreases, as the vertical diameter

increases as the second tunnel passes. The magnitude of this induced distortion reduces with increasing pillar depth, and is negligible for pillar depths greater than 3 tunnel diameters (Figure 2.16).

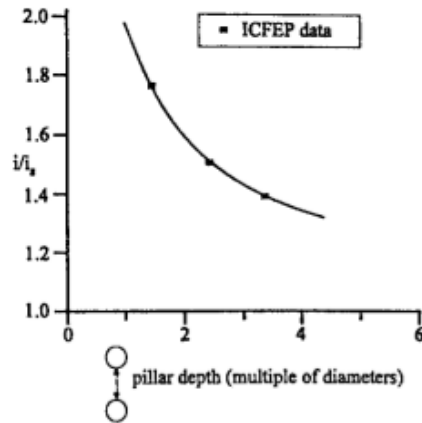


Figure 2.15 Position of inflection point with pillar depth (Addenbroke & Potts, 1996)

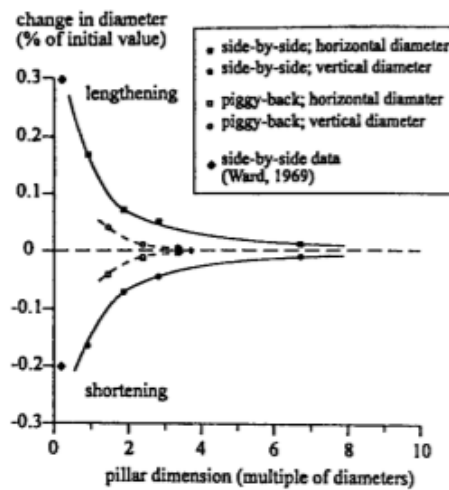


Figure 2.16 Response of 1st lining to passage of 2nd tunnel (Addenbroke & Potts, 1996)

A study was conducted by Kooi & Verruijt (2001) in order to investigate the interaction of circular holes in an infinite elastic medium. Method of bi-polar coordinates and Schwarz' alternating method is used for the solution of stresses and displacements, respectively. In order to confirm the results, data is compared with the results of numerical analysis conducted by using FLAC 2D and PLAXIS 2D computer programs. The tangential stress along the line between the two tunnels has been calculated analytically, and the results are compared with the numerical results obtained using the computer programs are shown in Figure 2.17. As shown in Figure 2.17, the results of the two computer programs are very similar and also the results obtained by analytical solution is close to those results. However, numerical solutions give slightly larger tangential stresses especially near the boundaries of the parallel openings (Kooi & Verruijt, 2001).

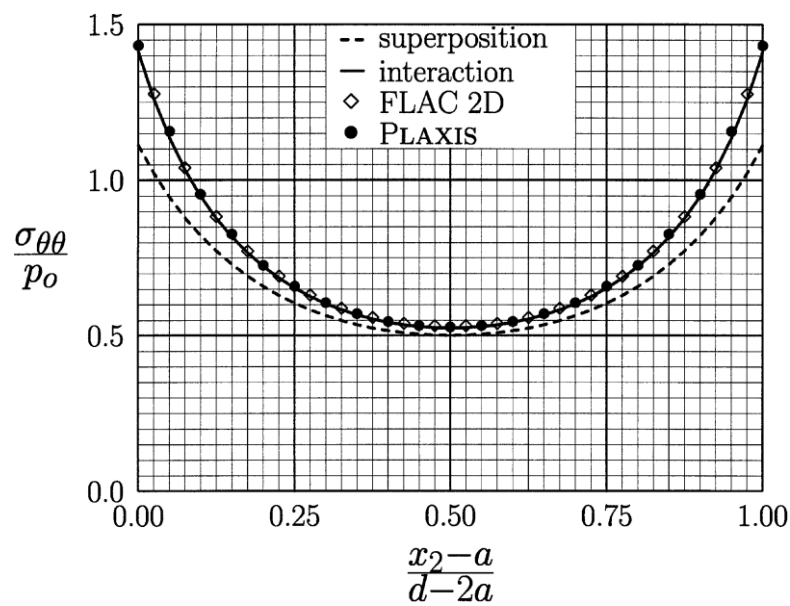


Figure 2.17 Results compared with FLAC 2D and PLAXIS
(Kooi & Verruijt, 2001)

Kooi & Verruijt (2001), state that the interaction between the parallel tunnels causes 15% larger displacements in the center of the openings for $d/a = 4$ where, d is the center to center distance between the parallel tunnels and a is the diameter of the tunnel. As shown in Figure 2.18, the continuous curve is drawn by using the computer program results, whereas the dashed curve is drawn by simply using the superposition of the single tunnel which neglects the interaction (Kooi & Verruijt, 2001).

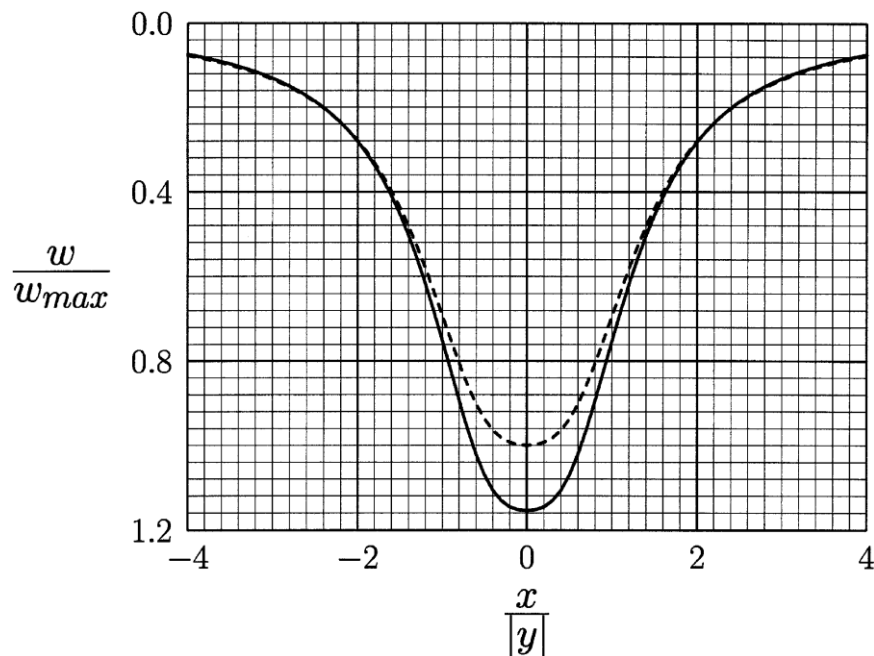


Figure 2.18 Scaled displacements for $d/a=4$ and $y=d$ (Kooi & Verruijt, 2001)

Yu and Akagi (2003), studied the interaction of parallel tunnels in terms of both numerical analysis and superposition of analytical solutions. Pillar width, depth of the tunnel, and soil properties are variable parameters which are taken into account in the scope of the study. Numerical results are compared with the data which is obtained from site measurements and analytical solutions. A numerical model was solved by using PLAXIS and results were compared with

the superposition of analytical solutions and site measurements. The results are shown in Figure 2.19. Yu and Akagi (2003), stated that the interaction between parallel tunnels is an important factor which affects the ground settlement behaviour. It was observed that, in stiffer soils, the results of the ground settlement by FEM (PLAXIS) solution are approximately same with the results obtained from site measurements and obtained by Logan & Poulos method.

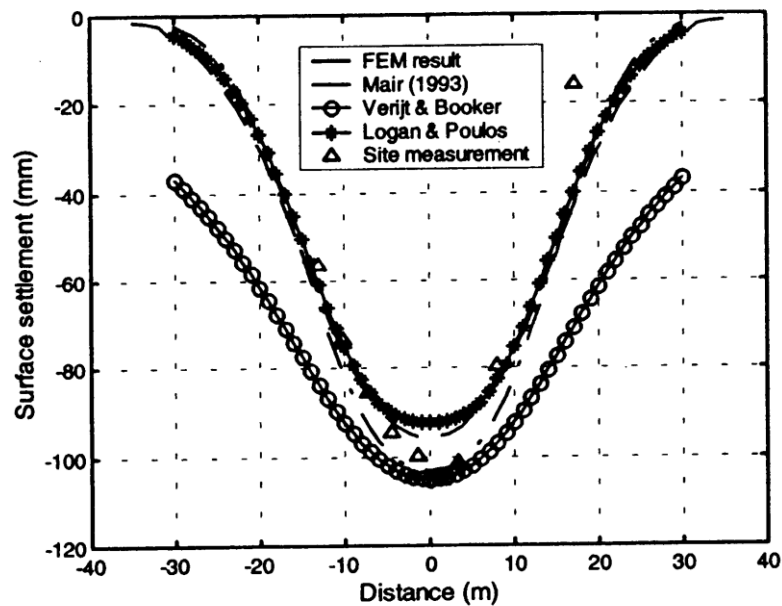


Figure 2.19 Comparison of ground settlements of twin tunnels
(Yu and Akagi, 2003)

Yu and Akagi, (2003), investigated also the effect of pillar width and burial depth on the interaction behaviour. Figure 2.20 compares the interaction factor for different values of burial depth and relative separation. Yu and Akagi, (2003), concluded that the interaction factor is almost zero when relative separation (D/H) is larger than 3 where D is the center to center distance between parallel tunnels and H is the depth of tunnel. Also burial depth is an

important factor to the interaction factor. When burial depth is large interaction is smaller (Yu & Akagi, 2003).

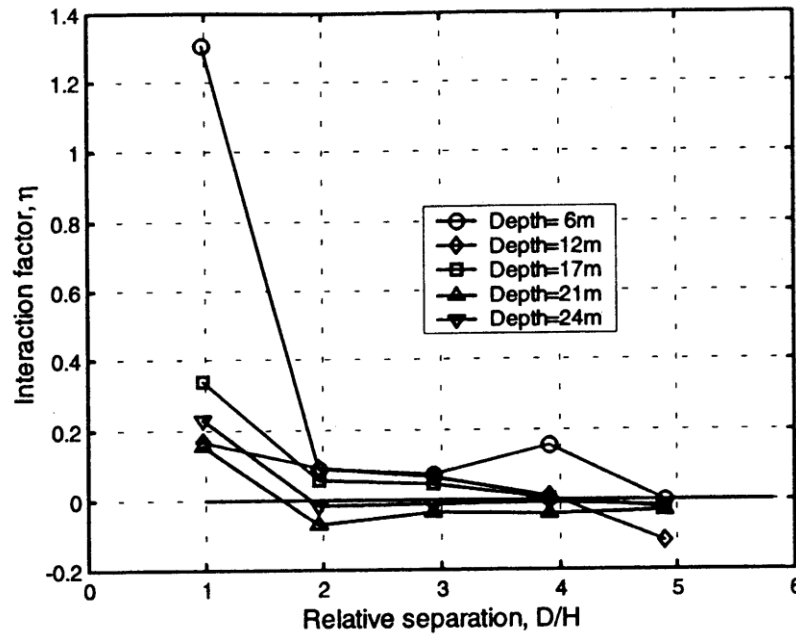


Figure 2.20 Interaction factor with depth (Yu and Akagi, 2003)

A study was conducted by Gerçek (2005), to investigate the interaction between closely spaced and unsupported parallel underground openings. A series of finite element analyses were performed by using Phase² computer program on two non-circular parallel underground openings. The basic geometrical parameters are shown in Figure 2.21.

Comparison of the analyses were performed by comparing the factor of safety values obtained from the analyses. The effect of pillar width (W_p) on the interaction between two parallel openings of the same size is investigated for the W_p / W_1 ratios of 0.5, 1.0 and 1.5. According to the analyses results, when

$W_p / W_1 > 1.5$ interaction between parallel underground openings becomes negligible. The results are shown in Figure 2.22 (Gerçek, 2005).

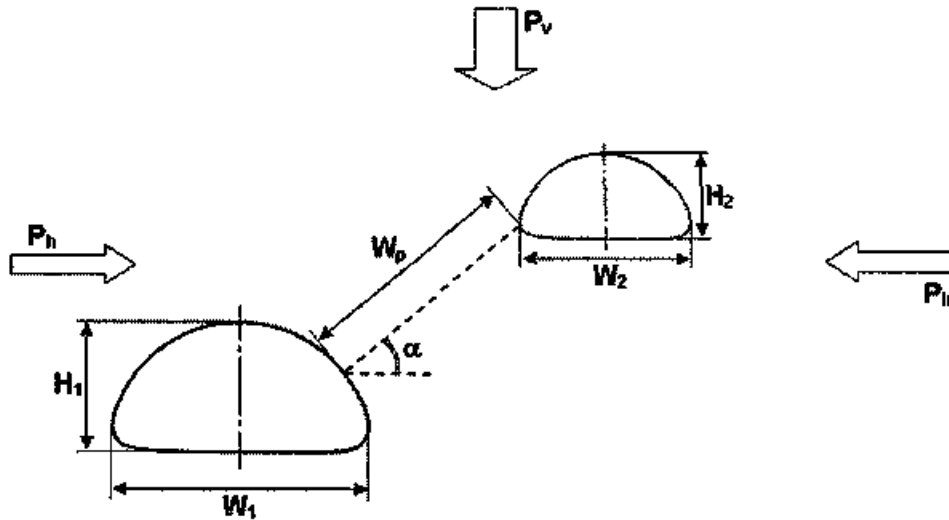


Figure 2.21 Geometrical parameters and in-situ stress field in the numerical analyses (Gerçek, 2005)

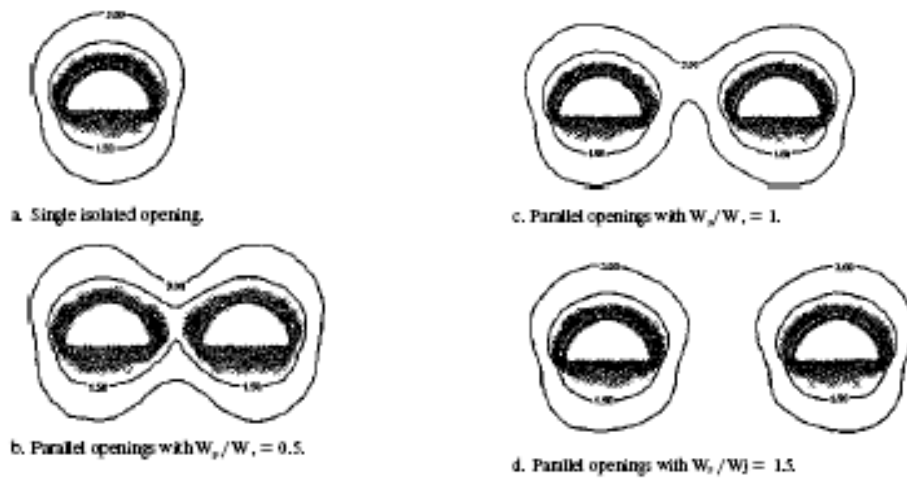


Figure 2.22 Effect of pillar width on the degree of interaction (Gerçek, 2005)

Gerçek (2005), investigated the effect of position of the openings with respect to each other for both same sized and different sized openings. Three different alignments are considered as horizontal alignment ($\alpha=0^\circ$), diagonal alignment ($\alpha=45^\circ$) and vertical alignment ($\alpha=90^\circ$). The results are shown in Figure 2.23. The case in which the openings aligned vertically, gives worse results in terms of stability for both same sized and different sized openings (Gerçek, 2005).

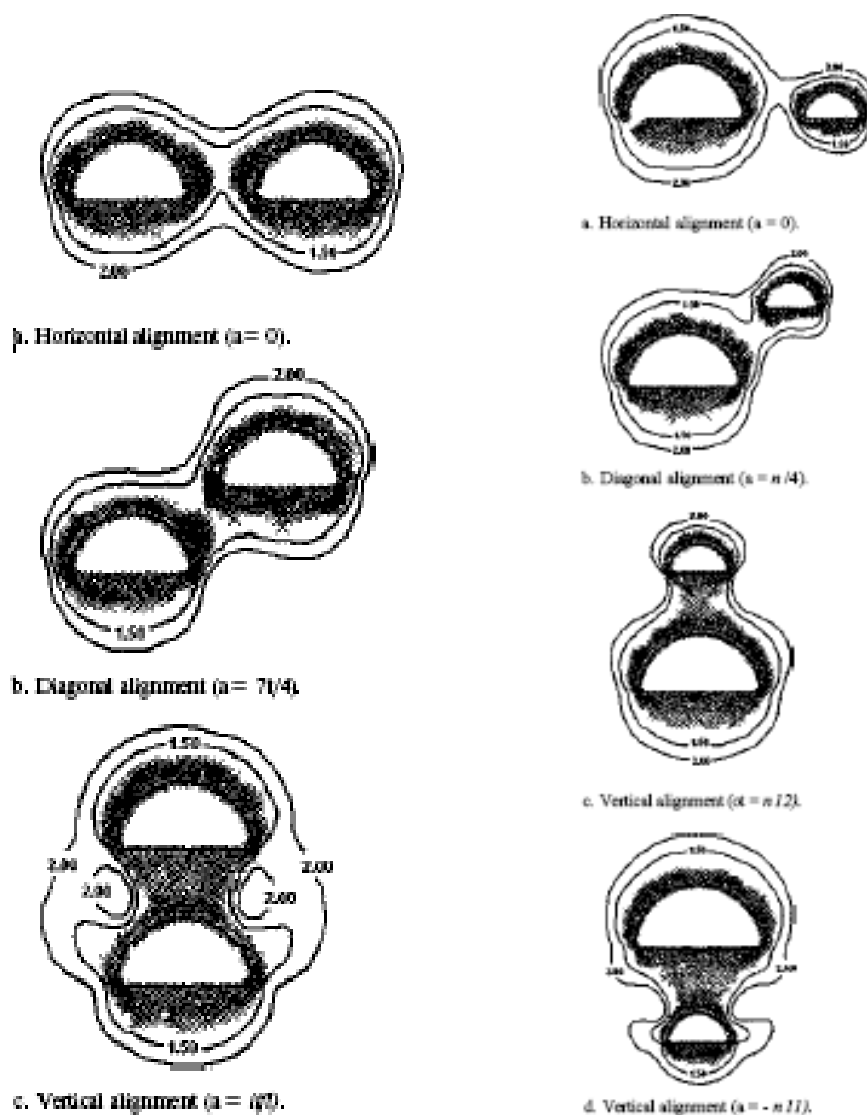


Figure 2.23 The effect of position of openings (Gerçek, 2005)

A study was conducted by Chehade & Shahrour (2007) in order to examine the influence of the relative position and construction procedure on the interaction between twin tunnels. In this study numerical analyses were conducted for three configurations of twin tunnels as: aligned-horizontally, vertically and inclined as shown in Figure 2.24.

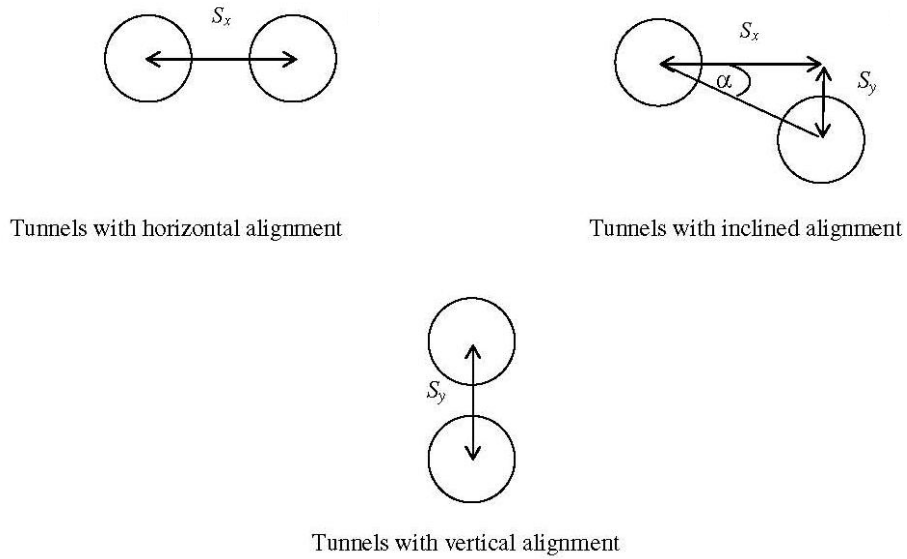


Figure 2.24 Configurations considered in the analyses of the interaction between twin tunnels (Chehade & Shahrour 2007)

The finite element program PLAXIS is used to carry out the analyses. A stress release factor of, $\beta=0.5$, is used in the analyses during the simulation of the construction stages. This factor is simply the ratio of the stress release before the installation of the tunnel lining. Figure 2.25 illustrates the generated mesh used for the analysis of horizontally-aligned tunnels with a spacing ratio of $S_x/D = 2$, where S_x is the center to center distance between parallel tunnels and D is the diameter of the tunnel (Chehade & Shahrour 2007).

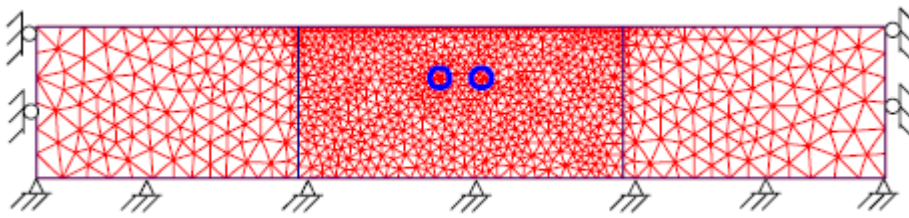
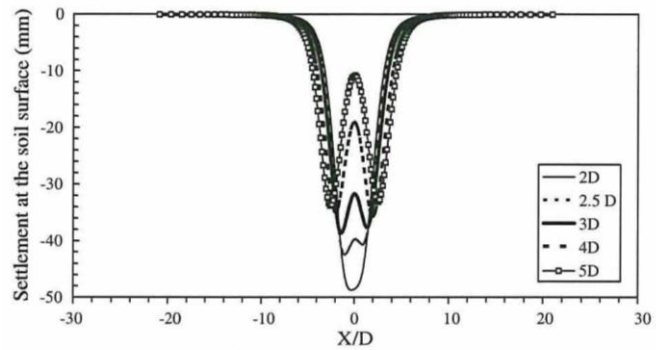


Figure 2.25 Mesh used in the analysis of tunnels with horizontal alignment
(Chehade & Shahrour 2007)

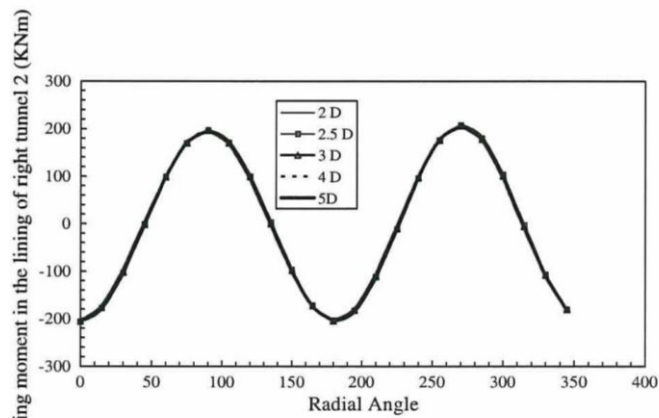
For horizontal alignment five values of spacing ratio , S_x / D , are used in the analyses as 2, 2.5, 3, 4 and 5. It is observed that the settlement profile and magnitude of the settlement depend on the separation distance between tunnels. The magnitude of the settlement is maximum when the spacing is closest which is the configuration of $S_x/D = 2$. The construction of the first tunnel does not effect the second one in terms of settlement behaviour, for the spacing ratio, S_x/D , values of larger than 3. The results of the analyses showed that the spacing and construction do not affect the internal forces in the tunnel, since spacing is large enough as shown in Figure 2.26 (Chehade & Shahrour 2007).

For the tunnels with vertical alignment two types of analyses were conducted. In the first type of analysis, the construction of the lower tunnel starts after the construction of the upper tunnel completed, on the other hand in the second type of analysis the construction of the lower tunnel is the first. First type of analyses give higher settlement and internal forces than the second type of analyses as shown in Figure 2.27. For tunnels parallel inclined again two configurations were analyzed which are mentioned above. The vertical distance between the tunnel axes kept constant as $S_y = 2D$ and in the first configuration $\alpha=45^\circ$ and in the second one $\alpha=39^\circ$ is selected. The results are similar with vertical aligned tunnels when the construction procedure is taken into

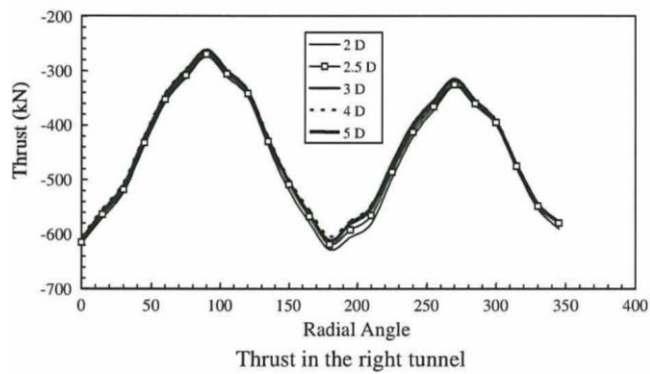
consideration. The results are summarized in Figure 2.28 (Chehade & Shahrour 2007).



Soil settlement induced by the construction of the twin-tunnel

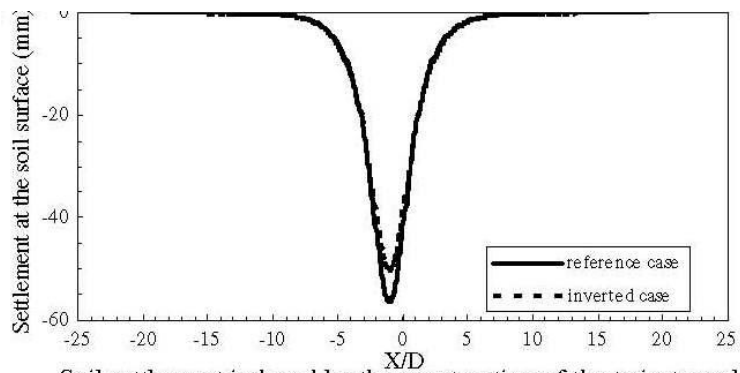


Bending moment in the right tunnel

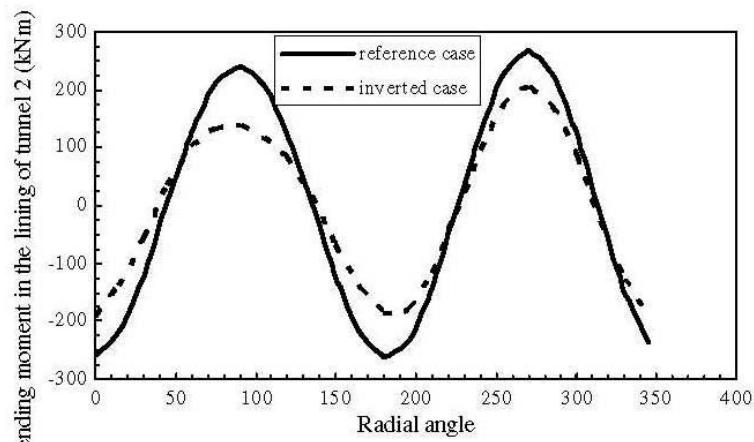


Thrust in the right tunnel

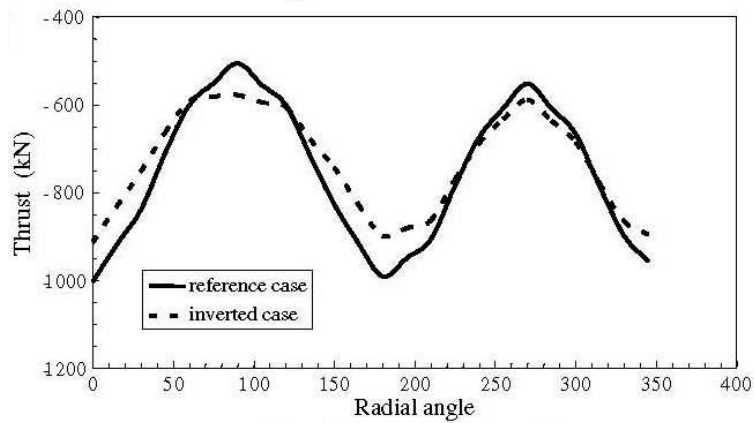
Figure 2.26 Horizontally aligned tunnels: settlement, bending moment and thrust in the right tunnel (Chehade & Shahrour 2007)



Soil settlement induced by the construction of the twin-tunnels
Reference case: upper tunnel constructed at first
Inverted case: lower tunnel constructed at first



Bending moment in the lower tunnel



Thrust in the lower tunnel

Figure 2.27 Vertically aligned tunnels: settlement, bending moment and thrust in the tunnel (Chehade & Shahrour 2007)

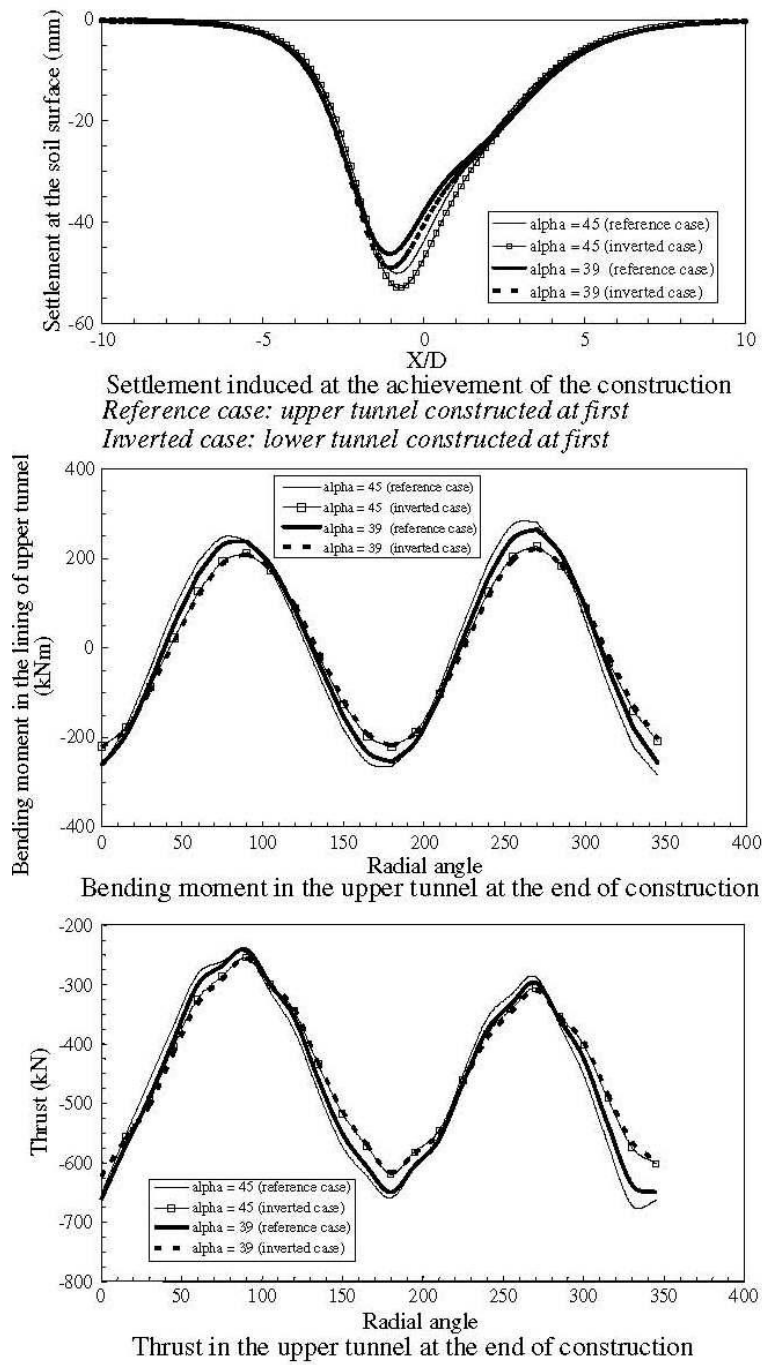


Figure 2.28 Inclined aligned tunnels: settlement, bending moment and thrust in the tunnel (Chehade & Shahrour 2007)

2.4 Numerical Solutions on 3D

Ng, Lee and Tang (2004), conducted a study in order to investigate the interactions between two parallel tunnels. A series of numerical analyses in 3D were performed to simulate the two parallel tunnels constructed by NATM technique. The three dimensional model is shown in Figure 2.29 and the analyses were carried out by using the finite element method program ABAQUS.

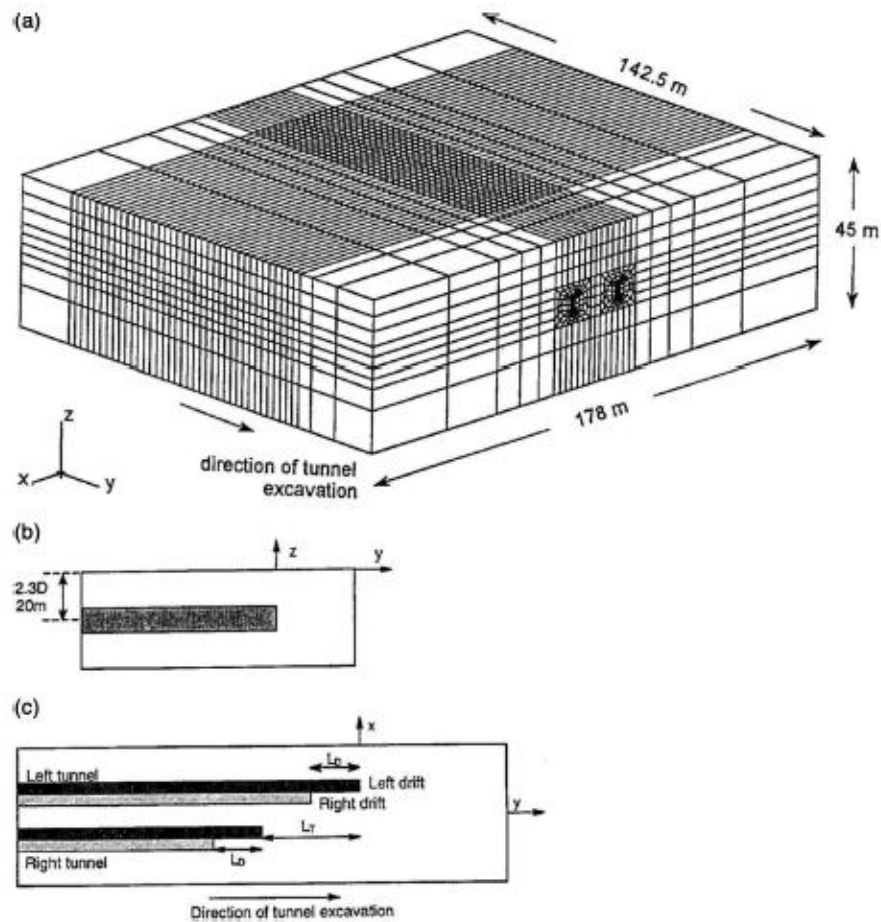


Figure 2.29 The 3D model used in the analyses (Ng, Lee and Tang, 2004)

The main variable parameter used in the analyses was the lagged distance between the left tunnel and the right tunnel. Five different values of lag distances in terms of diameter of the tunnel ($L_T = 0D, 0.6D, 1.2D, 2.3D, \text{ and } 3.5D$) between the left tunnel (firstly excavated) and the right tunnel (secondly excavated) were studied and analysed. In the analyses the pillar width between the tunnels was kept constant as $1.0D$. Ng, Lee and Tang (2004) concluded the results of the analyses as follows:

The deformation at the pillar location decreases because of the parallel tunnel interaction. The lagging distance, (L_T), between parallel tunnels has a strong influence on the behaviour of the horizontal movement. Shortening of the horizontal diameter of the tunnel approximately changes linearly with the change of L_T . On the other hand, the decrease in vertical diameter of the tunnel seems to be independent of the lagging distance, L_T (Ng, Lee and Tang, 2004).

The settlement profile above the firstly excavated tunnel shifts towards lagging tunnel when the lag distance is larger than zero. The location of the maximum settlement value offsets to the centerline of the pillar width until the lagging distance is approximately equal to 2.5 times of the tunnel diameter ($L_T=2.5D$). Beyond this lagging distance value the offset value becomes constant. The magnitude of the offset value may be a good indicator for the load sharing mechanism. Smaller offset values indicate that the load is shared by two tunnels more uniformly. The lagging distance between two tunnels effects the load sharing mechanism, however the magnitude of the maximum settlement is independent from the lagging distance, L_T (Ng, Lee and Tang, 2004).

The bending moment diagrams of the tunnel linings are similar in shape but different in magnitude. While, the bending moment values of the leading (left) tunnel is the largest, the bending moment values of the lagging (right) tunnel is the smallest. The difference between the magnitude of the bending moment values is related to the lagging distance, for lagging distances larger than zero. As the lagging distance, L_T , increases the leading tunnel carries larger load than the lagging tunnel which results in larger bending moments on the leading tunnel's lining. Pillar springline and the invert are the locations at which the effect of the L_T on axial forces is more evident than other locations of the tunnel. The axial forces increase at the left springline of the left tunnel and decrease at the right springline at the right tunnel due to the interaction between parallel tunnels as lagging distance increases (Ng, Lee and Tang, 2004).

2.5 Experimental Studies

An experimental study was conducted by Kim, Burd and Milligan (1998) as model testing of closely spaced tunnels in clay. In this study, the interaction problem between the soil and structure of closely spaced parallel and perpendicular tunnels in clay is studied by using laboratory model tests. Especially, short term effects of twin tunnel interaction is investigated which is observed directly after the installation of the tunnel. The tests are conducted for both horizontally parallel and vertically parallel tunnels in plane strain tank and cylindrical test tank, respectively. Plain strain test tank is shown in Figure 2.30 (Kim, Burd & Milligan, 1998).

A test was carried out in order to determine final and incremental bending moments acting on the instrumented existing tunnel. The results are presented in Figure 2.31. As seen from the figure, maximum bending moments occur at

the tunnel springlines ($\theta = 90^\circ$ and $\theta = 270^\circ$) and incremental bending moments are greatest at the pillar springline. (Kim, Burd & Milligan, 1998)

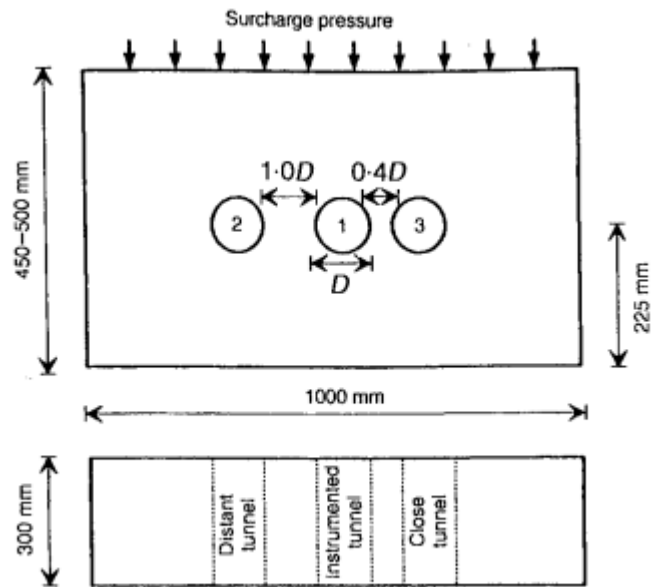


Figure 2.30 Plain Strain Test Tank Configuration
(Kim, Burd & Milligan, 1998)

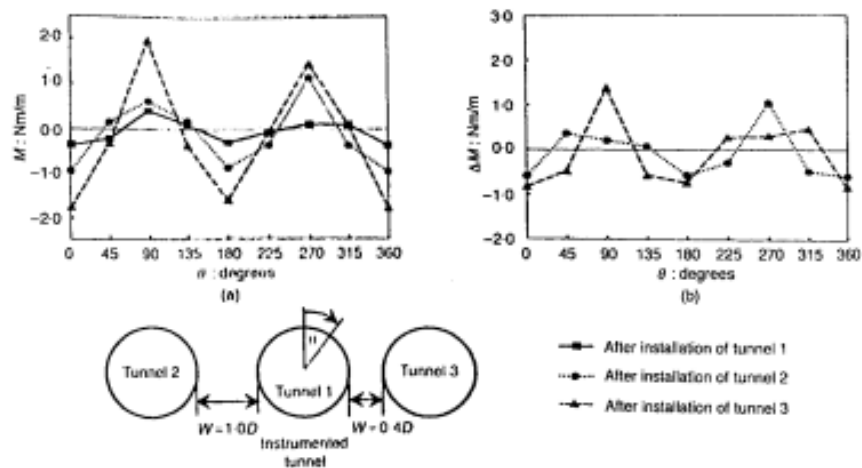


Figure 2.31 Total and incremental bending moments
(Kim, Burd & Milligan, 1998)

Also, the variation of incremental bending moment at the pillar springline with pillar width, liner stiffness and consolidation properties of the clay is investigated. The results are presented in Figure 2.32 and as shown in figure, the magnitude of normalized incremental bending moment decreases with increasing pillar width and reducing lining stiffness. The magnitude of normalized incremental bending moment also tends to increase with over consolidation ratio ,OCR (Kim, Burd & Milligan, 1998).

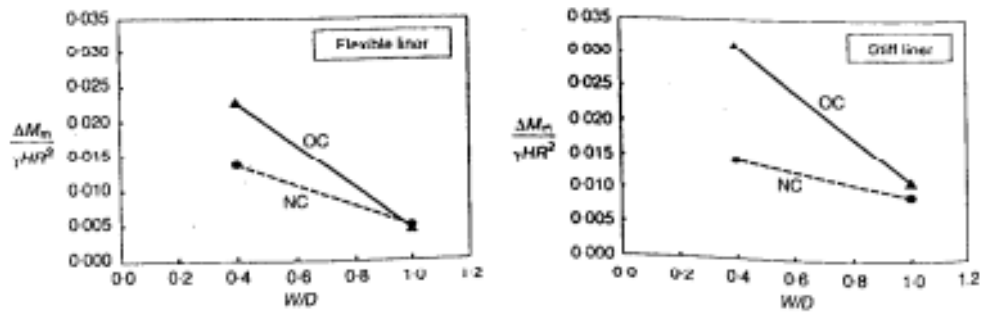


Figure 2.32 Variation of pillar springline incremental bending moment with W/D (Kim, Burd & Milligan, 1998)

Displacement values were also measured in order to determine the deformation behaviour. Figure 2.33 showed that the incremental displacements are intensified at the pillar springline and crown of the instrumented tunnel for $W/D=0.4$. Figure 2.34 showed the variation of the incremental diameter change with changing pillar width and consolidation properties of the clay. The interaction effects increase as the pillar width decreases. Figure 2.34 indicates that, displacement interaction effects tend to increase with increasing values of over consolidation ratio, OCR. However, in Figure 2.33 the displacements observed in the overconsolidated clay were generally smaller than those obtained in the equivalent normally consolidated test. Kim, Burd & Milligan

(1998), concluded that the result is unsurprising and is a consequence of the lower surcharge pressure used for the overconsolidated samples (Kim, Burd & Milligan, 1998).

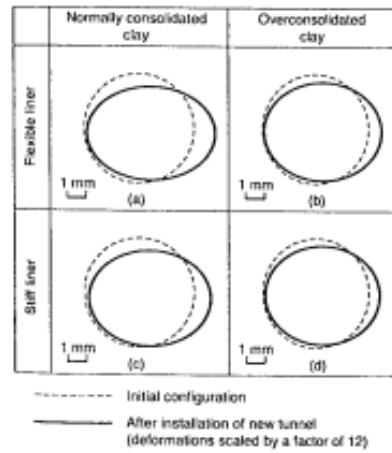


Figure 2.33 Deformed cross-sections for $W/D=0.4$
(Kim, Burd & Milligan, 1998)

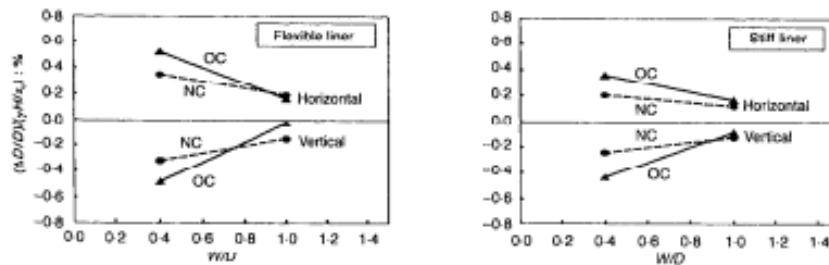


Figure 2.34 Variation of incremental diameter change with W/D
(Kim, Burd & Milligan, 1998)

Chu, Hsu, Chang and Lin (2006), performed an experimental study in order to determine the mechanical behavior of a twin tunnel in multi layered formations. A series of model tests were performed in two layered and three layered formations as shown in Figure 2.35.

There are four types of materials which are used in the model tests named as from I to IV. The type IV is the one which has the highest stiffness among other types. For model test, the parallel tunnels are always placed in the material which has higher stiffness than the others. The upper and lower formations are selected as the same material type (type I, II or III) for model tests in three layered formations. Also numerical simulations are performed by fictitious stress method (FSM) to model the mechanical behavior of a twin tunnel in multi layered formations (Chu, Hsu, Chang and Lin, 2006).

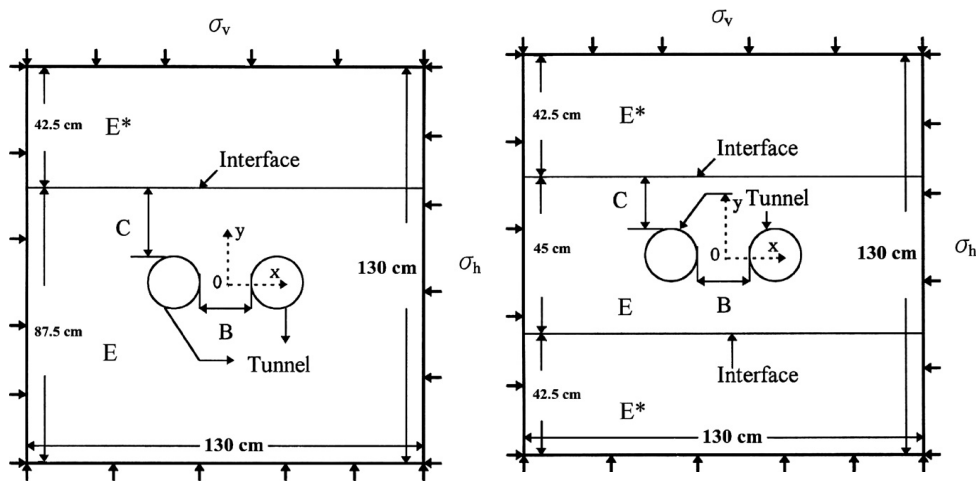


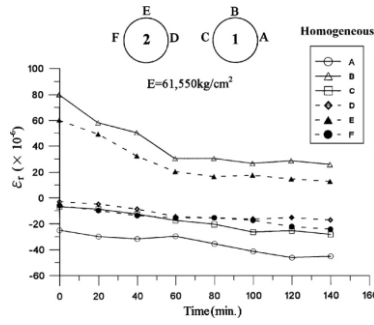
Figure 2.35 Schematic plot of the model test of twin tunnels in two and three layered formations (Chu, Hsu, Chang and Lin, 2006)

The results of the experimental studies are shown in Figure 2.36 for single layer, two layered and three layered formations. As shown in Figure 2.36 (a), the measured strains of the first excavated tunnel, marked as 1, are larger than the strains measured for the subsequently excavated tunnel. The strains become constant after a certain value for both tunnels. For the parallel tunnels placed in two and three layered formations, similar tendencies are determined. As the stiffness of the top formation, placed above the parallel tunnels, increases the

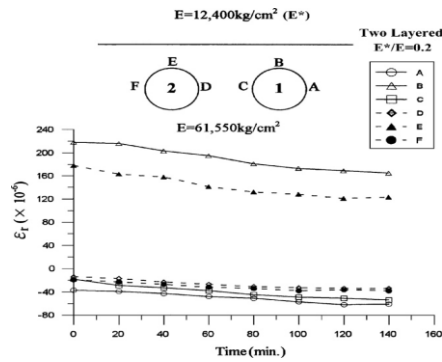
displacements at the crowns decrease. The measured strain for the three layered formations is less than the measured strain for the two layered formations for the same stiffness ratio as shown in Figure 2.37 (Chu, Hsu, Chang and Lin, 2006).

Other results of the study are as follows:

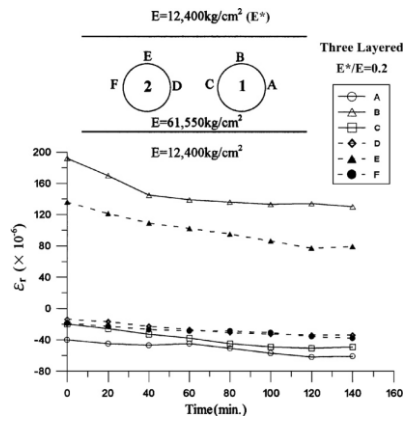
The results of the numerical analyses and model tests are close to each other which means FSM may be used for the solution of mechanical behaviour of parallel tunnels in multi-layered formations. The displacement at the tunnel crown is proportional with the stiffness of the upper formation for two layered model tests. For three layered formations, the displacements at the crown and invert are directly related with the stiffness of the upper and lower surrounding formations. As the ratio of horizontal stress to vertical stress closes to one the stress and displacement distribution become more symmetrical (Chu, Hsu, Chang and Lin, 2006).



(a)



(b)



(c)

Figure 2.36 Distribution of radial strains with time, (a) homogeneous material, (b) two-layered formations, (c) three layered formations (Chu, Hsu, Chang and Lin, 2006)

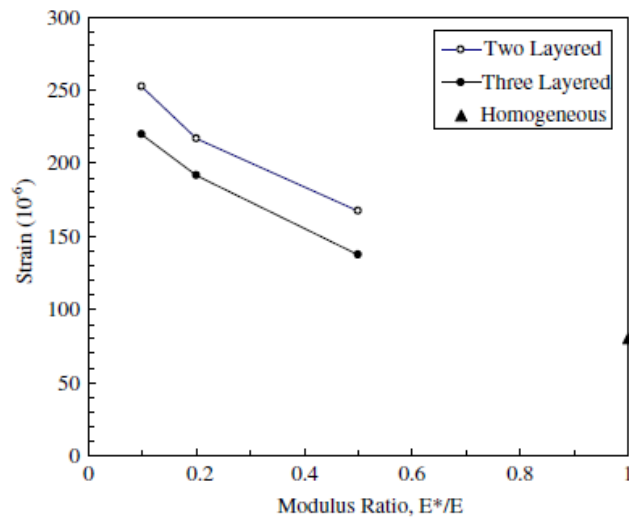


Figure 2.37 Measured strains at the crowns for different stiffness ratios
(Chu, Hsu, Chang and Lin, 2006)

2.6 Case Studies

There are two studies about case histories of Hsuehshan Tunnels in Taiwan. Both of the studies were performed in 2005, one of them dealt with interaction behaviour of two tunnels while the other study dealt with the interaction behaviour during the excavation for three parallel tunnels.

Chern and Hsiao (2005), conducted a study in order to determine the interaction behaviour of the Hsuehshan tunnels. The criterion proposed by Chern and Hsiao in 1997 for the assessment of the effects of tunnel interaction is examined by using the actual measurements of the tunnel. In the study which was conducted in 1997 it was concluded that the interactive effects between parallel tunnels are strongly related to distance between tunnels and strength to stress ratio of the surrounding soil (Chern and Hsiao, 2005).

Based on this study a graph is proposed in order to determine the variation of the severe interaction and slight or no interaction zones with W/B and strength/stress ratios as shown in Figure 2.38. The data of the 11 case histories from the Second Freeway Project in Taiwan plotted on this figure. All cases that observed abnormal conditions on the tunnel fall in the shaded area where severe interaction was expected. On the other hand, the cases with no abnormal conditions observed fall in the zone of slight or no interaction. A similar study is conducted for Hsuehshan Tunnels, also. Assessment of the tunnel interaction in Hsuehshan Tunnels is shown in Figure 2.39. It was concluded that the criterion can provide a guide to the planning of tunnel alignment by using the rock properties and in situ stress level estimated (Chern and Hsiao, 2005).

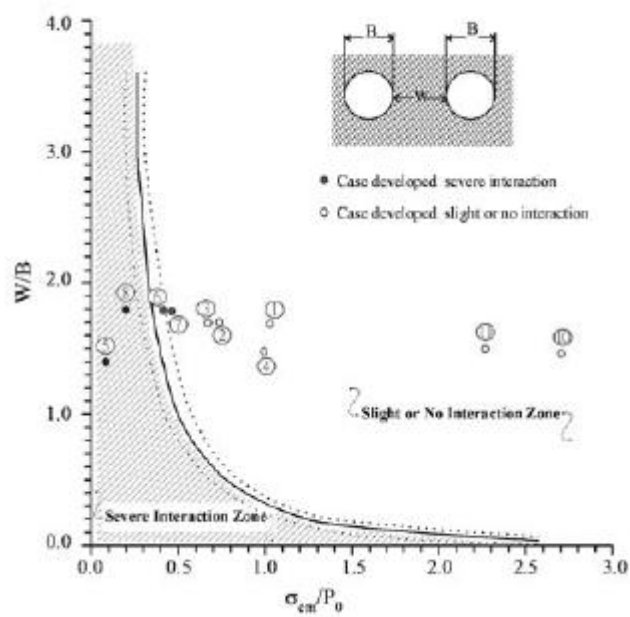


Figure 2.38 Proposed criterion to delineate the interactive effect (Chern and Hsiao, 2005)

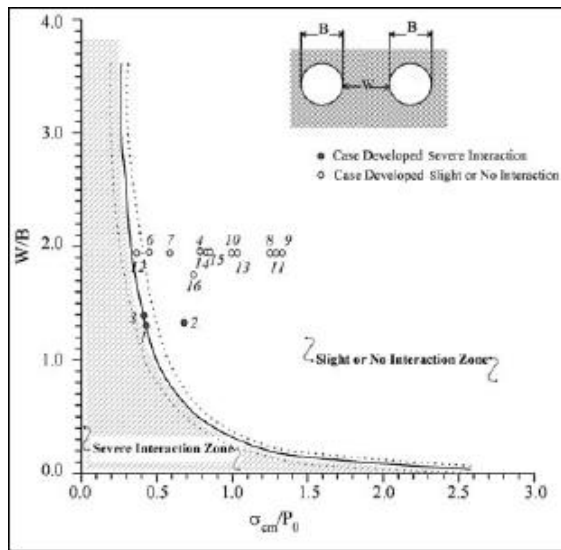


Figure 2.39 Assessment of tunnel interaction in Hsuehshan Tunnels
(Chern and Hsiao, 2005)

Lee, Lu and Lee (2005), conducted another study in order to determine the interaction behaviour during the excavation for three parallel tunnels constructed in Hsuehshan Tunnels. Numerical analyses were performed using PLAXIS finite element method computer program. The cross section of the three tunnels is given in Figure 2.40.

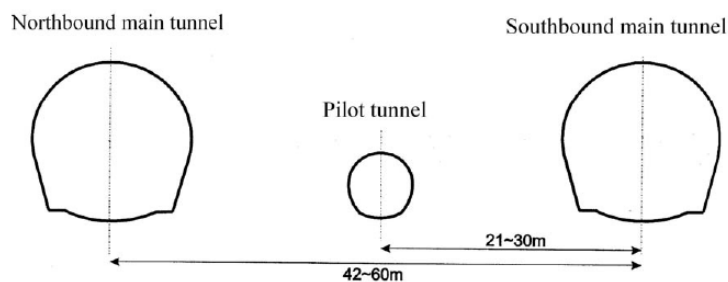


Figure 2.40 The cross section layout of the Hsuehshan Tunnels
(Lee, Lu and Lee, 2005)

The results of the analyses are as follows:

The displacements of the horse-shoe shaped tunnels are larger than the circular shaped tunnels and also, the distribution of the horse-shoe shaped tunnel is not in equilibrium when it is compared with the circular tunnel. The tunnel deformation is larger when the geological conditons are worse. As the pillar width reduces the displacements increase and the interaction of parallel tunnels is more evident. Especially, the interaction between parallel tunnels gets more severe when the net spacing between the two tunnels is smaller than the two times of the sum of the adjacent tunnel radius.

Karakus, Ozsan and Basarir (2005), conducted a study on finite element analysis for the twin metro tunnel constructed in Ankara Clay. In this study, finite element method analyses were performed in order to compare the results of the ground movements into the tunnel with the measured values at site. Finite elemet mesh used in the analysis and construction sequences are given in Figure 2.41 and 2.42, respectively.

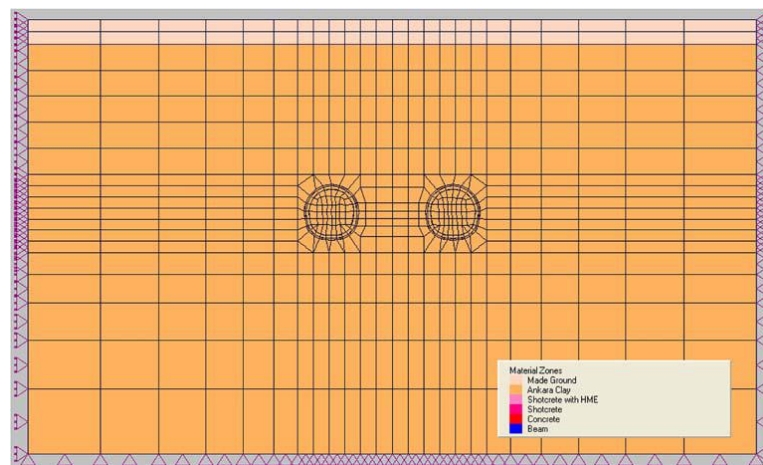


Figure 2.41 Finite element mesh used in the analyses
(Karakus, Ozsan and Basarir, 2005)

The results from the FEM analysis show that vertical displacements are quite similar with the site measurements; on the other hand, the horizontal displacements were calculated different from the site measurements. However, it was determined that the use of topographical methods gives more similar results. For that reason, it was concluded that especially in soft ground, measurements of the displacements should be performed by using a more reliable method (Karakus, Ozsan and Basarir, 2005).

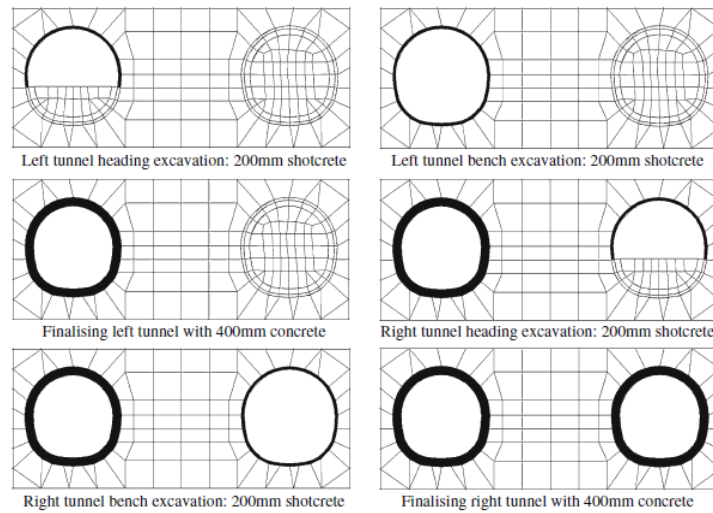


Figure 2.42 Construction sequences adopted in the FEM analyses
(Karakus, Ozsan and Basarir, 2005)

Both the measured horizontal and vertical displacements at the right tunnel are approximately 2-3 times more than the left tunnel which is previously constructed. It was commented on this result that the difference between displacement measurements could be due to the small pillar width between the tunnels which causes larger plastic regions around the tunnels (Karakus, Ozsan and Basarir, 2005).

CHAPTER 3

NUMERICAL MODELING

3.1 Introduction

This study is focused on the assessment of the interaction response of parallel NATM tunnels in weathered rock. A parametric study was performed for this purpose. Parametric analyses were carried out to determine the effects of two main parameters as pillar width and soil stiffness on the interaction behaviour of parallel NATM tunnels. Numerical analyses are performed by using Plaxis 3D Tunnel geotechnical finite element package, which is especially preferred for three-dimensional deformation and stability analysis of tunnels. In the proceeding paragraphs a short description of the program will be given.

There exist mainly four elements of Plaxis 3D Tunnel program as, Input, Calculation, Output and Curves. The boundary conditions, geometry of the problem and material properties may be defined in input program. Basically, the boundaries of the problem, excavation boundaries and boundaries of the soil layers are defined by using points and lines. The structural elements may be defined by plates, anchors or geogrids according to the type of the element. In this study plate elements are used in order to simulate the lining of the tunnels. The cross-section of the NATM tunnel is defined by using tunnel designer tool provided by the program. Material types that are available for the plates are either elastic or elastoplastic behaviour according to the type of the plate. Axial stiffness, EA , and flexural stiffness, EI , Poisson's ratio, ν , and unit weight of the plate, w , should be given appropriately for the elastic behaviour.

Material models which are available for modelling the soil behaviour are linear elastic model, Mohr – Coulomb model, jointed rock model, hardening soil model and soft soil creep model. For all these soil models mentioned above, three types of behaviours can be used named as, drained behaviour, undrained behaviour and non-porous behaviour in order to simulate the pore pressure behaviour in the soil. Hardening soil model will be described briefly since, this type of soil model is used in the analyses. Schanz (1998), stated that different types of soil such as stiff and soft soils can be simulated by using hardening soil model which is an advanced soil model. Stress dependent soil stiffness is the basic feature of hardening soil model. Also, definition of advanced soil parameters as unloading-reloading modulus, E_{ur} , and unloading-reloading Poisson's ratio, ν_{ur} , are available for hardening soil model. Since tunnelling is an unloading-reloading type of construction this soil model is more applicable than the other models. Parameters that can be defined in the hardening soil model are shown in Table 3.1 (Plaxis 3D Tunnel User's Manual, 2001).

Plaxis 3D Tunnel finite element program allows the user to create automatic mesh generation but, before the mesh generation boundary conditions should be properly defined. Standard fixities can be used to define the boundary conditions which restrain the horizontal displacement of vertical outer boundaries and vertical and horizontal displacements of bottom boundary. After the definition of the geometry, boundary conditions and the assignment of the soil and material properties an automatic 2D mesh is defined. Plaxis 3D Tunnel finite element program models the mesh by using 3D parallel planes model and 15 nodes wedge elements. These 15 nodes wedge elements are composed of 6 node triangles in xy direction. This type of volume element for soil behaviour gives a second order interpolation for displacements and the integration involves six stress points. Position of the nodes and stress points are shown in Figure 3.1.

Table 3.1 Parameters of hardening soil model

PARAMETER	EXPLANATION	UNIT
c	Effective cohesion	kPa
ϕ	Effective angle of internal friction	°
Ψ	Angle of dilatancy	°
E_{50}	Secant stiffness in standard drained triaxial test	kPa
E_{oed}	Tangent stiffness for primary oedometer loading	kPa
m	Power for stress-level dependency of stiffness	-
E_{ur}	Unloading-reloading stiffness ($E_{ur}=3E_{50}$)	kPa
ν_{ur}	Poisson's ratio for unloading-reloading ($\nu_{ur}=0.2$)	-
K_0	K_0 value for normal consolidation ($K_0=1-\sin\phi$)	-

The geometry of the problem and 2D mesh are created on the XY-Plane and the three dimensional model is simply the extension of the parallel created planes in Z direction. During the extension operation work planes at which the construction stages will be performed can also be created. Work-planes are vertical planes with different z-coordinates. The activation and de-activation of the soil elements, structural elements and loads are performed on these work planes. The horizontal distance along z-direction between successive work planes can be same or different in accordance with the construction procedure. Steps involved in the creation of 3D mesh are shown in Figure 3.2. After the generation of 3D mesh, groundwater level is defined if there exist and pore water pressures are generated.

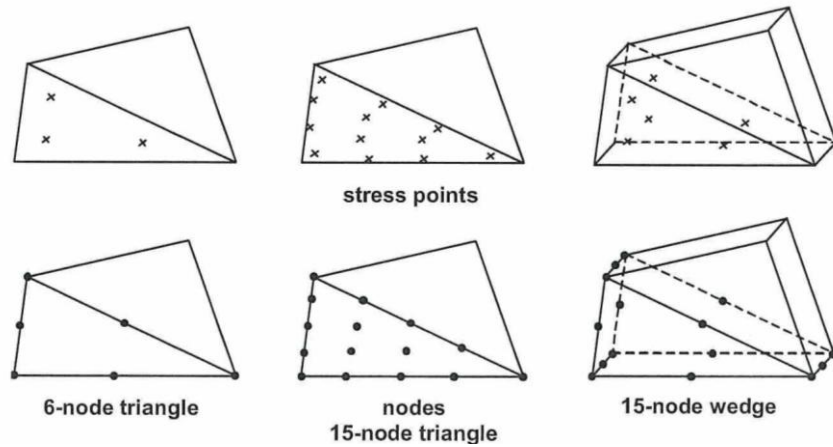


Figure 3.1 Position of the nodes and stress points
(Plaxis 3D Tunnel User's Manual, 2001)

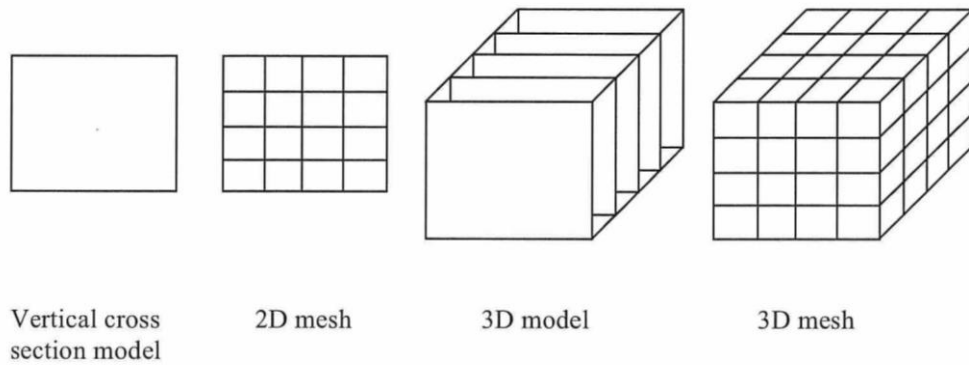


Figure 3.2 Creating a 3D model and finite element mesh
(Plaxis 3D Tunnel User's Manual, 2001)

After the generation of the 3D finite element model, the construction procedure can be simulated in calculations window. Plaxis 3D Tunnel finite element program calculates the elasto-plastic deformations for different loading

conditions. The program allows the user to define the actual construction stages which will take place at site. Construction stages can be modelled simply by activating and de-activating the soil clusters and structural elements. Also during the calculations, the change of pore water pressures may be defined if it is necessary and surcharge loads may be applied. Sometimes, it may be needed to simulate only a part of a construction stage, e.g. tunnel excavation. This type of an analysis can be achieved by inserting a ΣM_{stage} value less than 1 in the advanced menu. Also, safety analyses can be performed by using the c-phi reduction analysis option.

After the execution of the calculation phases which is defined in calculation program, the program allows the user to view the finite element solution of the selected phases. In the output program, it is possible to view the deformed mesh, total displacements, incremental displacements, total strains, effective stresses, total stresses, plastic points, active and excess pore pressures and internal forces of the structural elements. The internal forces of structural elements may be viewed both for the selected phase and envelope of the sectional forces up to selected phase.

Another component of the Plaxis 3D Tunnel finite element program is the curves program. By using the curves program, load displacement curves, stress paths and stress vs. strain diagrams may be plotted for previously selected nodes at the beginning of the calculations. The program also, allows the user to draw multiple curves on a single chart.

3.2 Geometry and Definition

As mentioned in the previous chapters, increase in demand for tunnels may lead the construction of new tunnels next to existing ones. In these cases the interaction between the previously constructed tunnel and new one becomes an important subject. For this reason, a parametric study is performed in order to investigate the behaviour of two parallel NATM tunnels constructed in weathered rock. Parametric analyses were carried out to determine the effects of two main parameters as pillar width and soil stiffness on the interaction response of parallel NATM tunnels. Numerical analyses were performed by using Plaxis 3D Tunnel geotechnical finite element package. The geometry of the problems for different pillar width values of 0.5D, 1.0D, 1.5D and 2.0D are shown in Figure 3.3, Figure 3.4, Figure 3.5 and Figure 3.6, respectively.

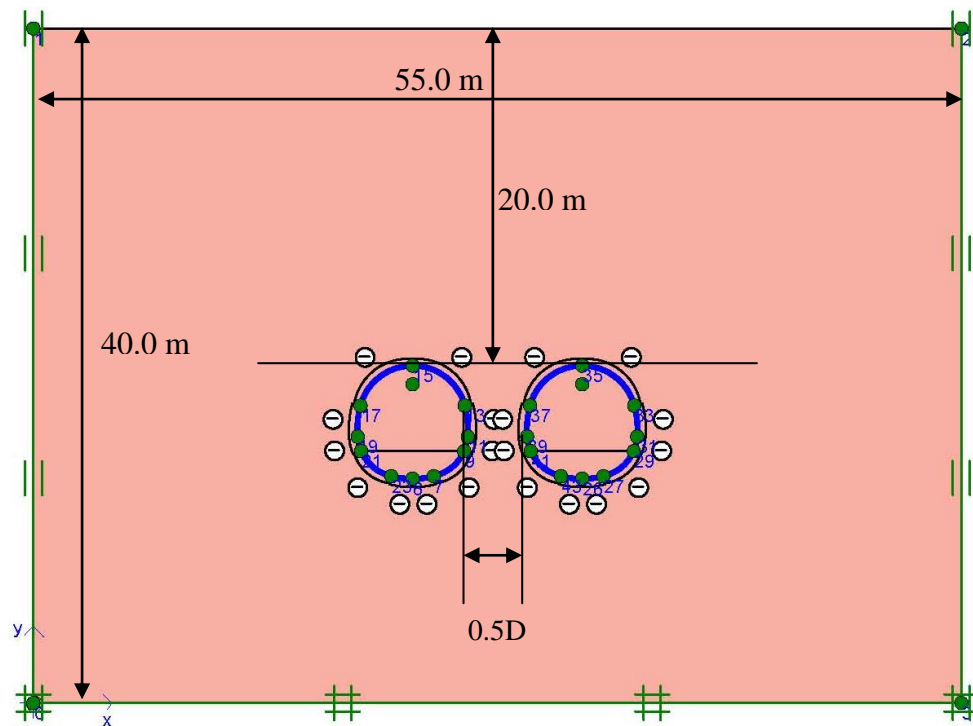


Figure 3.3 Geometry of the problem (Pillar width = 0.5D)

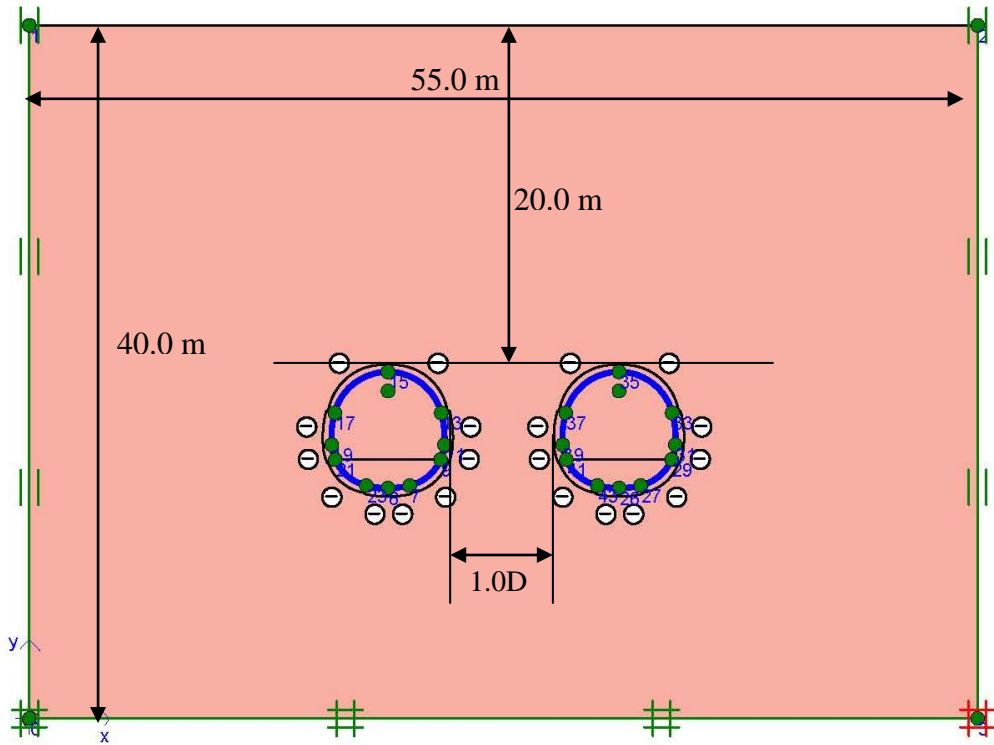


Figure 3.4 Geometry of the problem (Pillar width = 1.0D)

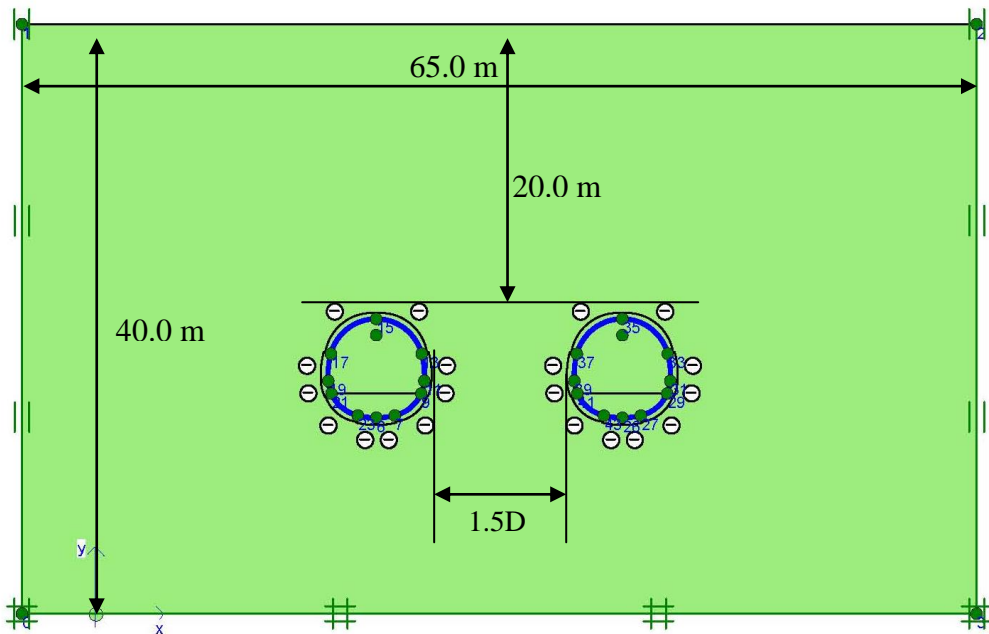


Figure 3.5 Geometry of the problem (Pillar width = 1.5D)

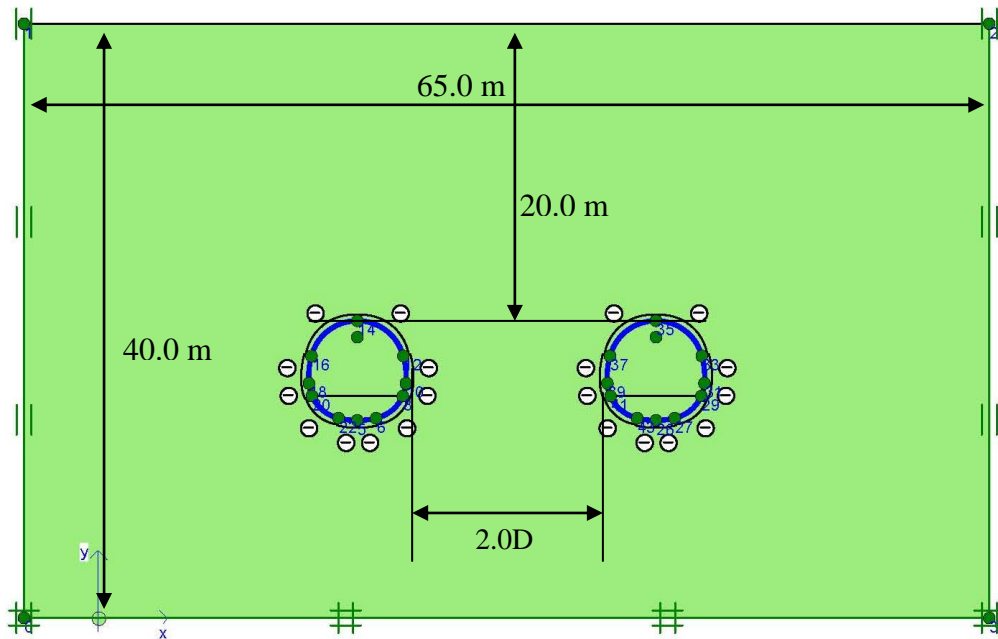


Figure 3.6 Geometry of the problem (Pillar width = 2.0D)

The geometrical properties of the NATM tunnel cross-section and corresponding cross-sectional view of the tunnel are given in Table 3.2 and Figure 3.7, respectively.

Table 3.2 Geometrical properties of the tunnel cross-section

Angle	(°)	Radius	(m)
α_1	12.98	R_1	5.60
α_2	53.45	R_2	2.60
α_3	19.58	R_3	5.60
α_4	18.99	R_4	3.20
α_5	75.00		

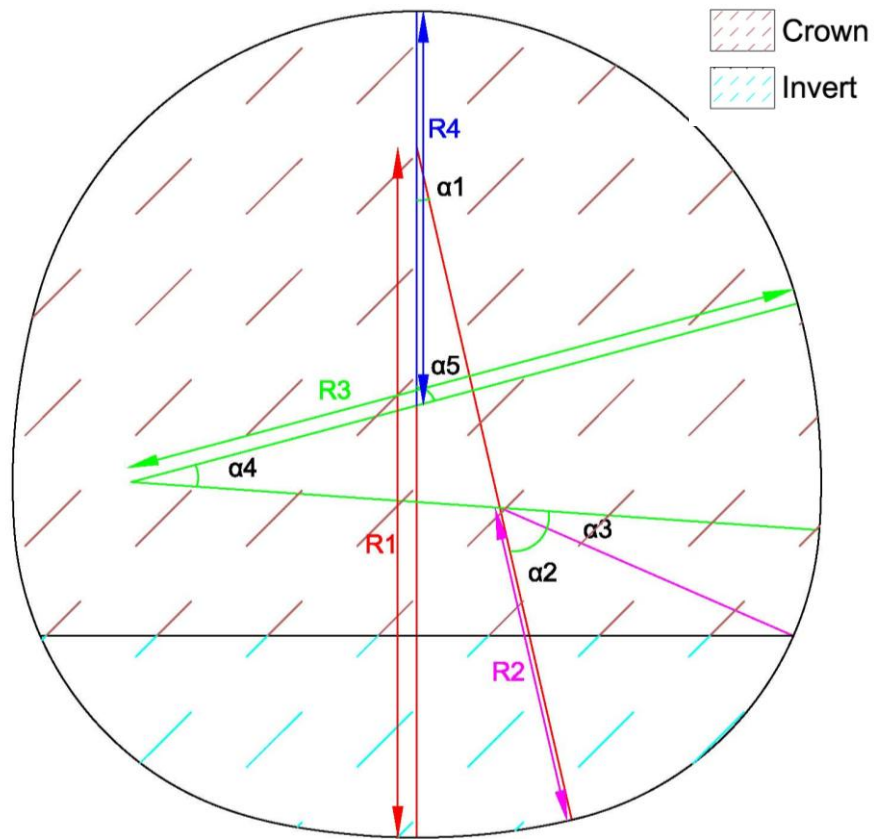


Figure 3.7 Cross-section of the NATM Tunnel

After the definition of the problem geometry on Plaxis 3D Tunnel finite element program, the 2D and 3D mesh are generated automatically. The generated mesh for 2D and 3D are given in Figure 3.8 and 3.9, respectively. The 3D mesh is defined by the extension of the 2D mesh at every 1 meter along the z-direction. Total length along z-direction is selected as 50 meters, since as the mesh dimensions and number of calculation steps increases, calculation time increases, also.

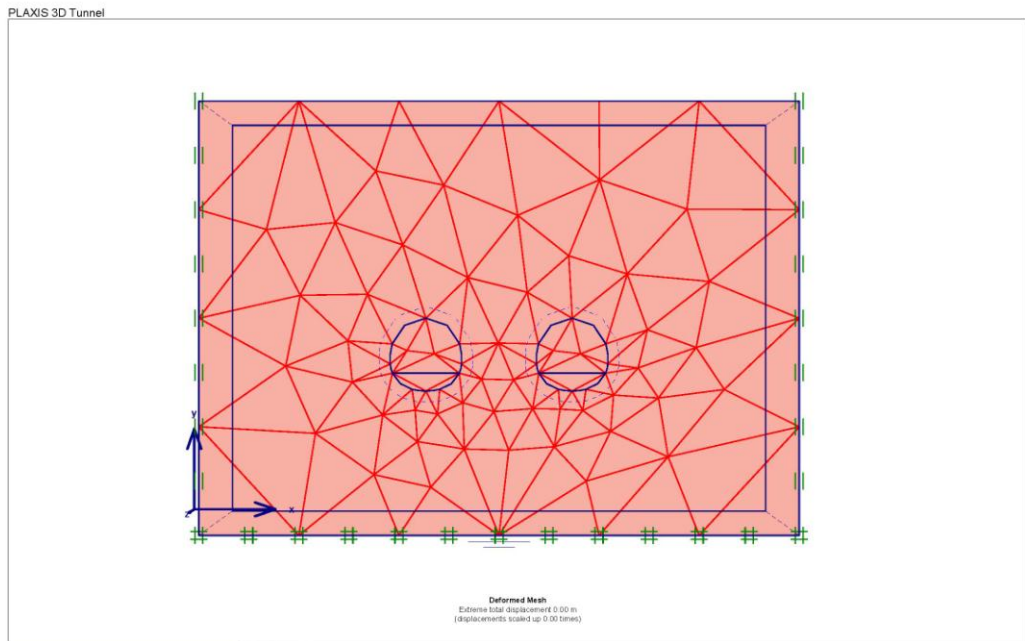


Figure 3.8 Generated mesh on 2D

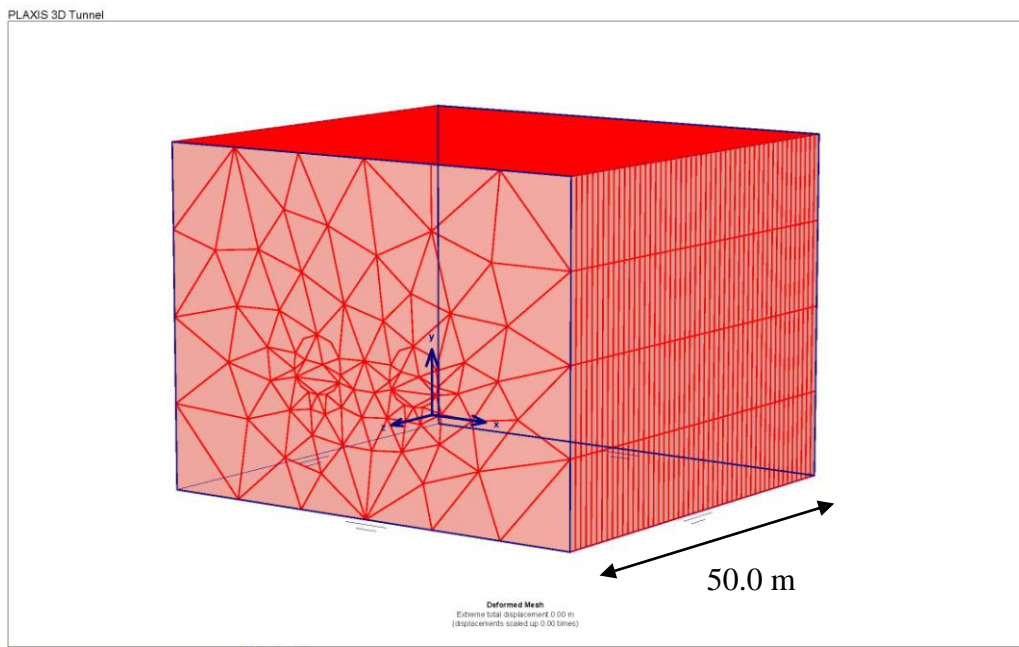


Figure 3.9 Generated mesh on 3D

3.3 Modeling Parameters

3.3.1 Soil Parameters

Mechanical properties of soil elements were defined by using hardening soil model. Hardening soil model requires basically five input parameters as, elastic modulus (E), Poisson's ratio (ν), friction angle (ϕ), cohesion (c) and dilatancy angle (ψ), as mentioned in previous parts. The parametric study was carried out for different values of elastic modulus. Another variable parameter used in the analyses is the modulus of elasticity of soil. Five different values of stiffness of the soil are used as, 25 MPa, 50 MPa, 75 MPa, 100 MPa and 500 MPa. While the modulus of elasticity of soil is changed, other geomechanical properties of the soil, such as cohesion, internal angle of friction, Poisson's ratio and dilatancy angle are all kept constant during the parametric analyses. The parameters used in this study are presented in Table 3.3. The dilatancy angle of the soil is taken as zero and interface elements are used between soil and lining elements in order to model the interaction between the structure and soil. A strength reduction factor, (R_{inter}), is defined which relates the interface strength to the soil strength in the order of 2/3 of the soil strength as recommended in the Plaxis User's Manual.

Table 3.3 Material properties of soil

Parameter	Symbol	Soil	Unit
Type of Material Behaviour		Drained	-
Unit Weight	γ	22	kN/m ³
Poisson's Ratio	ν	0.30	-
Cohesion	c'	10	kN/m ²
Internal Friction Angle	ϕ	33	°
Elastic modulus	E	variable	kN/m ²
Dilatancy Angle	ψ	0	°
Strength Reduction Factor	R_{inter}	0.622	-

3.3.2 Lining Parameters

The lining material of the tunnel is modeled as shotcrete material. Plate elements are used in order to model the shotcrete. Linear elastic material model is used in the analyses which requires the elastic modulus, (E), and Poisson's ratio, (ν), of the shotcrete. Two types of shotcrete material is defined to the program as soft shotcrete and hardened shotcrete. The use of these materials will be explained in proceeding chapter in detail. The main difference between the soft shotcrete and the hardened shotcrete is the stiffness of the material. The stiffness of the materials are calculated by using the formulas given below by American Concrete Institute (ACI) Code and Turkish Standard TS500 Code, respectively.

$$E_c = 4700\sqrt{f_c} \text{ (MPa)} \dots\dots\dots(3.1)$$

$$E_c = 3250\sqrt{f_{ck}} + 14000 \text{ (MPa)} \dots\dots\dots(3.2)$$

The material properties of the soft shotcrete and hardened shotcrete are given below in Table 3.4.

Table 3.4 Material properties of shotcrete

Parameter	Symbol	Soft Shotcrete	Hardened Shotcrete	Unit
Type of Material Behaviour		Elastic	Elastic	-
Thickness	t	20	20	cm
Unit Weight	γ	24	24	kN/m ³
Elastic modulus	E	10 000 000	28 500 000	kN/m ²
Poisson's ratio	ν	0.20	0.20	-

3.4 Construction Procedure

As mentioned in the previous chapters, the slices in z direction was created at every 1 meter and total length of the model along z direction is 50 meters. The excavation of the tunnel is executed in two parts as crown and invert excavation. The advancement of the tunnel is assumed as 1 meter both for the crown and invert. The lagged distance between the excavation of crown and invert is 4 meters and kept constant during the construction process.

Staged construction with $\Sigma M_{\text{stage}} < 1.0$ option is used in the construction stages at which excavation takes place. This option is used in order to simulate the relaxation behaviour of the soil before the installation of shotcrete. This ΣM_{stage} value is selected as 0.50 and kept constant for all construction phases performed in the analyses.

After the excavation stage, firstly, the soft shotcrete is activated around the excavated parts. Then, in the proceeding construction stage the material type of the previously activated plates are changed with hardened shotcrete. Also, in the same construction stage the excavation of the next slices is performed. This continuous construction process is repeated until the construction of the first tunnel (left-hand side) is completed. The construction procedure of the second tunnel (right-hand side) is the same as for the first tunnel. The excavation and activation of the shotcrete of the crown and invert performed simultaneously for the slices which is located four meters apart from each other. This type of a construction procedure is used in order to decrease the calculation time. The typical construction stage procedure is given in Figure 3.10.

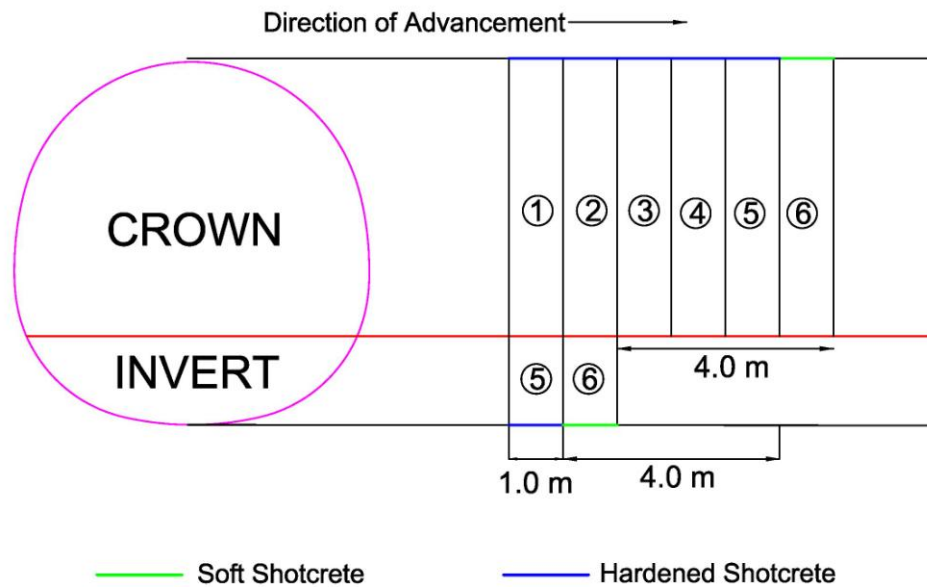












Figure 3.10 Typical construction stage procedure

3.5 Analysis Details

The main objective of the study is to determine the effects of construction of a new tunnel next to an existing one on the previously constructed tunnel, as mentioned before. Pillar width and the soil stiffness are the two variables which are changed during the parametric analyses. Table 3.5 shows the variables used in the analyses. As shown in Table 3.5, only one set of an analysis is performed for the maximum and minimum values of soil stiffness, since these extreme cases show more different behaviour when it is compared with other results. On the other hand, four different pillar width values are analyzed for the intermediate value of soil stiffness (75 MPa) since it is more representative.

Table 3.5 Variables of the parametric study

		MODULUS OF ELASTICITY OF SOIL (MPa)				
		25	50	75	100	500
PILLAR WIDTH	0.5D					
	1.0D					
	1.5D					
	2.0D					

After the analyses were completed displacements and sectional forces (bending moment and shear force) are examined in six different part of the mid-length cross-section of the previously constructed (left-hand side) tunnel. These six locations are shown in Figure 3.11. Typical displacement, bending moment and shear force diagrams are given in Figure 3.11, Figure 3.12 and Figure 3.13, respectively. Each of these regions are named as from 1 to 6 are investigated as the second tunnel (right-hand side) advances in the direction of the first tunnel which has already been constructed. The data to determine the behaviour of the sectional forces (bending moment and shear force) and displacement are collected at construction stages in which the advancement of the second tunnel is equal to 0 meter, 10 meters, 20 meters, 25 meters, 30 meters, 40 meters and finally 50 meters. 0 meter of advancement means that the construction of the second tunnel has not started yet; on the other hand, 50 meters of advancement means that the construction of the second tunnel is completed. Figure 3.14 shows the top view of the construction stages relative to the mid-length cross section at which the data is collected.

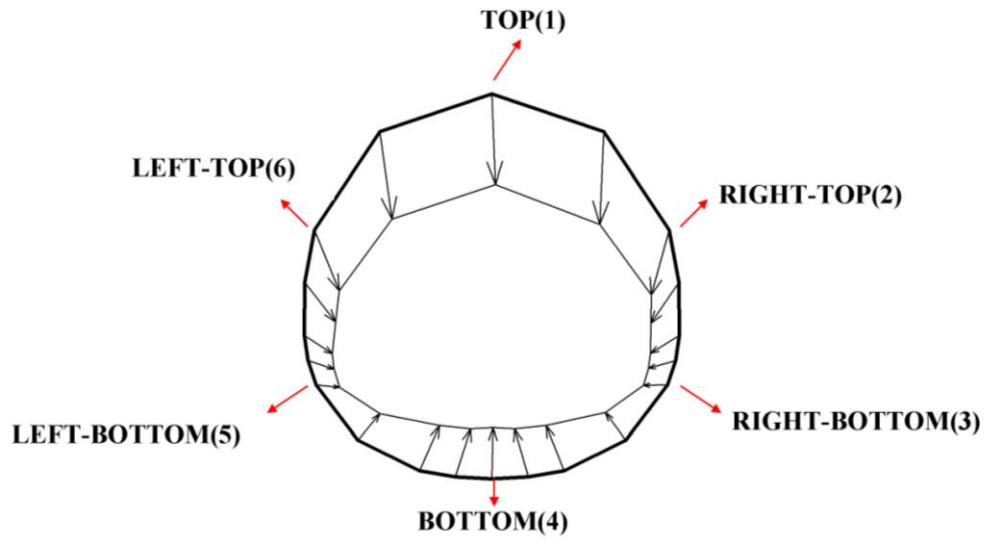


Figure 3.11 Typical displacement diagram

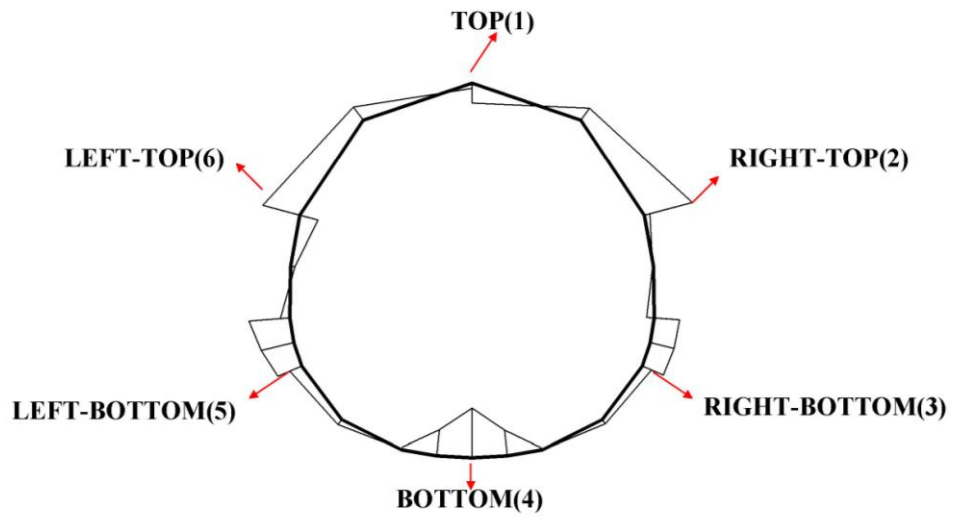


Figure 3.12 Typical bending moment diagram

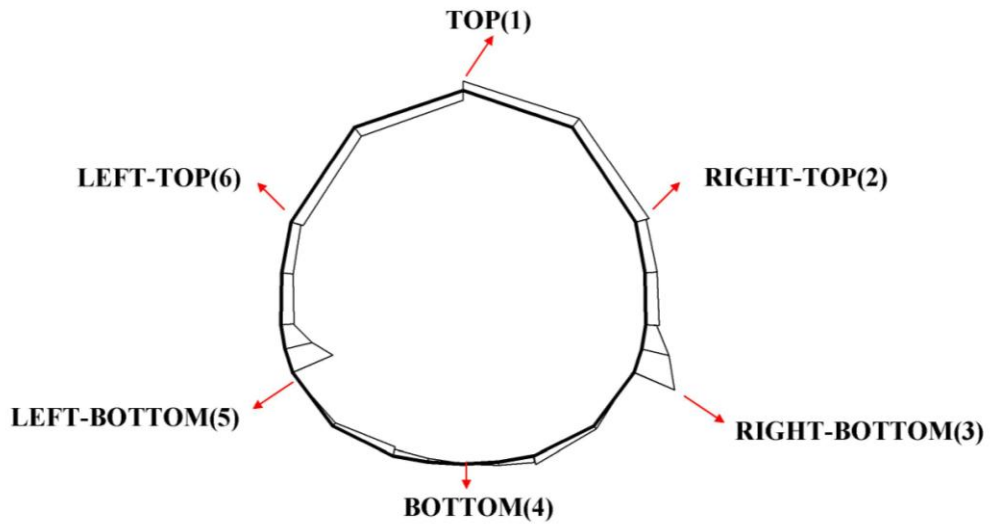


Figure 3.13 Typical shear force diagram

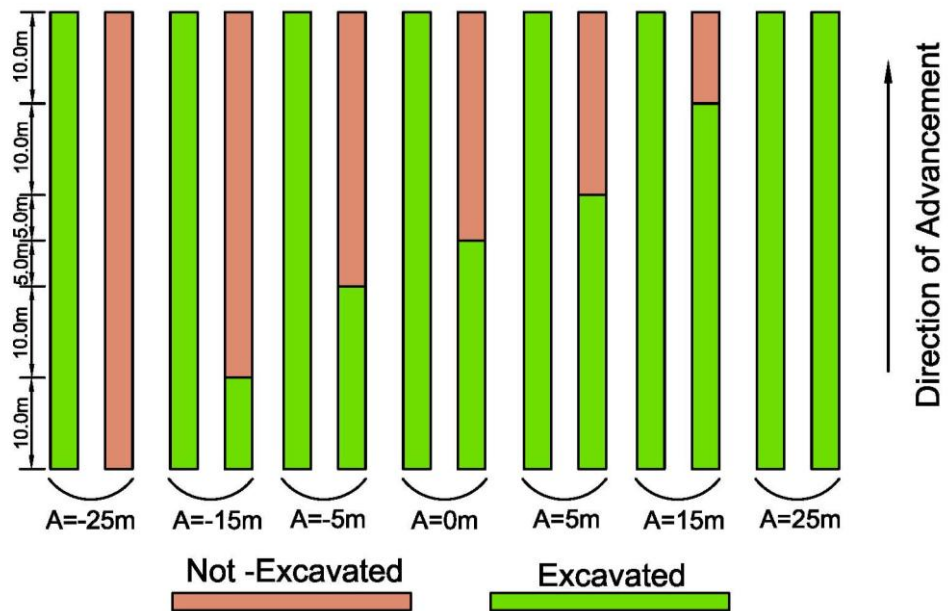


Figure 3.14 Construction stages at which data is collected

CHAPTER 4

DISCUSSION OF THE RESULTS

The results of the parametric study and evaluation of the results are presented in this chapter. The effect of the changing variables on the behaviour of displacement, bending moment and shear force are also discussed. The results of the analyses are classified in three main groups as behaviour of displacement, bending moment and shear force. These three main groups are evaluated in sub-groups according to the place of interest as mentioned in the previous chapters.

4.1 Behaviour of Displacements

The behaviour of the displacement as the second tunnel advances is given in this part. The behaviour of the displacement is evaluated in six different location of the mid-length cross-section of the previously constructed tunnel as top (1), right-top (2), right-bottom (3), bottom (4), left bottom (5) and left-top (6). The results presented below are given only for representing the typical behaviour. The rest of the results are given in related appendices.

4.1.1 Behaviour of Displacement at 1

Analysis results show that the displacement at the top side of the tunnel tends to increase as the advancement level of the second tunnel increases. The increase in displacement is determined both for the different soil stiffness

values and different pillar width values. As it is expected, displacement values are larger when the modulus of elasticity of soil is smaller for the same pillar width. The behaviour of the displacement at the top side of the tunnel is evaluated in terms of both the displacement values and percent change in these values. Figure 4.1 and Figure 4.2 show the typical displacement behaviour of the top side of the tunnel for the same pillar width.

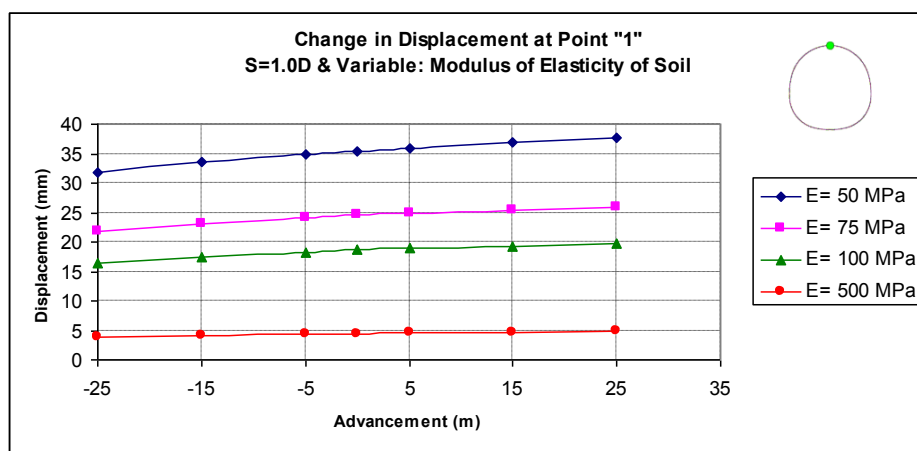


Figure 4.1 Displacement values at the top side of the tunnel

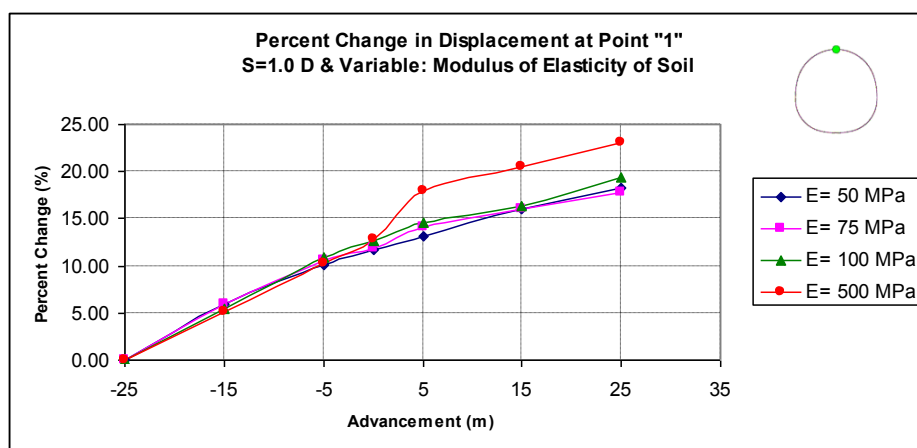


Figure 4.2 Percent change in displacement at the top side of the tunnel

Another set of analyses is performed by keeping constant the modulus of elasticity of soil and changing the pillar width. Analysis results show that the displacement at the top side of the tunnel tends to increase as the second tunnel advances for all pillar width values. Displacement values are larger when the pillar width is smaller for the same elastic modulus. Figure 4.3 and Figure 4.4 show the typical displacement behaviour of the top side of the tunnel for the same soil stiffness.

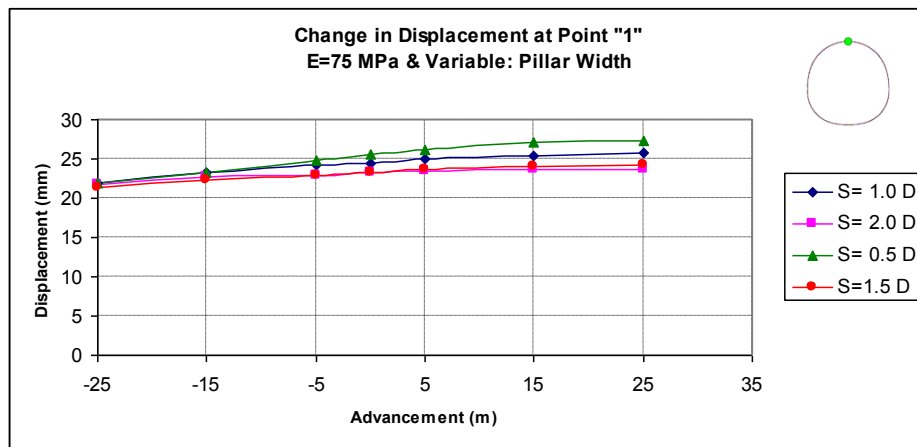


Figure 4.3 Displacement values at the top side of the tunnel

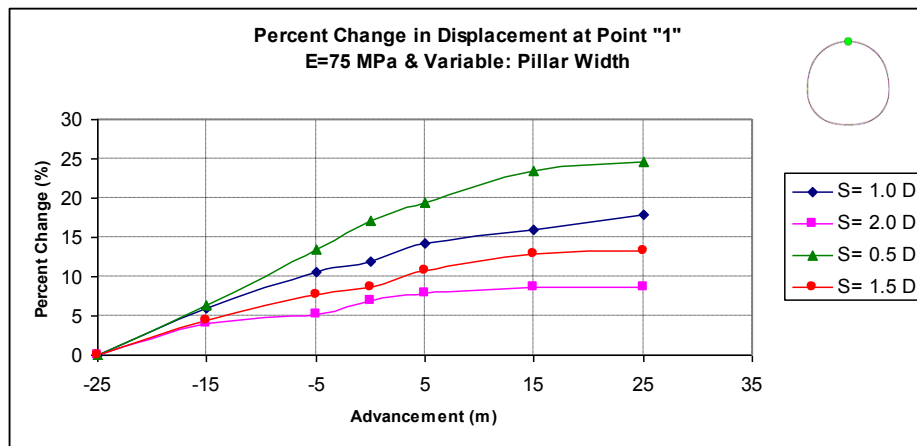


Figure 4.4 Percent change in displacement at the top side of the tunnel

Figure 4.4 shows that the rate of increase in displacement values decreases as the advancement of the second tunnel increases for the same soil stiffness. Figure 4.2 shows that the amount of increase in displacement at the top side of the tunnel is independent from the modulus of elasticity of soil and the increase is in the order of 20% for the pillar width is equal to the 1 diameter of the tunnel. The percent change in displacement at the top side of the tunnel reduces to approximately 10% for the pillar width is equal to the 2 times of the tunnel diameter. The percent increase in displacement at the top side of the tunnel is approximately 25% and 15% for the pillar width values of 0.5D and 1.5D, respectively. Figure 4.5 shows the change in percent increase for different pillar width values mentioned above. As shown in Figure 4.5 the increase in displacement at the top side of the tunnel decreases linearly as the pillar width increases. It may be concluded that the amount of percent increase and the pillar width are inversely proportional with each other.

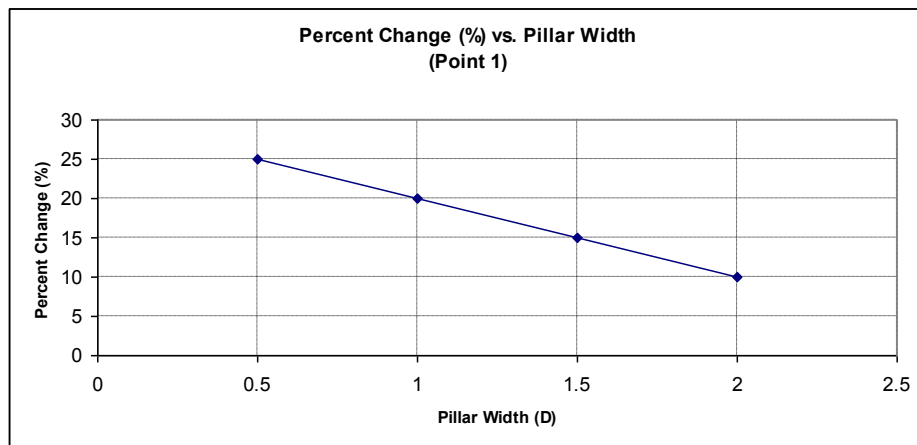


Figure 4.5 Change in percent increase for different pillar width values

4.1.2 Behaviour of Displacement at 2

Analysis results show that the displacement at the right-top side of the tunnel tends to increase as the advancement level of the second tunnel increases. The increase in displacement is determined both for the different soil stiffness values and different pillar width values. As it is expected, displacement values are larger when the modulus of elasticity of soil is smaller for the same pillar width. The behaviour of the displacement at the right-top side of the tunnel is evaluated in terms of both the displacement values and percent change in these values. Figure 4.6 and Figure 4.7 show the typical displacement behaviour of the right-top side of the tunnel for the same pillar width.

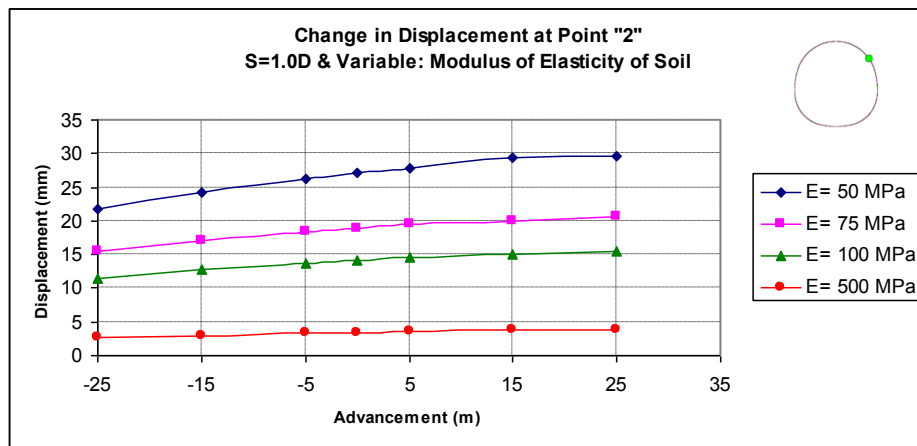


Figure 4.6 Displacement values at the right-top side of the tunnel

Another set of analyses is performed by keeping the modulus of elasticity of soil constant and changing the pillar width. Analysis results show that the displacement at the right-top side of the tunnel tends to increase as the second tunnel advances for all pillar width values. Displacement values are larger when the pillar width is smaller for the same elastic modulus. Figure 4.8 and

Figure 4.9 show the typical displacement behaviour of the right-top side of the tunnel for the same soil stiffness.

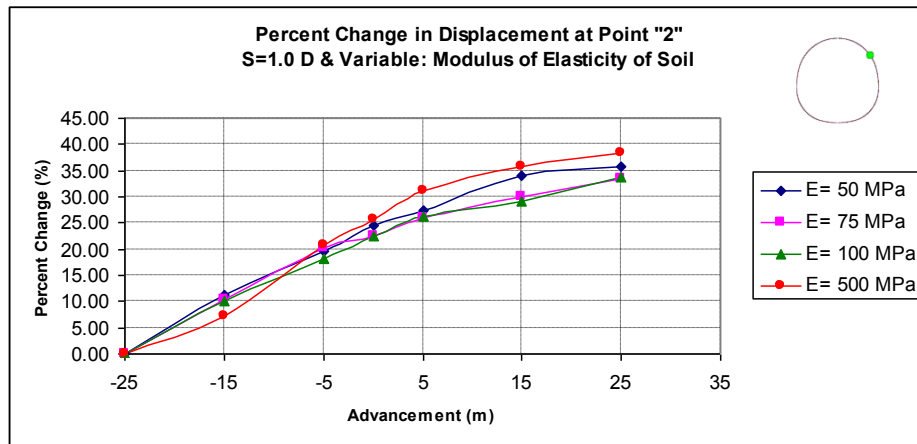


Figure 4.7 Percent change in displacement at the right-top side of the tunnel

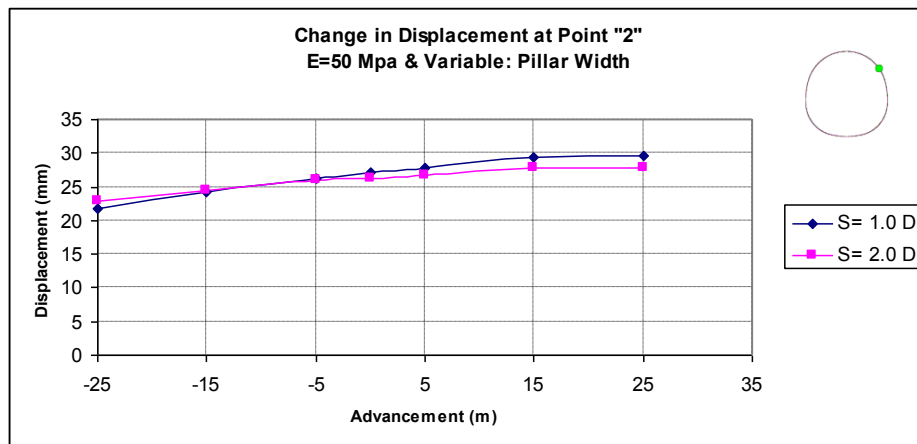


Figure 4.8 Displacement values at the right-top side of the tunnel

Figure 4.9 shows that the rate of increase in displacement values decreases as the advancement of the second tunnel increases for the same soil stiffness. Figure 4.7 shows that the amount of increase in displacement at the right-top side of the tunnel is independent from the modulus of elasticity of soil and the

increase is in the order of 35% for the pillar width is equal to the 1 diameter of the tunnel. The percent change in displacement at the right-top side of the tunnel reduces to approximately 20% for the pillar width is equal to the 2 times of the tunnel diameter. The percent increase in displacement at the right-top side of the tunnel is approximately 35% and 25% for the pillar width values of 0.5D and 1.5D, respectively. Figure 4.10 shows the change in percent increase for different pillar width values mentioned above. As shown in Figure 4.10 the increase in displacement at the right-top side of the tunnel is nearly constant for the pillar width values smaller than 1.0D and decreases linearly as the pillar width increases.

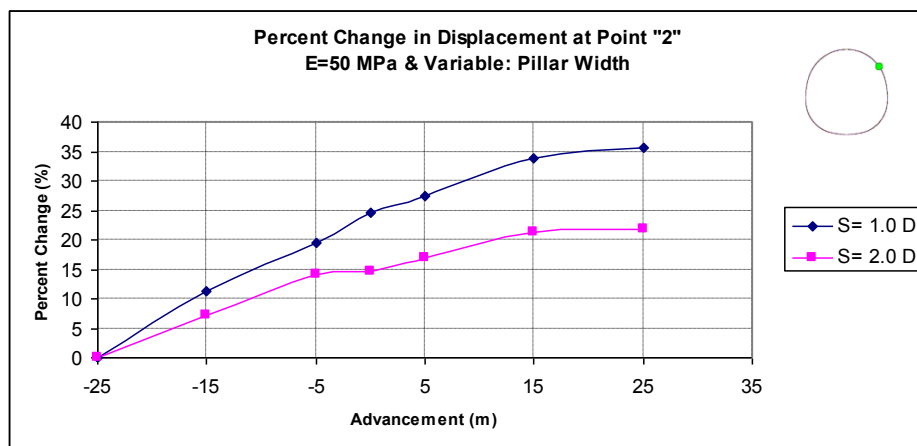


Figure 4.9 Percent change in displacement at the right-top side of the tunnel

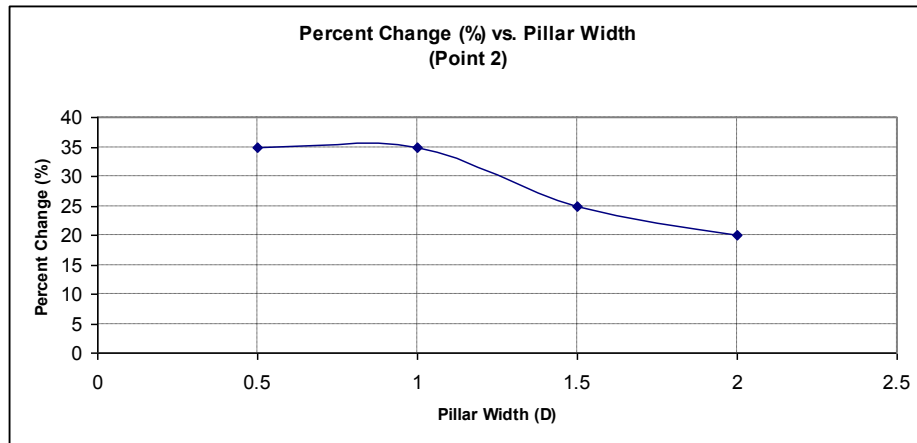


Figure 4.10 Change in percent increase for different pillar width values

4.1.3 Behaviour of Displacement at 3

Analysis results show that the displacement at the right-bottom side of the tunnel tends to increase as the advancement level of the second tunnel increases. The increase in displacement is determined both for the different soil stiffness values and different pillar width values. As it is expected, displacement values are larger when the modulus of elasticity of soil is smaller for the same pillar width. The behaviour of the displacement at the right-bottom side of the tunnel is evaluated in terms of both the displacement values and percent change in these values. Figure 4.11 and Figure 4.12 show the typical displacement behaviour of the right-bottom side of the tunnel for the same pillar width.

Another set of analyses is performed by keeping the modulus of elasticity of soil constant and changing the pillar width. Analysis results show that the displacement at the right-bottom side of the tunnel tends to increase as the second tunnel advances for all pillar width values. Displacement values are larger when the pillar width is smaller for the same elastic modulus. Figure

4.13 and Figure 4.14 show the typical displacement behaviour of the right-bottom side of the tunnel for the same soil stiffness.

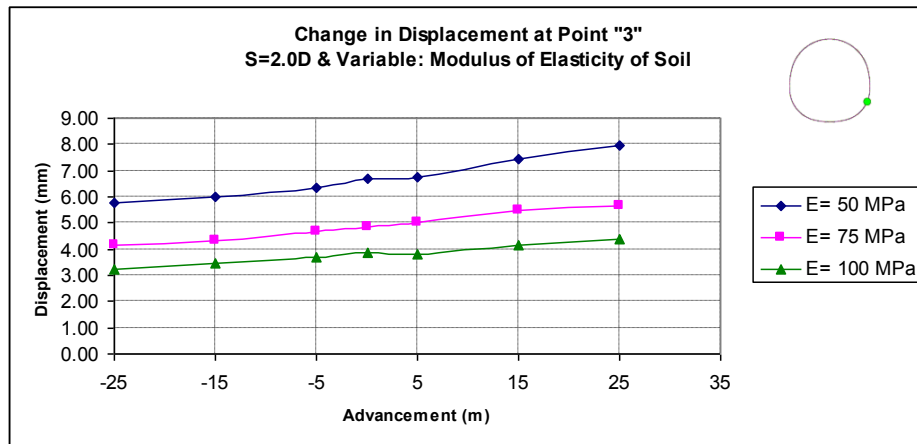


Figure 4.11 Displacement values at the right-bottom side of the tunnel

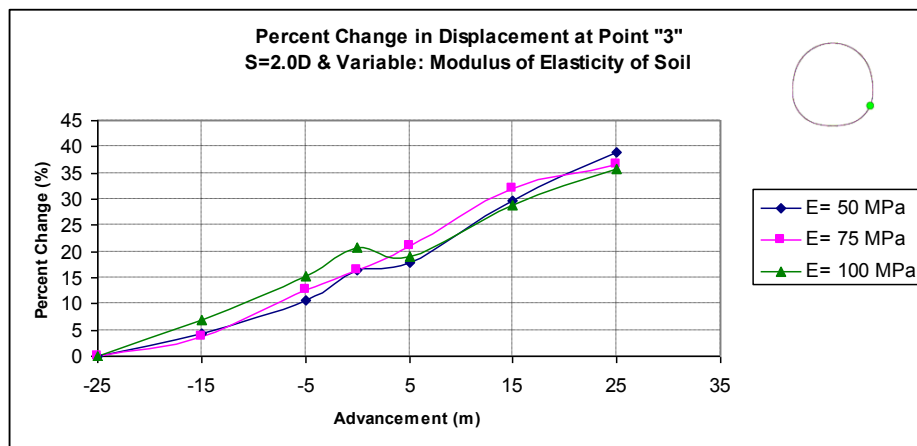


Figure 4.12 Percent change in displacement at the right-bottom side of the tunnel

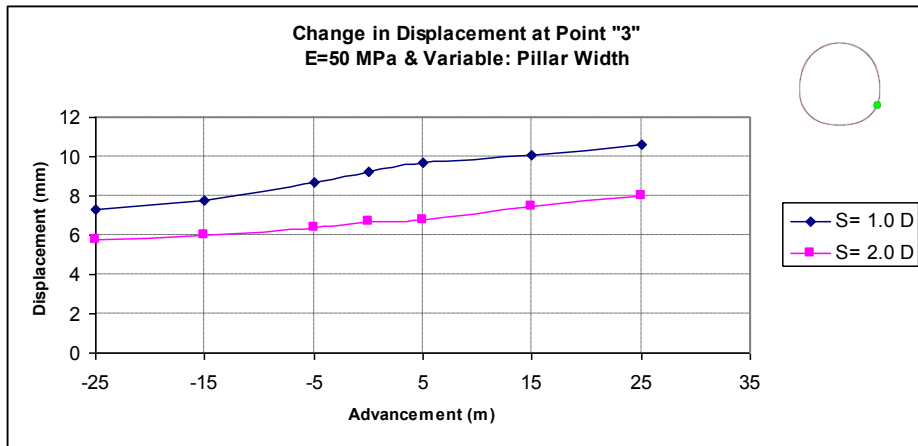


Figure 4.13 Displacement values at the right-bottom side of the tunnel

Figure 4.14 shows that the rate of increase in displacement is nearly constant for the same soil stiffness. In opposition to the results obtained for top and right-top of the tunnel, it is not possible to obtain a direct relationship between the percent increase and pillar width for the case of right-bottom. This situation may be arisen since, the displacement values are very small and small changes on these values result in large percent changes.

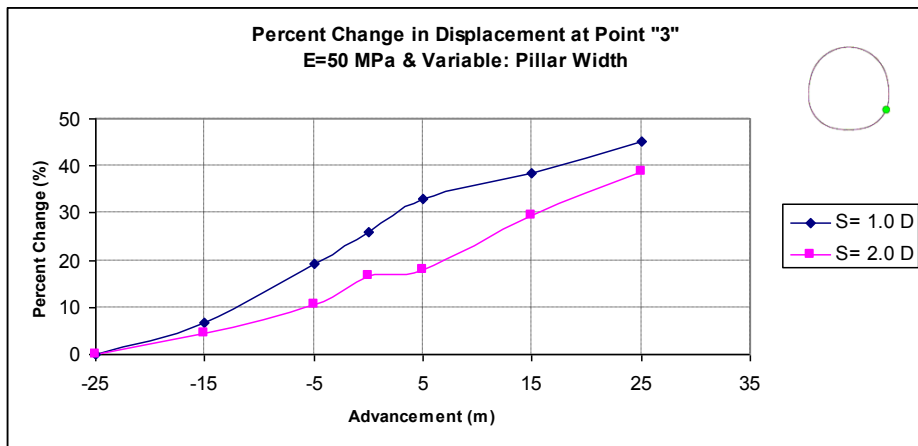


Figure 4.14 Percent change in displacement at the right-bottom side of the tunnel

4.1.4 Behaviour of Displacement at 4

Analysis results show that the displacement at the bottom side of the tunnel tends to decrease as the advancement level of the second tunnel increases. The decrease in displacement is determined both for the different soil stiffness values and different pillar width values. As it is expected, displacement values are larger when the modulus of elasticity of soil is smaller for the same pillar width. The behaviour of the displacement at the bottom side of the tunnel is evaluated in terms of both the displacement values and percent change in these values. Figure 4.15 and Figure 4.16 show the typical displacement behaviour of the bottom side of the tunnel for the same pillar width.

Another set of analyses is performed by keeping the modulus of elasticity of soil constant and changing the pillar width. Analysis results show that the displacement at the bottom side of the tunnel tends to decrease as the second tunnel advances for all pillar width values. Displacement values are smaller when the pillar width is smaller for the same elastic modulus, since the amount of decrease is larger than in higher pillar width values. Figure 4.17 and Figure 4.18 show the typical displacement behaviour of the bottom side of the tunnel for the same soil stiffness.

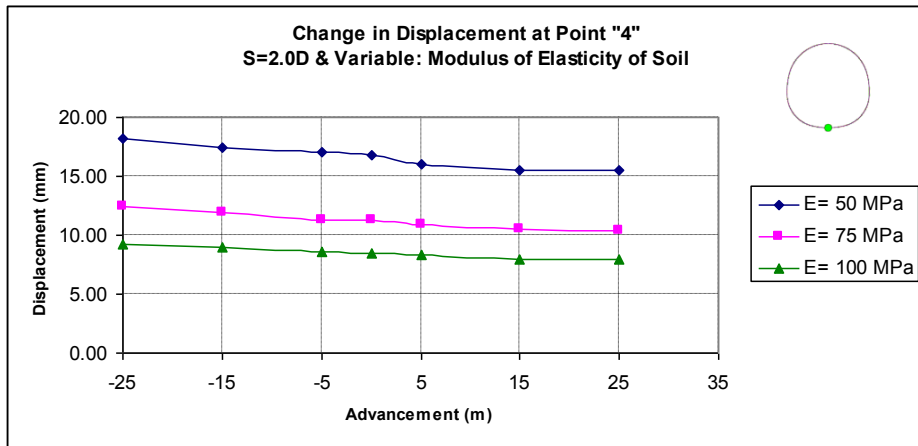


Figure 4.15 Displacement values at the bottom side of the tunnel

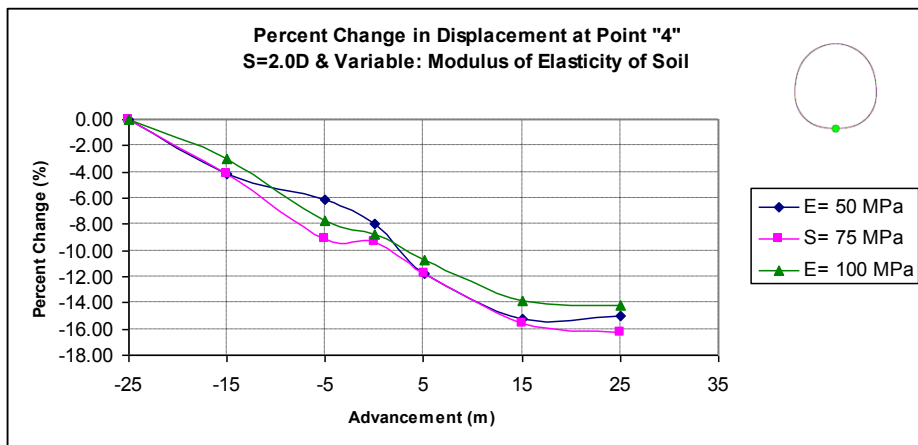


Figure 4.16 Percent change in displacement at the bottom side of the tunnel

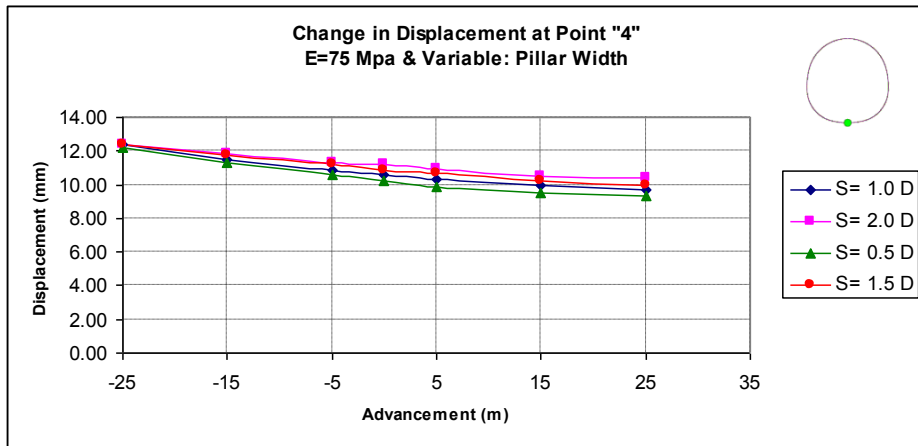


Figure 4.17 Displacement values at the bottom side of the tunnel

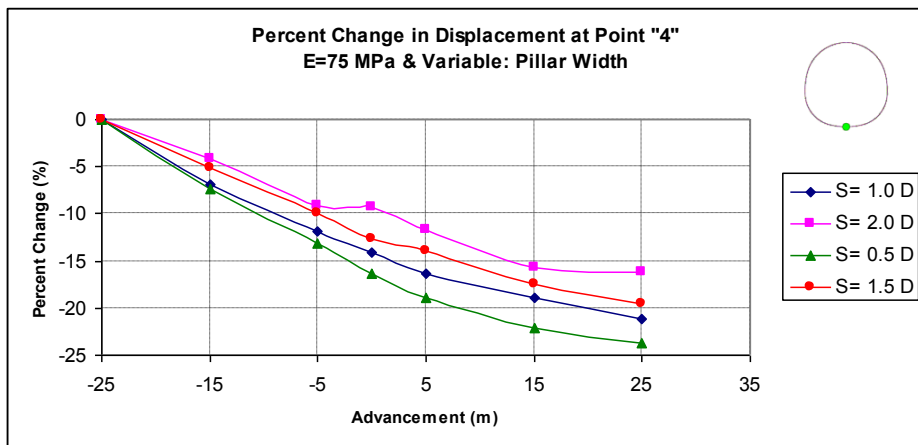


Figure 4.18 Percent change in displacement at the bottom side of the tunnel

Figure 4.18 shows that the rate of decrease in displacement values decreases as the advancement of the second tunnel increases for the same soil stiffness. Figure 4.16 shows that the amount of decrease in displacement at the bottom side of the tunnel is independent from the modulus of elasticity of soil and the decrease is in the order of 15% for the pillar width is equal to the 2 times of the diameter of the tunnel. The percent change in displacement at the bottom side

of the tunnel increases to approximately 22.5% for the pillar width is equal to the 1 tunnel diameter. The percent decrease in displacement at the bottom side of the tunnel is approximately 23.8% and 21.2% for the pillar width values of 0.5D and 1.5D, respectively. Figure 4.19 shows the change in percent decrease for different pillar width values mentioned above. As shown in Figure 4.19 the decrease in displacement at the bottom side of the tunnel is nearly linearly changing with increasing pillar width but after the point at which pillar width is 1.5D the rate of increase sharply increases. This graph may be used as an extrapolation of larger pillar width values in such a way that the effect of the second tunnel decreases greatly with increasing pillar width values of small intervals.

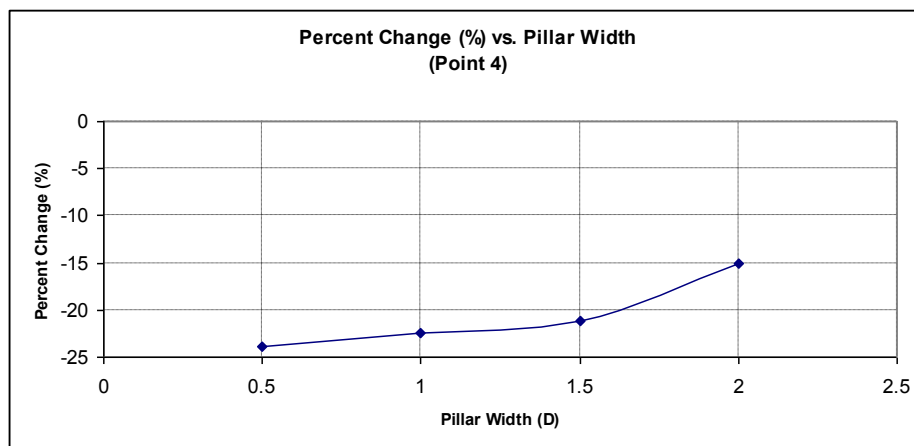


Figure 4.19 Change in percent increase for different pillar width values

4.1.5 Behaviour of Displacement at 5

Analysis results show that the displacement at the left-bottom side of the tunnel tends to decrease as the advancement level of the second tunnel increases. The decrease in displacement is determined both for the different soil stiffness values and different pillar width values. As it is expected, displacement values

are larger when the modulus of elasticity of soil is smaller for the same pillar width. The behaviour of the displacement at the left-bottom side of the tunnel is evaluated in terms of both the displacement values and percent change in these values. Figure 4.20 and Figure 4.21 show the typical displacement behaviour of the left-bottom side of the tunnel for the same pillar width.

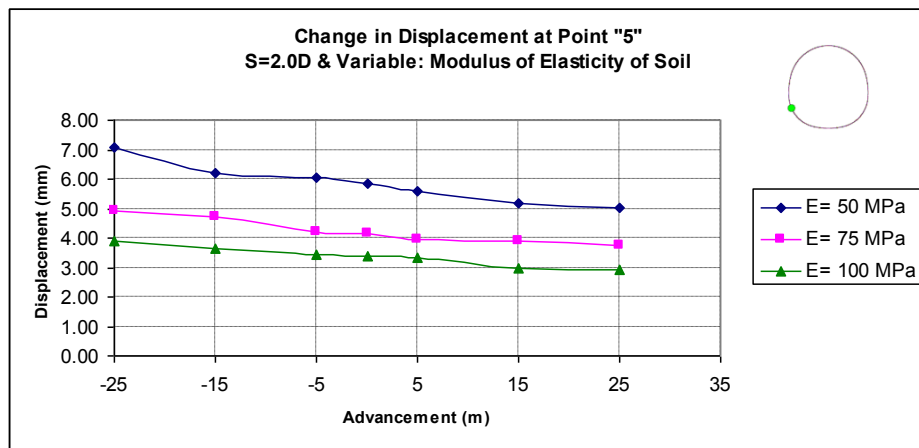


Figure 4.20 Displacement values at the left-bottom side of the tunnel

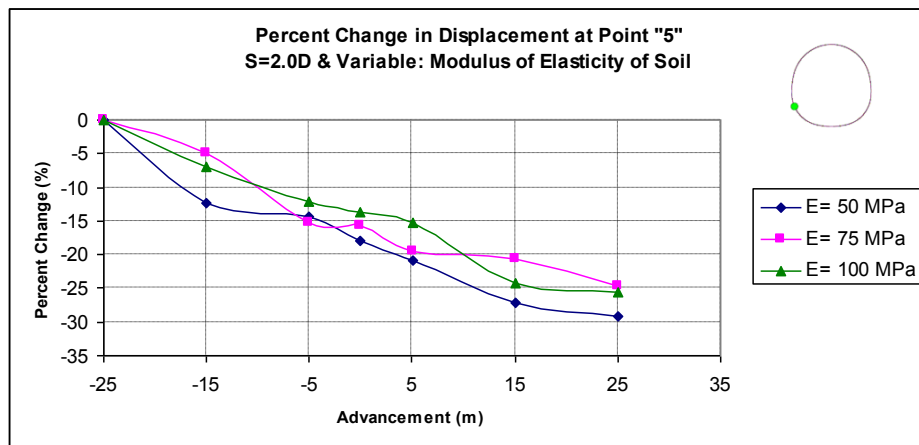


Figure 4.21 Percent change in displacement at the left-bottom side of the tunnel

Another set of analyses is performed by keeping the modulus of elasticity of soil constant and changing the pillar width. Analysis results show that the displacement at the left-bottom side of the tunnel tends to decrease as the second tunnel advances for all pillar width values. Displacement values are smaller when the pillar width is smaller for the same elastic modulus, since the amount of decrease is larger than in higher pillar width values. Figure 4.22 and Figure 4.23 show the typical displacement behaviour of the left-bottom side of the tunnel for the same soil stiffness.

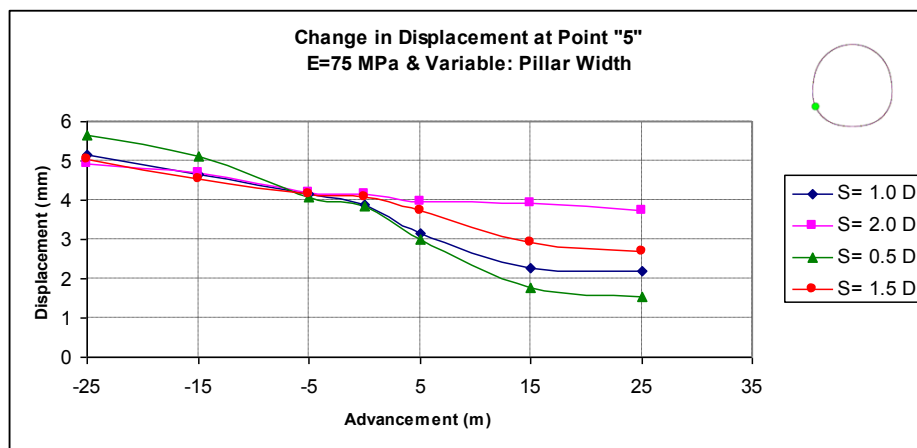


Figure 4.22 Displacement values at the left-bottom side of the tunnel

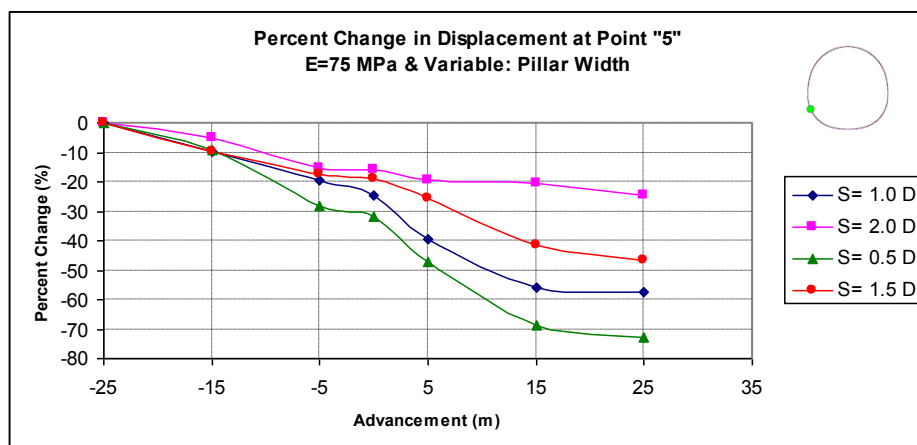


Figure 4.23 Percent change in displacement at the left-bottom side of the tunnel

Figure 4.23 shows that the rate of decrease in displacement becomes nearly zero after the passage of the second tunnel for the same soil stiffness. As it is mentioned above for the right-bottom displacement values of the tunnel, it is not possible to obtain a direct relationship between the percent increase and pillar width for the case of left-bottom, also. This situation may be arisen since, the displacement values are very small and small changes on these values result in large percent changes.

4.1.6 Behaviour of Displacement at 6

Analysis results show that the displacement at the left-top side of the tunnel is nearly same as the advancement level of the second tunnel increases. As it is expected, displacement values are larger when the modulus of elasticity of soil is smaller for the same pillar width. On the other hand, left top side of the tunnel is the location at which the effect of second tunnel is minimum. The change in displacement is nearly zero. A very slight increase in displacement is determined in the order of 5% and this increase level is independent from the soil stiffness. The behaviour of the displacement at the left-top side of the tunnel is evaluated in terms of both the displacement values and percent change in these values. Figure 4.24 and Figure 4.25 show the typical displacement behaviour of the left-top side of the tunnel for the same pillar width.

Another set of analyses is performed by keeping the modulus of elasticity of soil constant and changing the pillar width. According to analysis results it is determined that the displacement at the left-top side of the tunnel is nearly same for all different pillar width values in case of same soil stiffness. A very slight increase in displacement is determined in the order of 5% independent from the pillar width. Figure 4.26 and Figure 4.27 show the typical

displacement behaviour of the left-bottom side of the tunnel for the same soil stiffness.

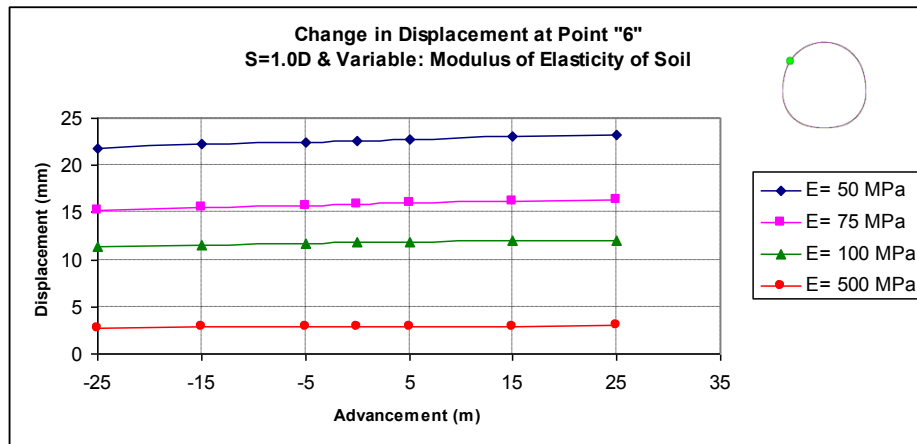


Figure 4.24 Displacement values at the left-top side of the tunnel

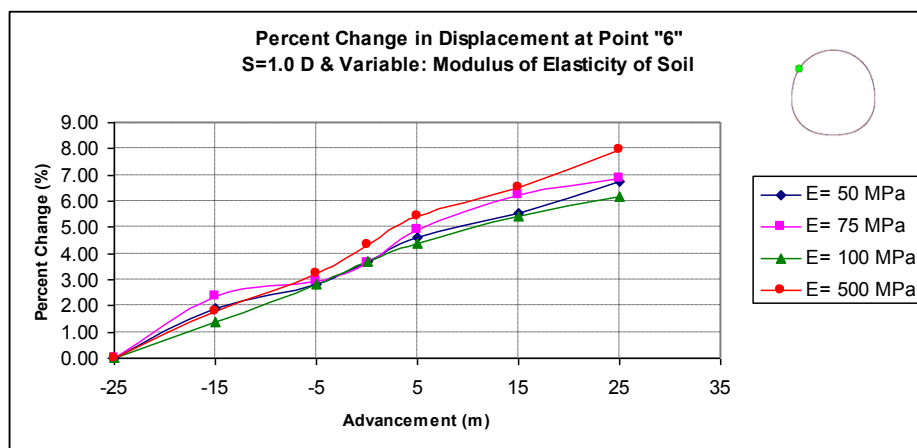


Figure 4.25 Percent change in displacement at the left-top side of the tunnel

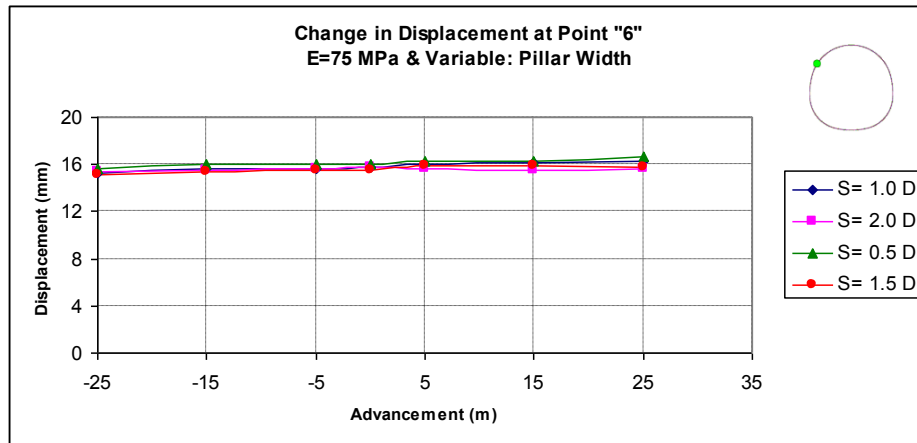


Figure 4.26 Displacement values at the left-top side of the tunnel

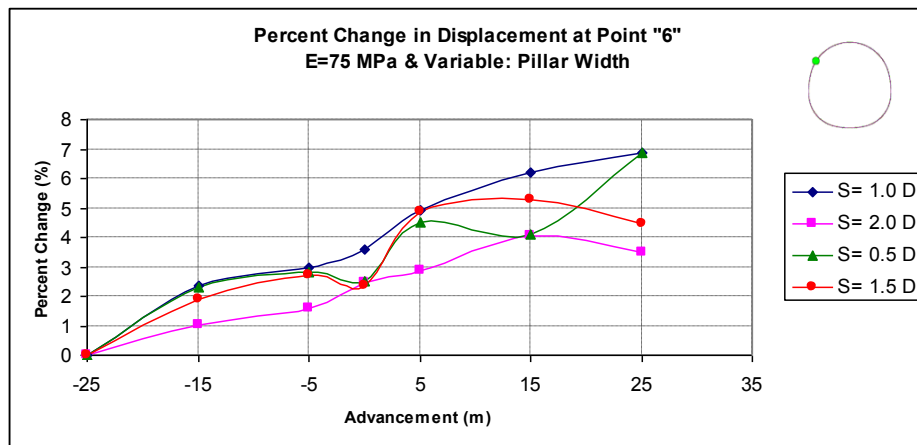


Figure 4.27 Percent change in displacement at the left-top side of the tunnel

4.2 Behaviour of Bending Moments

The behaviour of the bending moment as the second tunnel advances is given in this part. The behaviour of the bending moment is evaluated in six different location of the mid-length cross-section of the previously constructed tunnel as top (1), right-top (2), right-bottom (3), bottom (4), left bottom (5) and left-top

(6). The results presented below are given only for representing the typical behaviour. The rest of the results are given in related appendices.

4.2.1 Behaviour of Bending Moment at 1

Analysis results show that the bending moment at the top side of the tunnel tends to increase as the second tunnel advances. This increasing behaviour is valid for both different soil stiffnesses and different pillar width values. Bending moment values are larger when the modulus of elasticity of soil is smaller for the same pillar width. The behaviour of the bending moment at the top side of the tunnel is evaluated in terms of both the bending moment values and percent change in these values. Figure 4.28 and Figure 4.29 show the typical bending moment behaviour of the top side of the tunnel for the same pillar width.

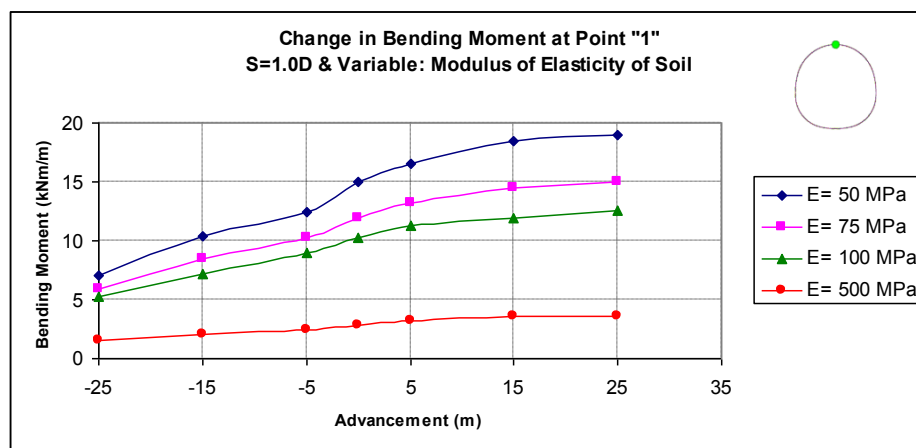


Figure 4.28 Bending moment values at the top side of the tunnel

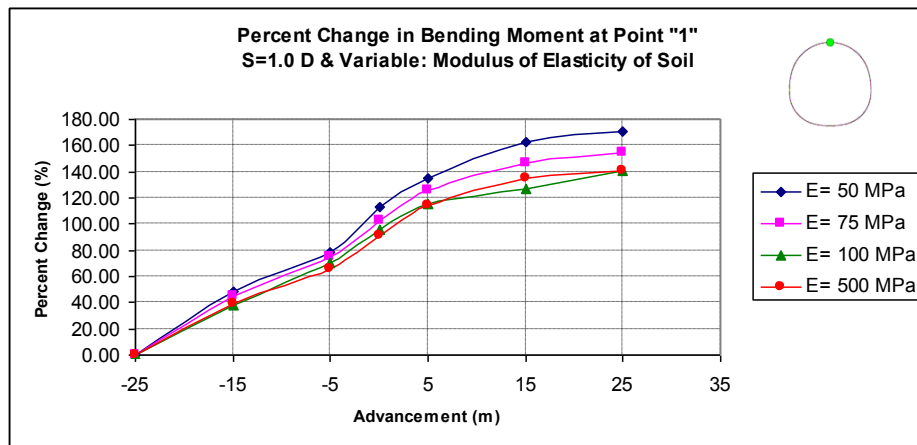


Figure 4.29 Percent change in bending moment at the top side of the tunnel

Another type of analyses is performed by keeping the modulus of elasticity of soil constant and changing the pillar width. According to analysis results, the bending moment at the top side of the tunnel tends to increase as the second tunnel advances for all pillar width values. Bending moment values are larger when the pillar width is smaller for the same elastic modulus. The increase in bending moment values is more evident when the spacing left between the tunnels is smaller than $1.5D$. Figure 4.30 and Figure 4.31 show the typical bending moment behaviour of the top side of the tunnel for the same soil stiffness.

Figure 4.31 shows that the rate of increase in bending moment values is low at the first half of the construction stages, especially for pillar width values greater than $1.0 D$, and the rate of increase is maximum when the second tunnel passes the mid-length section for the same soil stiffness. The rate of increase is again low as the advancement of the second tunnel is greater than 40 meters. Figure 4.29 shows that the percent increase in bending moment at the top side of the tunnel is nearly independent from the modulus of elasticity of soil and

the increase is in the order of 150% for the pillar width is equal to the 1 diameter of the tunnel. The percent change in bending moment at the top side of the tunnel reduces to approximately 40% for the pillar width is equal to the 2 times of the tunnel diameter. The percent increase in bending moment at the top side of the tunnel is approximately 280% and 65% for the pillar width values of 0.5D and 1.5D, respectively. Figure 4.32 shows the change in percent increase for different pillar width values mentioned above. As shown in Figure 4.32 the increase in bending moment at the top side of the tunnel increases dramatically when the pillar width is smaller than 1.5D. The amount of increase decreases to low values for pillar width greater than 1.5D.

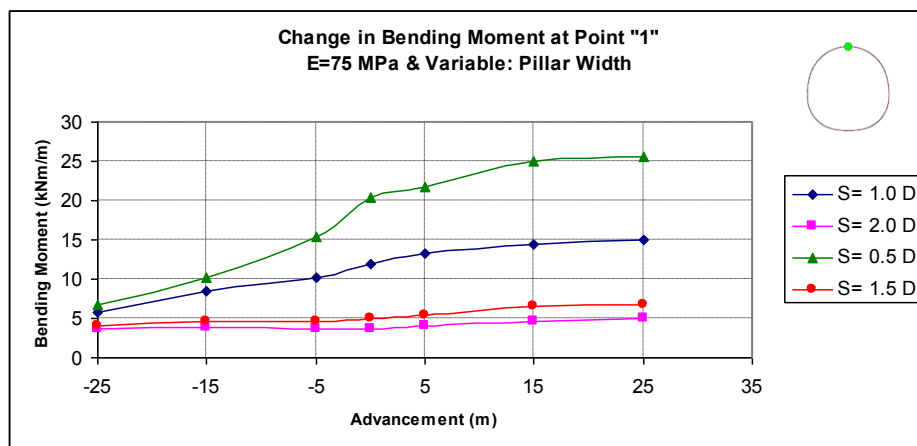


Figure 4.30 Bending moment values at the top side of the tunnel

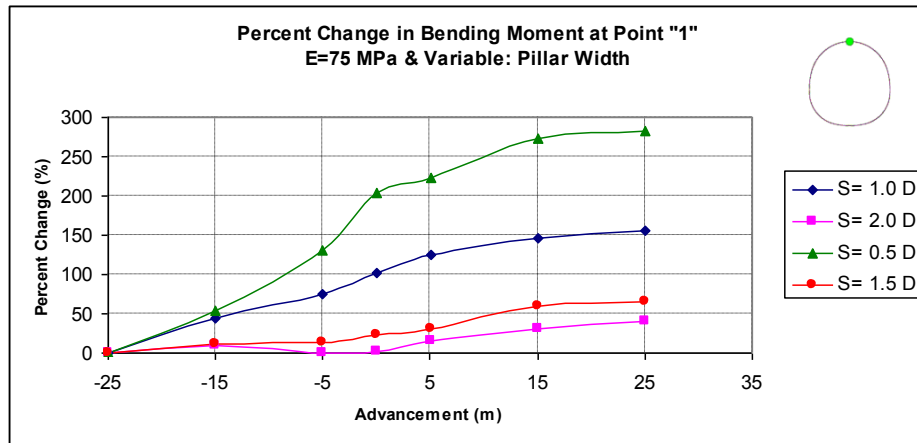


Figure 4.31 Percent change in bending moment at the top side of the tunnel

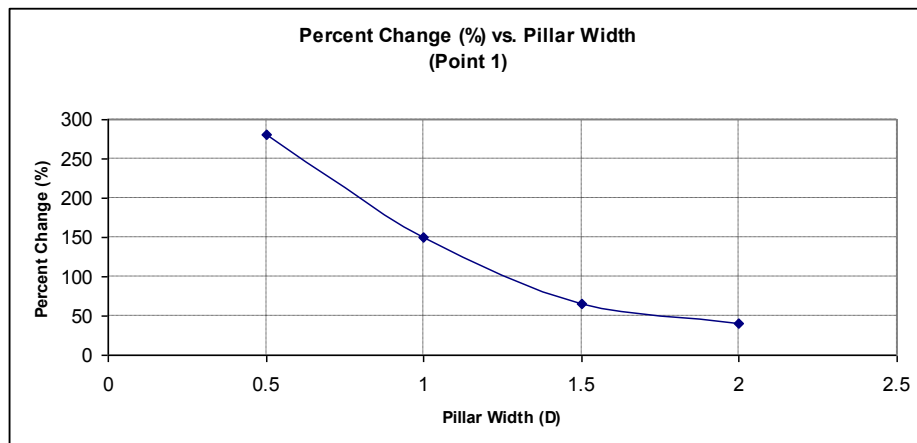


Figure 4.32 Change in percent increase for different pillar width values

4.2.2 Behaviour of Bending Moment at 2

Analysis results show that the bending moment at the right-top side of the tunnel strongly related with the spacing between the tunnels. Bending moment values tend to increase for spacings of 0.5D and 1.0D; on the other hand, bending moment values tend to decrease for spacings of 1.5D and 2.0D as the

second tunnel advances. Bending moment values are larger when the modulus of elasticity of soil is smaller for the same pillar width. The behaviour of the bending moment at the right-top side of the tunnel is evaluated in terms of both the bending moment values and percent change in these values. Figure 4.33 and Figure 4.34 show the typical bending moment behaviour of the right-top side of the tunnel for the same elastic modulus of soil.

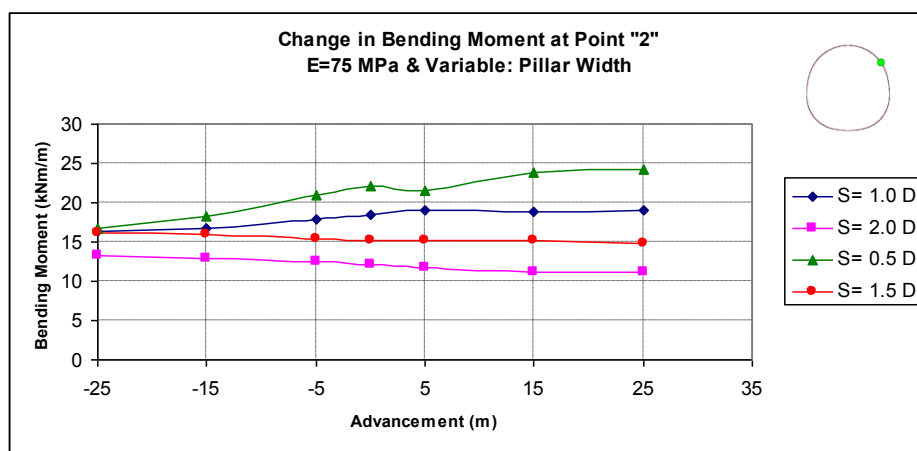


Figure 4.33 Bending moment values at the right-top side of the tunnel

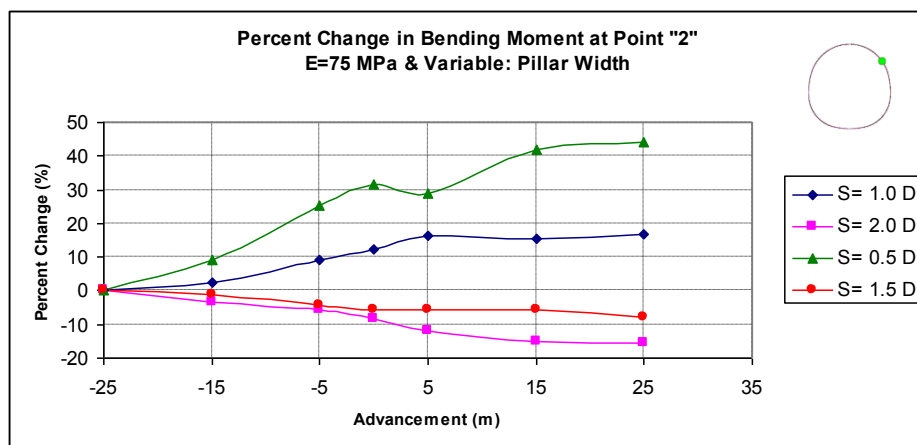


Figure 4.34 Percent change in bending moment at the right-top side of the tunnel

The data obtained from Figure 4.34 is used to determine the effect of pillar width on bending moment at the right-top side of the tunnel when the construction of second tunnel is completed. Figure 4.35 shows the percent change for different pillar width values of tunnel constructed in intermediate soil stiffness ($E=75$ MPa). As shown in Figure 4.35 the construction of the second tunnel does not affect the bending moment at the right-top side of the tunnel for an approximate spacing of $1.25D$.

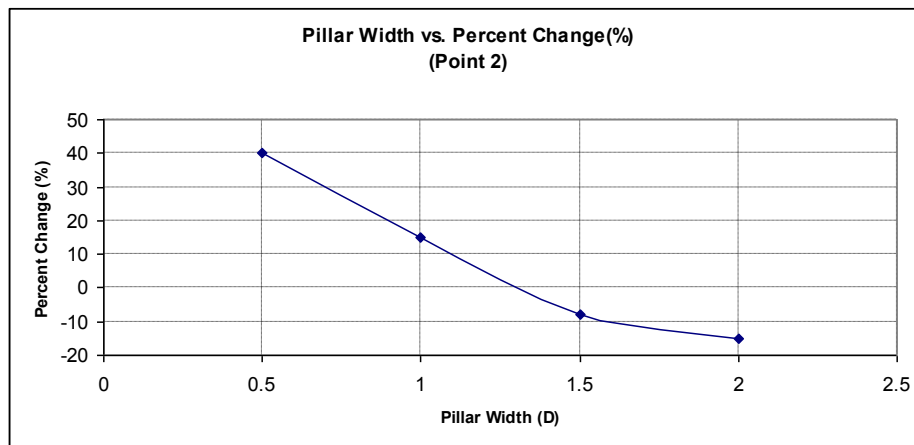


Figure 4.35 Change in percent increase for different pillar width values

4.2.3 Behaviour of Bending Moment at 3

Analysis results show that the bending moment at the right-bottom side of the tunnel tends to increase as the second tunnel advances. This increasing behaviour is valid for both different soil stiffnesses and different pillar width values. Bending moment values are larger when the modulus of elasticity of soil is smaller for the same pillar width. The behaviour of the bending moment at the right-bottom side of the tunnel is evaluated in terms of both the bending moment values and percent change in these values. Figure 4.36 and Figure 4.37

show the typical bending moment behaviour of the right-bottom side of the tunnel for the same pillar width.

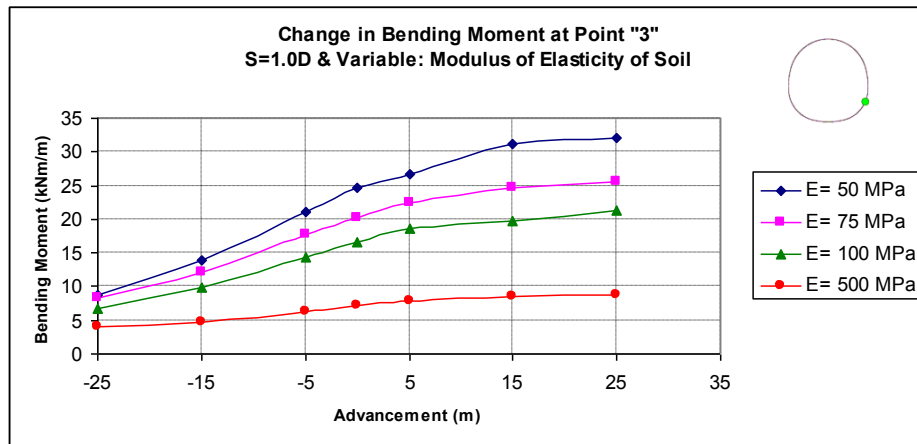


Figure 4.36 Bending moment values at the right-bottom side of the tunnel

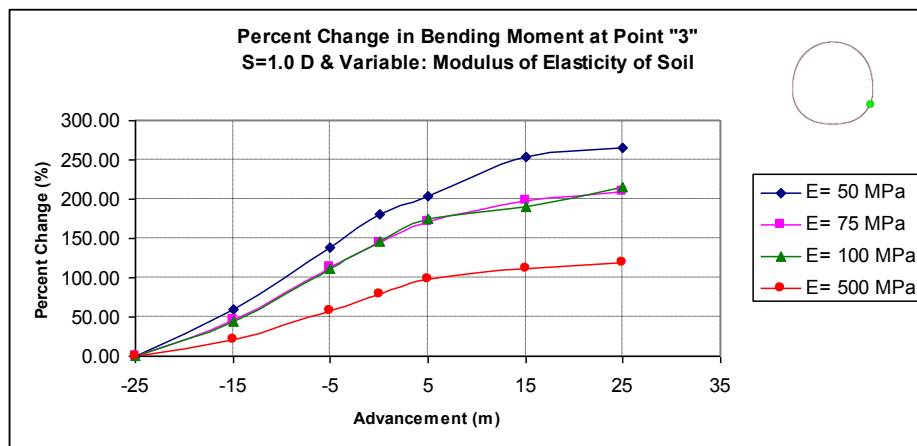


Figure 4.37 Percent change in bending moment at the right-bottom side of the tunnel

As shown in Figure 4.37, the increase in bending moment at the right-bottom side of the mid-length section is nearly same for the intermediate values of soil stiffness (e.g. 75 MPa and 100 MPa). A similar behaviour is determined from the analysis results of the case in which the pillar width is kept constant as 2.0 D and modulus of elasticity of the soil is changed. Three analyses were carried out by using three different soil stiffness values as 50 MPa, 75 MPa and 100 MPa for this case. The analysis results show that the final bending moment values at the right-bottom side of the tunnel vary only in the order of 15% difference. This result means that the effect of soil stiffness becomes negligible when the pillar width is larger than an approximate value of 2.0 D.

Another type of analyses is performed by keeping the modulus of elasticity of soil constant and changing the pillar width. According to analysis results, the bending moment at the right-bottom side of the tunnel tends to increase as the second tunnel advances for all pillar width values. Bending moment values are larger when the pillar width is smaller for the same elastic modulus. The bending moment values become closer when the spacing left between the tunnels is greater than 1.0D. Figure 4.38 and Figure 4.39 show the typical bending moment behaviour of the right-bottom side of the tunnel for the same soil stiffness.

The data obtained from Figure 4.39 is used to determine the effect of pillar width on bending moment at the right-bottom side of the tunnel when the construction of second tunnel is completed. Figure 4.40 shows the percent change for different pillar width values of tunnel constructed in intermediate soil stiffness ($E=75$ MPa). As shown in Figure 4.40 the tendency of the percent change in bending moment becomes nearly linear for the pillar width greater than 1.0 D. Assuming that, this trend is valid for the values greater than 2.0 D;

it is possible to conclude that the construction of a new tunnel does not affect the bending moment at the right-bottom side of the tunnel when the pillar width is beyond the value 3.0 D.

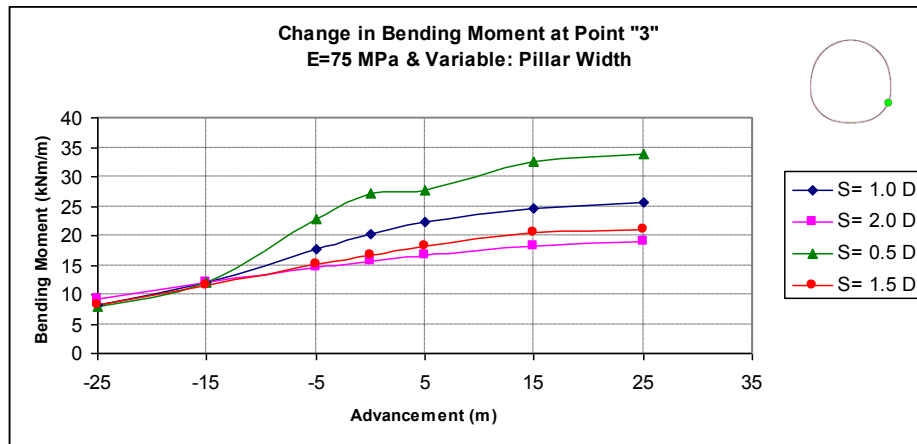


Figure 4.38 Bending moment values at the right-bottom side of the tunnel

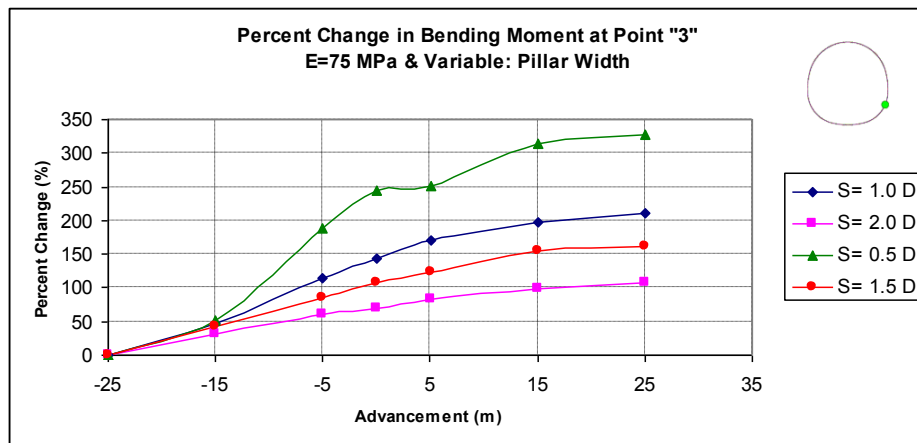


Figure 4.39 Percent change in bending moment at the right-bottom side of the tunnel

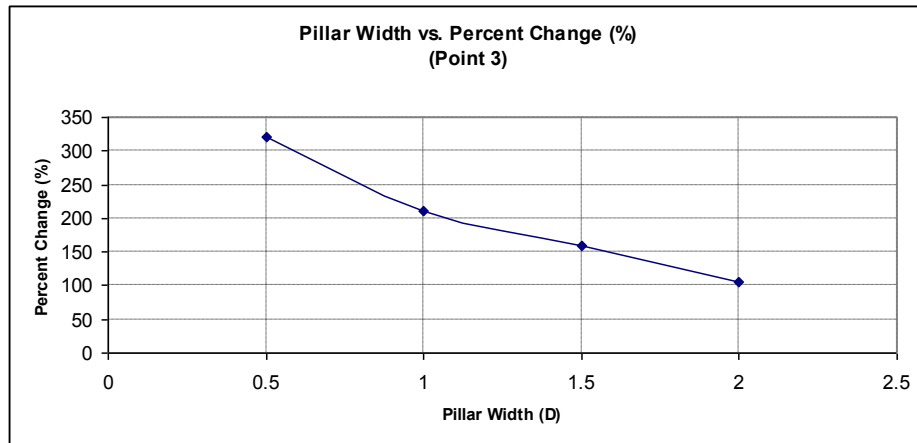


Figure 4.40 Change in percent increase for different pillar width values

4.2.4 Behaviour of Bending Moment at 4

Analysis results show that the bending moment at the bottom side of the tunnel tends to increase as the second tunnel advances. This increasing behaviour is valid for both different soil stiffnesses and different pillar width values. Bending moment values are larger when the modulus of elasticity of soil is smaller for the same pillar width. The behaviour of the bending moment at the bottom side of the tunnel is evaluated in terms of both the bending moment values and percent change in these values. Figure 4.41 and Figure 4.42 show the typical bending moment behaviour of the bottom side of the tunnel for the same pillar width.

Another type of analyses is performed by keeping the modulus of elasticity of soil constant and changing the pillar width. According to analysis results, the bending moment at the bottom side of the tunnel tends to increase as the second tunnel advances for all pillar width values. Bending moment values are larger when the pillar width is smaller for the same soil stiffness. The bending moment values are close to each other for successive values of pillar width.

Figure 4.43 and Figure 4.44 show the typical bending moment behaviour of the bottom side of the tunnel for the same soil stiffness.

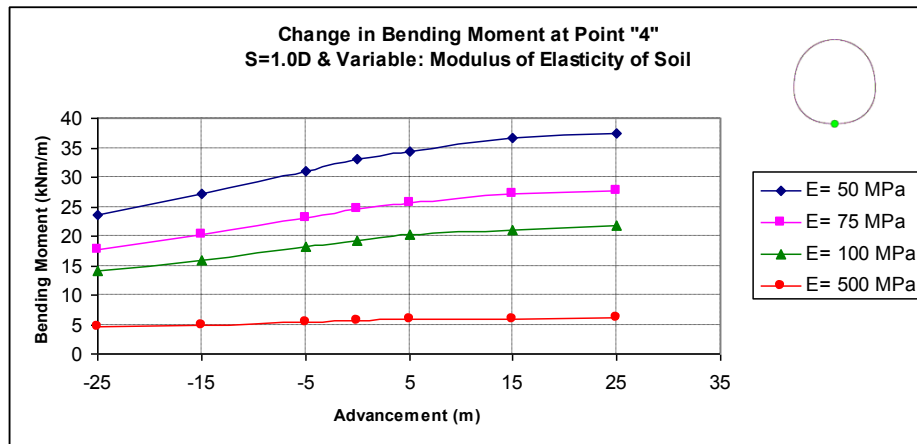


Figure 4.41 Bending moment values at the bottom side of the tunnel

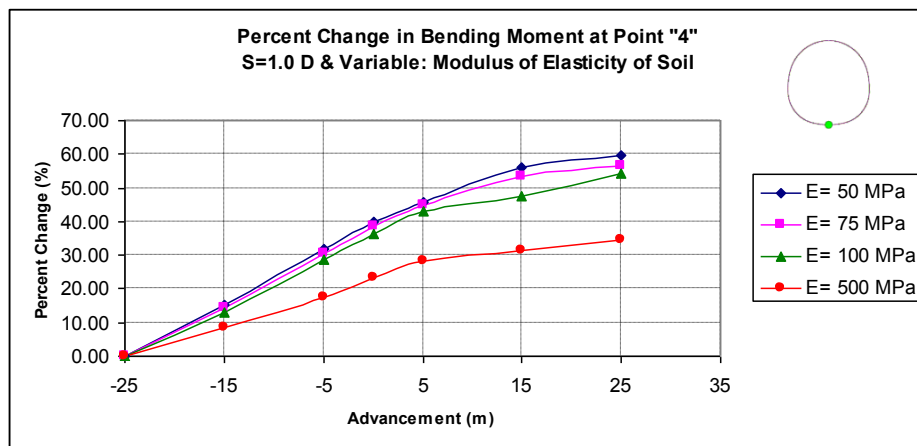


Figure 4.42 Percent change in bending moment at the bottom side of the tunnel

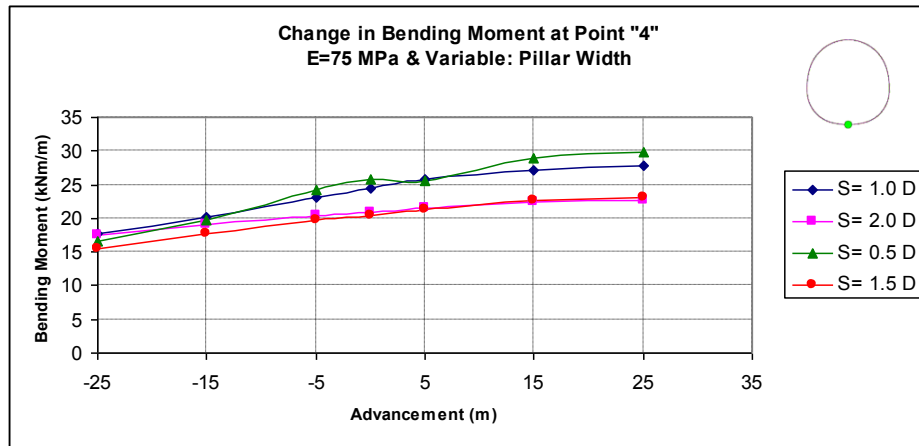


Figure 4.43 Bending moment values at the bottom side of the tunnel

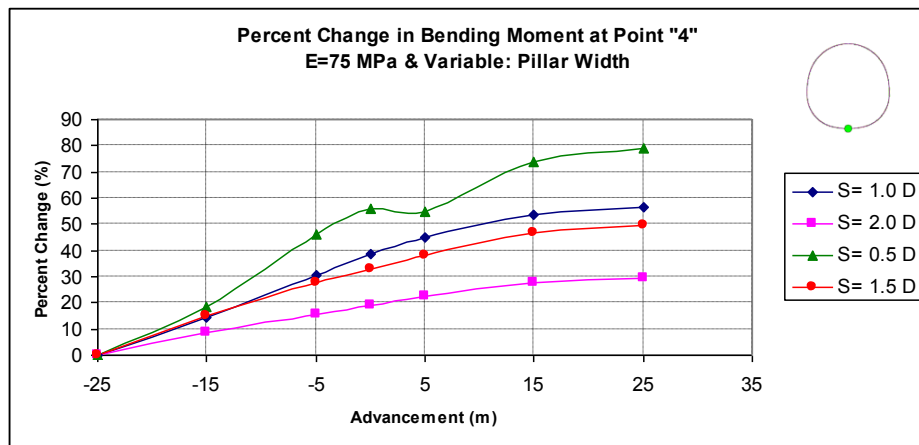


Figure 4.44 Percent change in bending moment at the bottom side of the tunnel

Figure 4.42 shows that the percent increase in bending moment at the bottom side of the tunnel is nearly independent from the modulus of elasticity of soil, excluding the largest value of 500 MPa, and the increase is in the order of 55% for the pillar width is equal to the 1 diameter of the tunnel. The percent change in bending moment at the bottom side of the tunnel reduces to approximately 30% for the pillar width is equal to the 2 times of the tunnel diameter. The

percent increase in bending moment at the bottom side of the tunnel is approximately 80% and 50% for the pillar width values of 0.5D and 1.5D, respectively. Figure 4.45 shows the change in percent increase for different pillar width values mentioned above. As shown in Figure 4.45 the increase in bending moment at the bottom side of the tunnel increases rapidly when the pillar width is smaller than 1.0 D and decreases rapidly when the pillar width is larger than 1.5 D. It may be estimated that the construction of the new tunnel does not affect the bending moment at the bottom of the tunnel for pillar width of greater than 2.5 D.

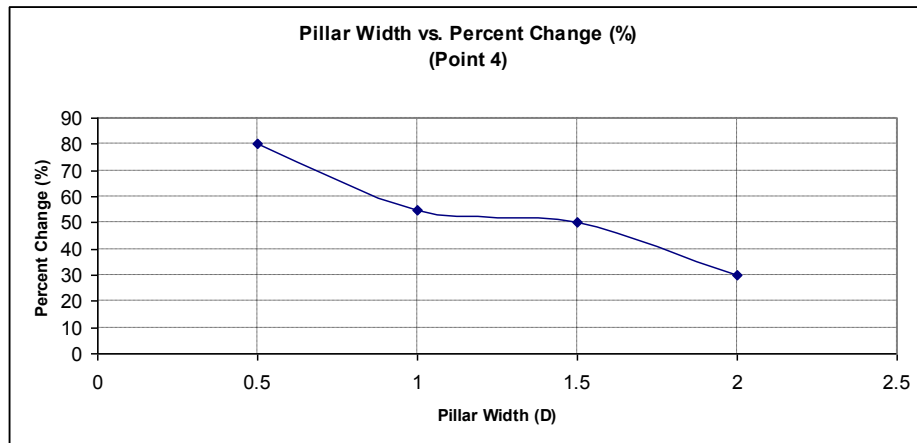


Figure 4.45 Change in percent increase for different pillar width values

4.2.5 Behaviour of Bending Moment at 5

Analysis results show that the bending moment at the left-bottom side of the tunnel tends to increase as the second tunnel advances. This increasing behaviour is valid for both different soil stiffnesses and different pillar width values. The amount of increase in bending moment is low especially for large pillar width values, if it is compared with other locations of interest. Bending moment values are larger when the modulus of elasticity of soil is smaller for

the same pillar width. The behaviour of the bending moment at the left-bottom side of the tunnel is evaluated in terms of both the bending moment values and percent change in these values. Figure 4.46 and Figure 4.47 show the typical bending moment behaviour of the left-bottom side of the tunnel for the same pillar width.

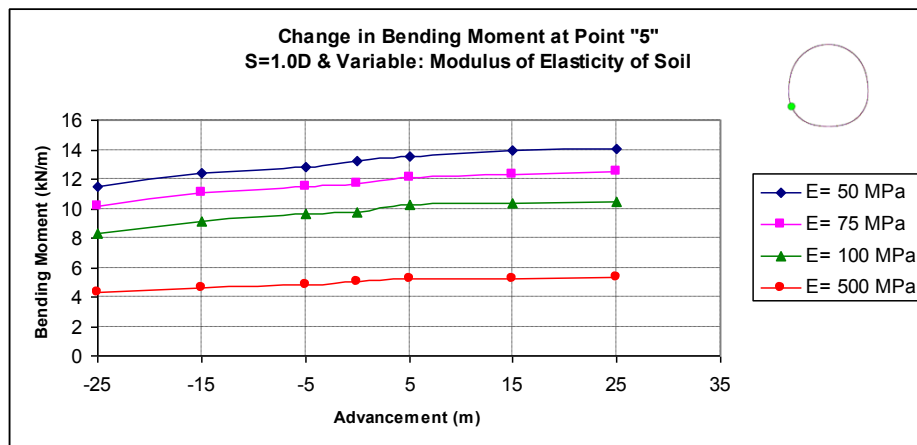


Figure 4.46 Bending moment values at the left-bottom side of the tunnel

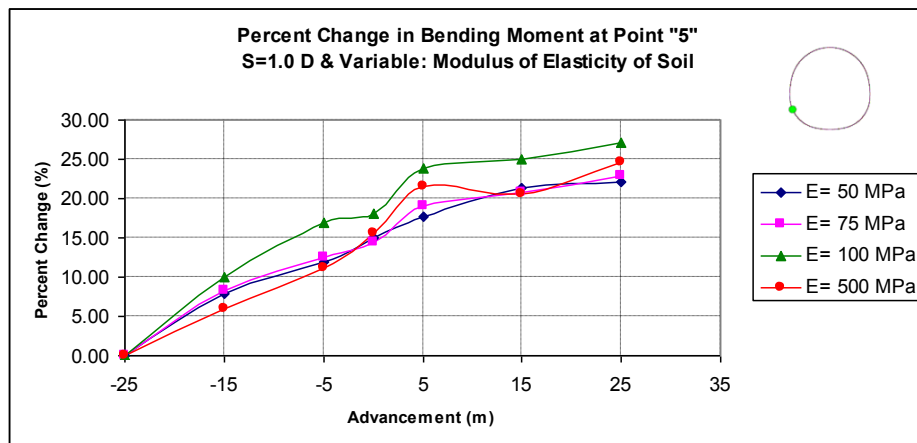


Figure 4.47 Percent change in bending moment at the left-bottom side of the tunnel

Another type of analyses is performed by keeping the modulus of elasticity of soil constant and changing the pillar width. According to analysis results, the bending moment at the left-bottom side of the tunnel tends to increase as the second tunnel advances for all pillar width values. Bending moment values are larger when the pillar width is smaller for the same soil stiffness. The increase in bending moment values are very small especially for pillar width values of equal or greater than 1.5 D. Figure 4.48 and Figure 4.49 show the typical bending moment behaviour of the left-bottom side of the tunnel for the same soil stiffness.

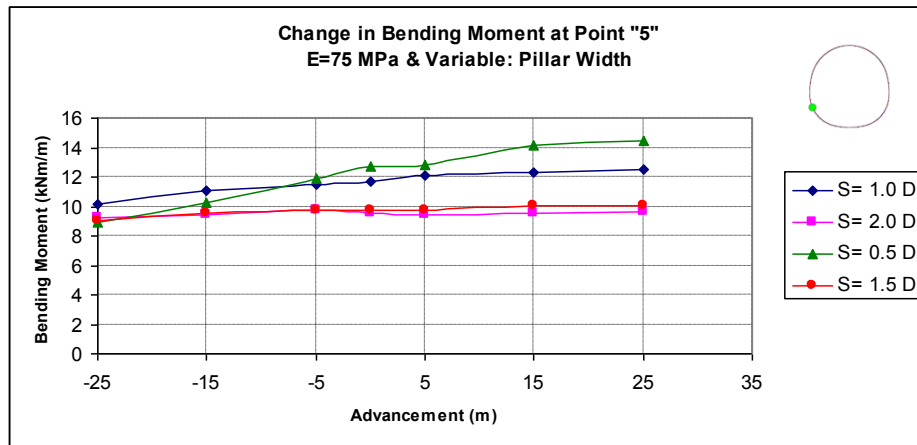


Figure 4.48 Bending moment values at the left-bottom side of the tunnel

Figure 4.47 shows that the percent increase in bending moment at the left-bottom side of the tunnel is nearly independent from the modulus of elasticity of soil and the increase is in the order of 25% for the pillar width is equal to the 1 diameter of the tunnel. The percent change in bending moment at the left-bottom side of the tunnel reduces to approximately 4% for the pillar width is equal to the 2 times of the tunnel diameter. The percent increase in bending

moment at the left-bottom side of the tunnel is approximately 60% and 10% for the pillar width values of 0.5D and 1.5D, respectively.

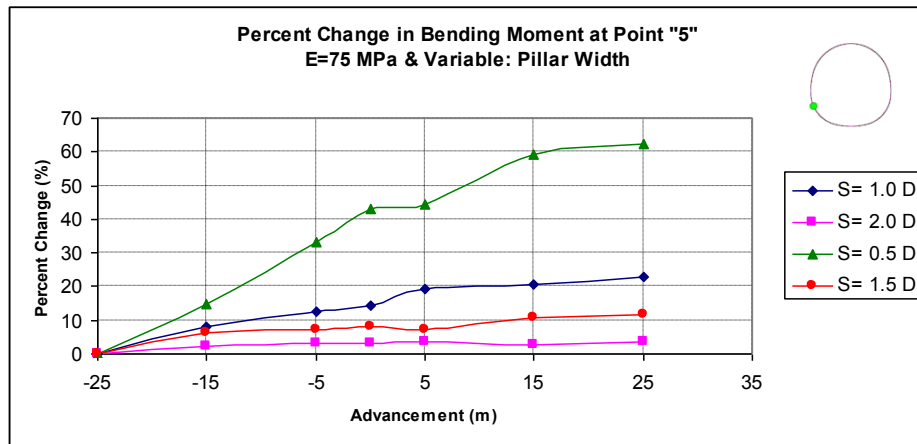


Figure 4.49 Percent change in bending moment at the left-bottom side of the tunnel

Figure 4.50 shows the change in percent increase for different pillar width values mentioned above. As shown in Figure 4.50 the increase in bending moment at the left-bottom side of the tunnel increases rapidly when the pillar width gets smaller than 1.5 D. It is graphically determined that the construction of the new tunnel does not affect the bending moment at the left-bottom of the tunnel for pillar width of greater than 2.0 D.

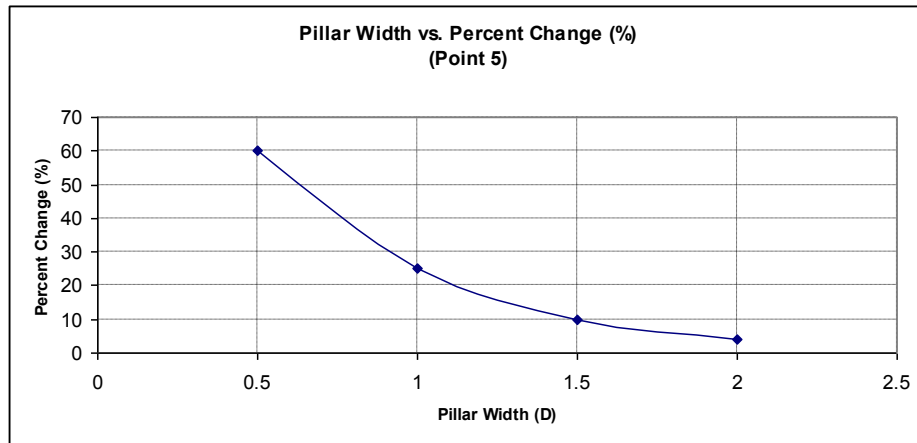


Figure 4.50 Change in percent increase for different pillar width values

4.2.6 Behaviour of Bending Moment at 6

Analysis results show that the bending moment at the left-top side of the tunnel tends to increase as the second tunnel advances. This increasing behaviour is valid for both different soil stiffnesses and different pillar width values. Bending moment values are larger when the modulus of elasticity of soil is smaller for the same pillar width. The behaviour of the bending moment at the left-top side of the tunnel is evaluated in terms of both the bending moment values and percent change in these values. Figure 4.51 and Figure 4.52 show the typical bending moment behaviour of the left-top side of the tunnel for the same pillar width.

Another type of analyses is performed by keeping the modulus of elasticity of soil constant and changing the pillar width. According to analysis results, the bending moment at the left-top side of the tunnel tends to increase as the second tunnel advances for all pillar width values. Bending moment values are larger when the pillar width is smaller for the same soil stiffness. Figure 4.53

and Figure 4.54 show the typical bending moment behaviour of the left-top side of the tunnel for the same soil stiffness.

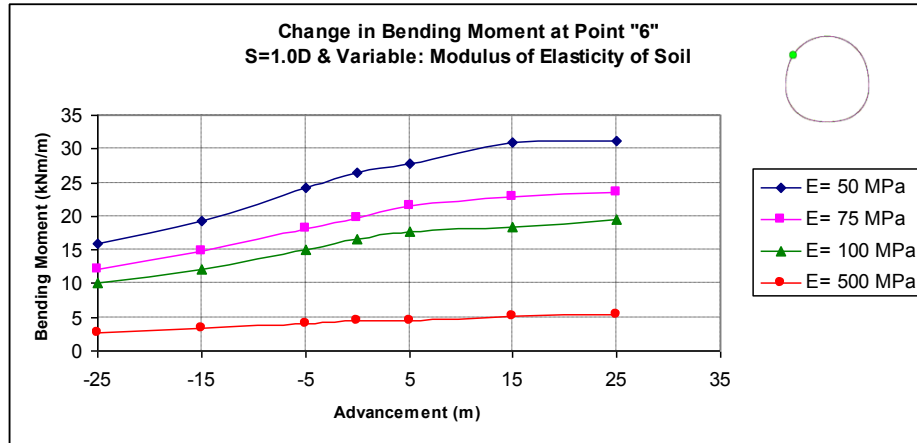


Figure 4.51 Bending moment values at the left-top side of the tunnel

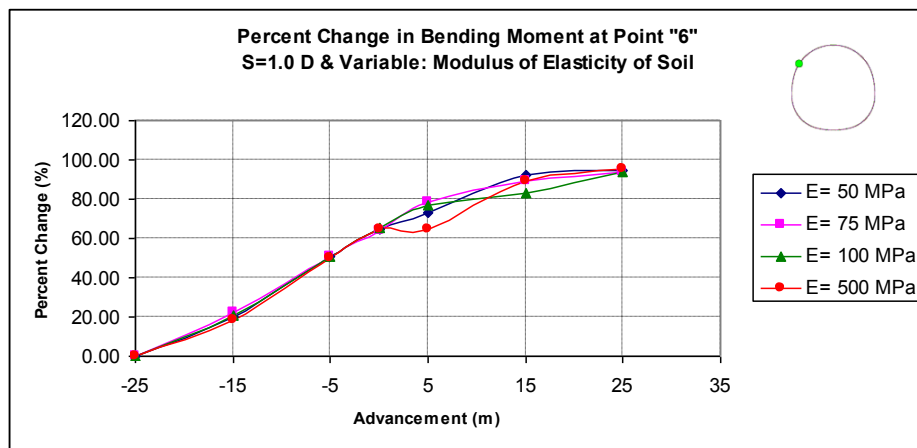


Figure 4.52 Percent change in bending moment at the left-top side of the tunnel

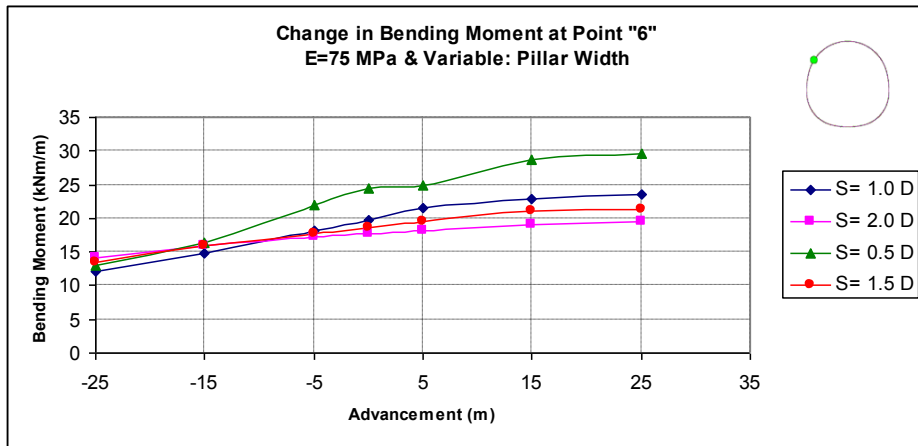


Figure 4.53 Bending moment values at the left-top side of the tunnel

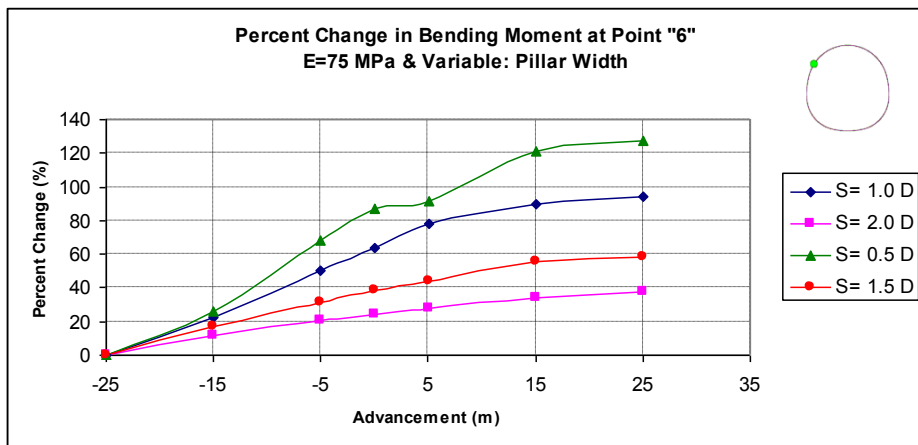


Figure 4.54 Percent change in bending moment at the left-top side of the tunnel

Figure 4.52 shows that the percent increase in bending moment at the left-top side of the tunnel is nearly independent from the modulus of elasticity of soil and the increase is in the order of 100% for the pillar width is equal to the 1 diameter of the tunnel. The percent change in bending moment at the left-top side of the tunnel reduces to approximately 40% for the pillar width is equal to the 2 times of the tunnel diameter. The percent increase in bending moment at

the left-top side of the tunnel is approximately 125% and 55% for the pillar width values of 0.5D and 1.5D, respectively. Figure 4.55 shows the change in percent increase for different pillar width values mentioned above. As shown in Figure 4.55 the rate of increase and the rate of decrease get smaller for the pillar width values of smaller than 1.0 D and larger than 1.5 D, respectively.

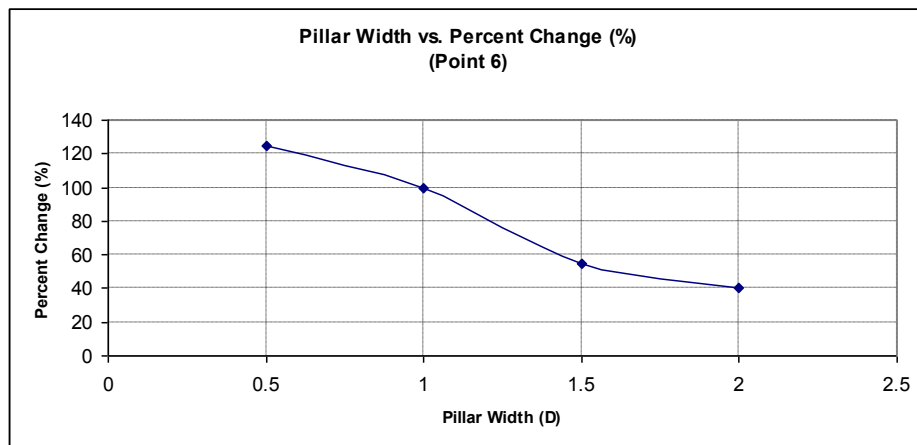


Figure 4.55 Change in percent increase for different pillar width values

4.3 Behaviour of Shear Forces

The behaviour of the shear forces as the second tunnel advances is given in this part. The behaviour of the shear force is evaluated in six different location of the mid-length cross-section of the previously constructed tunnel as top (1), right-top (2), right-bottom (3), bottom (4), left-bottom (5) and left-top (6). The top, left bottom and right bottom are the regions where the direction of the shear force is changed. That is why; these regions are investigated in terms of both the positive and negative shear forces. Shear force behaviour is more complicated than the behaviour of displacement and bending moments. It is not always possible to generalize the behaviour for changing variables. The results

presented below are given only for representing the typical behaviour. The rest of the results are given in related appendices.

4.3.1 Behaviour of Shear Force at 1

According to analysis results, positive shear forces at the top side of the tunnel start decreasing with the advancement of the second tunnel when the advancement is approximately 20 meters, positive shear forces start increasing. Finally, when the second tunnel passes away the mid-length section about 5 meters, positive shear forces become nearly constant. In opposition to the positive shear forces, negative shear forces at the top side of the tunnel firstly increase, secondly decrease and finally become stable. This behaviour is valid for both different soil stiffnesses and different pillar width values. Positive and negative shear force values are larger when the modulus of elasticity of soil is smaller for the same pillar width. The behaviour of the shear force at the top side of the tunnel is evaluated in terms of both the shear force values and percent change in these values. Figure 4.56, Figure 4.57, Figure 4.58 and Figure 4.59 show the typical shear force behaviour of the top side of the tunnel for the same pillar width.

As shown in Figure 4.58 and Figure 4.59 the difference between the maximum and minimum values of shear forces is maximum when the modulus of elasticity of soil is the largest. The positive shear forces result in values of 1.5 times about of its original value. On the other hand, negative shear forces result in values of 0.5 times about of its original value. These increase and decrease amounts are smaller for the cases of pillar width values larger than 1.0 times of the diameter of the tunnel.

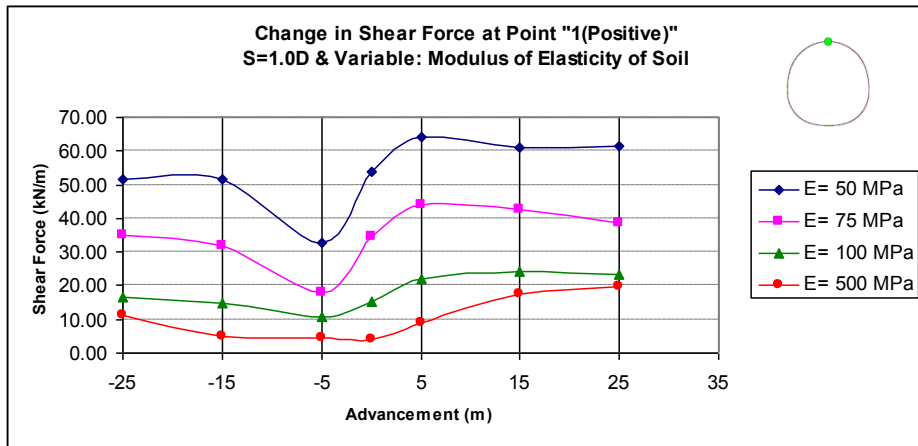


Figure 4.56 Shear force values at the top side of the tunnel

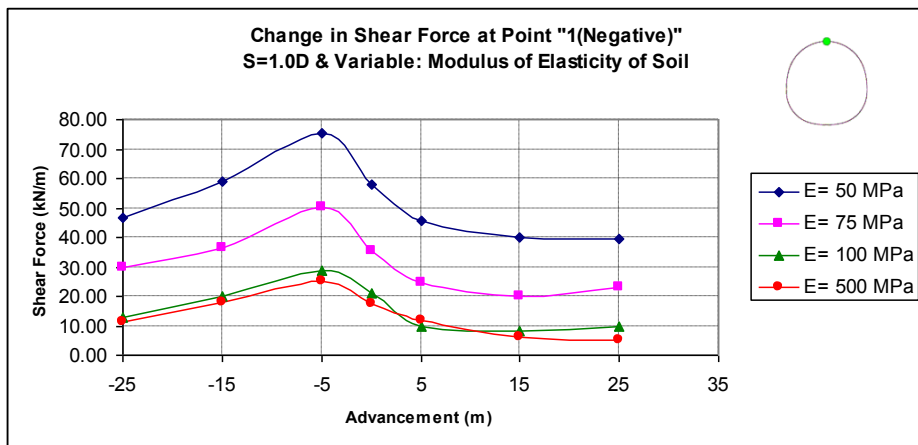


Figure 4.57 Shear force values at the top side of the tunnel

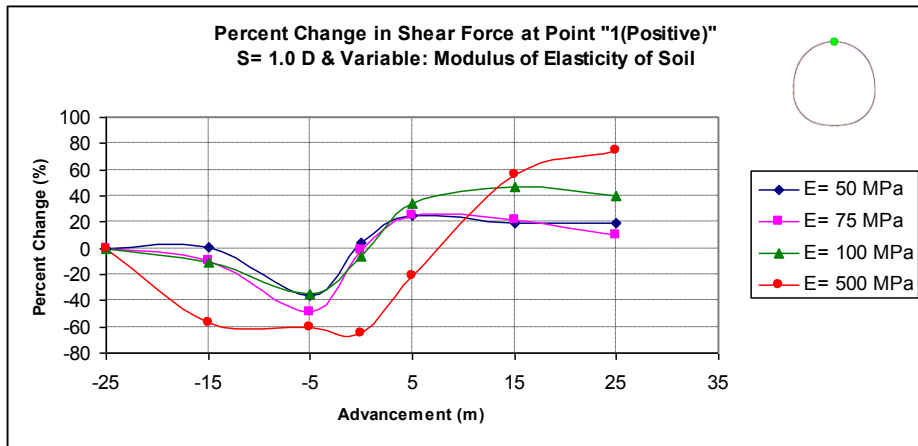


Figure 4.58 Percent change in shear force at the top side of the tunnel

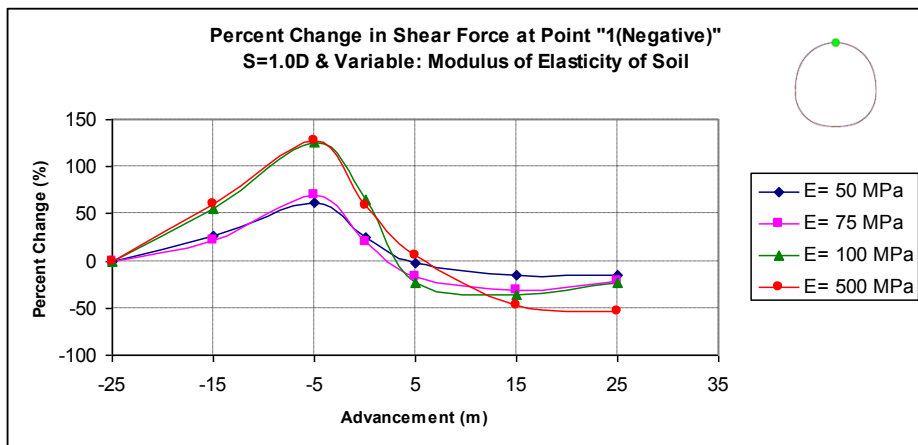


Figure 4.59 Percent change in shear force at the top side of the tunnel

A similar type of behaviour is determined for the cases in which soil stiffness is kept constant and pillar width is changed. The maximum difference occurs between the maximum and minimum values of shear forces for the smallest pillar width value. Figure 4.60, Figure 4.61, Figure 4.62 and Figure 4.63 show the typical shear force behaviour of the top side of the tunnel for the same soil stiffness.

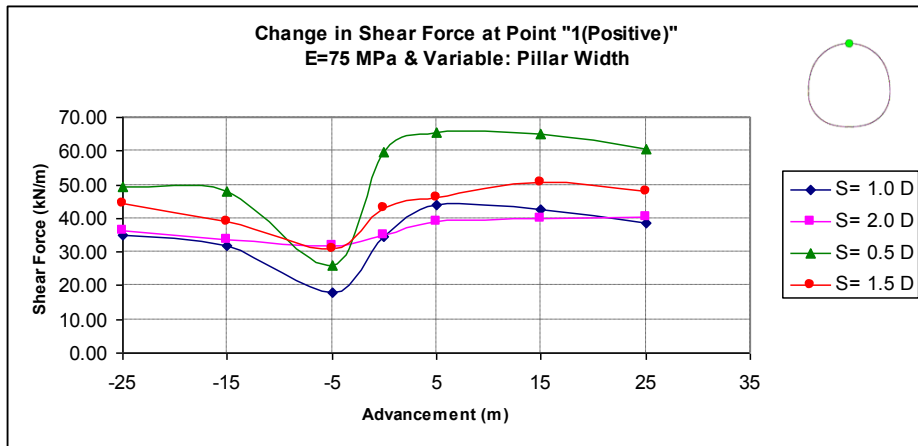


Figure 4.60 Shear force values at the top side of the tunnel

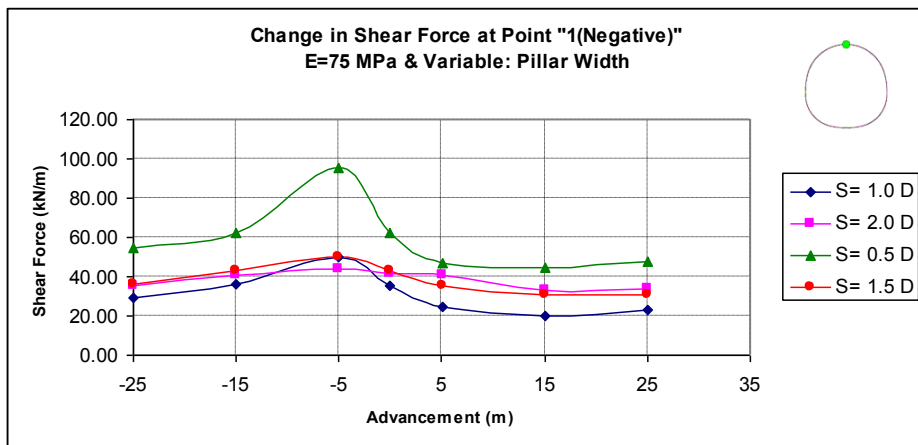


Figure 4.61 Shear force values at the top side of the tunnel

As shown in Figure 4.62 and Figure 4.63, most of the values of positive shear forces converge to a value of approximately 1.1 times of the original value and most of the values of negative shear forces converge to an average value of 0.9 times of the original value. To summarize the general behaviour of the shear forces at the top, it may be concluded that the larger stiffness with smallest

pillar width gives the maximum shear force difference with the value obtained before the construction of the second tunnel begins.

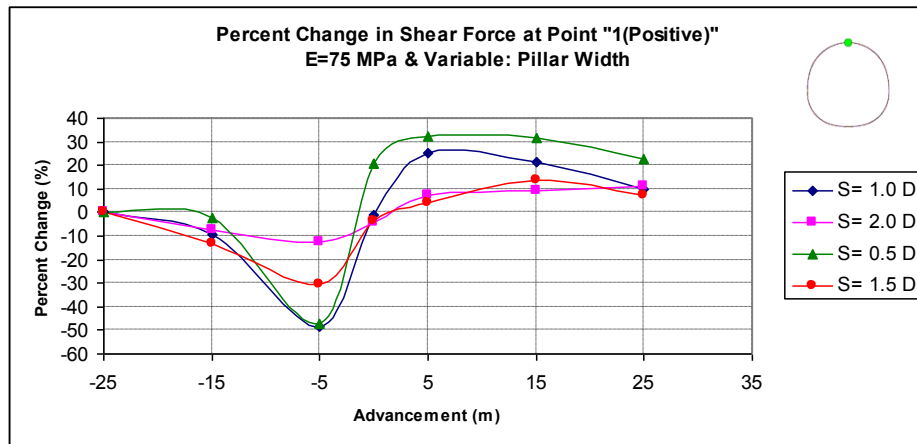


Figure 4.62 Percent change in shear force at the top side of the tunnel

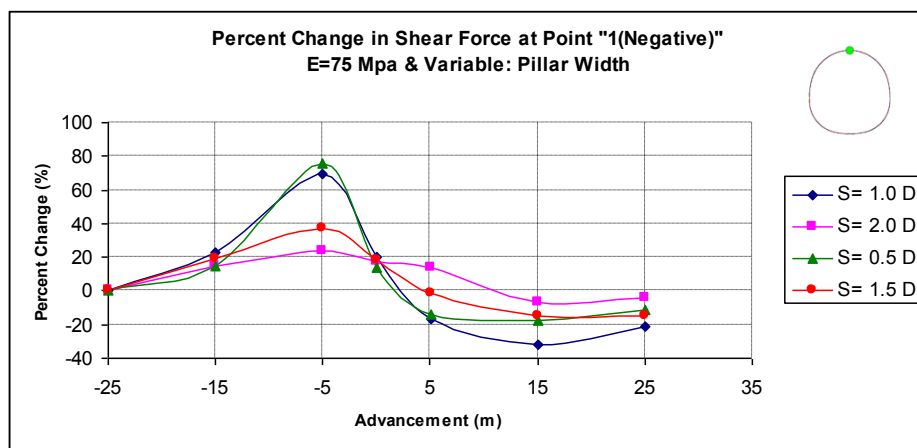


Figure 4.63 Percent change in shear force at the top side of the tunnel

4.3.2 Behaviour of Shear Force at 2

Analysis results show that the shear forces at the right-top side of the tunnel tend to decrease as the advancement level of the second tunnel increases. After the passage of the second tunnel from the mid-length section of the first tunnel, shear forces start increasing and nearly reach the original value at the end of the last construction stage. The values obtained at the last construction stage are generally lower than the values at the beginning. This behaviour is valid for both different soil stiffnesses and different pillar width values. Figure 4.64 and Figure 4.65 show the typical shear force behaviour of the right-top side of the tunnel for the same pillar width. As shown in Figure 4.65, the maximum decrease in shear force is nearly same for small stiffnesses (50, 75 and 100 MPa) and is about 40% decrease. The maximum decrease for modulus of elasticity of 500 MPa is smaller than this value. The change in shear forces ranges between 0-10% decrease at the last construction stage for the pillar width of 1.0 D.

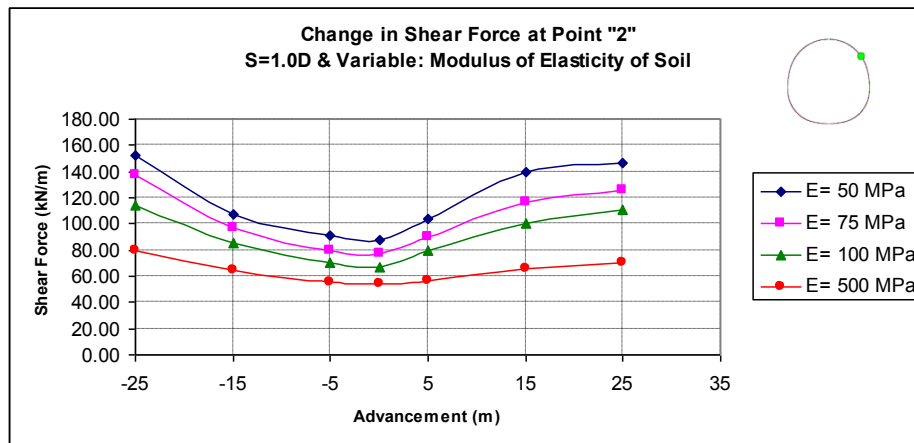


Figure 4.64 Shear force values at the right-top side of the tunnel

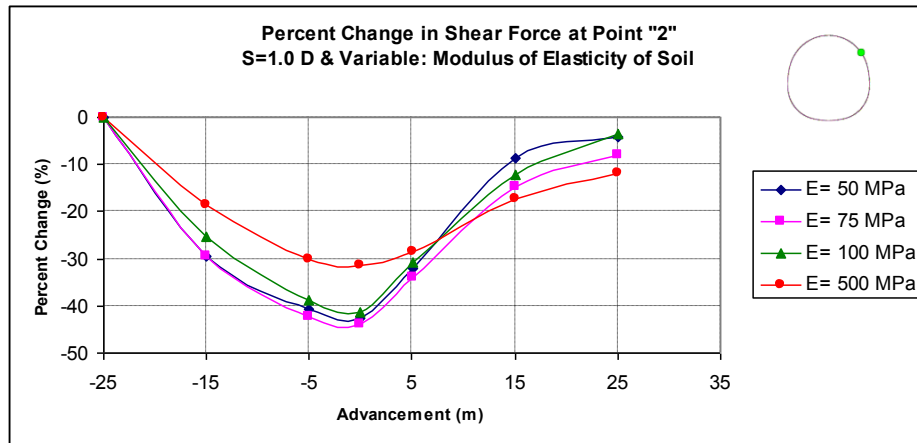


Figure 4.65 Percent change in shear force at the right-top side of the tunnel

A similar type of behaviour is determined for the cases in which soil stiffness is kept constant and pillar width is changed. The maximum amount of decrease occurs for the smallest pillar width value; but again shear force values return to a value just a little bit smaller than its original value. Figure 4.66 and Figure 4.67 show the typical shear force behaviour of the right-top side of the tunnel for the same soil stiffness. As shown in Figure 4.67, the shear force returns its original value for the pillar width of greater than 1.0 D.

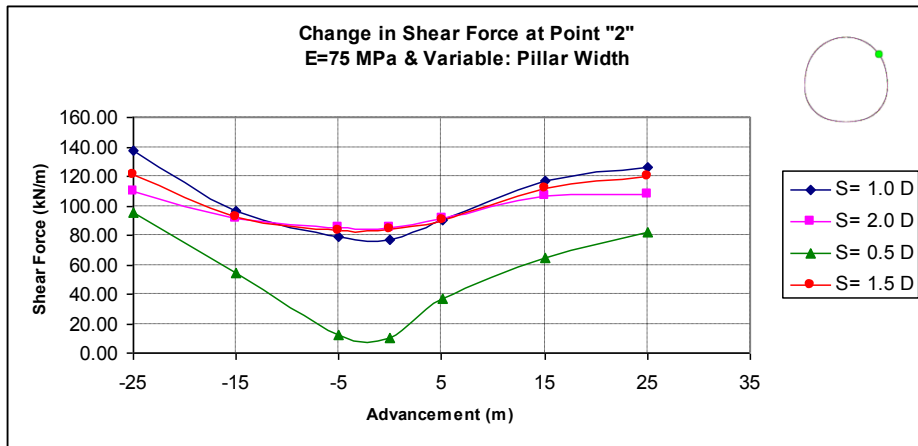


Figure 4.66 Shear force values at the right-top side of the tunnel

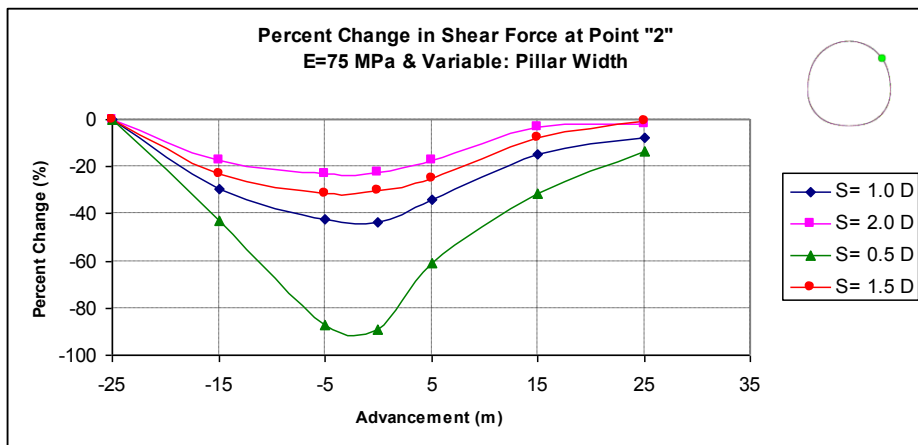


Figure 4.67 Percent change in shear force at the right-top side of the tunnel

4.3.3 Behaviour of Shear Force at 3

Analysis results show that the positive shear forces at the right-bottom side of the tunnel tend to increase as the advancement level of the second tunnel increases. After the passage of the second tunnel from the mid-length section of the first tunnel, positive shear forces start decreasing and nearly reach the

original value at the end of the last construction stage. In opposition to the positive shear forces, negative shear forces at the right-bottom side of the tunnel firstly decrease, secondly increase and finally reach its original value. This behaviour is valid for both different soil stiffnesses and different pillar width values. Figure 4.68, Figure 4.69, Figure 4.70 and Figure 4.71 show the typical shear force behaviour of the right-bottom side of the tunnel for the same pillar width.

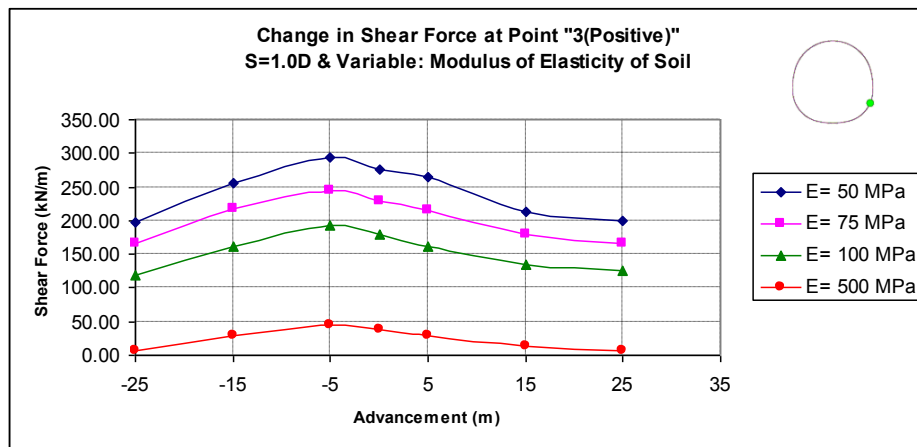


Figure 4.68 Shear force values at the right-bottom side of the tunnel

As shown in Figure 4.70 and Figure 4.71, positive and negative shear forces show similar behaviour for the modulus of elasticity of 50 MPa, 75 MPa and 100 MPa. On the other hand, especially, the case in which 500 MPa is analyzed, show a similar behaviour in a large scale, since the original value of the positive shear force is too low.

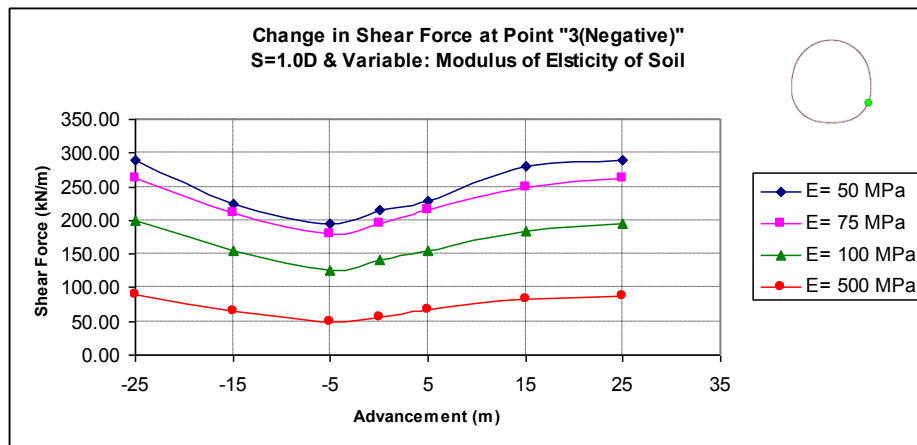


Figure 4.69 Shear force values at the right-bottom side of the tunnel

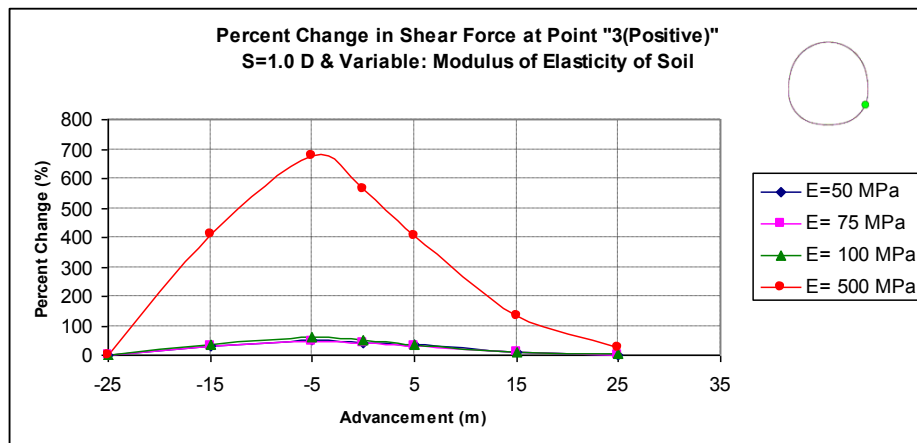


Figure 4.70 Percent change in shear force at the right-bottom side of the tunnel

Both the increase in positive shear forces and the decrease in negative shear forces reach their maximum and minimum values at the mid-length of the advancement and independent from the modulus of elasticity of soil. The average is about 50% and the average decrease is about 35% for pillar width of 1.0D.

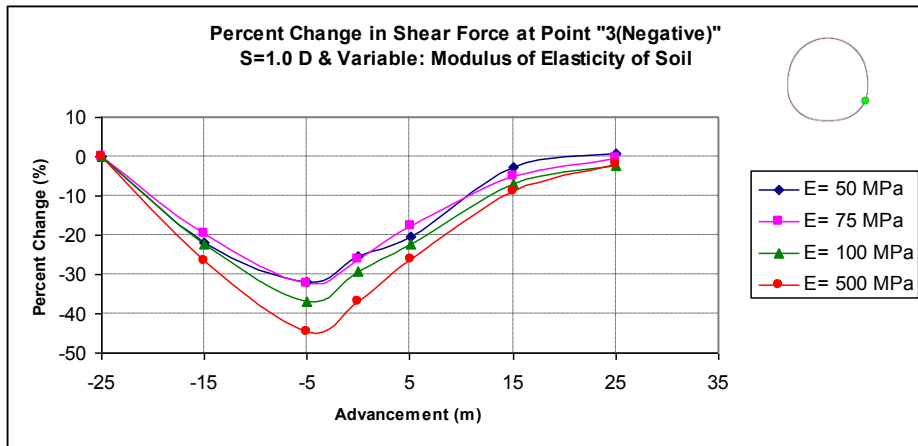


Figure 4.71 Percent change in shear force at the right-bottom side of the tunnel

A similar type of behaviour is determined for the cases in which soil stiffness is kept constant and pillar width is changed. Figure 4.72, Figure 4.73, Figure 4.74 and Figure 4.75 show the typical shear force behaviour of the right-bottom side of the tunnel for the same modulus of elasticity of soil.

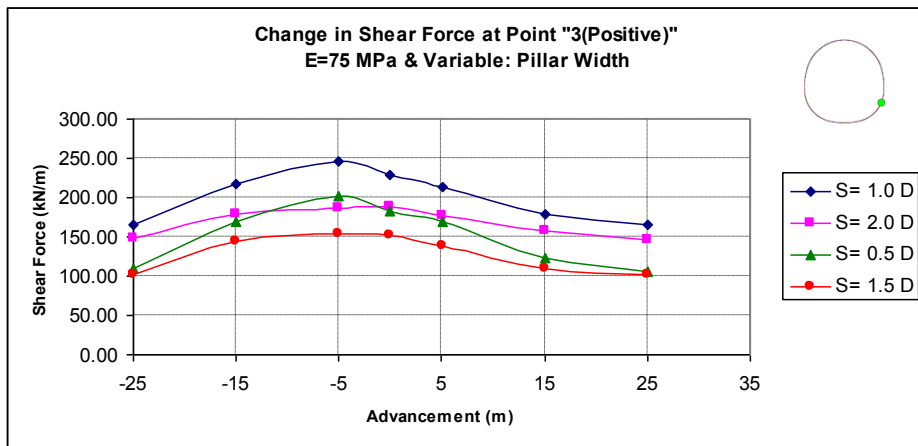


Figure 4.72 Shear force values at the right-bottom side of the tunnel

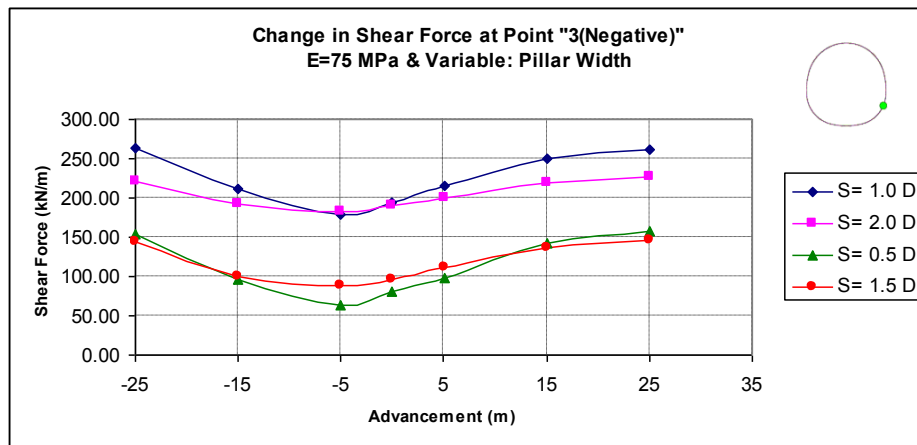


Figure 4.73 Shear force values at the right-bottom side of the tunnel

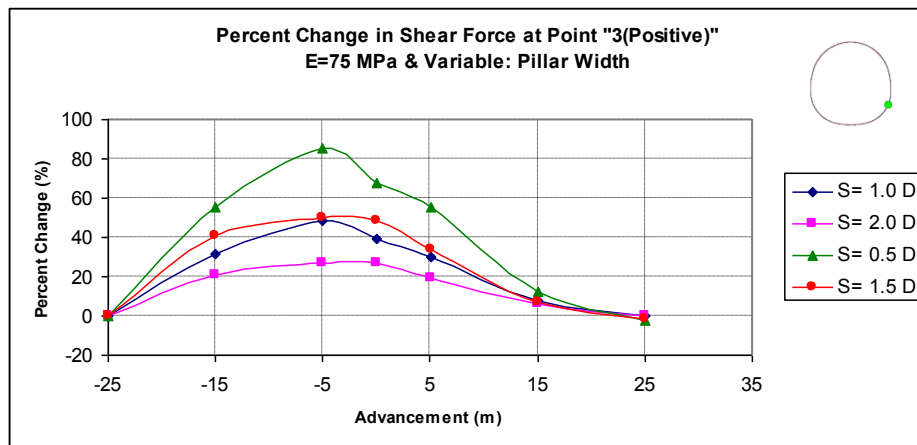


Figure 4.74 Percent change in shear force at the right-bottom side of the tunnel

As shown in Figure 4.74 and Figure 4.75, positive and negative shear forces at the right-bottom side of the tunnel show similar tendencies in different scales according to the pillar width. As the pillar width reduces, the maximum and minimum values get larger. By extrapolating the data obtained, it may be concluded that the differences will be more negligible when the pillar width is larger than 2.0 D.

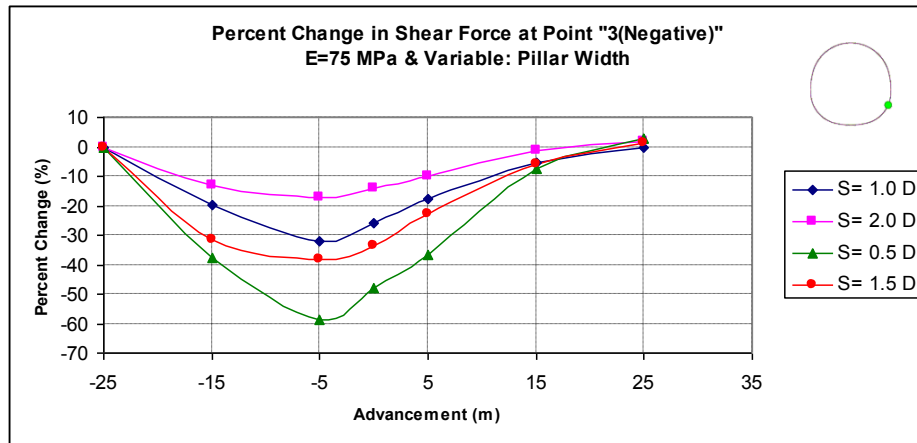


Figure 4.75 Percent change in shear force at the right-bottom side of the tunnel

4.3.4 Behaviour of Shear Force at 4

Analysis results show that the shear forces at the bottom side of the tunnel tend to increase as the advancement level of the second tunnel increases. After the passage of the second tunnel from the mid-length section of the first tunnel, shear forces start decreasing and nearly reach the original value at the end of the last construction stage. This behaviour is valid for both different soil stiffnesses and different pillar width values. Figure 4.76 and Figure 4.77 show the typical shear force behaviour of the bottom side of the tunnel for the same pillar width. As shown in Figure 4.76, the shear force at the bottom side of the tunnel is nearly equals to zero at the beginning of the construction of the second tunnel. Since, this initial value is so small, a minor increase in the shear forces at the bottom side of the tunnel results in very large amount of increase in terms of percent difference, as shown in Figure 4.77. As shown in these figures, as the stiffness of the soil decreases the difference between the maximum increase and initial value increases, but this behaviour is not taken into consideration since it is due to the small magnitude of the initial shear force value.

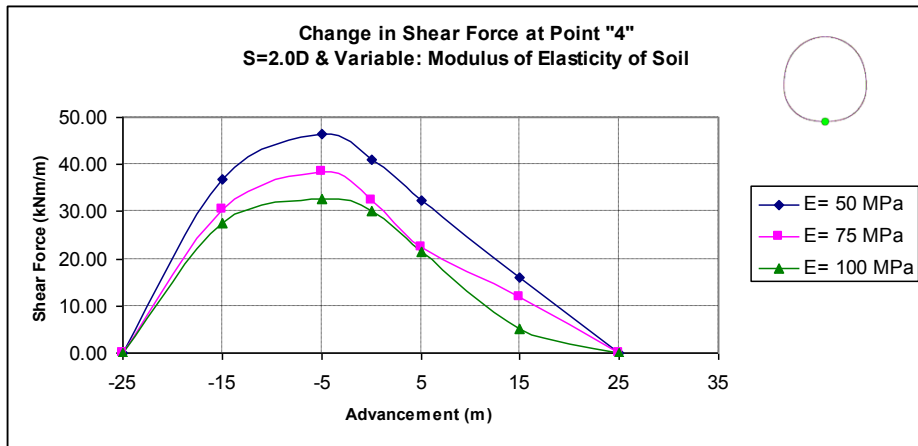


Figure 4.76 Shear force values at the bottom side of the tunnel

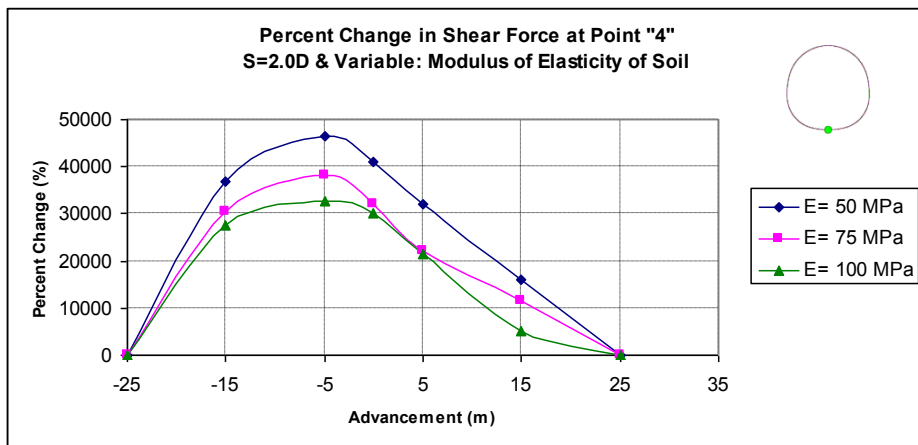


Figure 4.77 Percent change in shear force at the bottom side of the tunnel

Another type of analyses is performed by keeping the modulus of elasticity of soil constant and changing the pillar width. According to analysis results, the shear force behaviour at the bottom side of the tunnel is similar with the behaviour mentioned above. Shear force values are larger when the pillar width is smaller for the same soil stiffness. Figure 4.78 and Figure 4.79 show the typical shear force behaviour of the bottom side of the tunnel for the same soil

stiffness. As shown in Figure 4.78 and Figure 4.79, the behaviour of the shear forces is the same. Only difference is such that the difference between the maximum shear force and initial value is determined by the effect of the pillar width since the soil stiffness is kept constant. For the same soil stiffness small pillar width values give large differences.

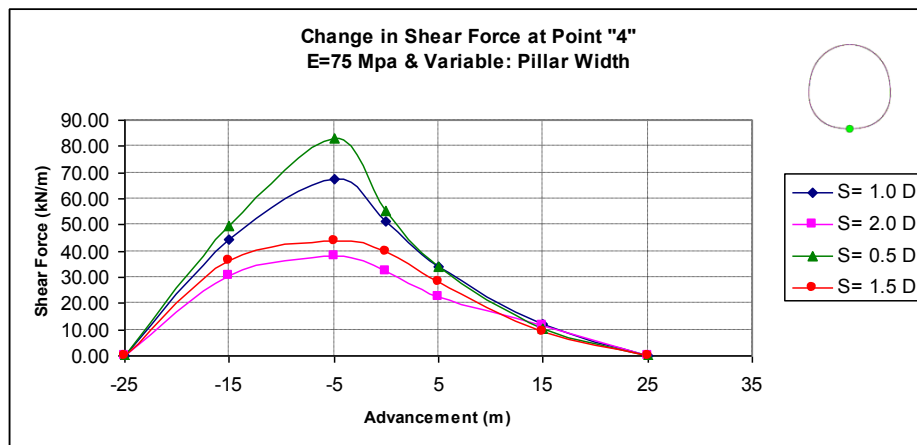


Figure 4.78 Shear force values at the bottom side of the tunnel

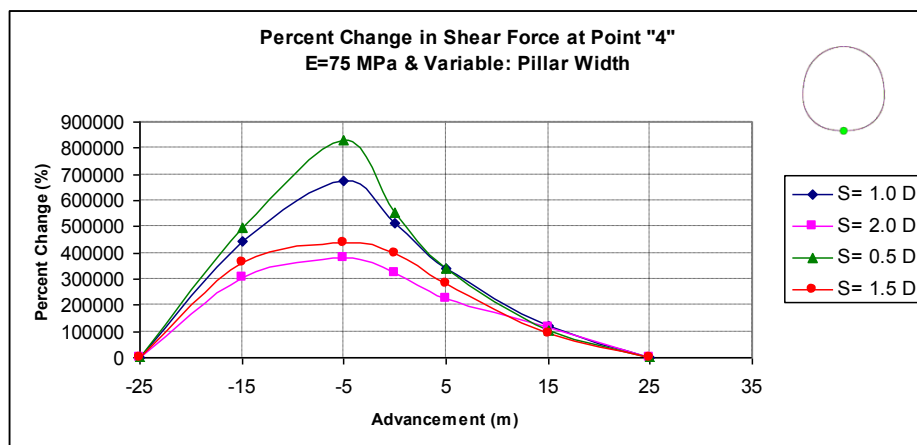


Figure 4.79 Percent change in shear force at the bottom side of the tunnel

4.3.5 Behaviour of Shear Force at 5

According to analysis results, it is determined that the shear forces at the left bottom side of the tunnel are not affected by the advancement of the second tunnel. The behaviour for both the positive and negative shear forces at the left-bottom side of the tunnel is given in Figure 4.80, Figure 4.81, Figure 4.82 and Figure 4.83.

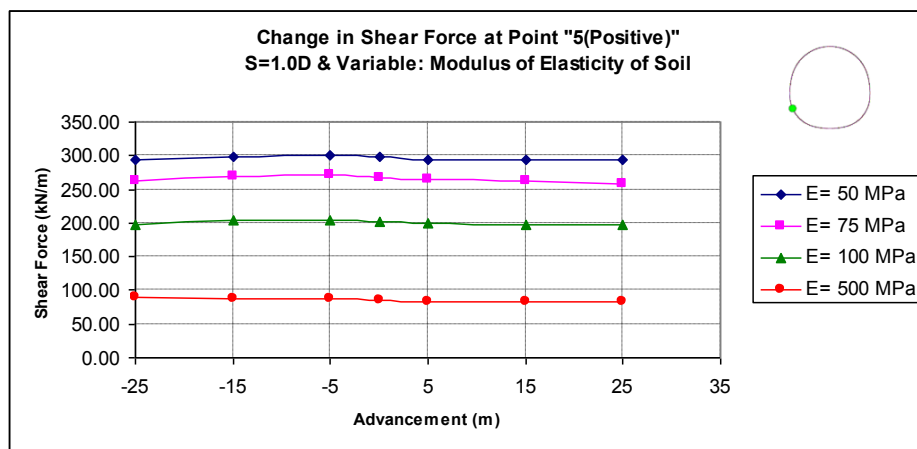


Figure 4.80 Shear force values at the left-bottom side of the tunnel

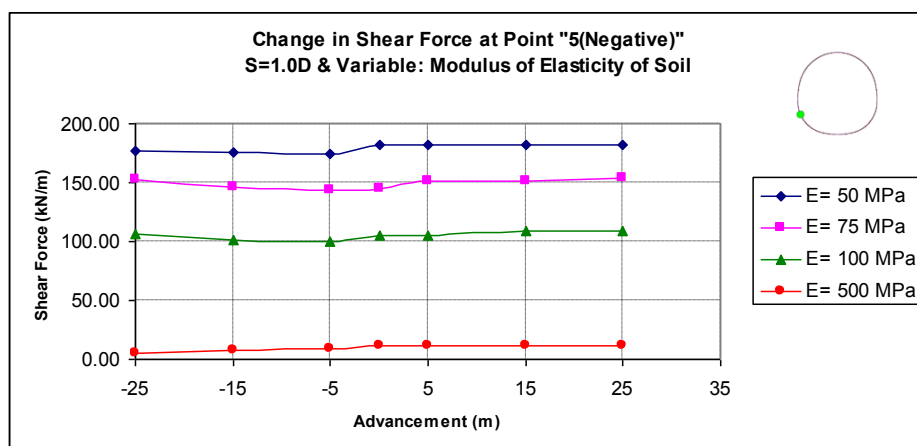


Figure 4.81 Shear force values at the left-bottom side of the tunnel

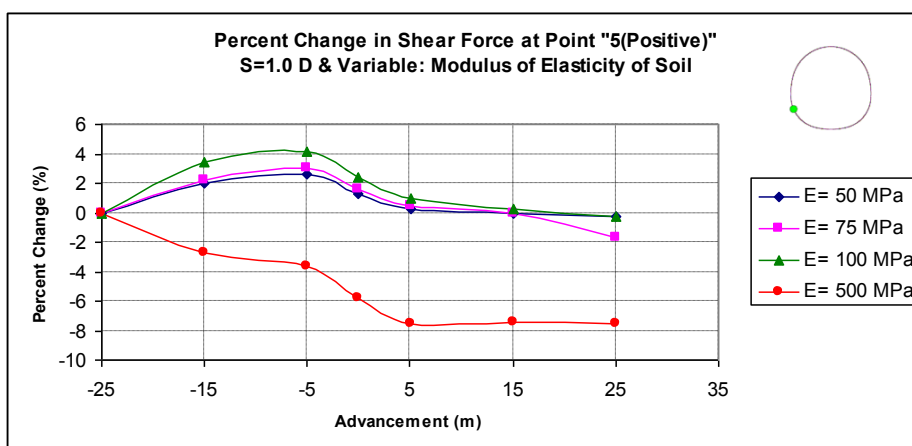


Figure 4.82 Percent change in shear force at the left-bottom side of the tunnel

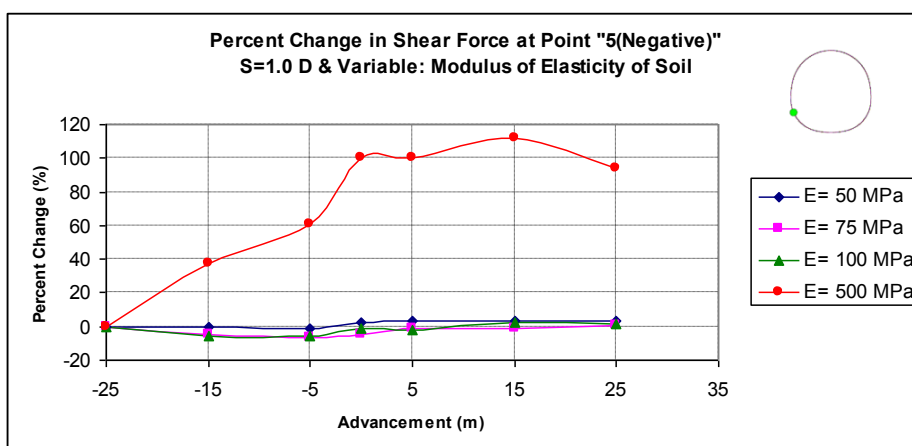


Figure 4.83 Percent change in shear force at the left-bottom side of the tunnel

As shown in figures, shear forces does not affected considerably especially for the elastic modulus of 50 MPa, 75 MPa and 100 MPa. On the other hand, negative shear forces are seemed to be affected by the advancement of the second tunnel for the case of 500 MPa of soil stiffness since the initial value is again very small in scale.

Another type of analyses is performed by keeping the modulus of elasticity of soil constant and changing the pillar width. Analysis results show that the shear forces at the left-bottom side of the tunnel are not affected by the advancement of the new tunnel. Positive and negative shear forces are not affected by the change of pillar width and the maximum rate of change does not exceed 5%.

4.3.6 Behaviour of Shear Force at 6

Analysis results show that the shear forces at the left-top side of the tunnel tend to decrease as the advancement level of the second tunnel increases. After the passage of the second tunnel from the mid-length section of the first tunnel, shear forces start increasing and nearly reach the original value at the end of the last construction stage. This behaviour is valid for both different soil stiffnesses and different pillar width values. Figure 4.84 and Figure 4.85 show the typical shear force behaviour of the left-top side of the tunnel for the same pillar width. As shown in Figure 4.85, the maximum decrease in shear force is nearly same for all soil stiffnesses and is about 20% decrease.

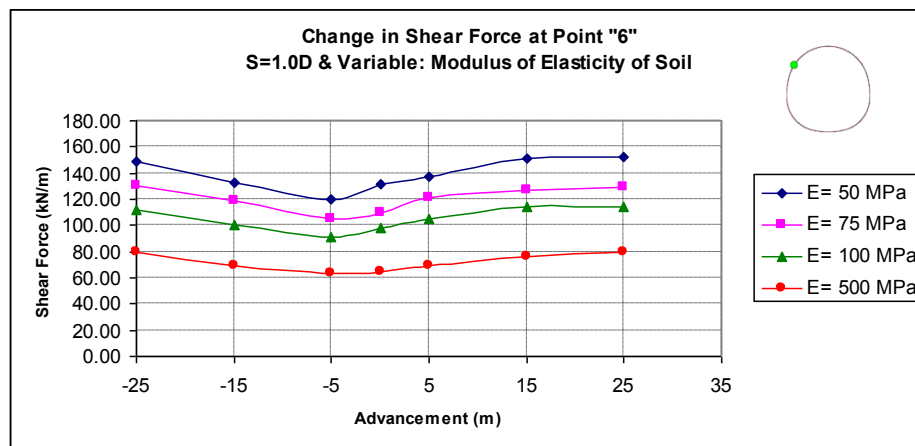


Figure 4.84 Shear force values at the left-top side of the tunnel

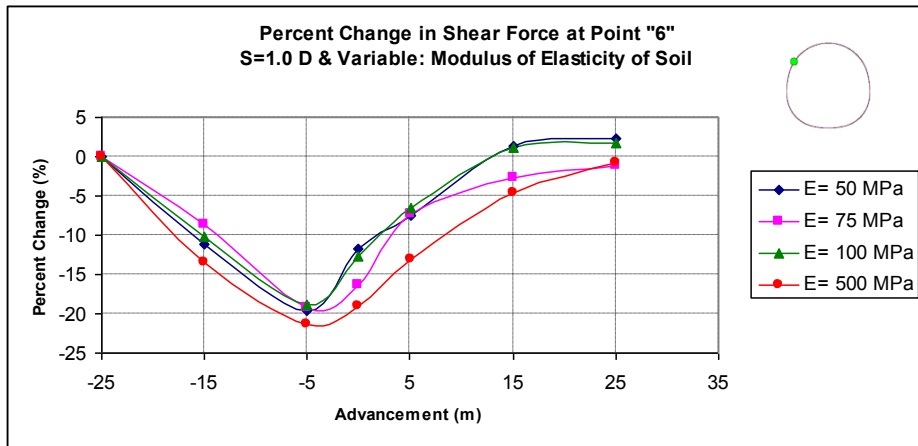


Figure 4.85 Percent change in shear force at the left-top side of the tunnel

A similar type of behaviour is determined for the cases in which soil stiffness is kept constant and pillar width is changed. The maximum amount of decrease occurs for the smallest pillar width value; but again shear force values return to its original value, nearly. Figure 4.86 and Figure 4.87 show the typical shear force behaviour of the left-top side of the tunnel for the same soil stiffness.

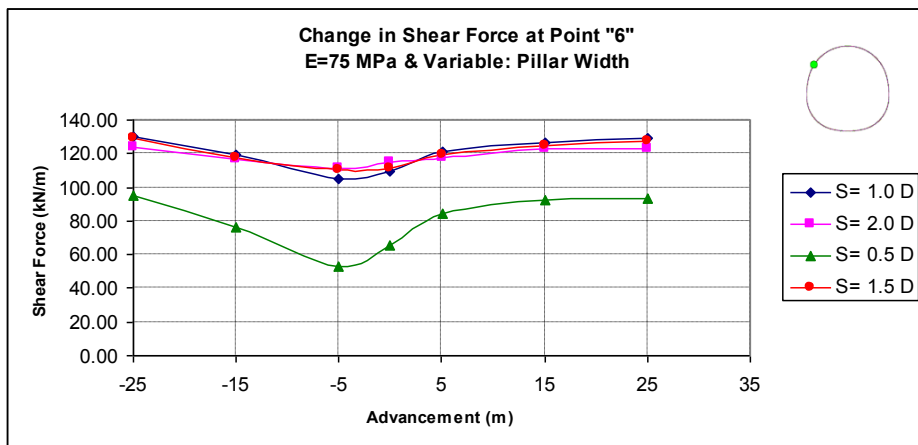


Figure 4.86 Shear force values at the left-top side of the tunnel

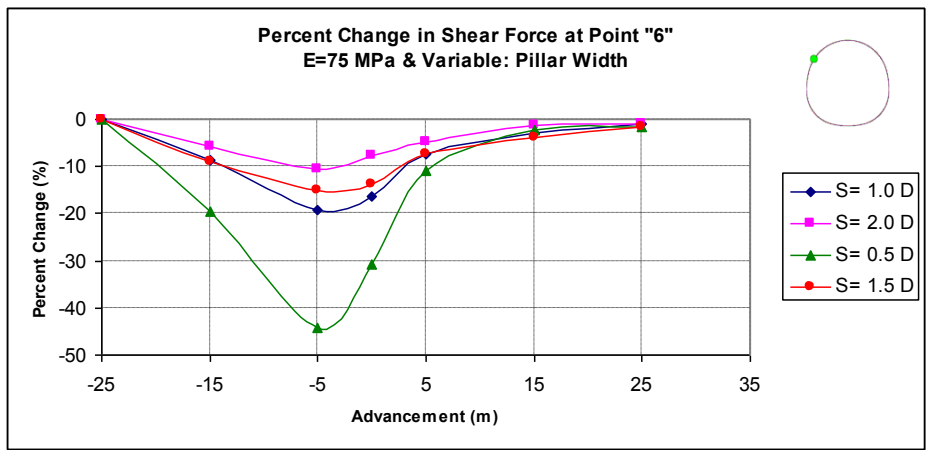


Figure 4.87 Percent change in shear force at the left-top side of the tunnel

CHAPTER 5

CONCLUSION

A parametric study has been carried out to determine the interaction effects of pillar width and the soil stiffness on the behaviour of displacement, bending moment and shear force of the previously constructed tunnel which is induced by the construction of a parallel tunnel. For the numerical modeling of generic cases, Plaxis 3D Tunnel geotechnical finite element package is used. Effects of pillar width, soil stiffness and the construction periods are presented.

The followings are the main conclusion of this study:

- As the second tunnel (right-hand side) advances in the direction of advancement, all displacement values at the locations of top, right-top, right-bottom and left-top increases. On the other hand, the displacement values decreases with the advancement at bottom and left-bottom of the previously constructed tunnel. This type of behaviour is valid for all cases of different pillar width and soil stiffness values. These parameters only affect the magnitude of the differences.
- The maximum amount of increase in displacements is determined generally for the cases of minimum soil stiffness and minimum pillar width combination for the increasing regions. The maximum increase is in the order of 55% and determined at the right-bottom of the tunnel. The minimum amount of increase is observed at the left-top side of the

tunnel and is in the order of 5% increase. On the other hand, the maximum amount of decrease is determined for the region left-bottom and is in the order of 70% decrease for combinations of 50 MPa soil stiffness with 1.0 D pillar width and 75 MPa soil stiffness with 0.5 D pillar width.

- In most of the cases of constant pillar width, the displacement values show similar tendencies independent from the soil stiffness which means that the displacement behaviour is controlled more dominantly by the pillar width than the soil stiffness.
- In general, plotted graphs of percent change of displacements vs. varying pillar width values show that pillar width values of greater than 2.5 – 3.0 D will show no or negligible interaction effects on displacements for tunnels constructed by NATM method in an average soil stiffness with shotcrete lining. Pillar width values smaller than 1.0 D show the interaction effects more evident. It is important to mention that, these recommendations may change for the linings of different stiffness.
- As the second tunnel (right-hand side) advances in the direction of advancement, all bending moment values at the locations of interest increases. Only, right-top side of the previously constructed tunnel shows a decreasing behaviour for the cases of pillar width equals to 1.5 D and 2.0 D. This type of behaviour is valid for all cases of different pillar width and soil stiffness values. These parameters only affect the magnitude of the differences.
- The maximum amount of increase in bending moment is determined generally for the cases of minimum soil stiffness and minimum pillar width. The maximum increase is in the order of 325% and determined at the right-bottom of the tunnel. The minimum amount of increase is

observed at the left-bottom side of the tunnel and is in the order of 4% increase.

- As compared with the displacement behaviour, change in soil stiffness results in more considerable changes in the behaviour of bending moments. But still, in some of the cases of constant pillar width, the bending moment values show similar tendencies independent from the soil stiffness which means that the bending moment behaviour is controlled more dominantly by the pillar width than the soil stiffness. While the small changes on soil stiffness result in negligible differences, a small increase or decrease in pillar width results in large differences on bending moments.
- In general, plotted graphs of percent change of bending moments vs. varying pillar width values show that pillar width values of greater than 2.5 – 3.0 D will show no or negligible interaction effects on bending moments for an average soil stiffness. Pillar width values smaller than 1.0 D show the interaction effects more evident.
- The shear force behaviour of the previously constructed tunnel is more complicated than the other investigated behaviours. The general trend for the most of the cases is such that the behaviour can be divided into two parts as the first half of the construction and the second half of the construction. The type of behaviour in the second half of the construction is usually the opposite of the first half of the construction. In the first half of the construction positive shear forces at the top, shear forces at the right-top, negative shear forces at right-bottom and shear forces at the left-top regions show decreasing behaviour. The remaining part of the regions shows increasing behaviour. Only left-bottom side of the tunnel is not affected by the construction of the new tunnel which result in no or negligible change in shear forces.

- The important point about the shear forces is that all investigated shear forces nearly return to their original value at the beginning after the construction of the second tunnel completed.
- The maximum amount of increase in shear force is determined generally for the cases of minimum soil stiffness and minimum pillar width. The maximum increase is determined at the bottom of the tunnel but, the amount of increase is incredibly high since the initial value is close to zero. The most considerable increase is determined at positive shear forces at right-bottom and negative shear forces at the top side of the tunnel and the increase is in the order of 80% for both of them.
- Analysis results show that all shear forces nearly return to their original values at the end of the construction of the second tunnel. In this point of view it may be concluded that the final values of shear forces are nearly independent from both the soil stiffness and the pillar width. On the other hand, intermediate construction stages may be critical especially for low values of soil stiffness and pillar width. In such a case a detailed analyses may be needed for the case which represents the real situation.

REFERENCES

Addenbrooke, T.I., Potts, D.M. (1996). "Twin tunnel construction – ground movements and lining behaviour," *1st International Geotechnical Aspects of Underground Construction in Soft Ground*, pp. 441-446.

Cheade Hage, F., Shahrour, I. (2007). "Numerical analysis of the interaction between twin-tunnels: Influence of the relative position and construction procedure." *Tunnelling and Underground Space Technology*, Vol. 23 (2008), pp. 210-214.

Chern, J.C., Hsiao, F.Y. (2005). "Interaction behaviour of the Hsuehshan Tunnels," *World 2005 Long Tunnels*, pp. 73-73.

Chu, B.L., Hsu, S.C., Chang, Y.L. and Lin, Y.S. (2007). "Mechanical behaviour of a twin tunnel in multi-layered formations," *Tunnelling and Underground Space Technology*, Vol. 22 (2007), pp. 351-362.

Dunaevskii, R.A. (1986). "Stresses and forces in linings of two non circular paralel tunnels." *Gidrotekhnicheskoe Stroitel'stvo*, Vol. 12 , pp. 25-27

Fotieva, N.N., Sheinin, V.I. (1966). "Distribution of stresses in the lining of a circular tunnel when driving a parallel tunnel", *Fundamenty i Mekhanika Gruntov*, No.6, pp.26-29.

Gerçek, H. (1988). "Interaction of parallel tunnels and roadways." *Madencilik*, Volume XXVII, No.1, pp. 39-50 (In Turkish)

Gerçek, H. (2005). "Interaction between parallel underground openings." *The 19th International Mining Congress and Fair of Turkey*, pp. 73-81.

Ghaboussi, J., Ranken, R.E. (1977). "Interaction between two parallel tunnels," *International Journal for Numerical and Analytical Methods in Geomechanics*, Volume 1, pp. 75-103.

Gnilsen, R. (1989). "*Underground Structures Design and Instrumentation*," Elsevier, Amsterdam, pp. 84-128.

Karakus, M., Ozsan, A., Basarir, H. (2007). "Finite element analysis for the twin metro tunnel constructed in Ankara clay, Turkey," *Bulletin of Engineering Geology and the Environment*, Vol. 66 (2007), pp. 71-79.

Kim, S.H., Burd, H.J., Milligan, G.W.E. (1998). "Model testing of closely spaced tunnels in clay," *Geotechnique*, Vol. 48, pp. 375-388.

Kolymbas, D. (2005). "*Tunnelling and Tunnel Mechanics A Rational Approach to Tunnelling*," Springer, pp. 171-173.

Kooi, C.B., Verruijt, A. (2001). "Interaction of circular holes in an infinite elastic medium," *Tunnelling and Underground Space Technology*, No. 16, pp. 59-62.

Lee, S.C., Lu, F.S., Lee, K.W. (2005). "Interaction behaviours during the excavation for three parallel tunnel," *World 2005 Long Tunnels*, pp. 91-104

Megaw, T.M., Bartlett, V. (1981). "*Tunnels: Planning, Design, Construction*," Volume 1, Ellis Horwood Limited, West Sussex, pp.11-18.

Ng, C.W.W., Lee, K.M., Tang, D.K.W. (2004). "Three dimensional numerical investigations of new Austrian tunneling method (NATM) twin tunnel interactions," *Canadian Geotechnical Journal*, Vol.41, pp. 523-539

Plaxis 3D Tunnel Material Models Manual. (2001). Delft University of Technology & PLAXIS B.V.

Plaxis 3D Tunnel Reference Manual. (2001). Delft University of Technology & PLAXIS B.V.

Sinha, R.S. (1989). "*Underground Structures Design and Instrumentation*," Elsevier, Amsterdam, pp. 17-19

TS 500, Requirements for Design and Construction of Reinforced Concrete Structures (February 2000)

APPENDIX A

DISPLACEMENTS

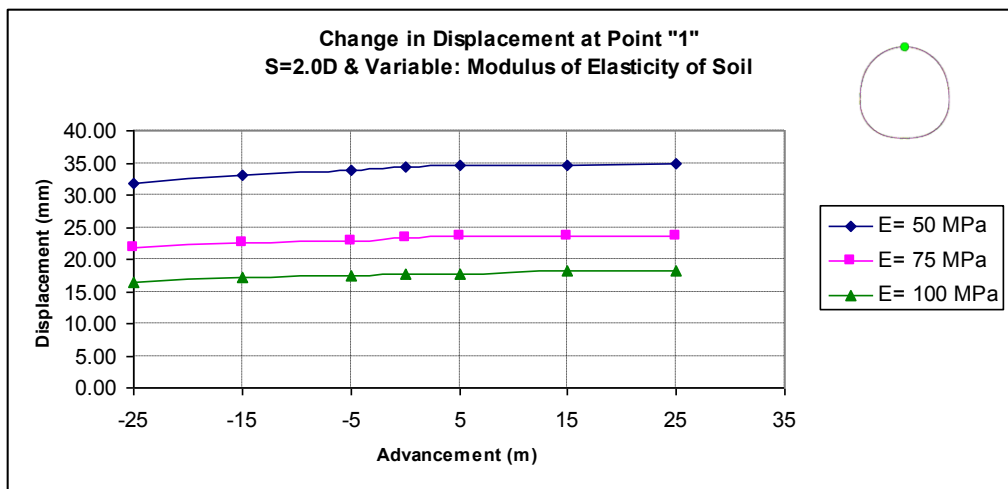


Figure A.1 Displacement values at the top side of the tunnel

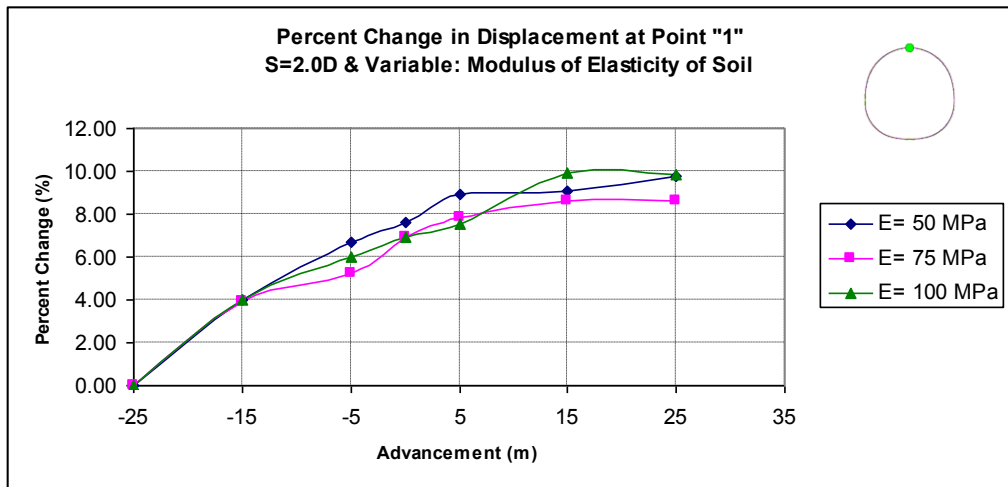


Figure A.2 Percent change in displacement at the top side of the tunnel

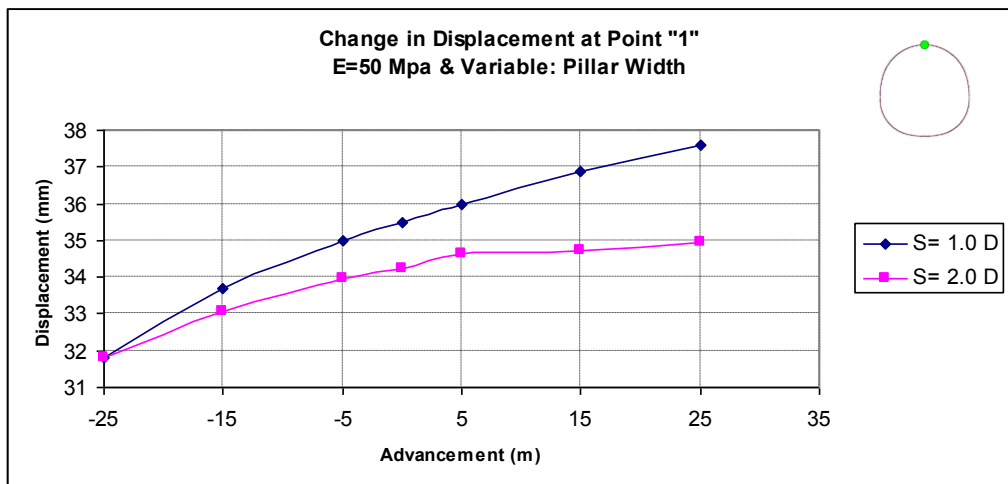


Figure A.3 Displacement values at the top side of the tunnel

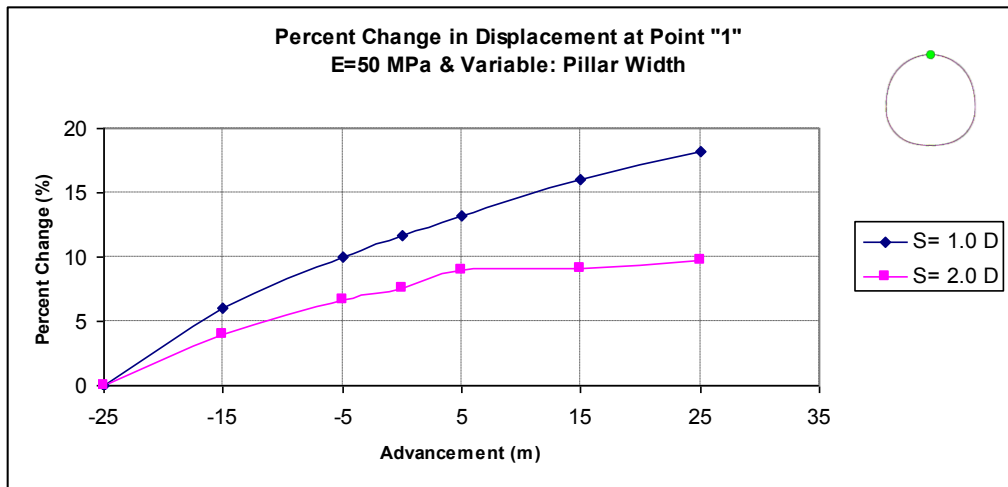


Figure A.4 Percent change in displacement at the top side of the tunnel

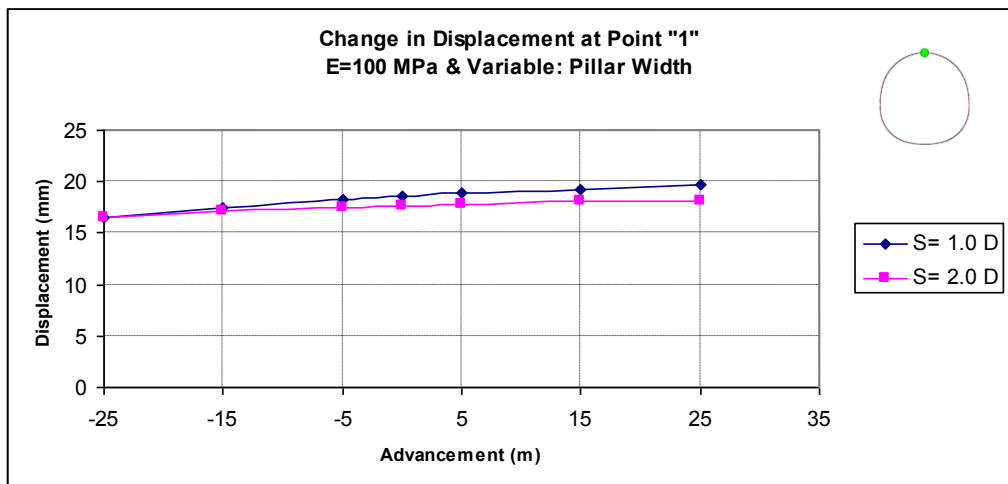


Figure A.5 Displacement values at the top side of the tunnel

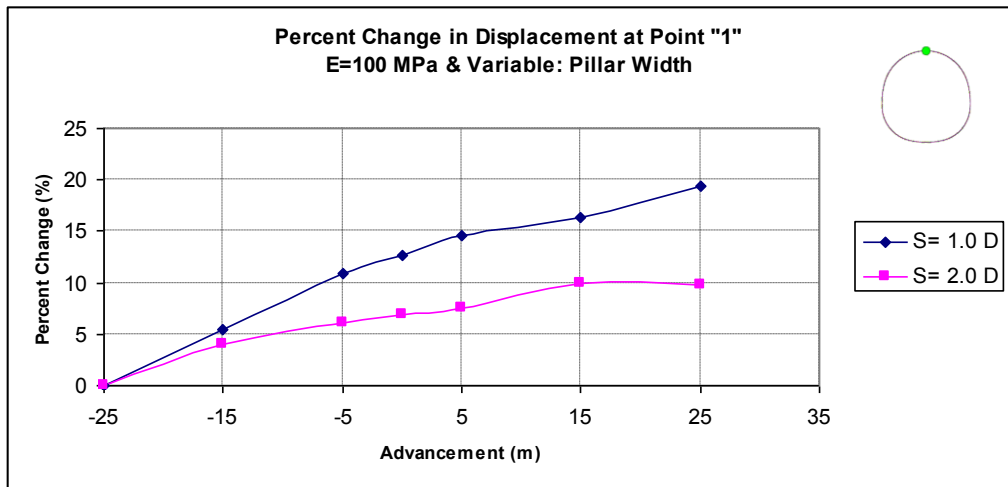


Figure A.6 Percent change in displacement at the top side of the tunnel

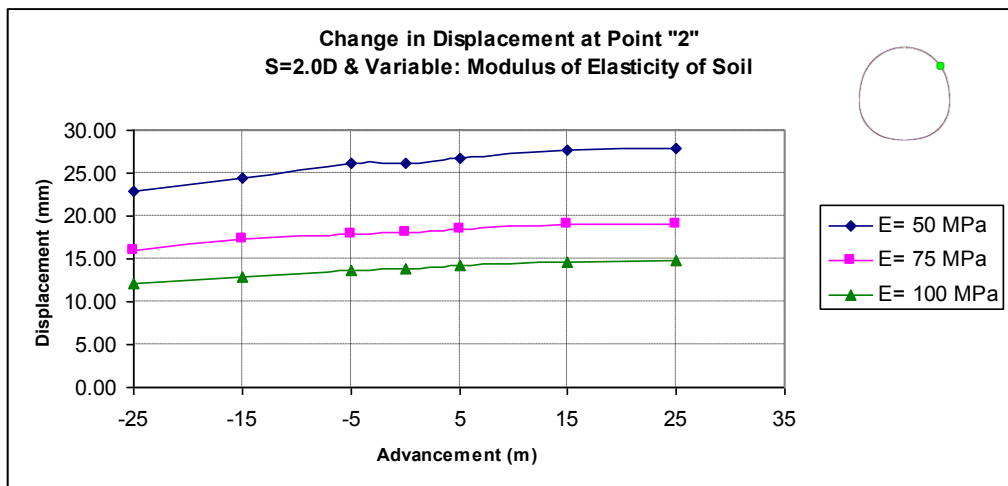


Figure A.7 Displacement values at the right-top side of the tunnel

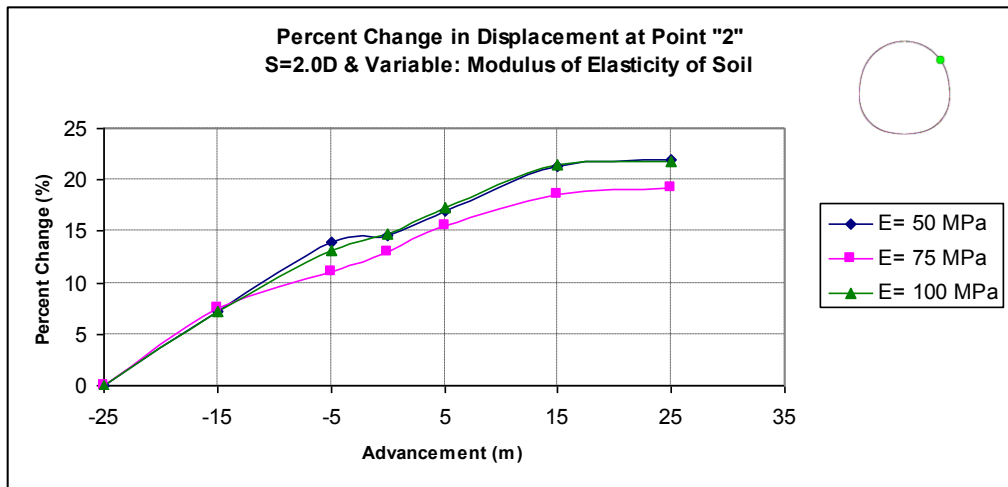


Figure A.8 Percent change in displacement at the right-top side of the tunnel

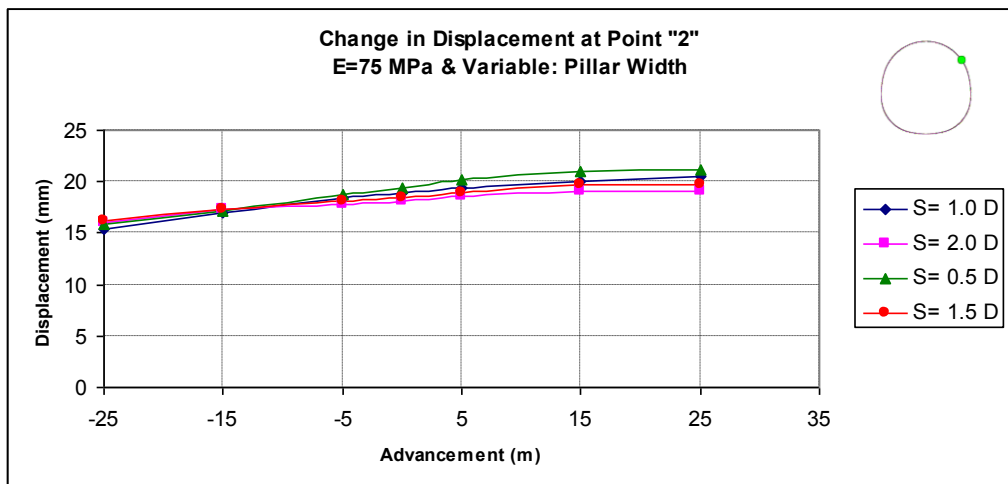


Figure A.9 Displacement values at the right-top side of the tunnel

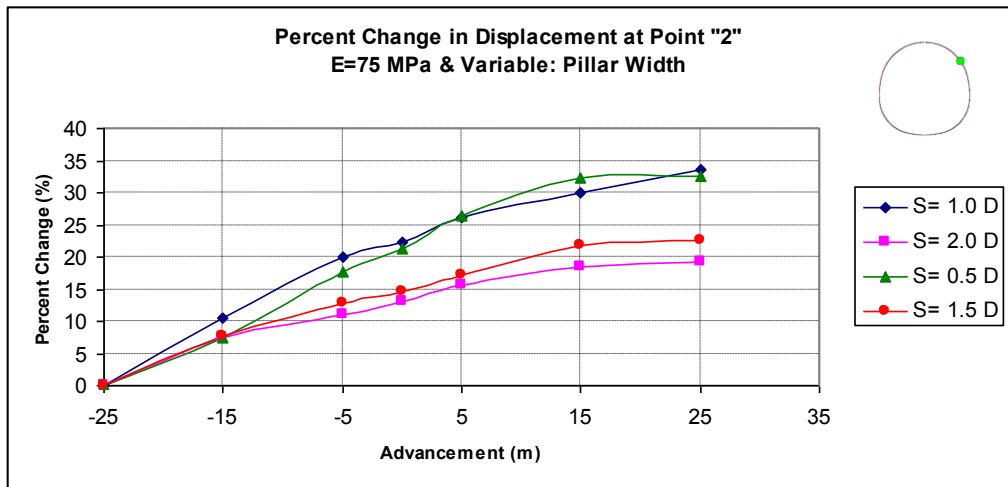


Figure A.10 Percent change in displacement at the right-top side of the tunnel

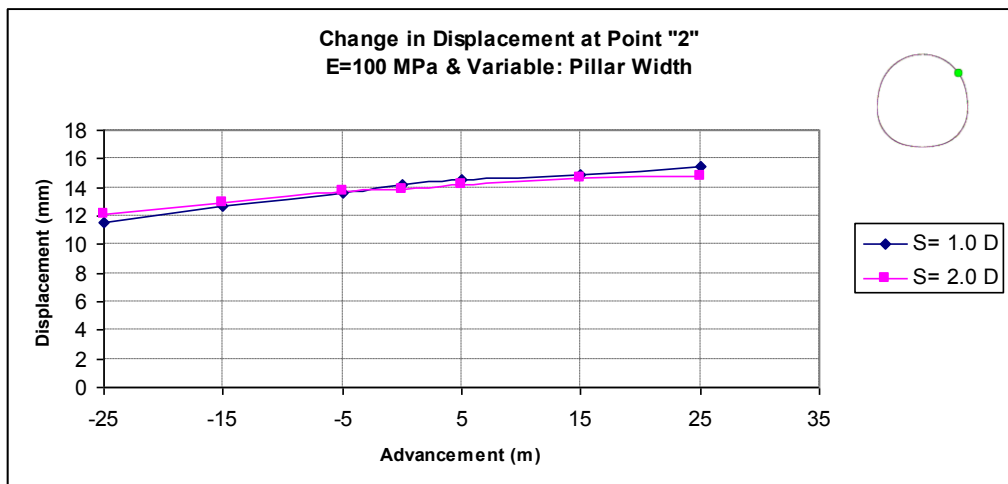


Figure A.11 Displacement values at the right-top side of the tunnel

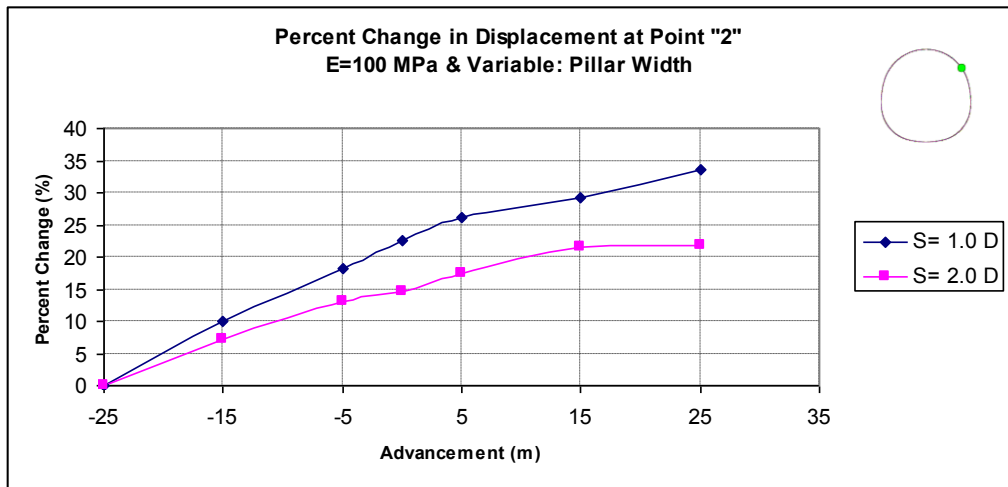


Figure A.12 Percent change in displacement at the right-top side of the tunnel

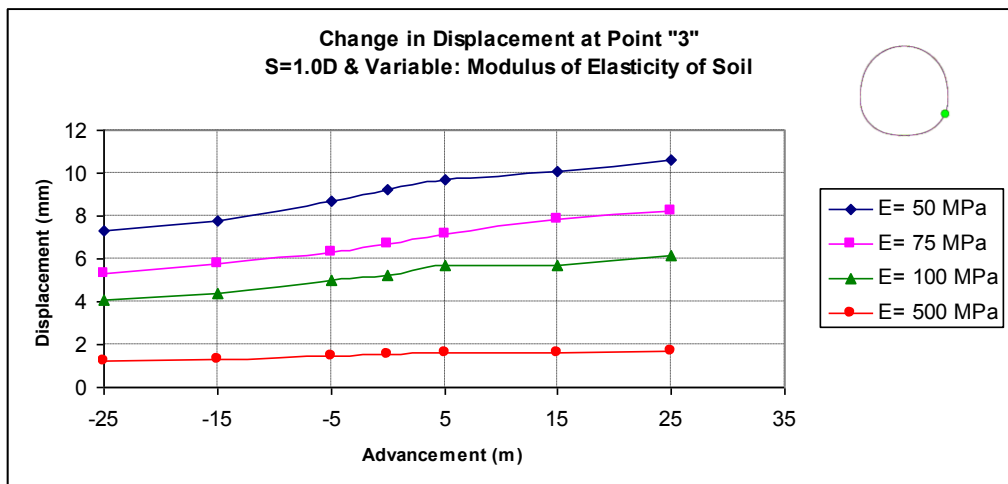


Figure A.13 Displacement values at the right-bottom side of the tunnel

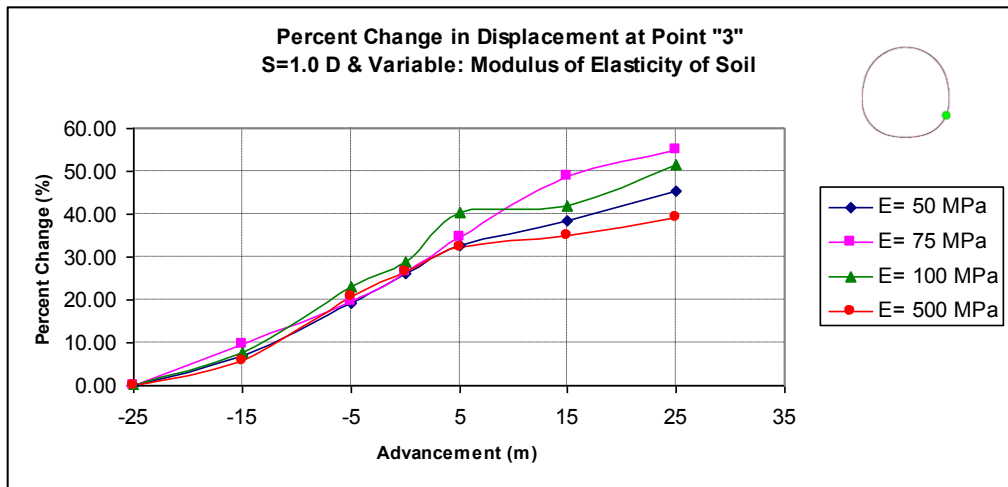


Figure A.14 Percent change in displacement at the right-bottom side of the tunnel

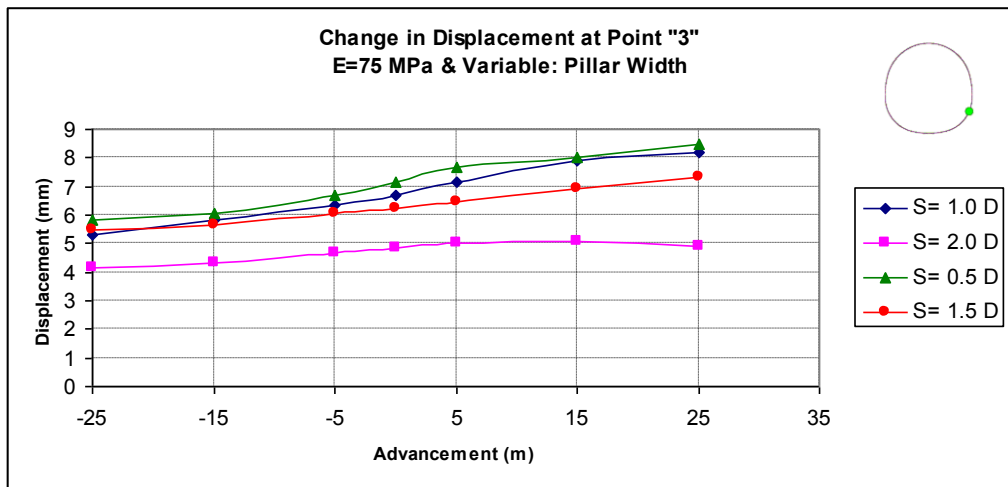


Figure A.15 Displacement values at the right-bottom side of the tunnel

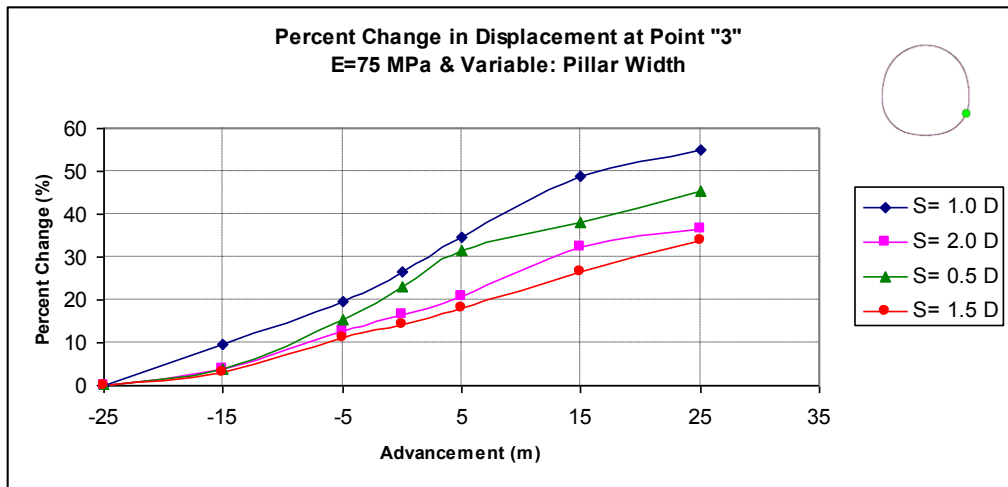


Figure A.16 Percent change in displacement at the right-bottom side of the tunnel

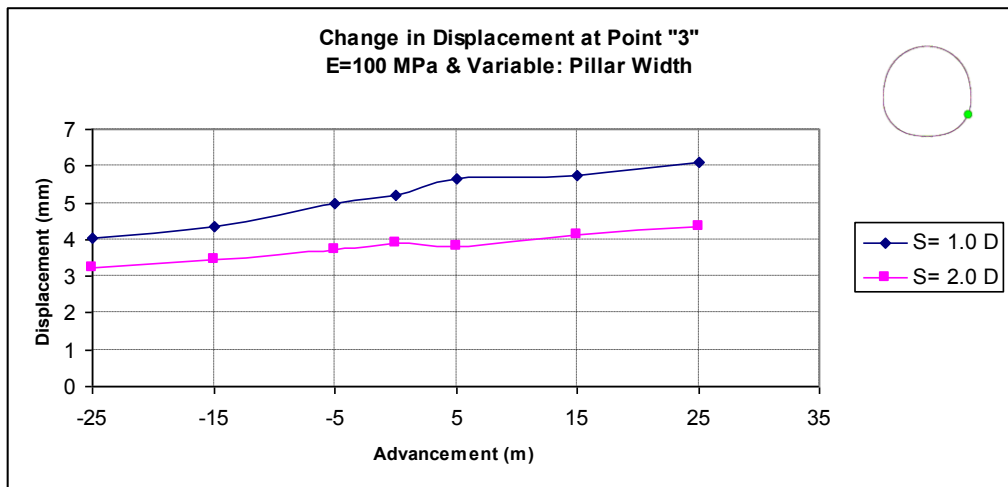


Figure A.17 Displacement values at the right-bottom side of the tunnel

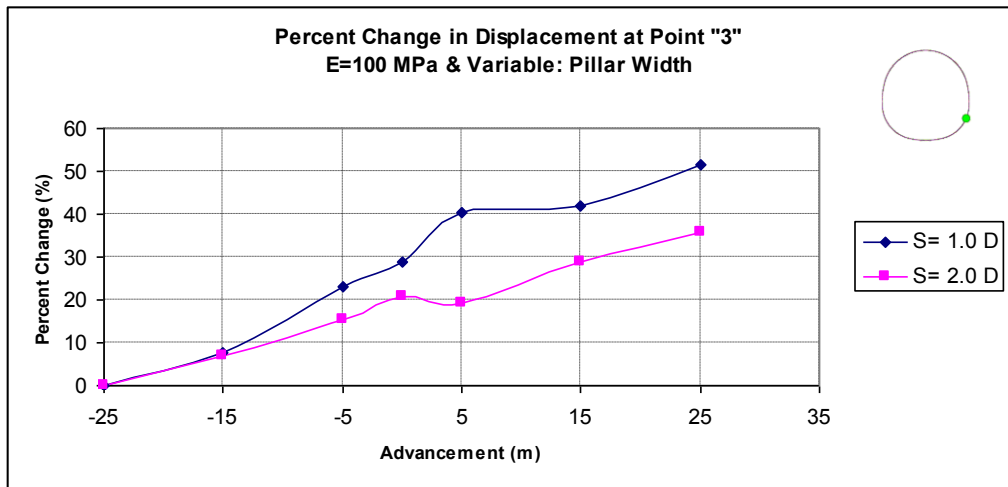


Figure A.18 Percent change in displacement at the right-bottom side of the tunnel

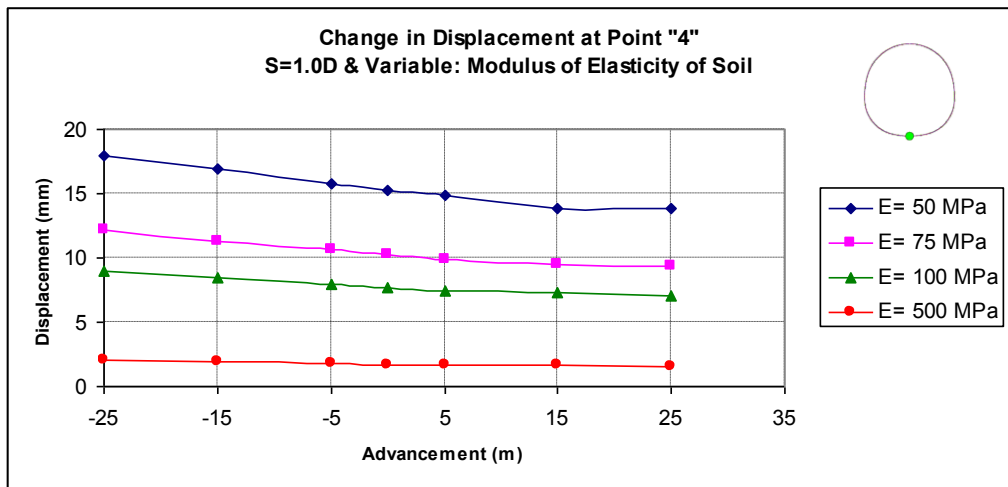


Figure A.19 Displacement values at the bottom side of the tunnel

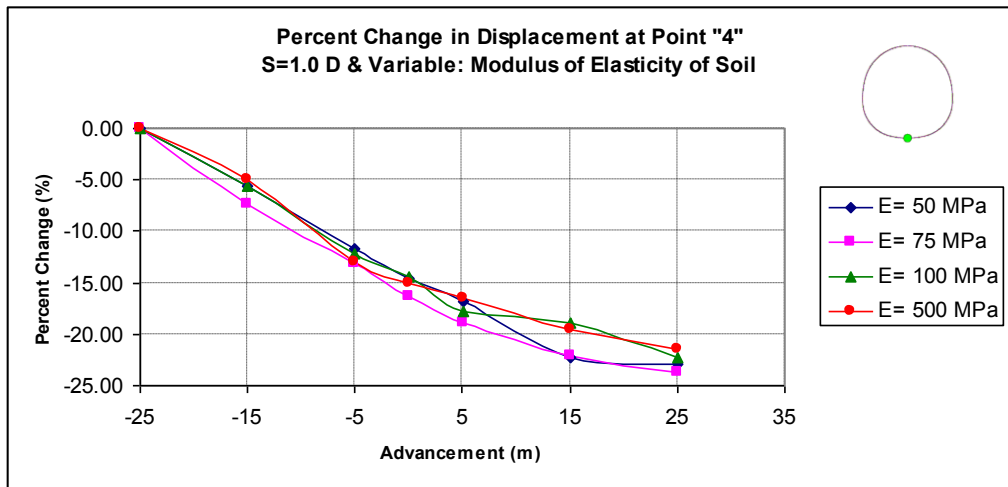


Figure A.20 Percent change in displacement at the bottom side of the tunnel

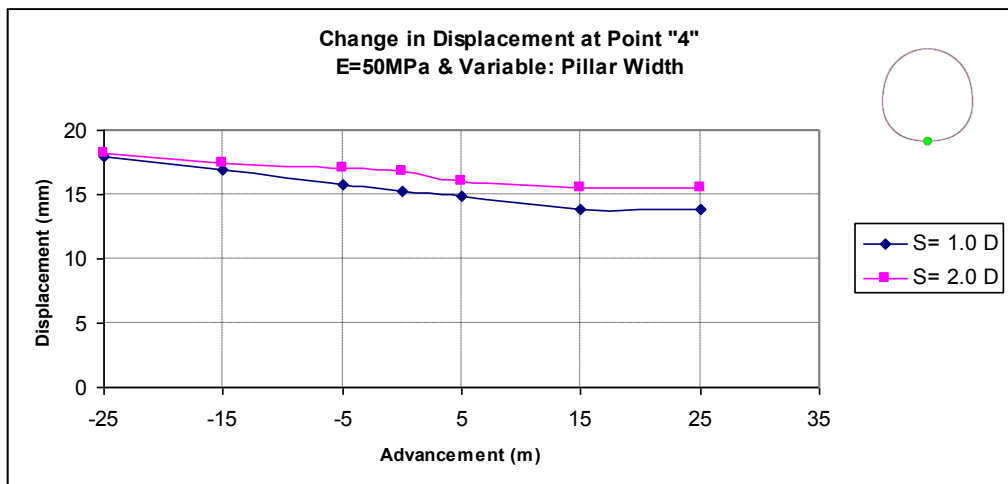


Figure A.21 Displacement values at the bottom side of the tunnel

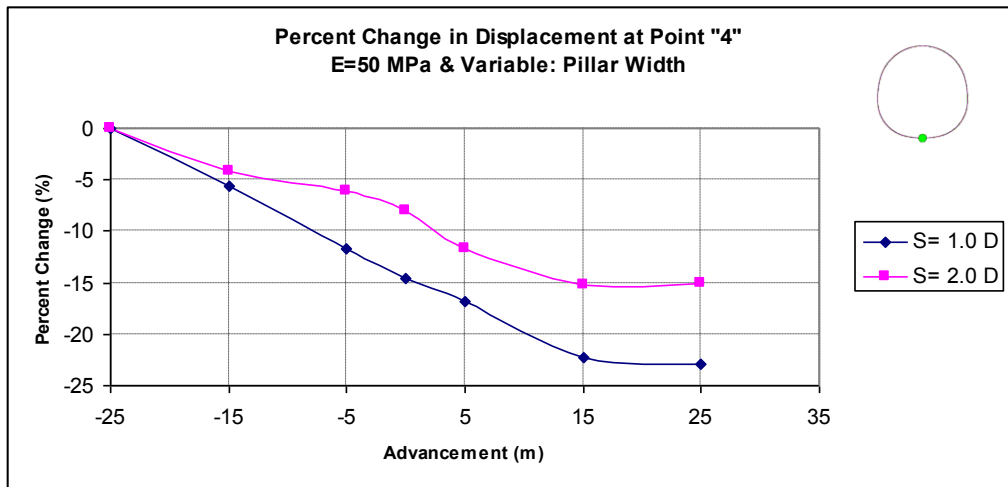


Figure A.22 Percent change in displacement at the bottom side of the tunnel

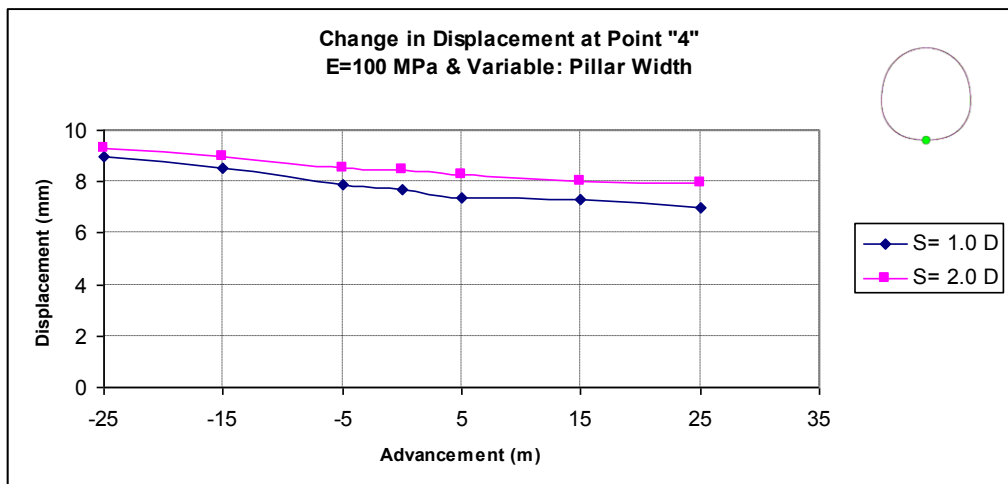


Figure A.23 Displacement values at the bottom side of the tunnel

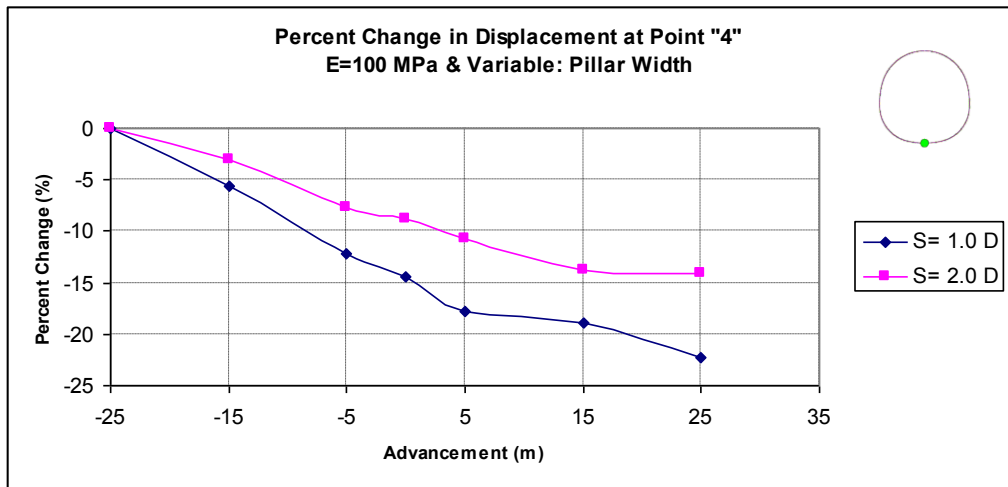


Figure A.24 Percent change in displacement at the bottom side of the tunnel

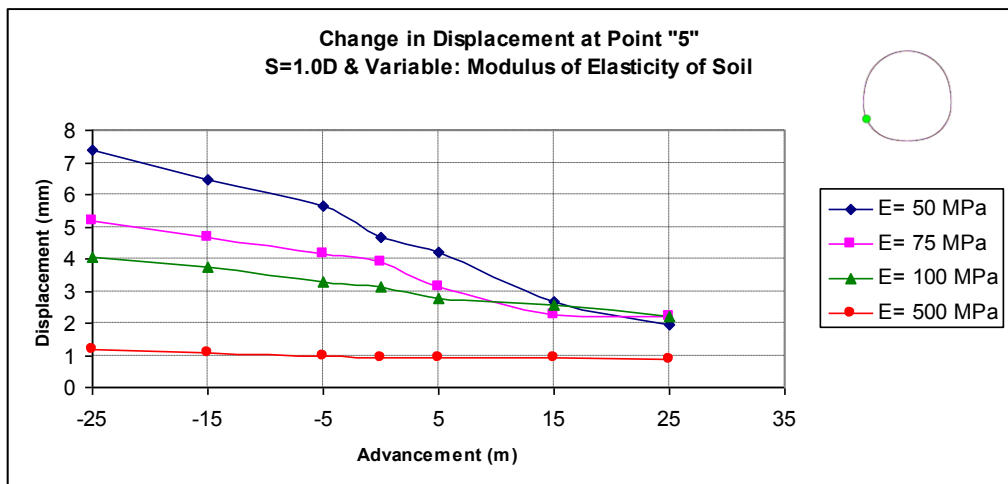


Figure A.25 Displacement values at the left-bottom side of the tunnel

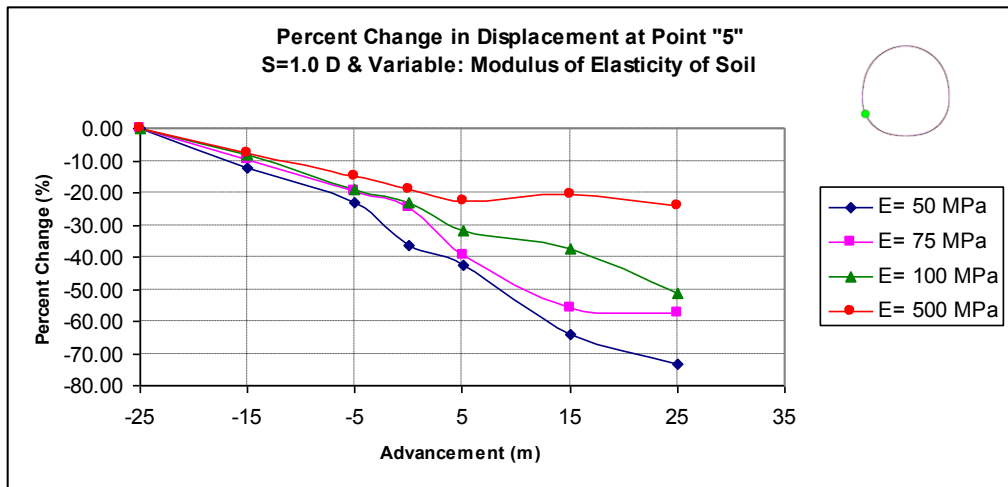


Figure A.26 Percent change in displacement at the left-bottom side of the tunnel

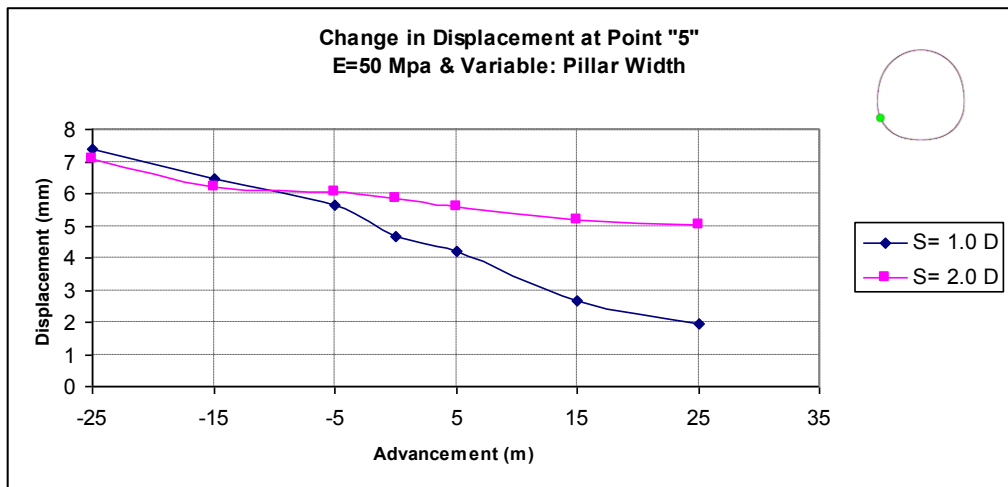


Figure A.27 Displacement values at the left-bottom side of the tunnel

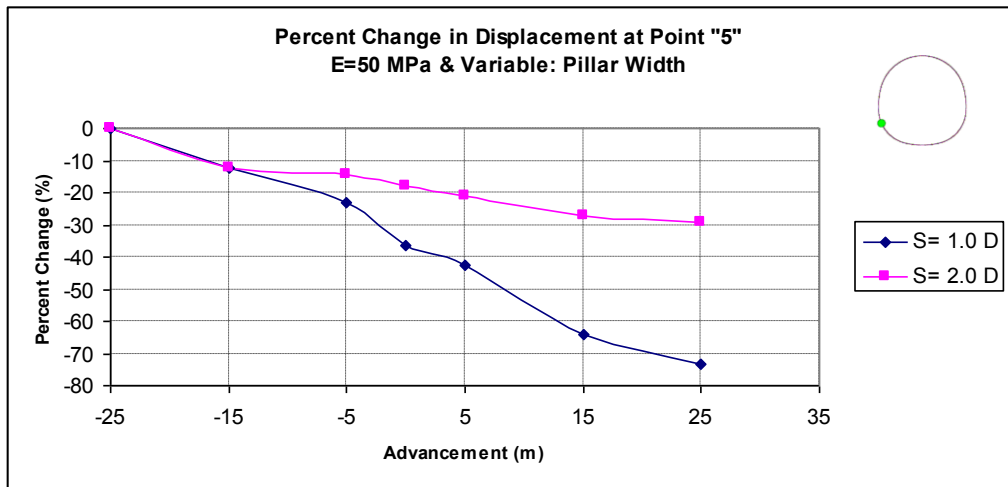


Figure A.28 Percent change in displacement at the left-bottom side of the tunnel

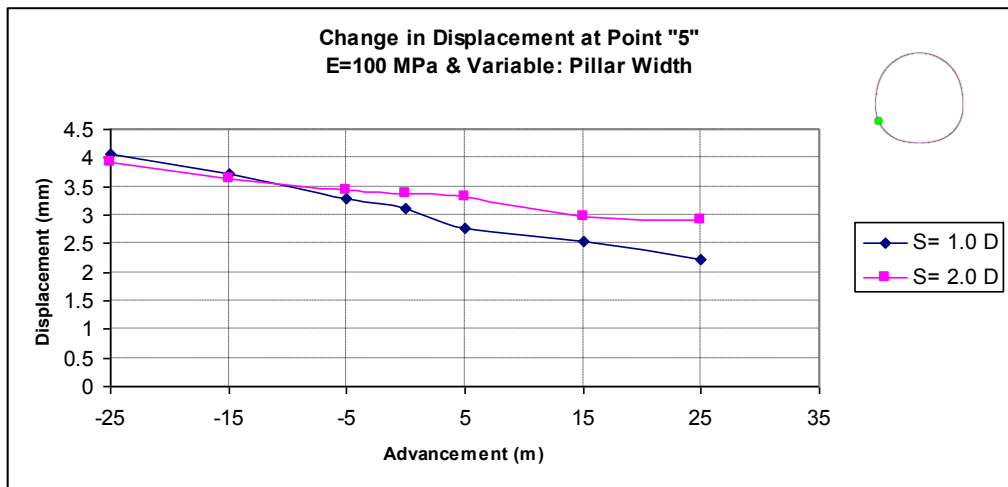


Figure A.29 Displacement values at the left-bottom side of the tunnel

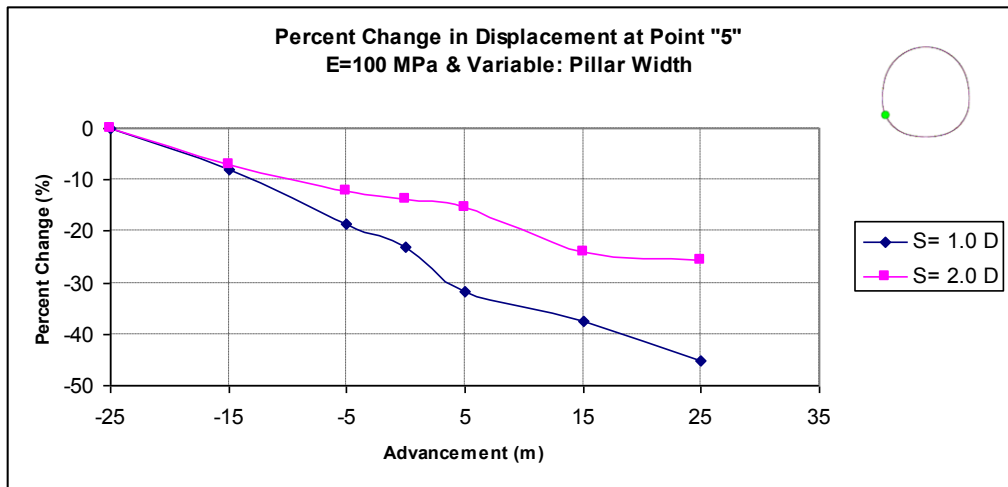


Figure A.30 Percent change in displacement at the left-bottom side of the tunnel

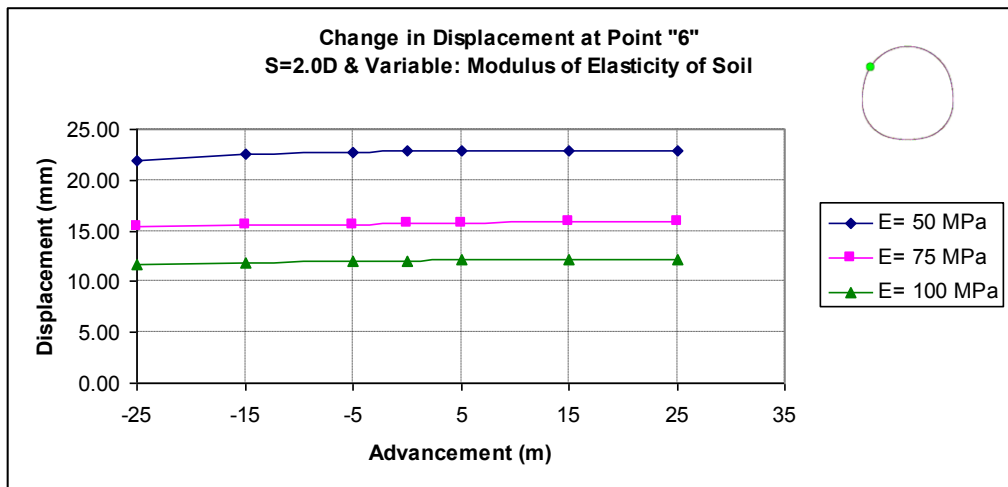


Figure A.31 Displacement values at the left-top side of the tunnel

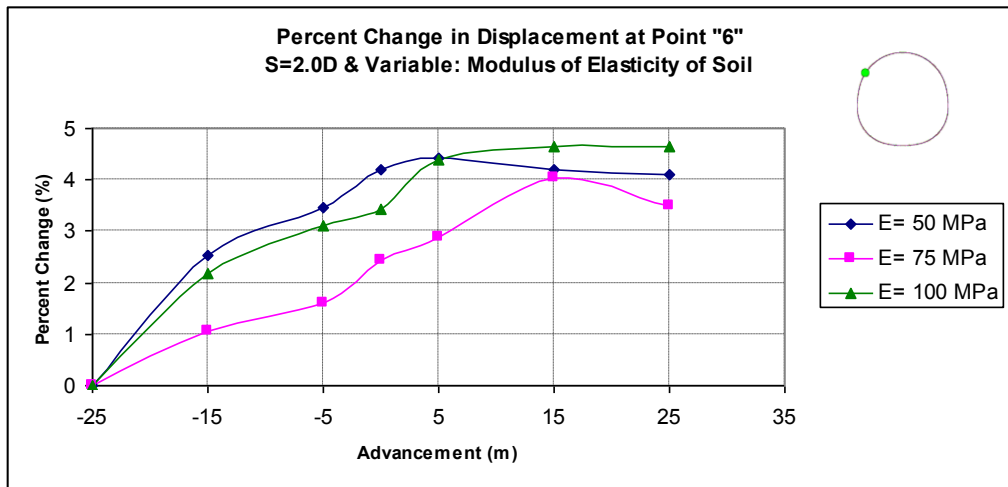


Figure A.32 Percent change in displacement at the left-top side of the tunnel

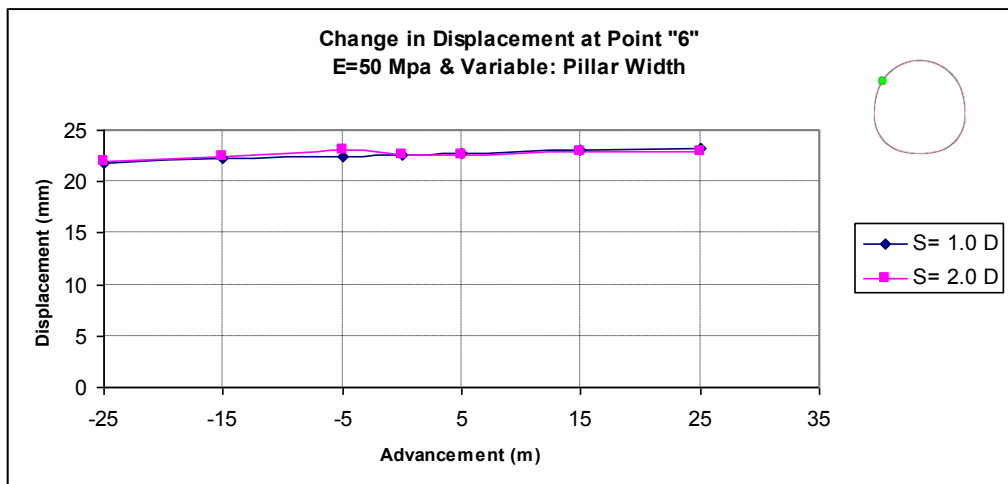


Figure A.33 Displacement values at the left-top side of the tunnel

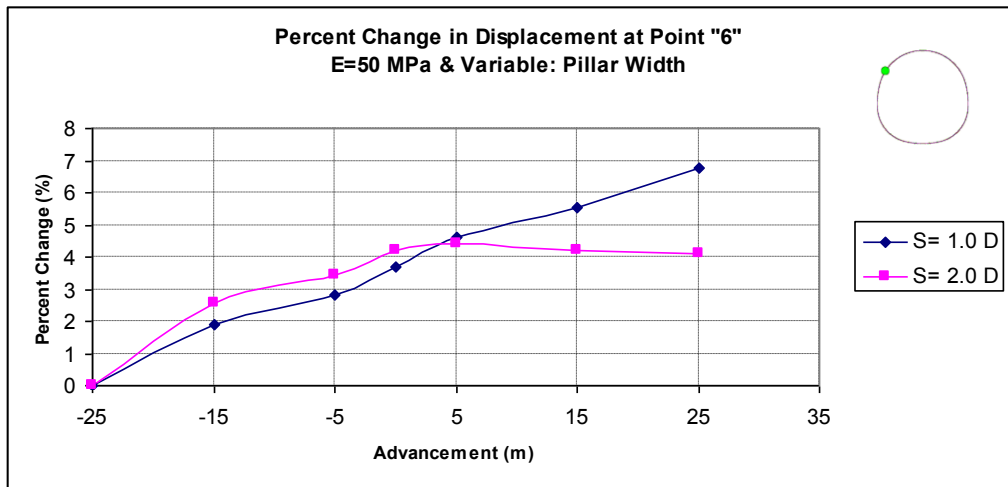


Figure A.34 Percent change in displacement at the left-top side of the tunnel

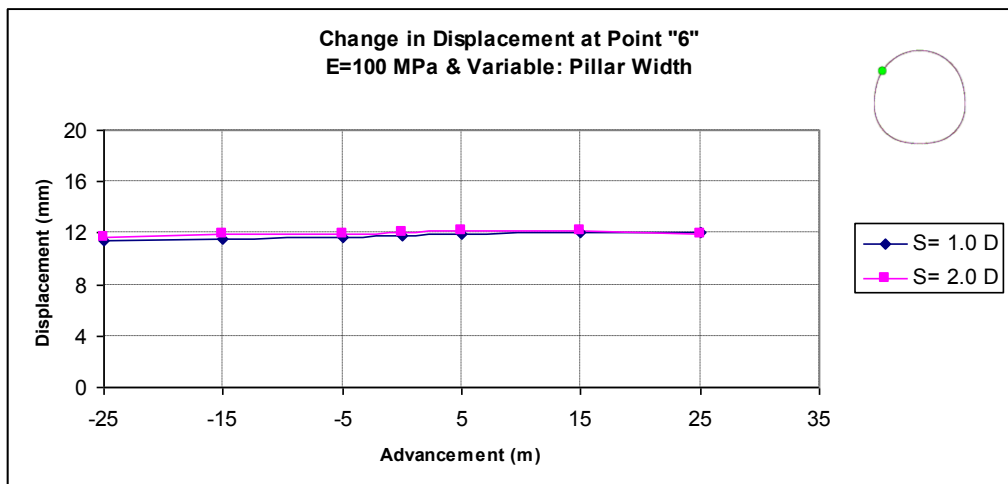


Figure A.35 Displacement values at the left-top side of the tunnel

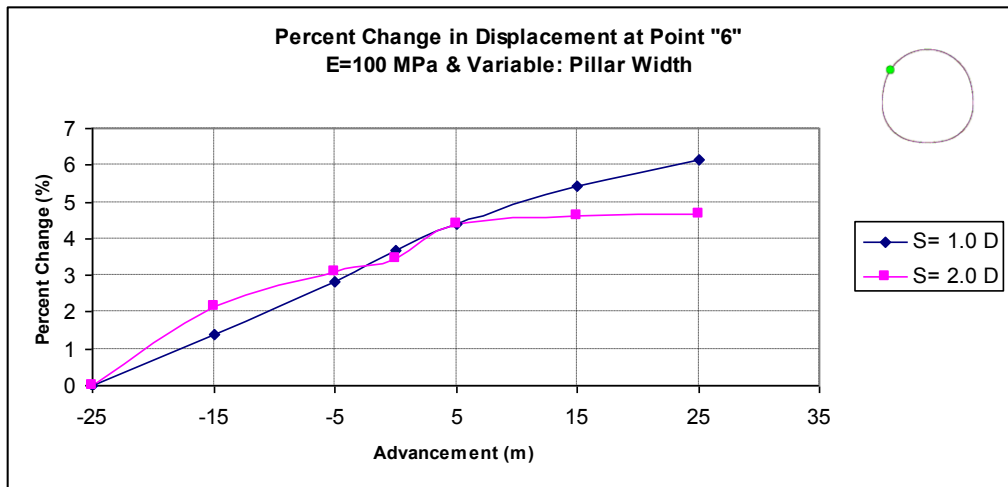


Figure A.36 Percent change in displacement at the left-top side of the tunnel

APPENDIX B

BENDING MOMENTS

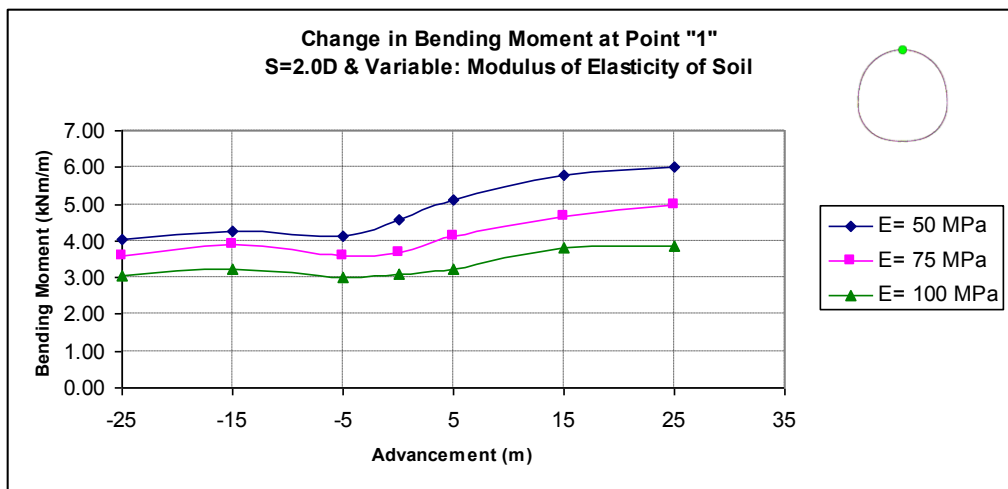


Figure B.1 Bending moment values at the top side of the tunnel

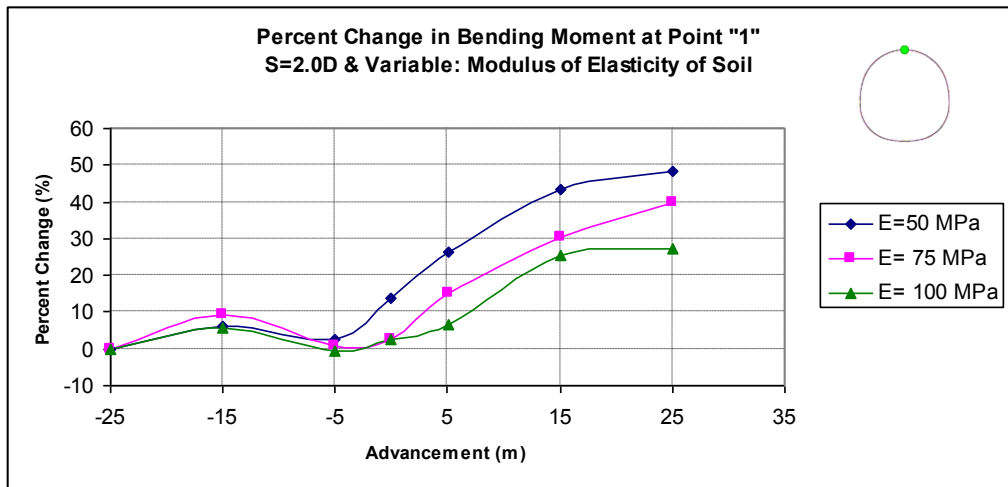


Figure B.2 Percent change in bending moment at the top side of the tunnel

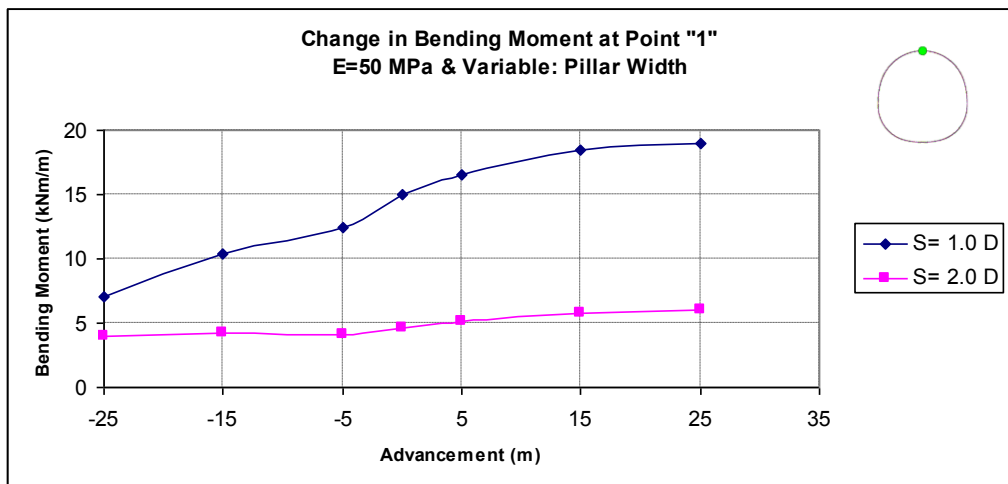


Figure B.3 Bending moment values at the top side of the tunnel

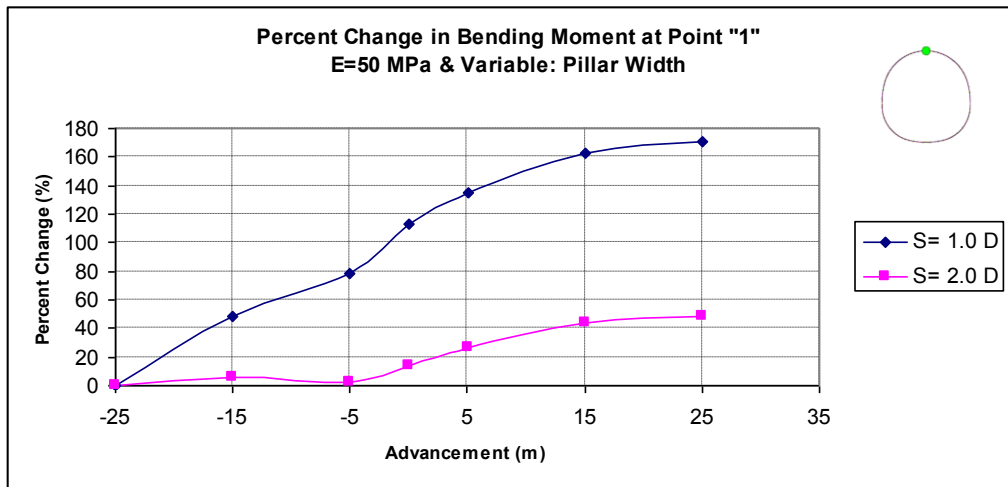


Figure B.4 Percent change in bending moment at the top side of the tunnel

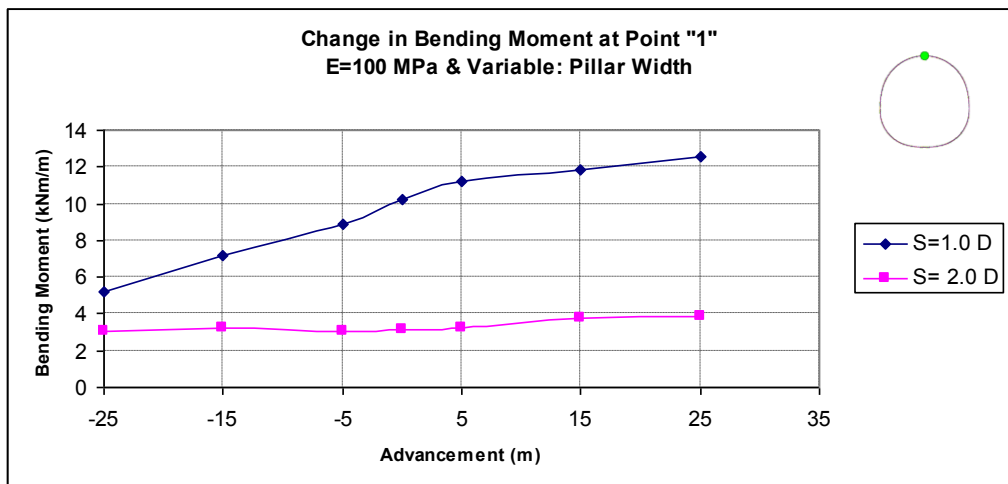


Figure B.5 Bending moment values at the top side of the tunnel

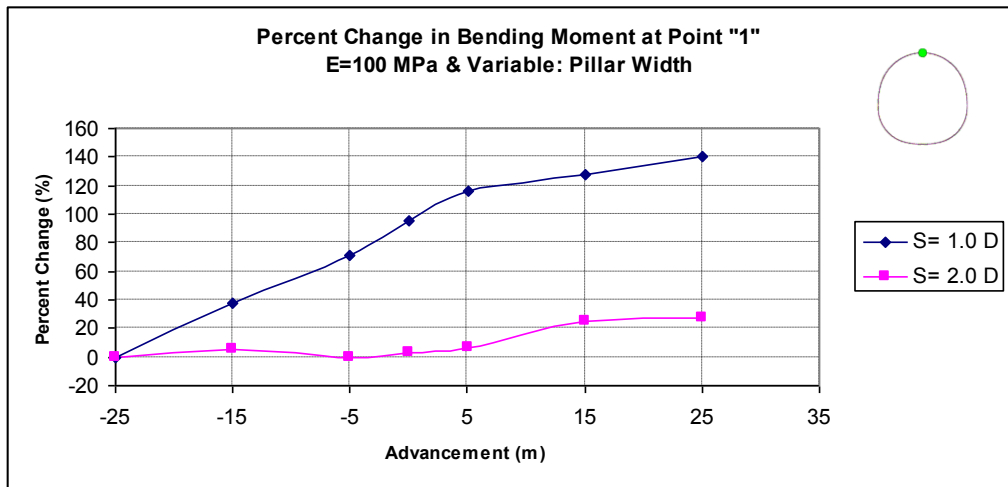


Figure B.6 Percent change in bending moment at the top side of the tunnel

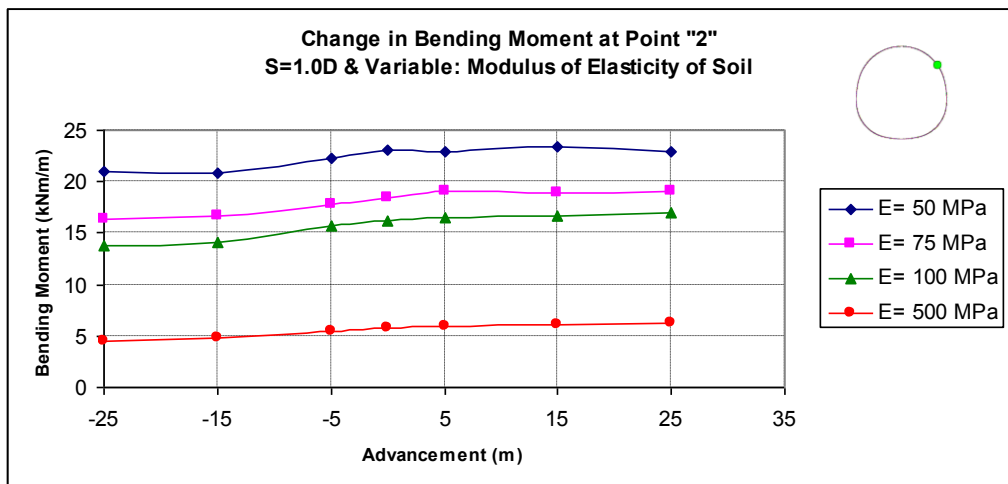


Figure B.7 Bending moment values at the right-top side of the tunnel

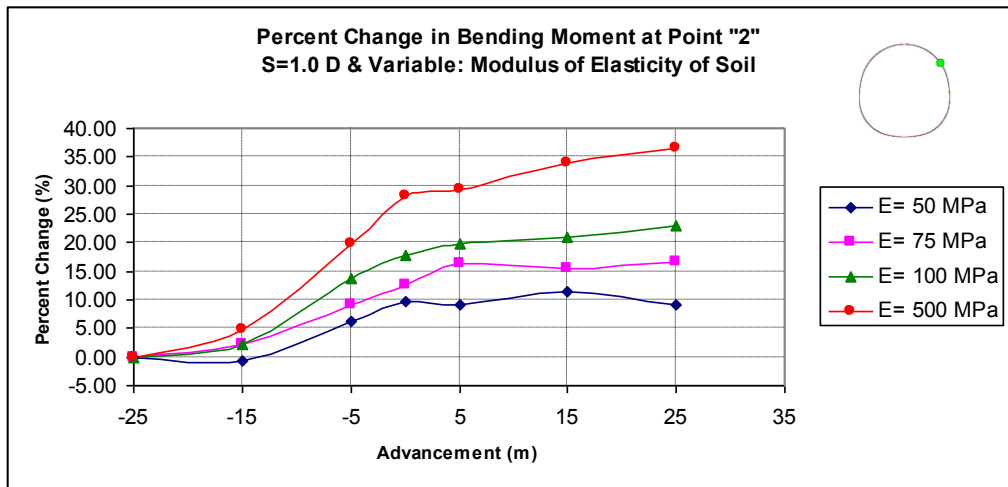


Figure B.8 Percent change in bending moment at the right-top side of the tunnel

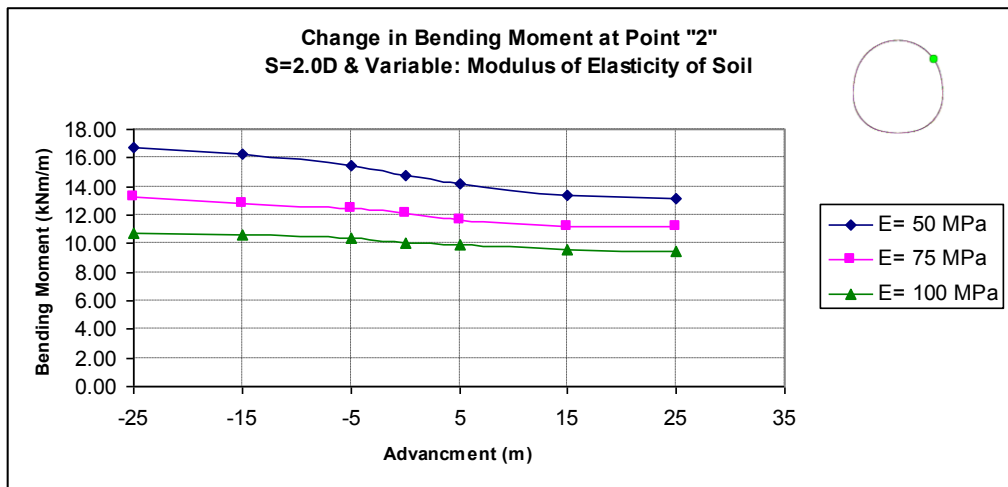


Figure B.9 Bending moment values at the right-top side of the tunnel

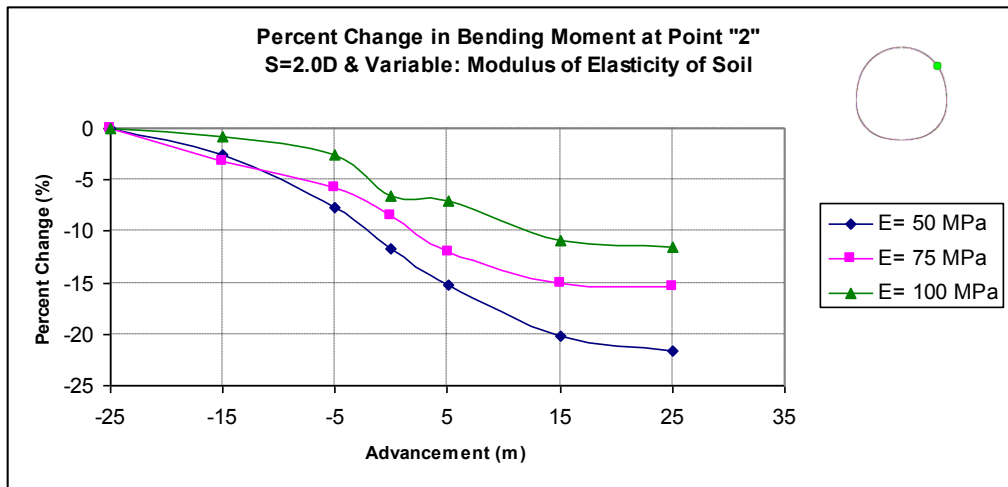


Figure B.10 Percent change in bending moment at the right-top side of the tunnel

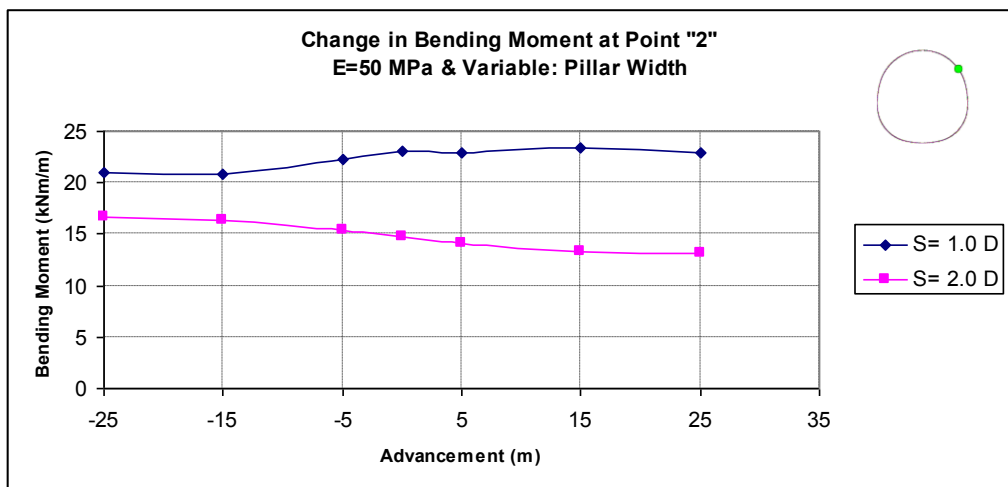


Figure B.11 Bending moment values at the right-top side of the tunnel

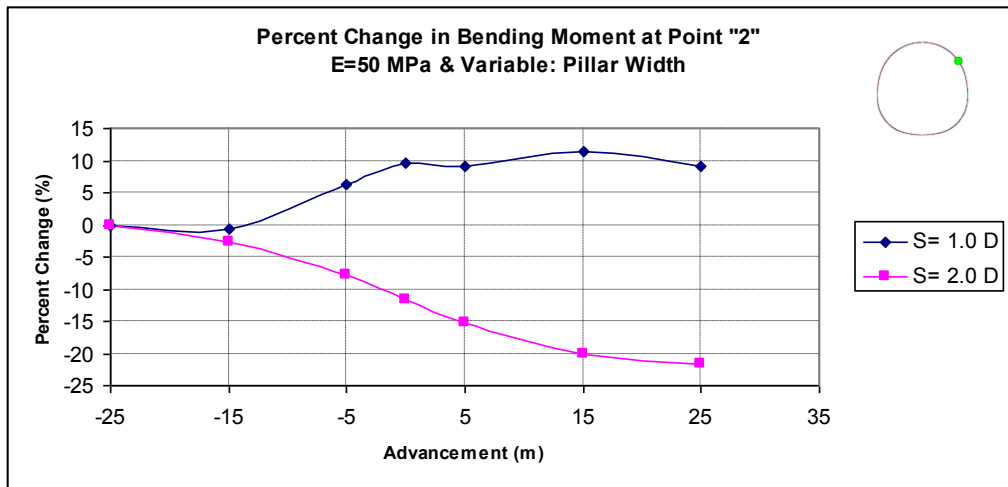


Figure B.12 Percent change in bending moment at the right-top side of the tunnel

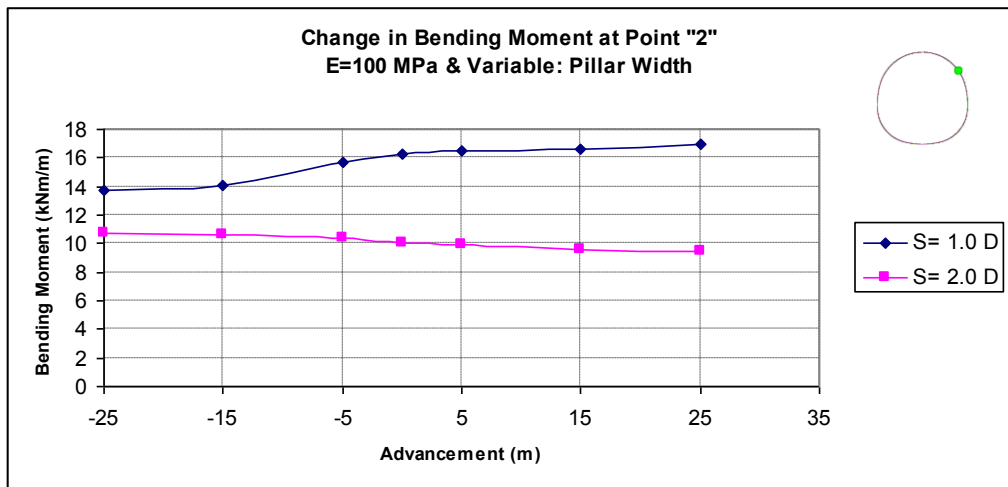


Figure B.13 Bending moment values at the right-top side of the tunnel

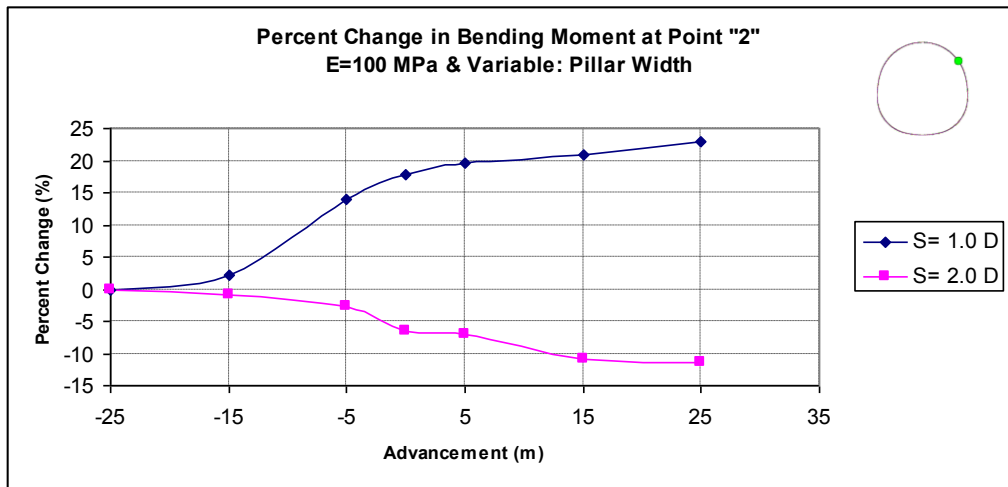


Figure B.14 Percent change in bending moment at the right-top side of the tunnel

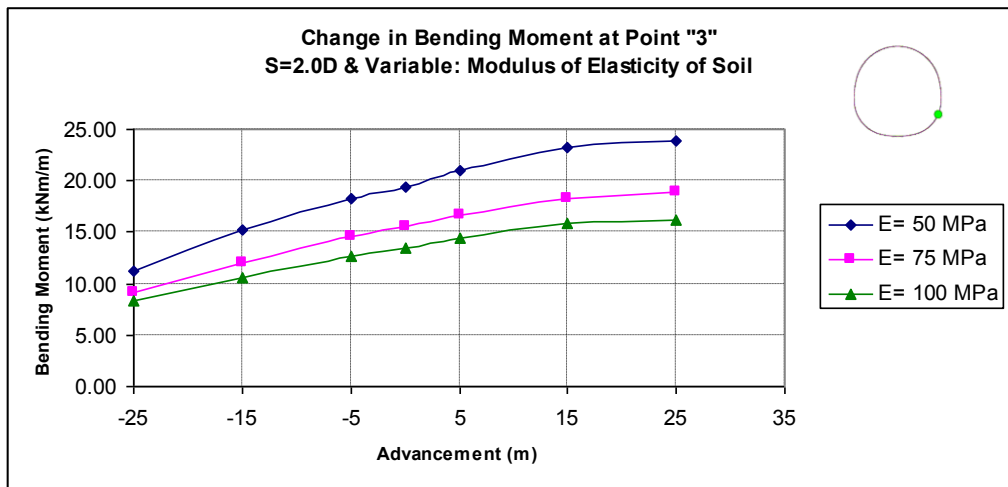


Figure B.15 Bending moment values at the right-bottom side of the tunnel

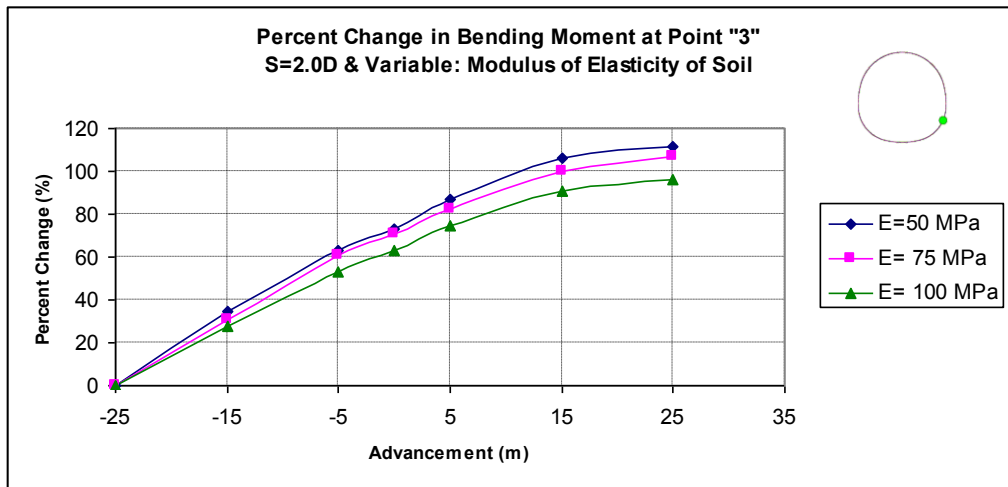


Figure B.16 Percent change in bending moment at the right-bottom side of the tunnel

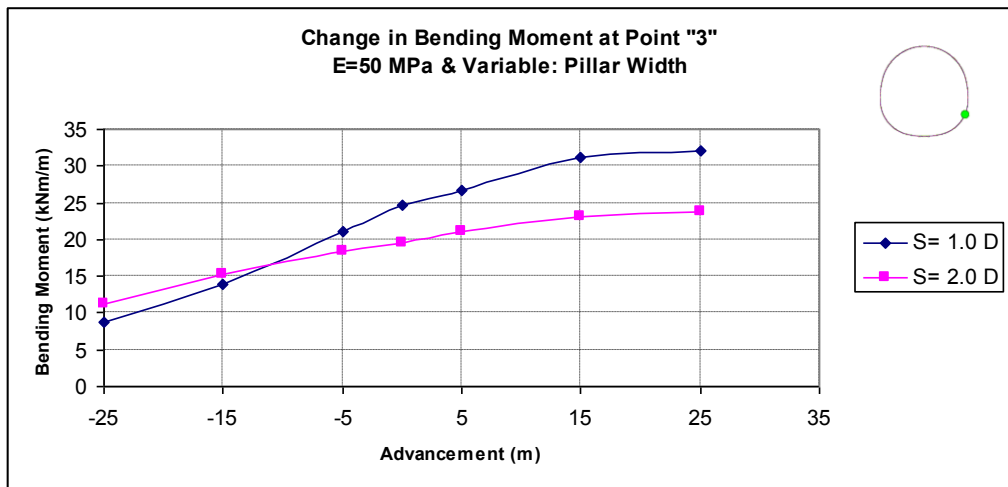


Figure B.17 Bending moment values at the right-bottom side of the tunnel

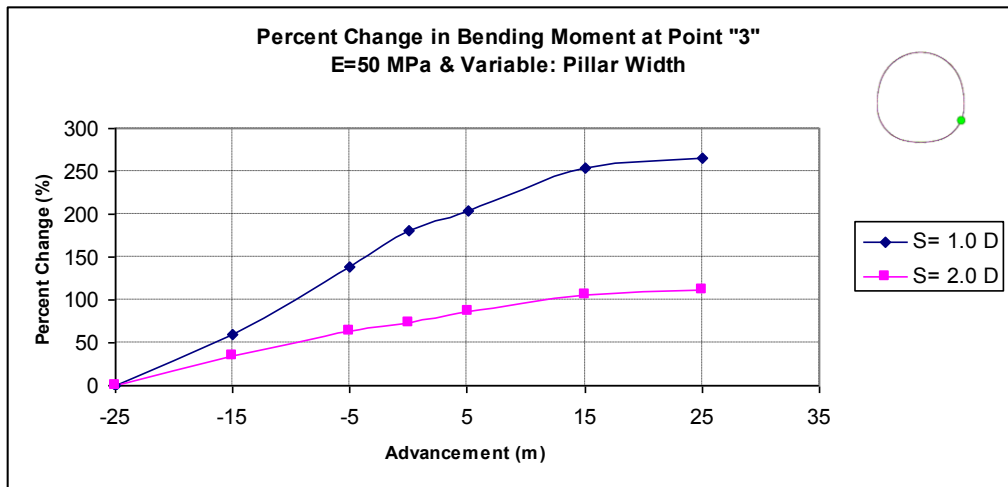


Figure B.18 Percent change in bending moment at the right-bottom side of the tunnel

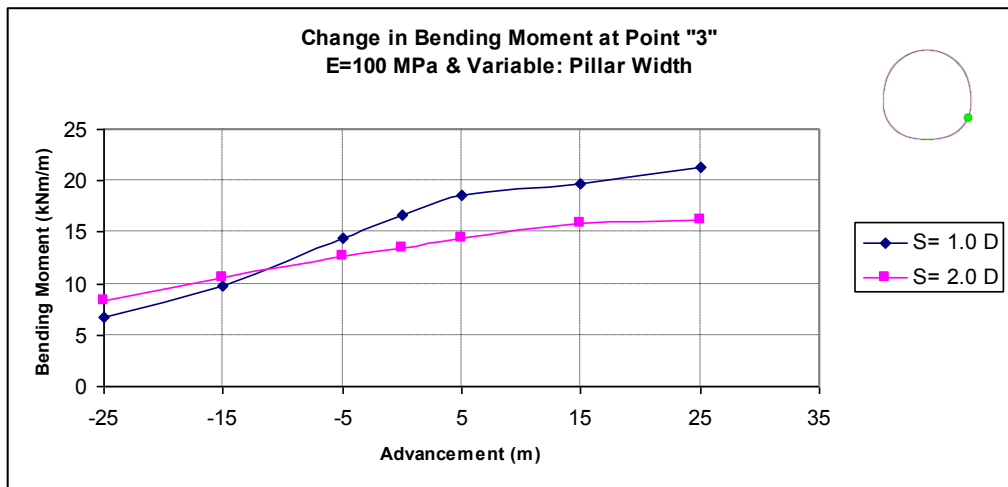


Figure B.19 Bending moment values at the right-bottom side of the tunnel

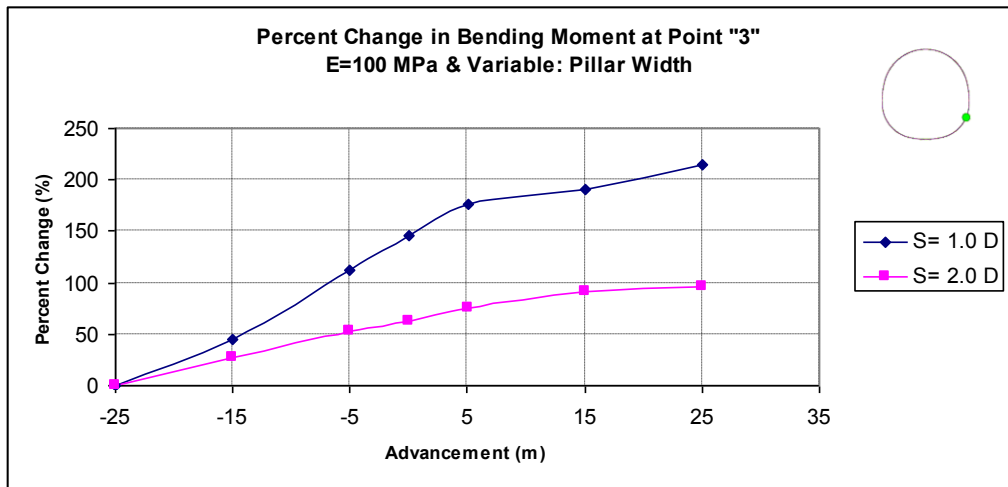


Figure B.20 Percent change in bending moment at the right-bottom side of the tunnel

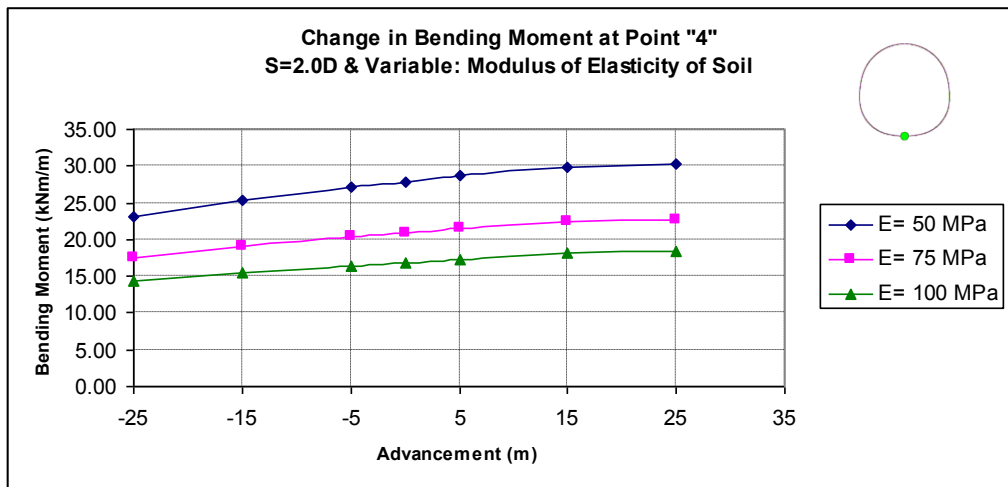


Figure B.21 Bending moment values at the bottom side of the tunnel

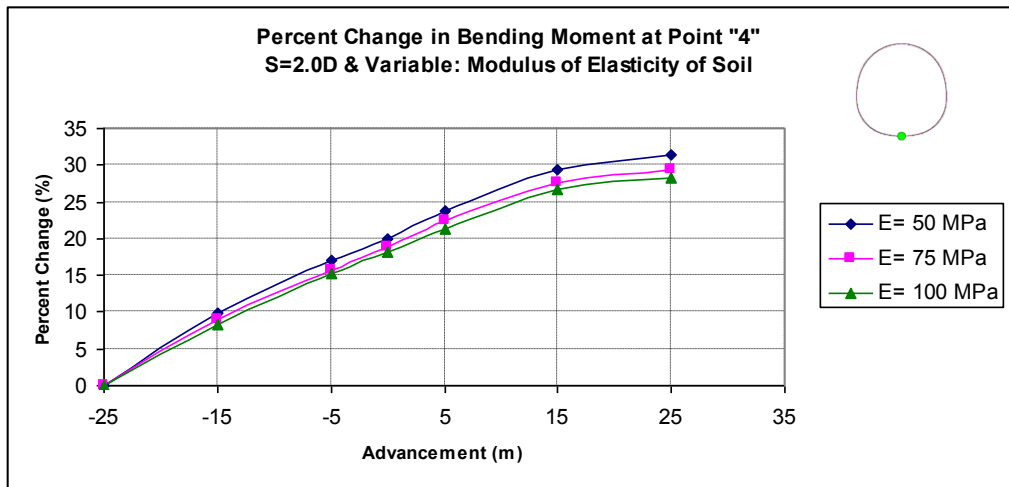


Figure B.22 Percent change in bending moment at the bottom side of the tunnel

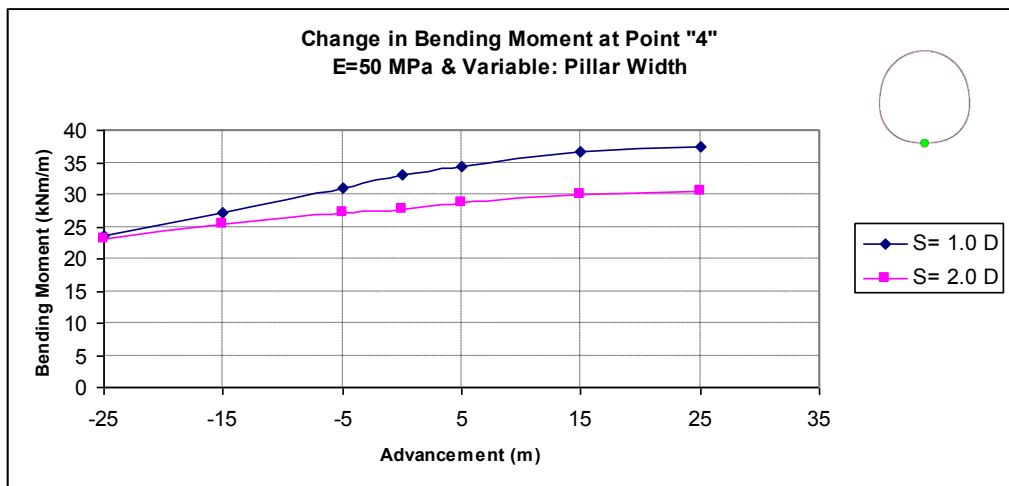


Figure B.23 Bending moment values at the bottom side of the tunnel

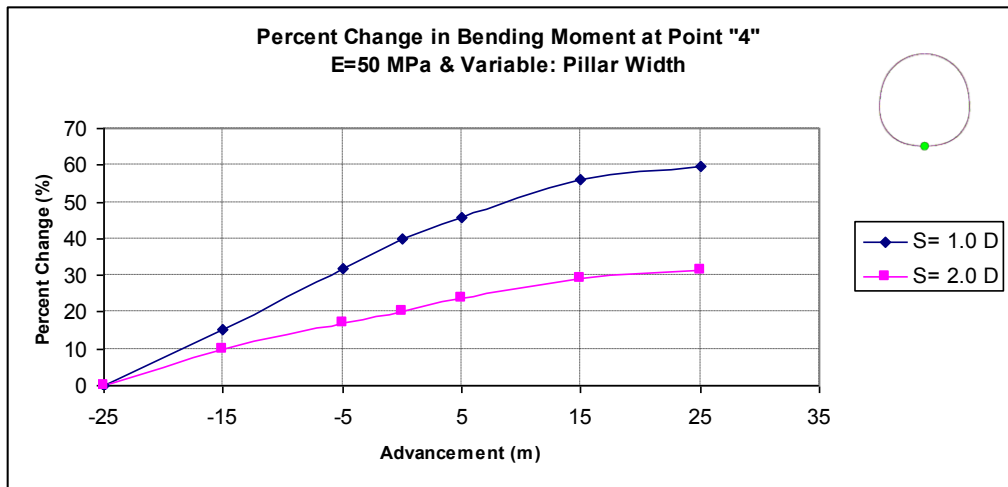


Figure B.24 Percent change in bending moment at the bottom side of the tunnel

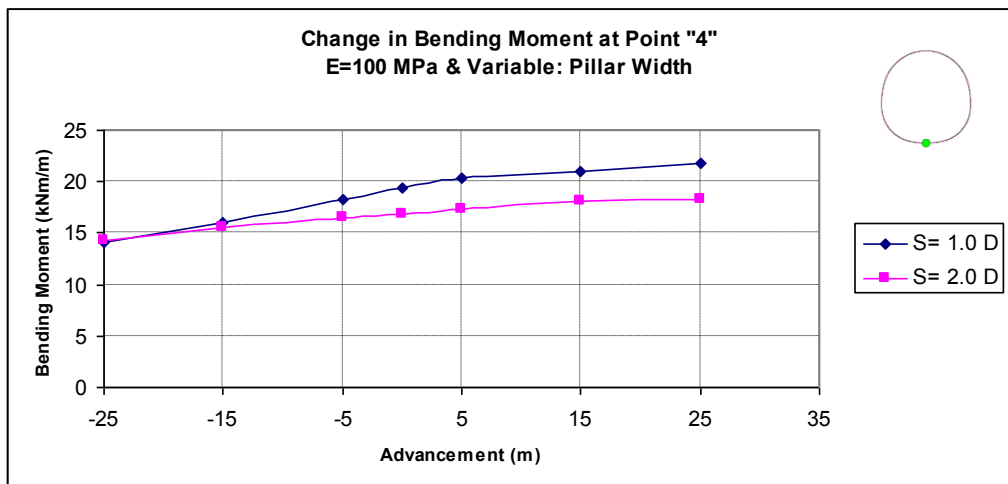


Figure B.25 Bending moment values at the bottom side of the tunnel

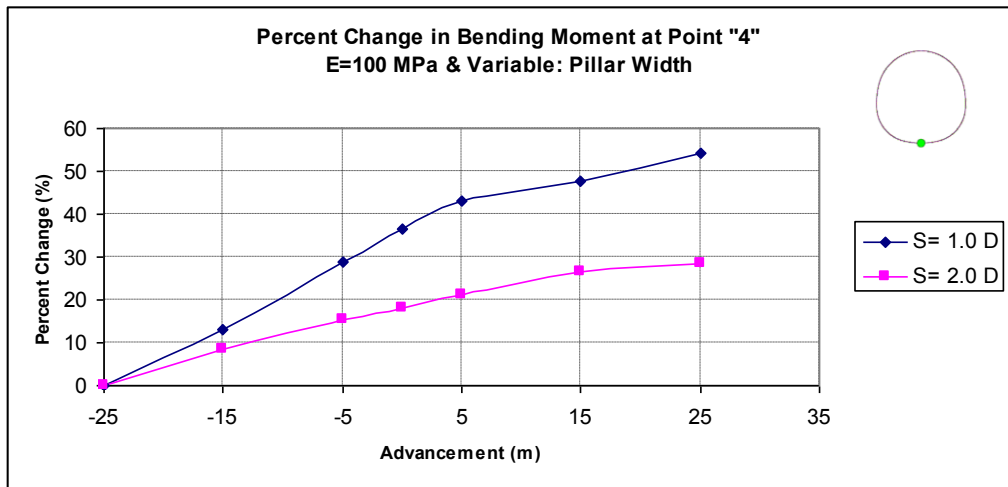


Figure B.26 Percent change in bending moment at the bottom side of the tunnel

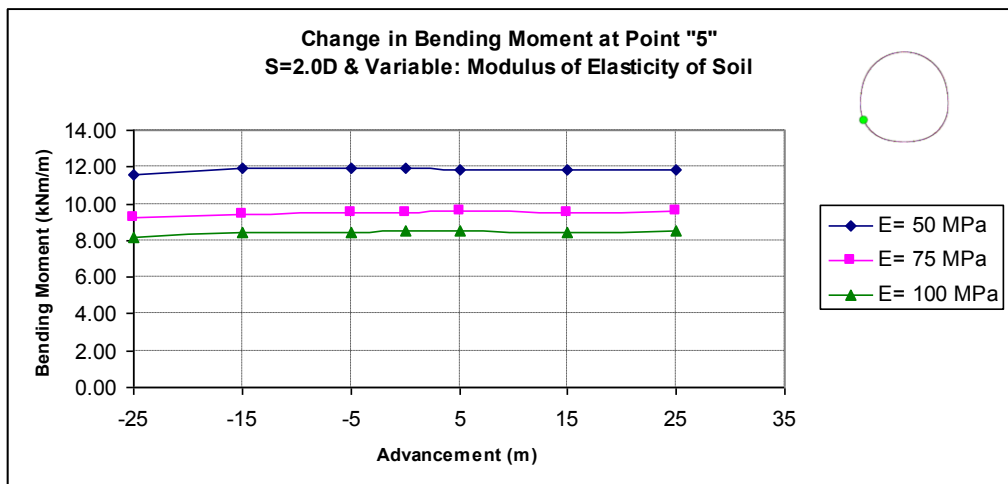


Figure B.27 Bending moment values at the left-bottom side of the tunnel

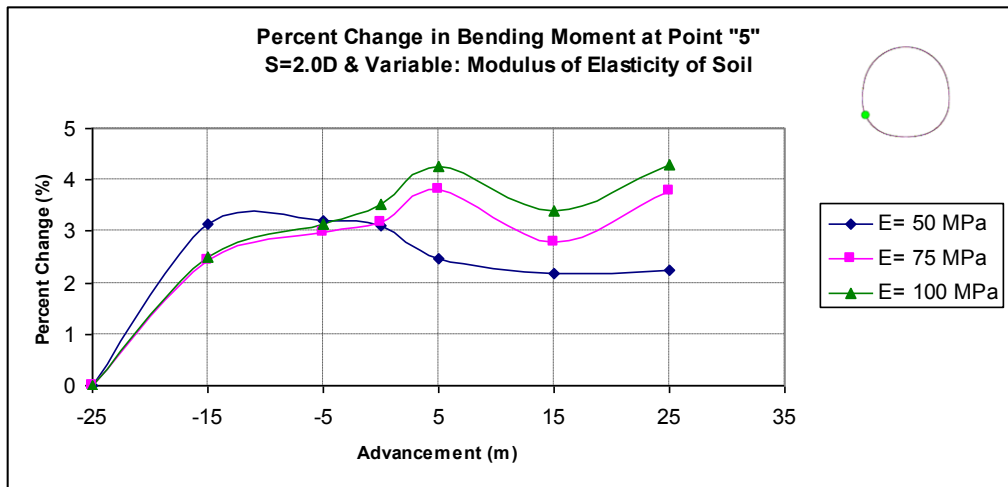


Figure B.28 Percent change in bending moment at the left-bottom side of the tunnel

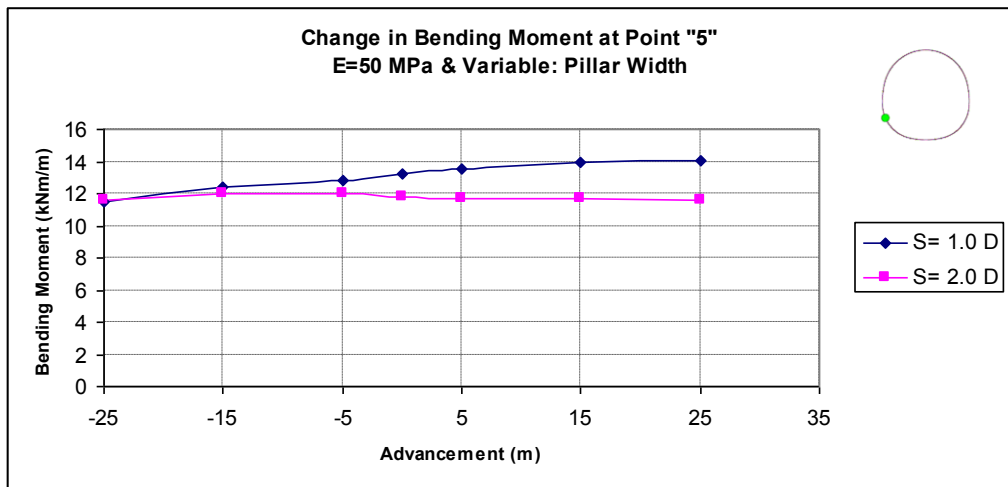


Figure B.29 Bending moment values at the left-bottom side of the tunnel

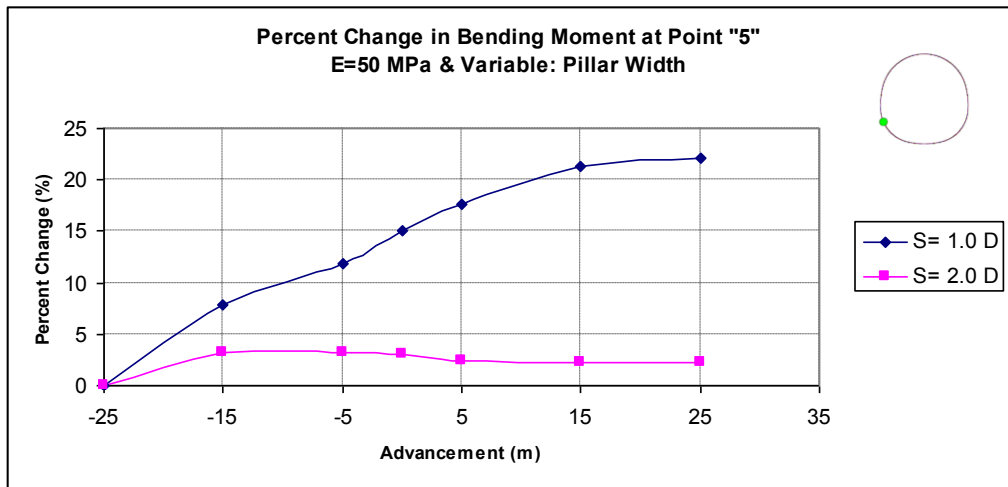


Figure B.30 Percent change in bending moment at the left-bottom side of the tunnel

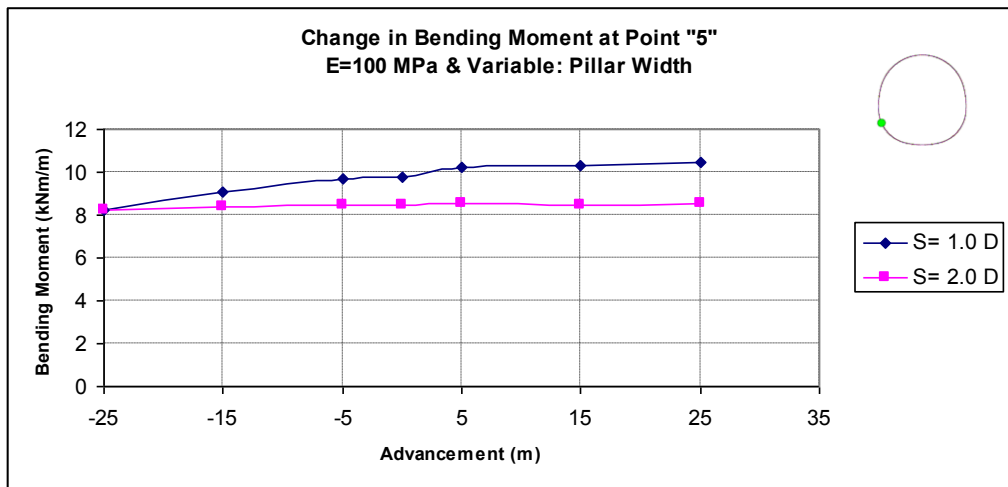


Figure B.31 Bending moment values at the left-bottom side of the tunnel

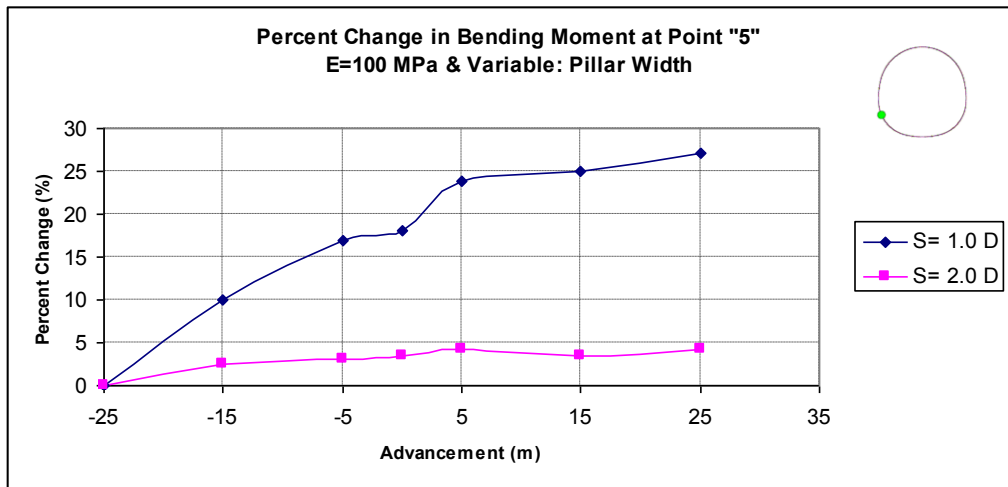


Figure B.32 Percent change in bending moment at the left-bottom side of the tunnel

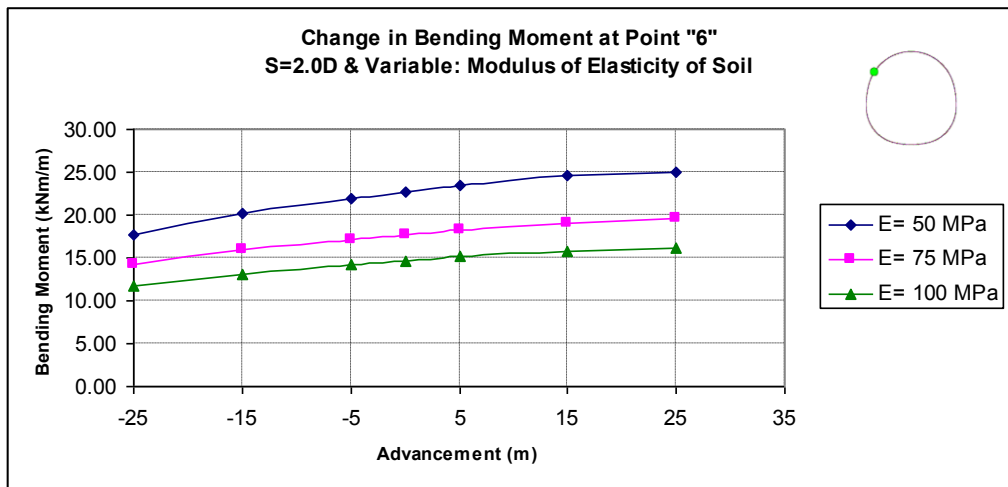


Figure B.33 Bending moment values at the left-top side of the tunnel

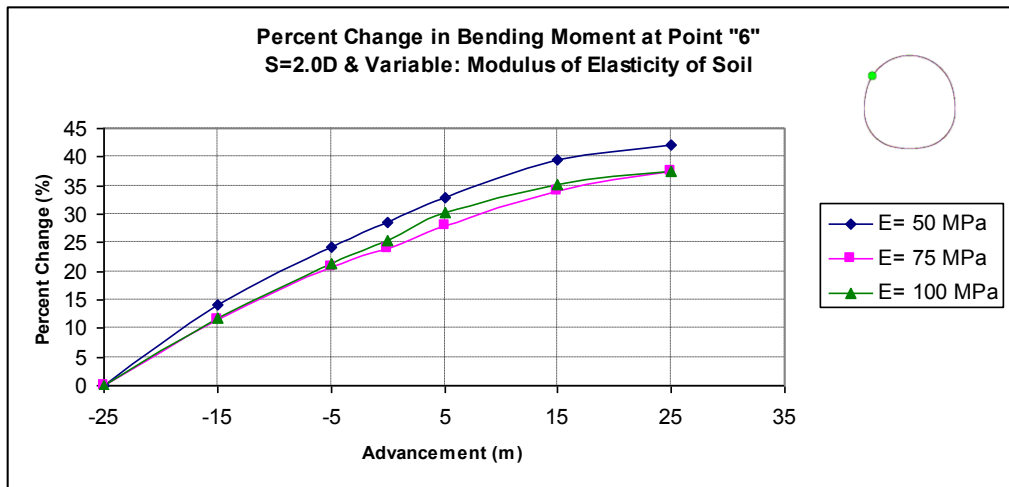


Figure B.34 Percent change in bending moment at the left-top side of the tunnel

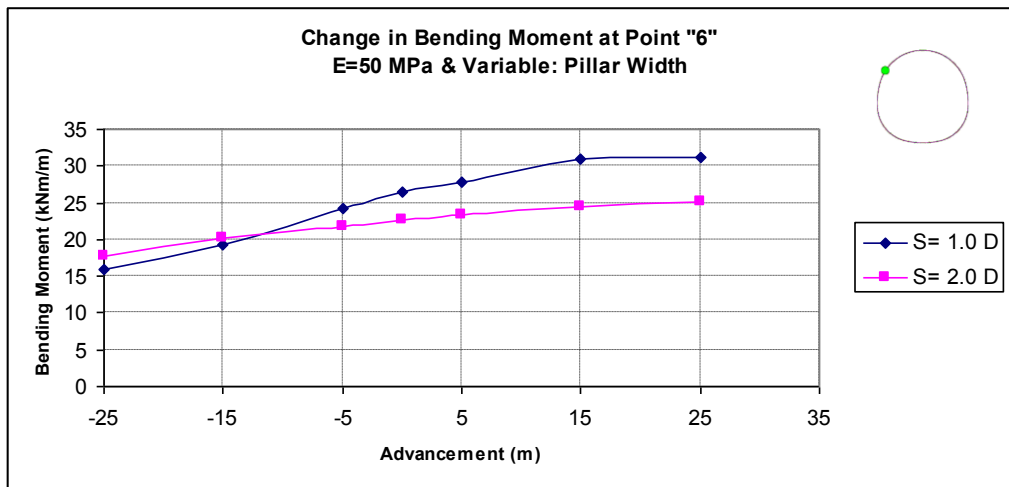


Figure B.35 Bending moment values at the left-top side of the tunnel

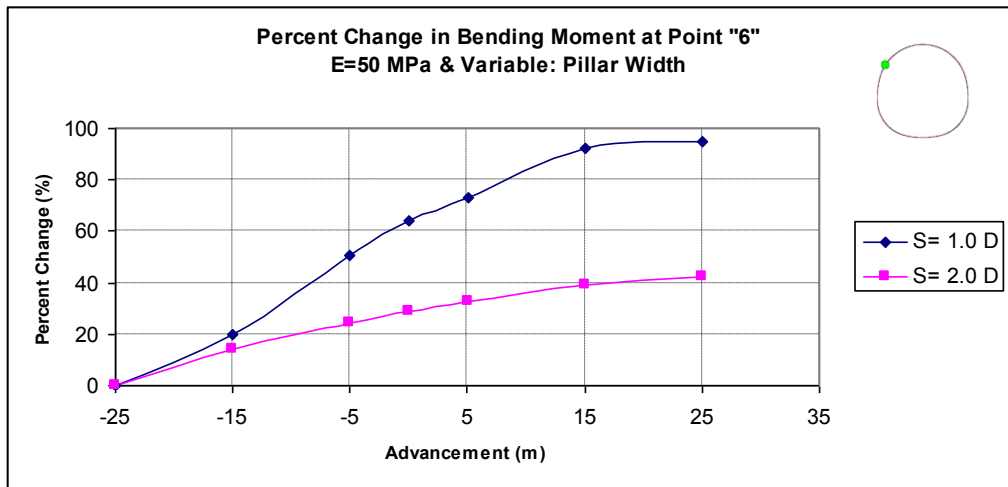


Figure B.36 Percent change in bending moment at the left-top side of the tunnel

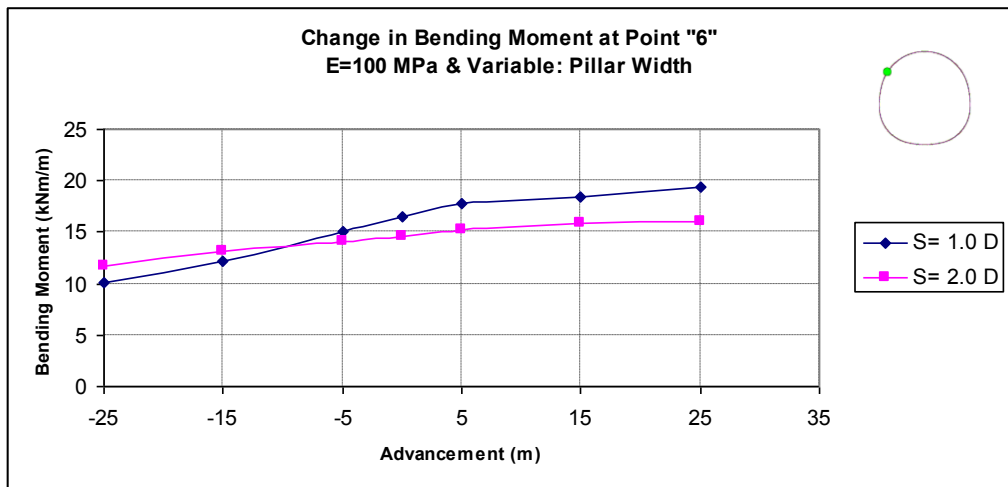


Figure B.37 Bending moment values at the left-top side of the tunnel

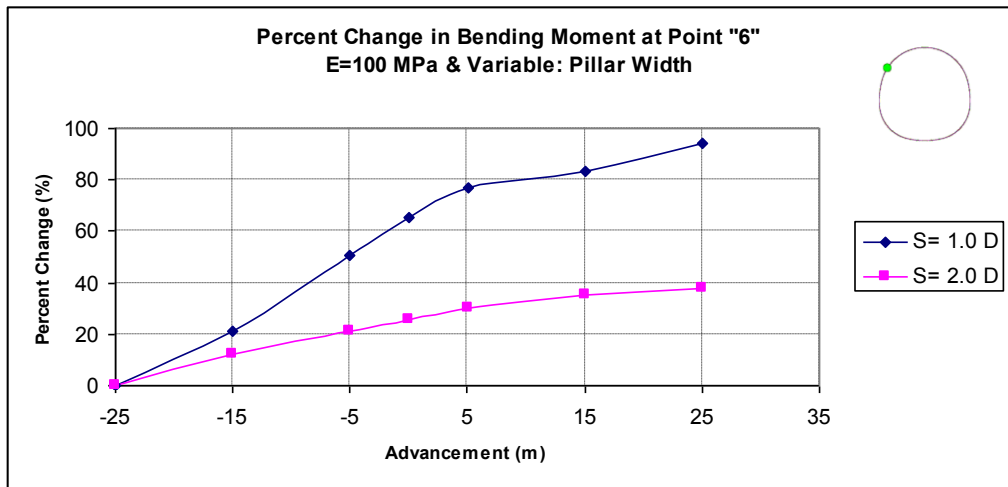


Figure B.38 Percent change in bending moment at the left-top side of the tunnel

APPENDIX C

SHEAR FORCES

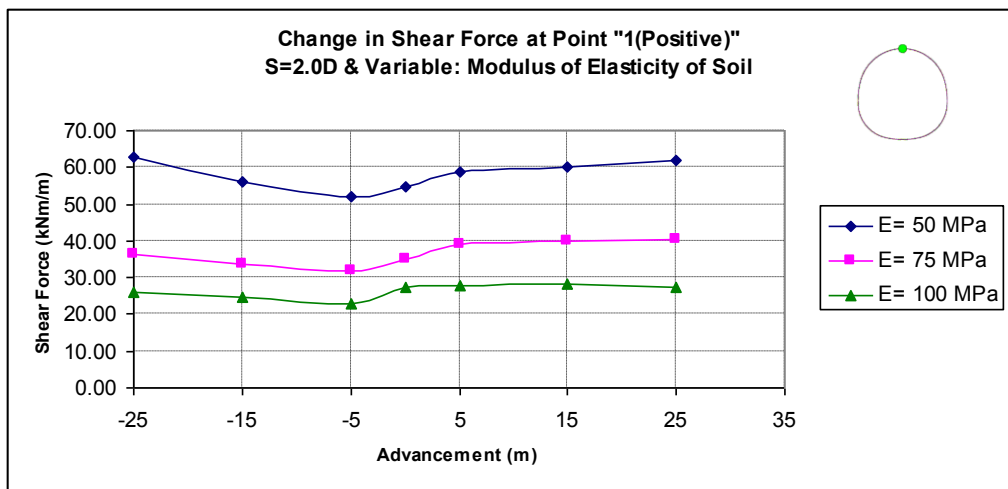


Figure C.1 Shear force values at the top side of the tunnel

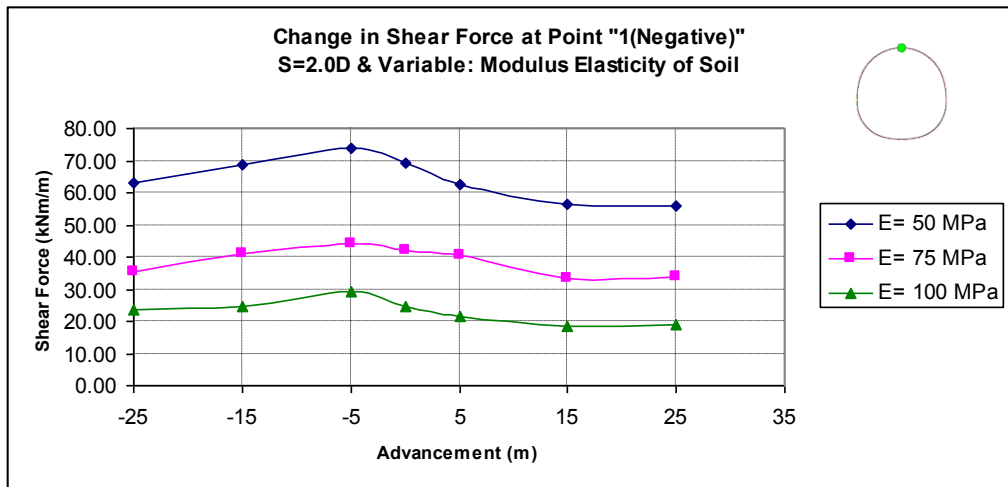


Figure C.2 Shear force values at the top side of the tunnel

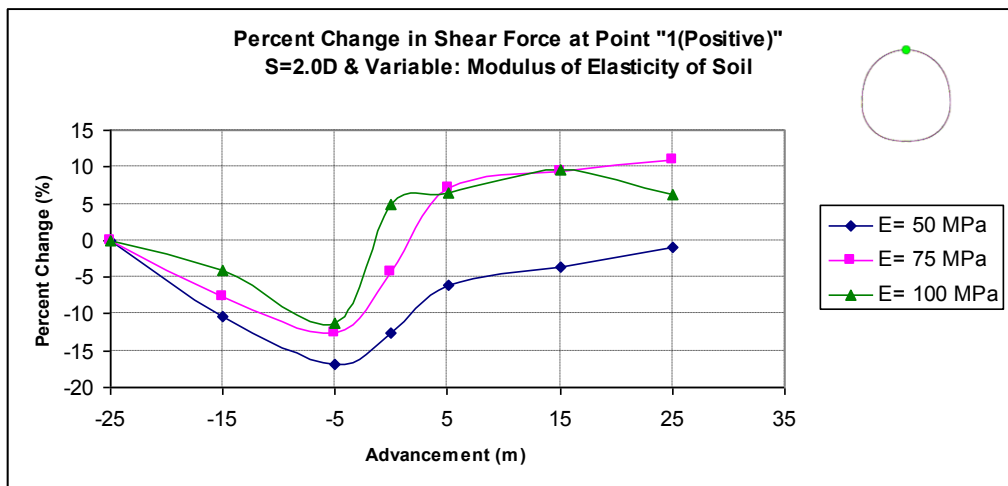


Figure C.3 Percent change in shear force at the top side of the tunnel

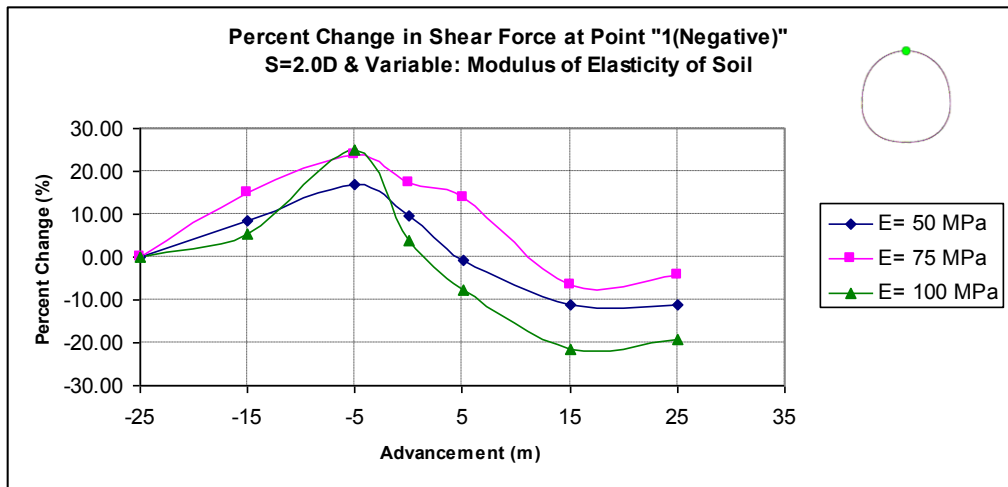


Figure C.4 Percent change in shear force at the top side of the tunnel

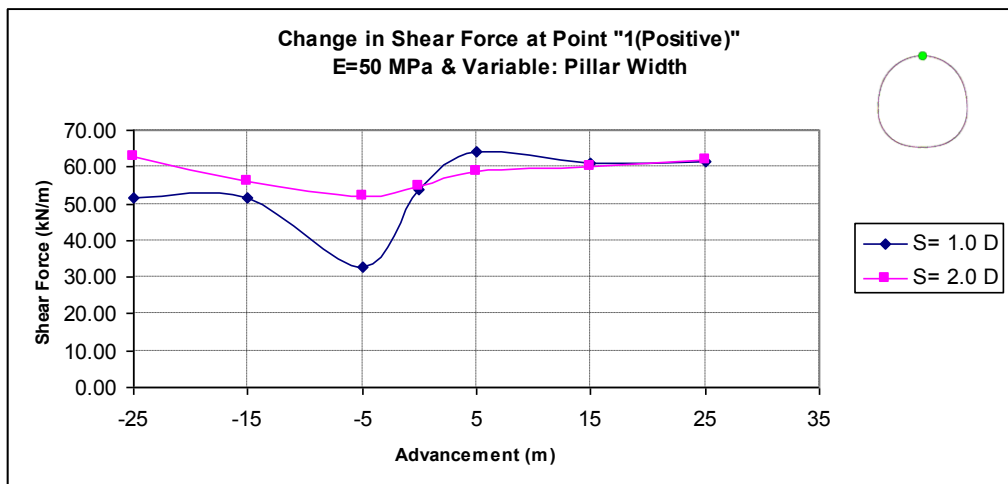


Figure C.5 Shear force values at the top side of the tunnel

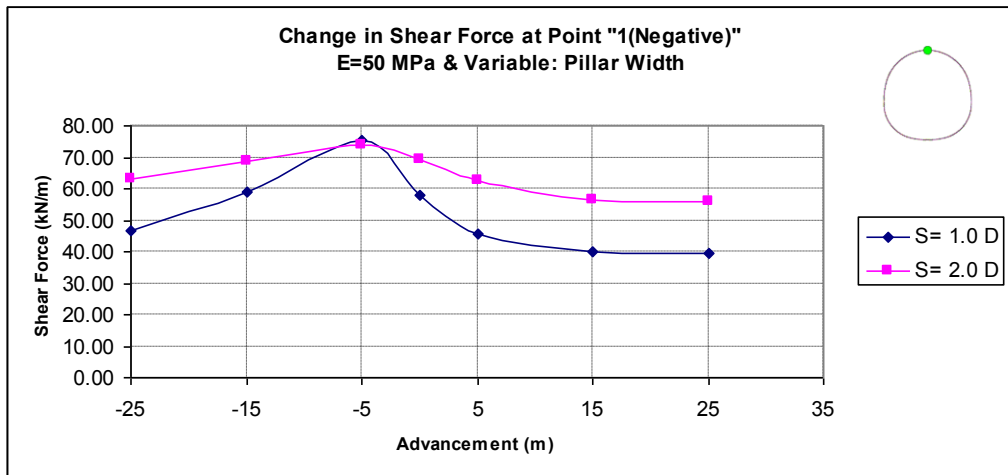


Figure C.6 Shear force values at the top side of the tunnel

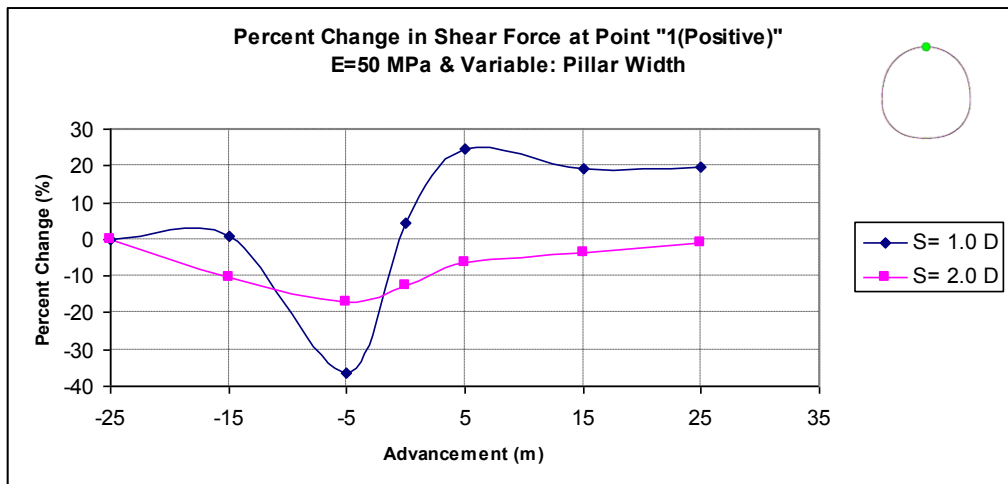


Figure C.7 Percent change in shear force at the top side of the tunnel

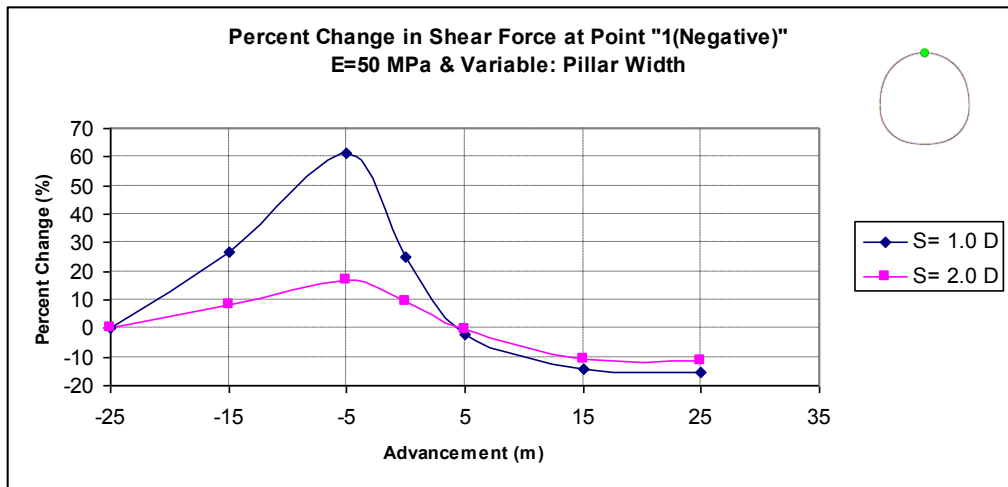


Figure C.8 Percent change in shear force at the top side of the tunnel

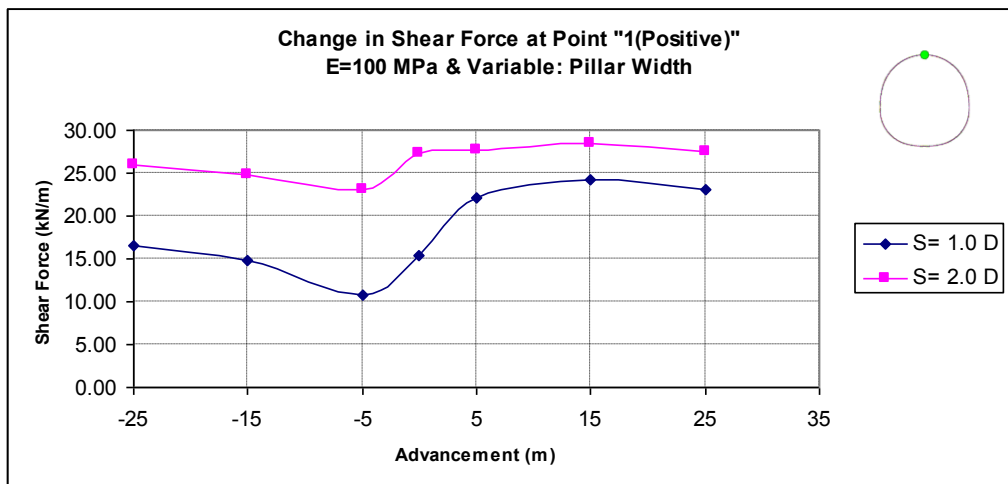


Figure C.9 Shear force values at the top side of the tunnel

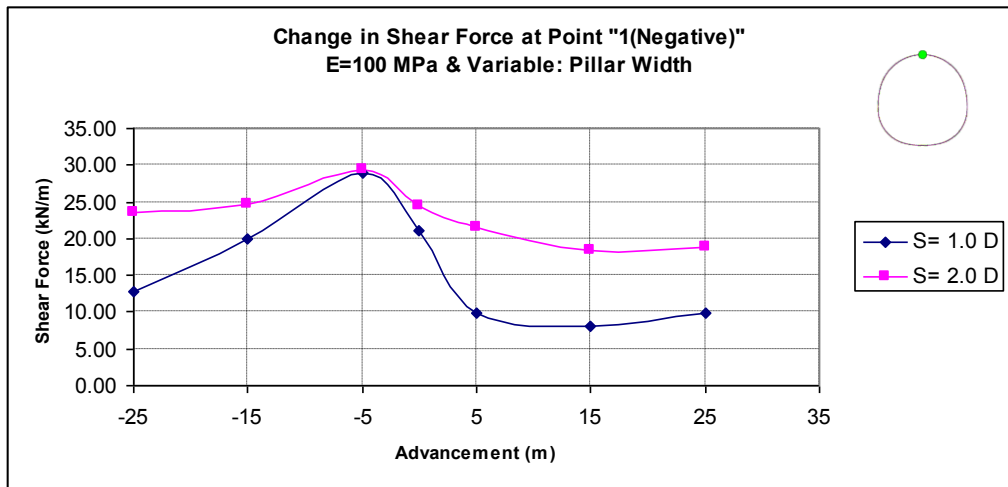


Figure C.10 Shear force values at the top side of the tunnel

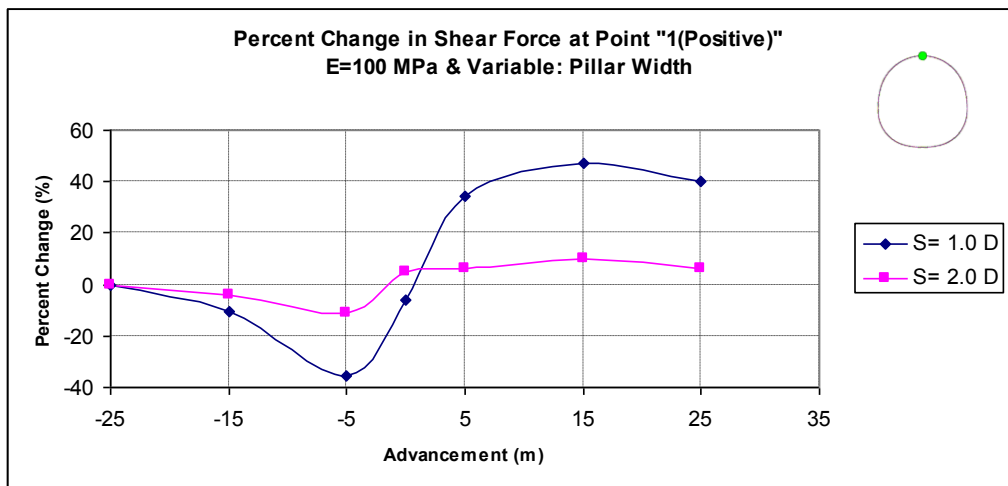


Figure C.11 Percent change in shear force at the top side of the tunnel

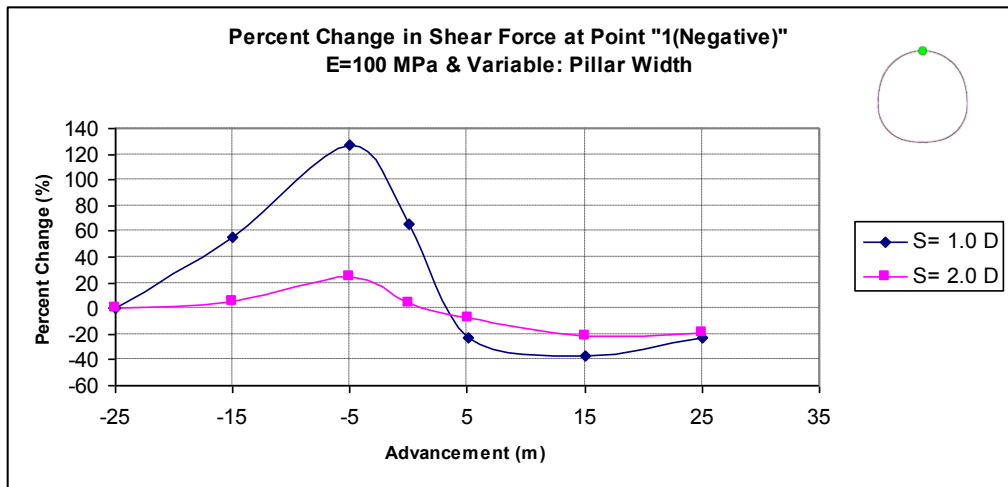


Figure C.12 Percent change in shear force at the top side of the tunnel

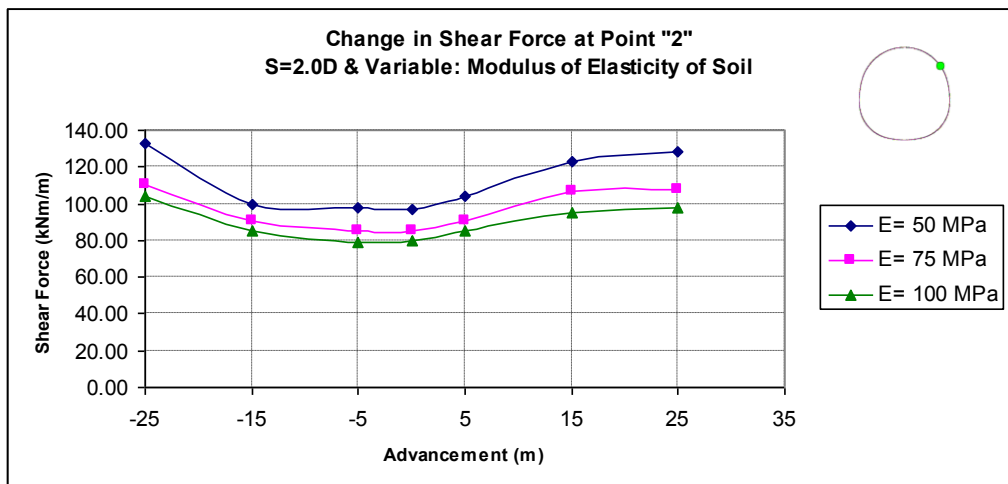


Figure C.13 Shear force values at the right-top side of the tunnel

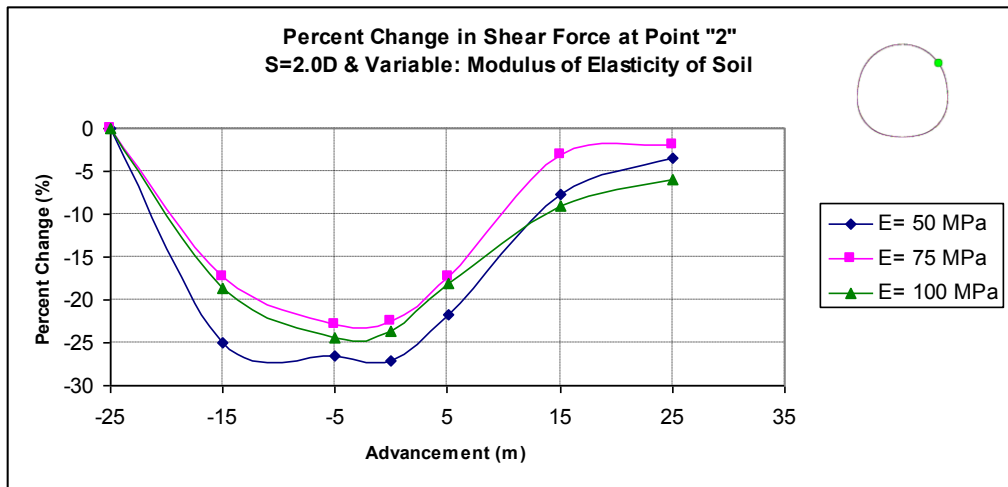


Figure C.14 Percent change in shear force at the right-top side of the tunnel

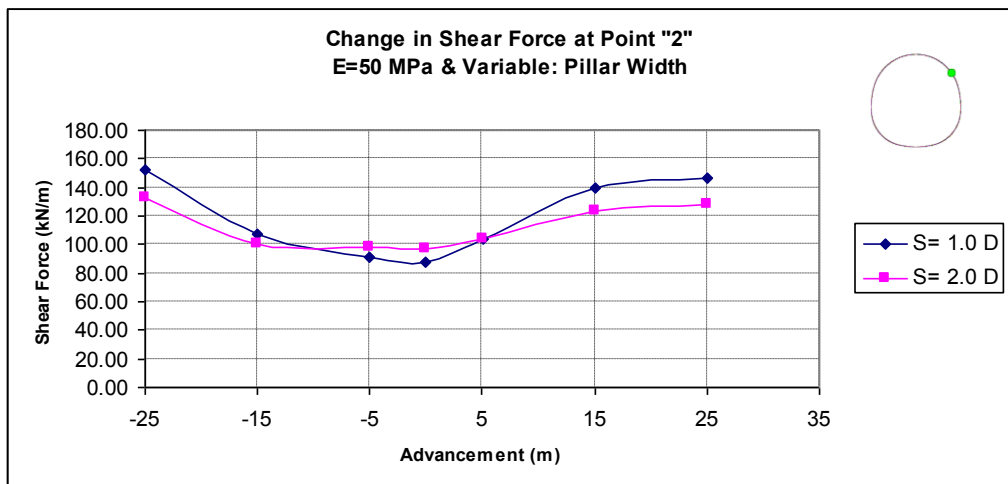


Figure C.15 Shear force values at the right-top side of the tunnel

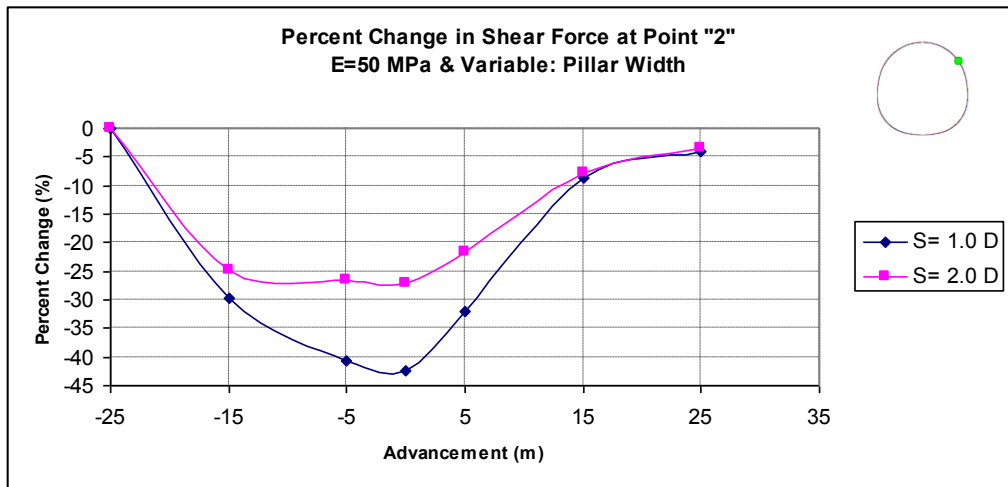


Figure C.16 Percent change in shear force at the right-top side of the tunnel

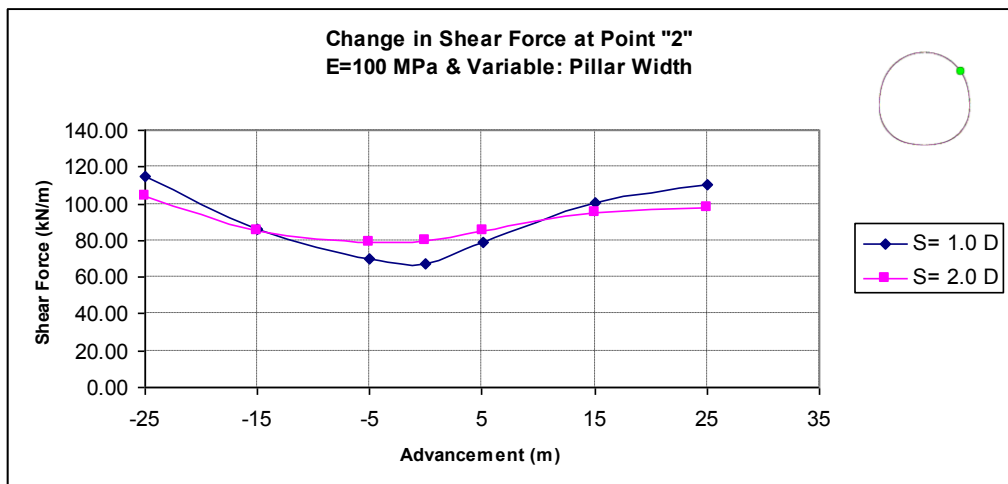


Figure C.17 Shear force values at the right-top side of the tunnel

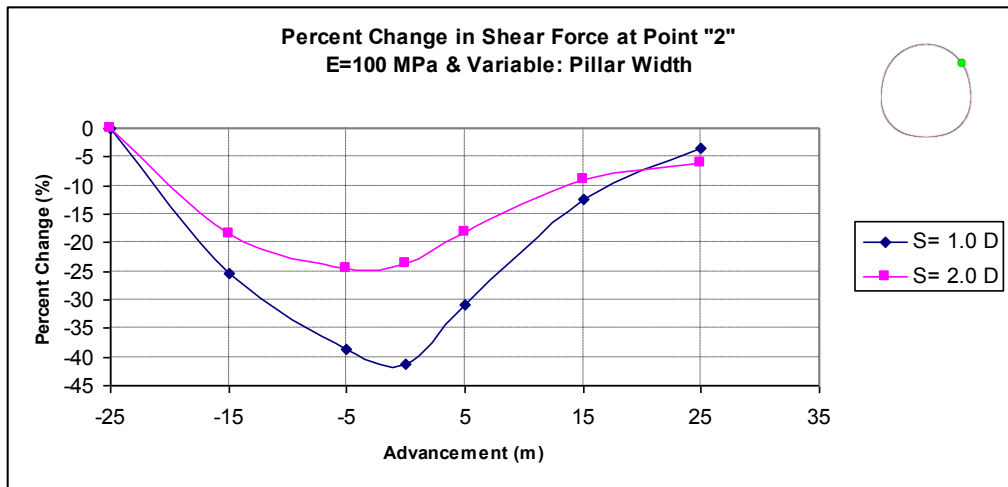


Figure C.18 Percent change in shear force at the right-top side of the tunnel

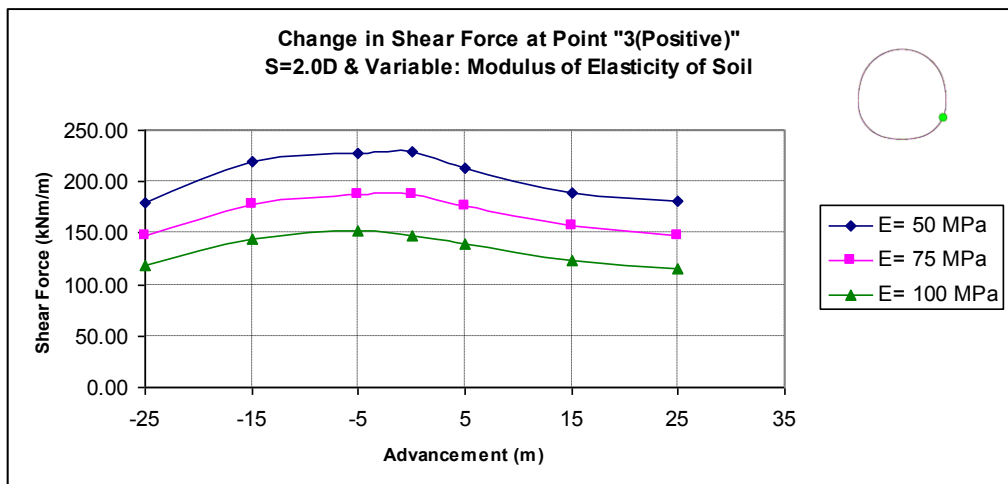


Figure C.19 Shear force values at the right-bottom side of the tunnel

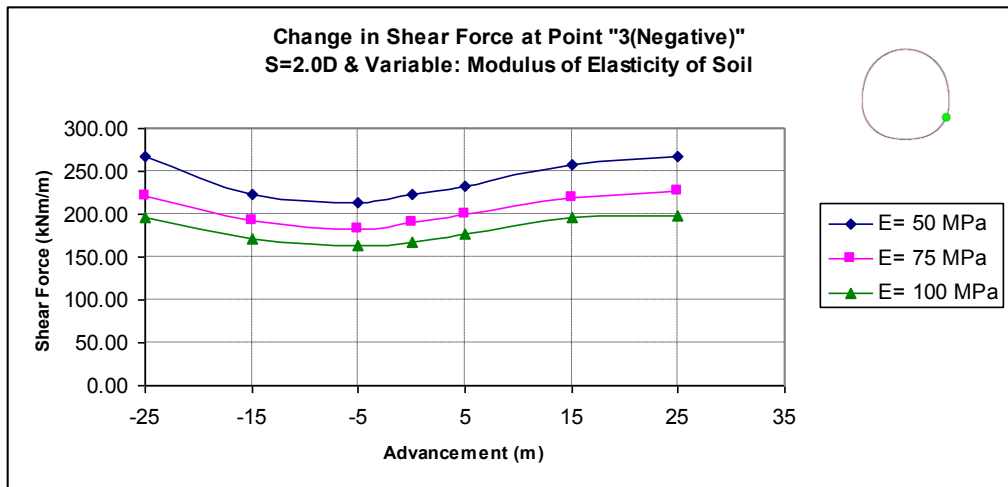


Figure C.20 Shear force values at the right-bottom side of the tunnel

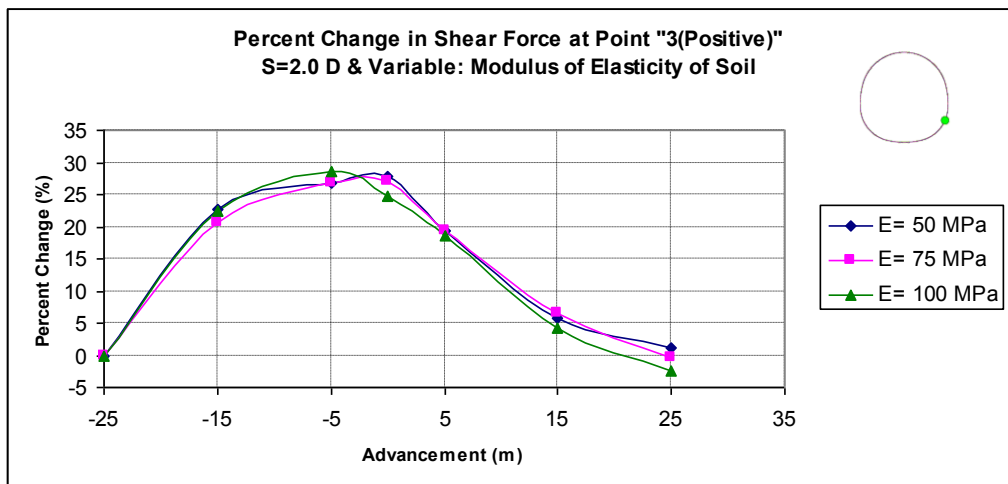


Figure C.21 Percent change in shear force at the right-bottom side of the tunnel

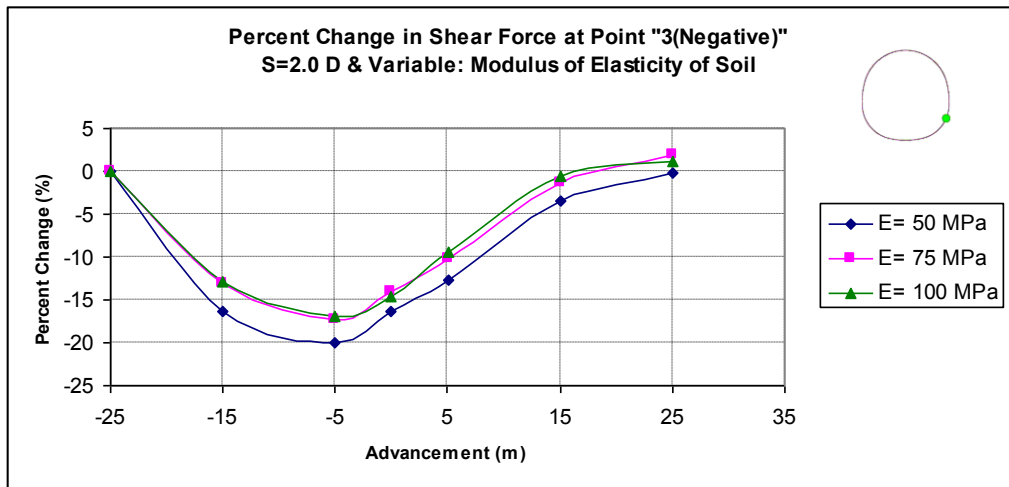


Figure C.22 Percent change in shear force at the right-bottom side of the tunnel

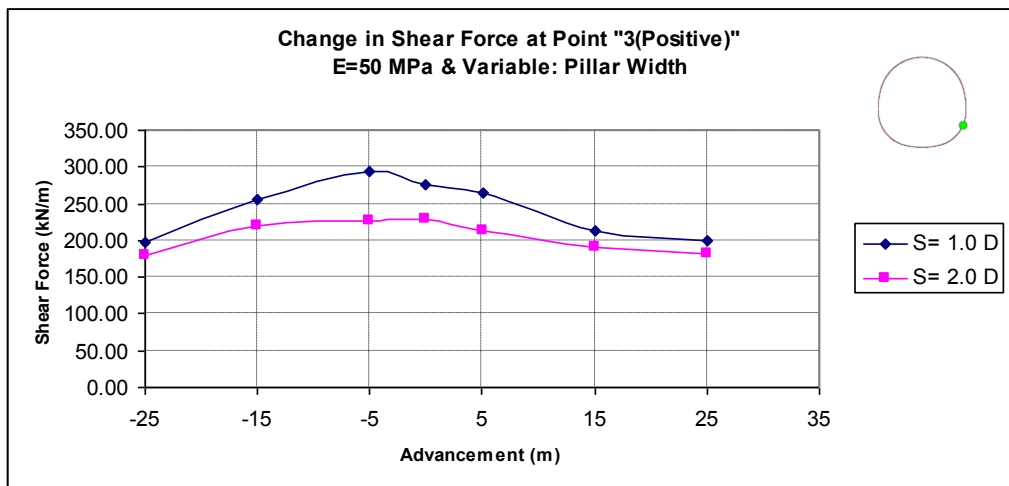


Figure C.23 Shear force values at the right-bottom side of the tunnel

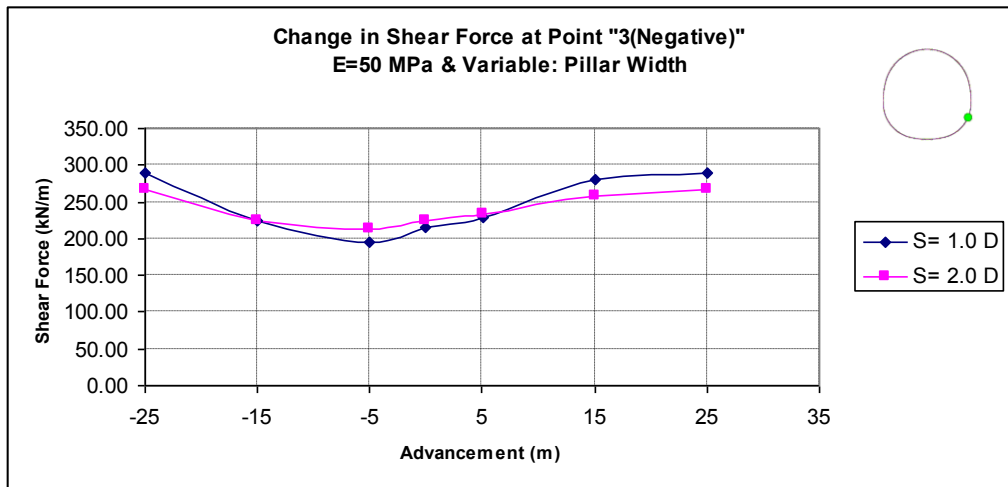


Figure C.24 Shear force values at the right-bottom side of the tunnel

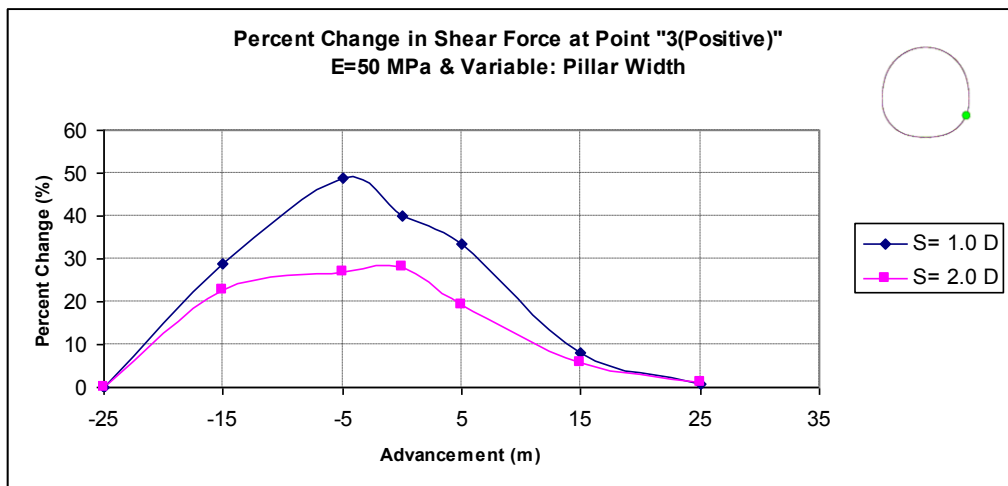


Figure C.25 Percent change in shear force at the right-bottom side of the tunnel

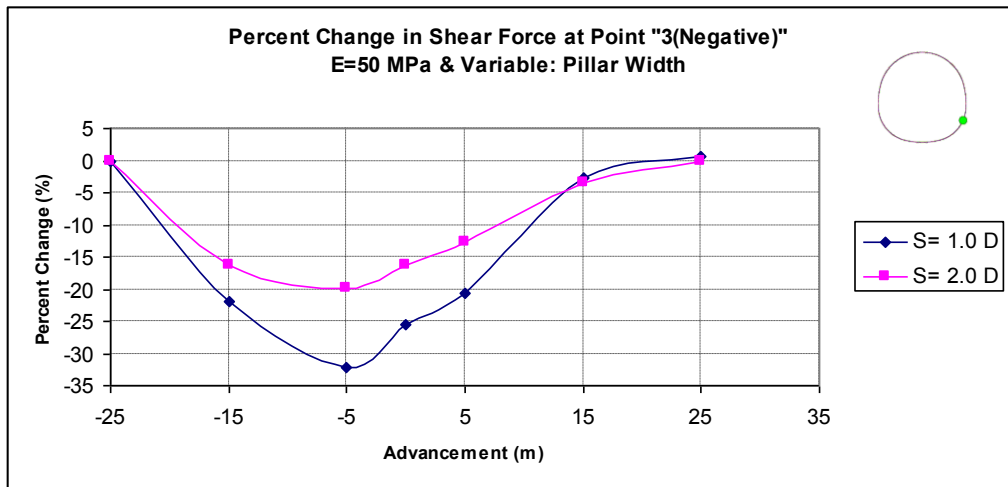


Figure C.26 Percent change in shear force at the right-bottom side of the tunnel

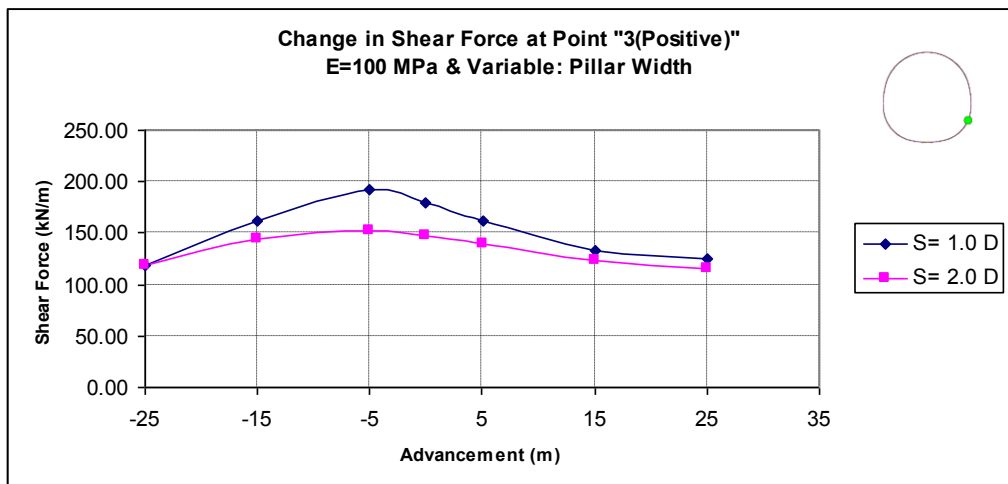


Figure C.27 Shear force values at the right-bottom side of the tunnel

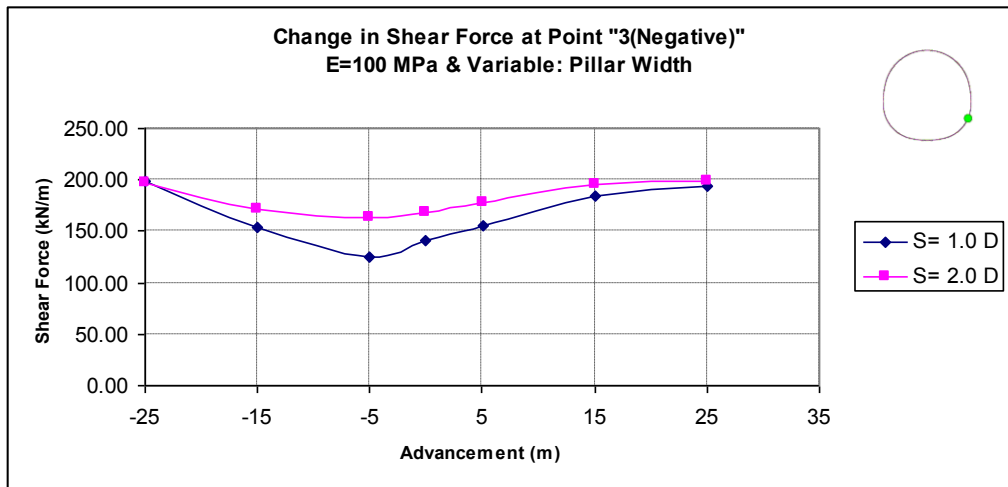


Figure C.28 Shear force values at the right-bottom side of the tunnel

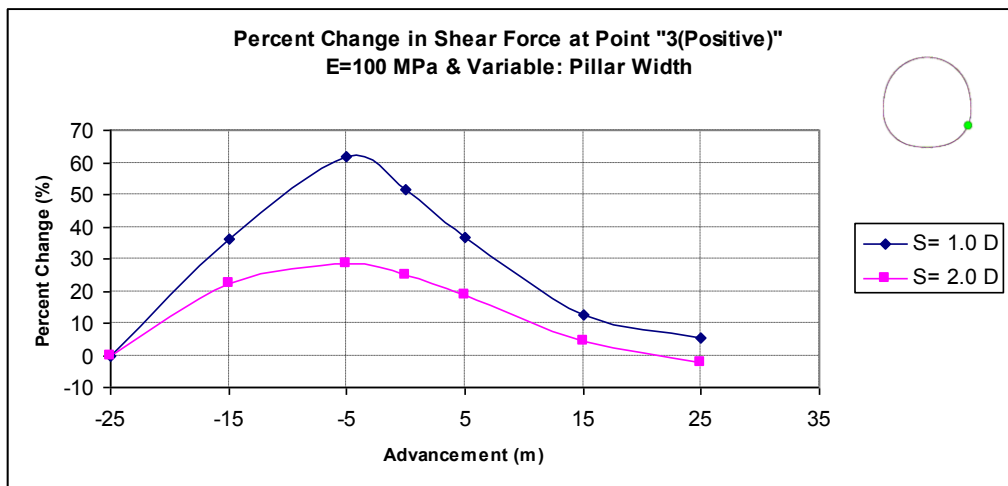


Figure C.29 Percent change in shear force at the right-bottom side of the tunnel

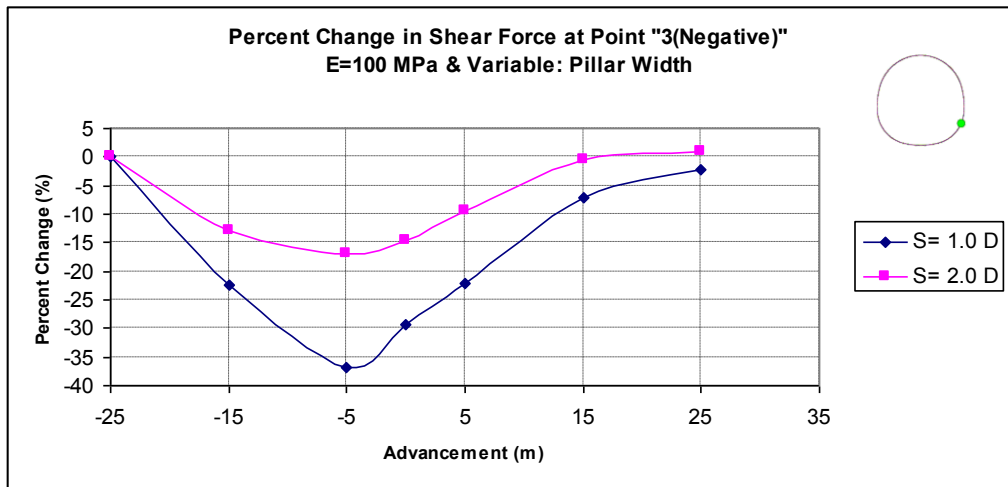


Figure C.30 Percent change in shear force at the right-bottom side of the tunnel

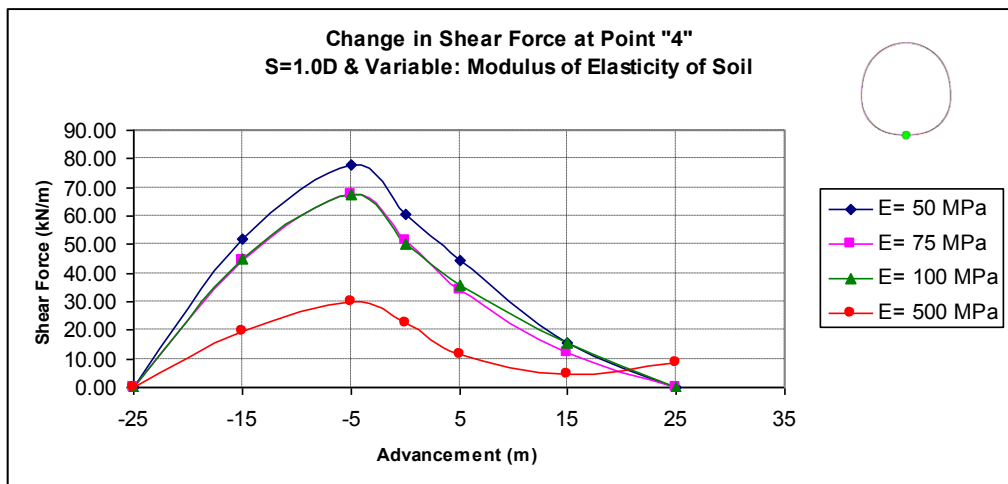


Figure C.31 Shear force values at the bottom side of the tunnel

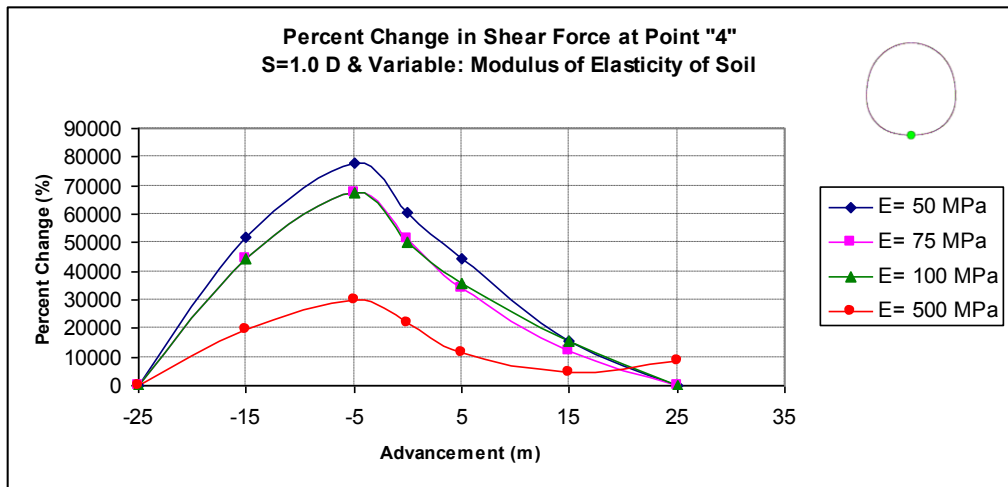


Figure C.32 Percent change in shear force at the bottom side of the tunnel

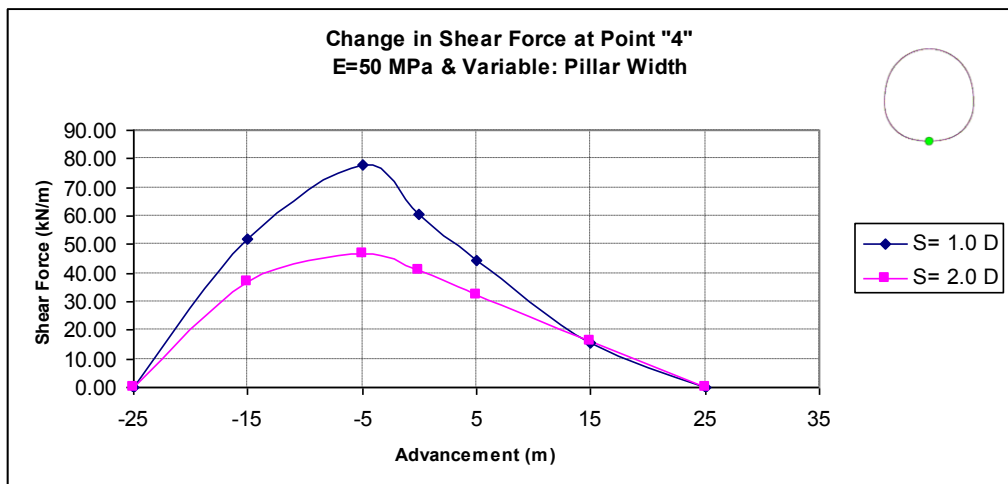


Figure C.33 Shear force values at the bottom side of the tunnel

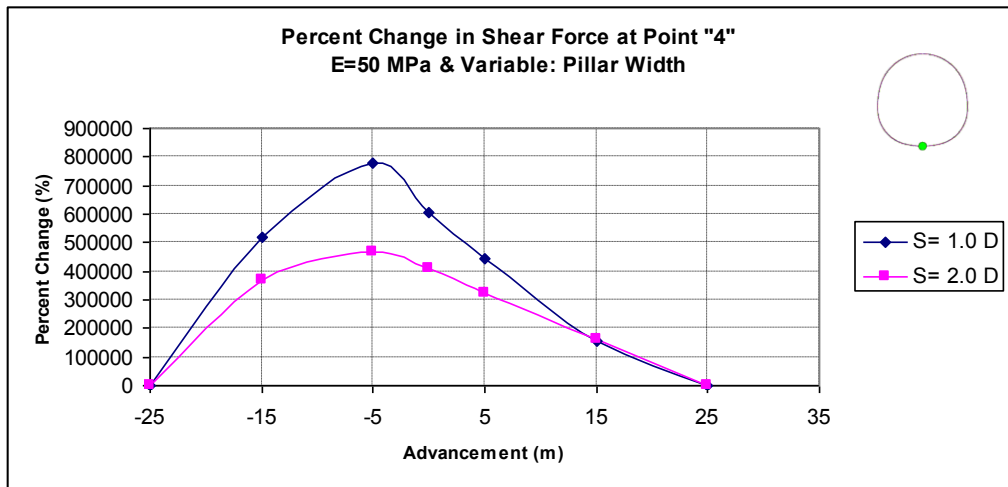


Figure C.34 Percent change in shear force at the bottom side of the tunnel

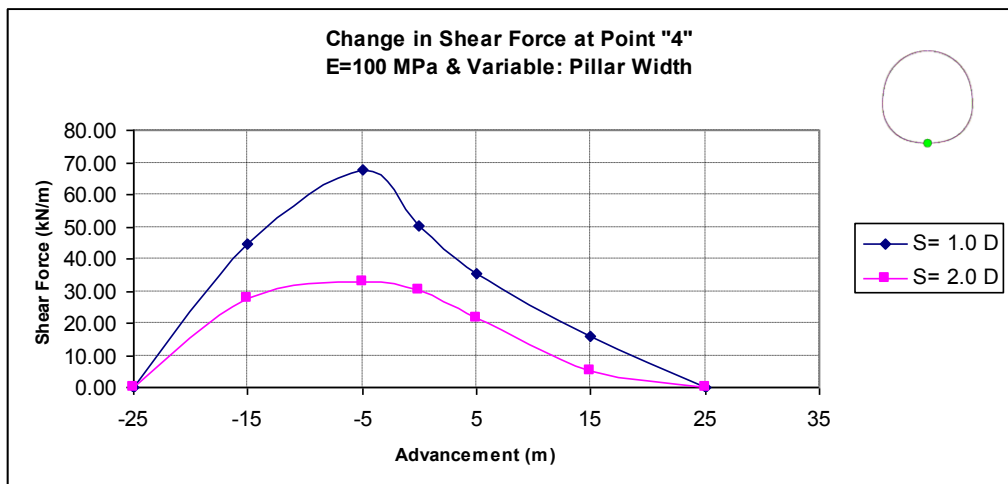


Figure C.35 Shear force values at the bottom side of the tunnel

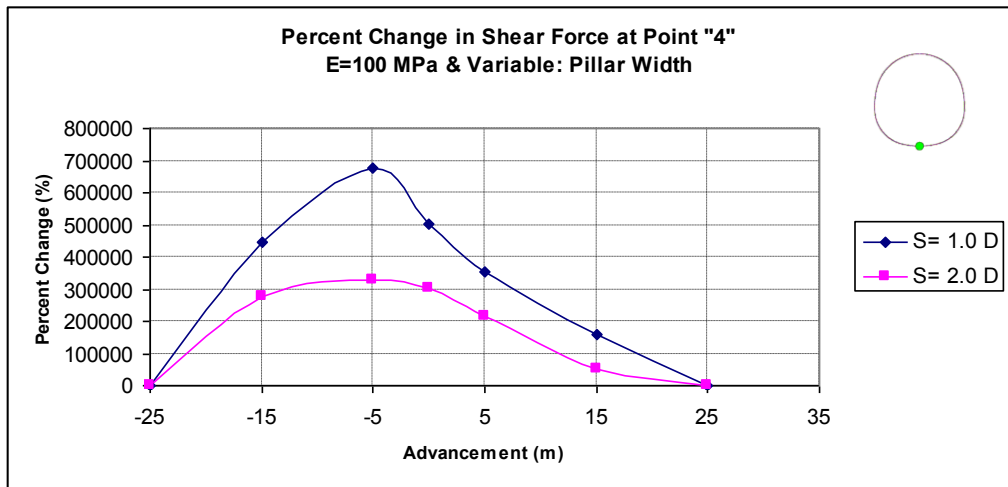


Figure C.36 Percent change in shear force at the bottom side of the tunnel

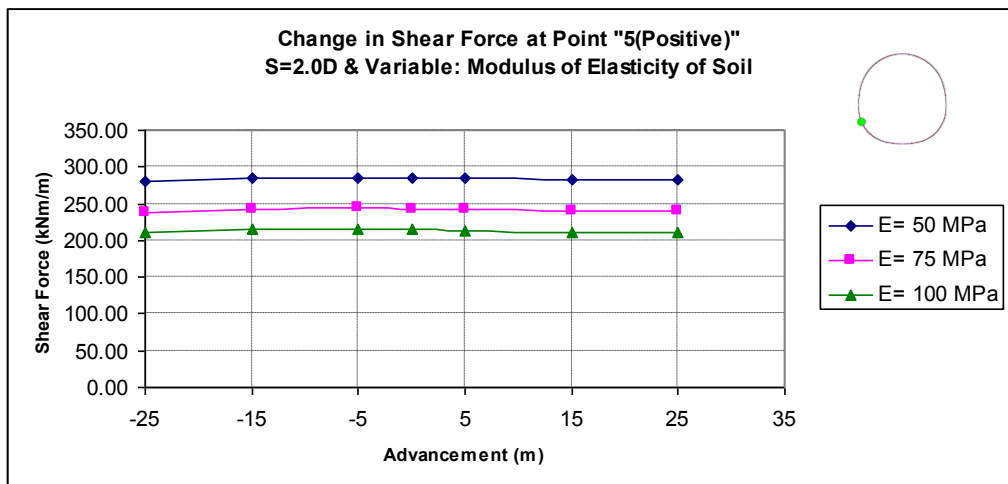


Figure C.37 Shear force values at the left-bottom side of the tunnel

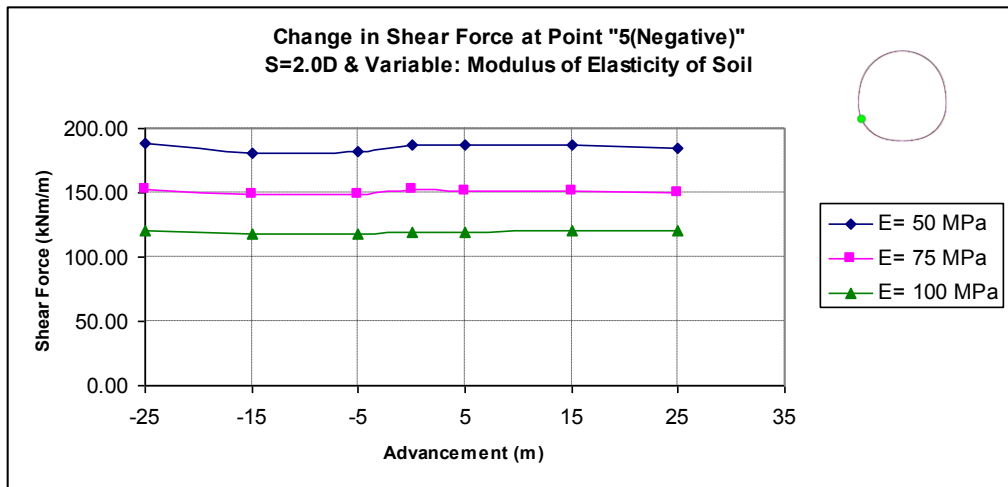


Figure C.38 Shear force values at the left-bottom side of the tunnel

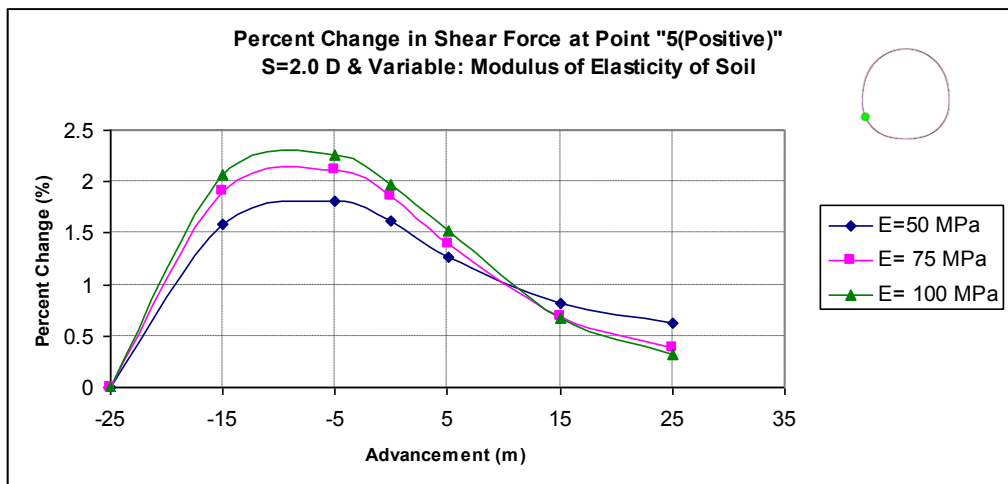


Figure C.39 Percent change in shear force at the left-bottom side of the tunnel

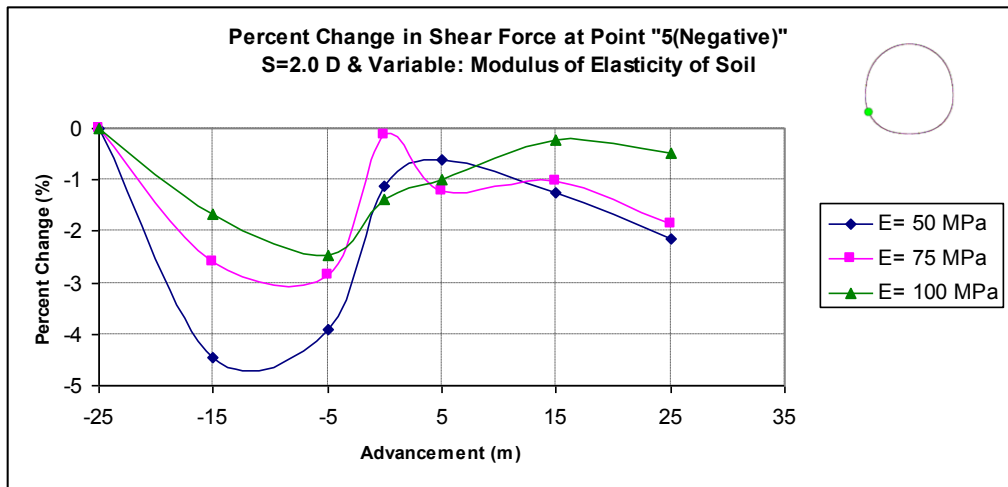


Figure C.40 Percent change in shear force at the left-bottom side of the tunnel

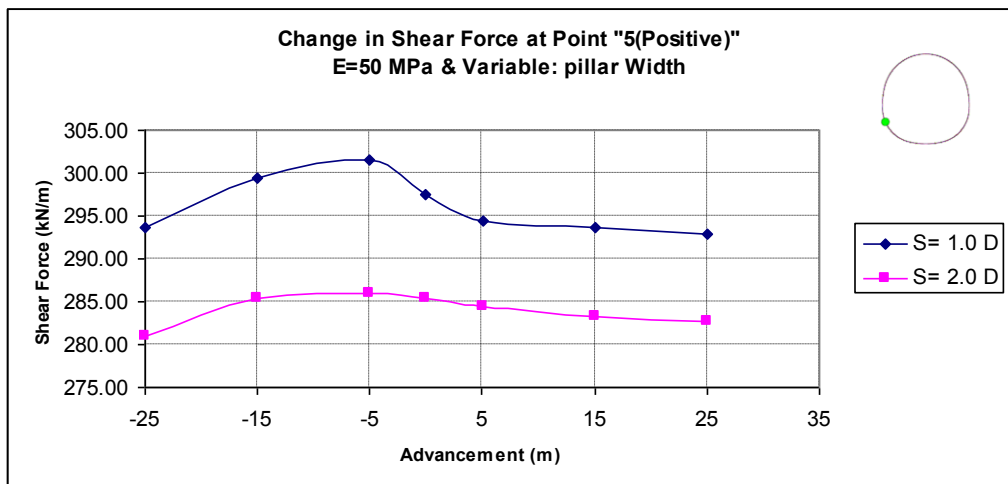


Figure C.41 Shear force values at the left-bottom side of the tunnel

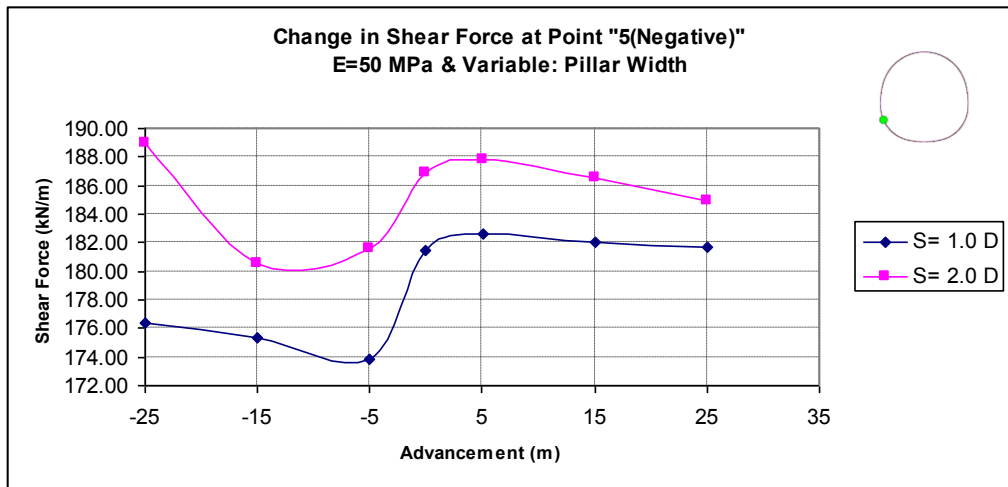


Figure C.42 Shear force values at the left-bottom side of the tunnel

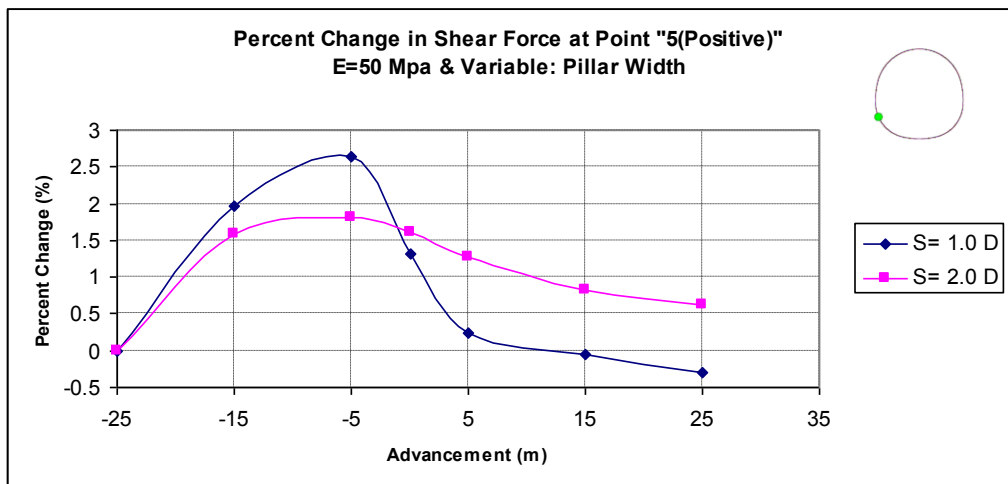


Figure C.43 Percent change in shear force at the left-bottom side of the tunnel

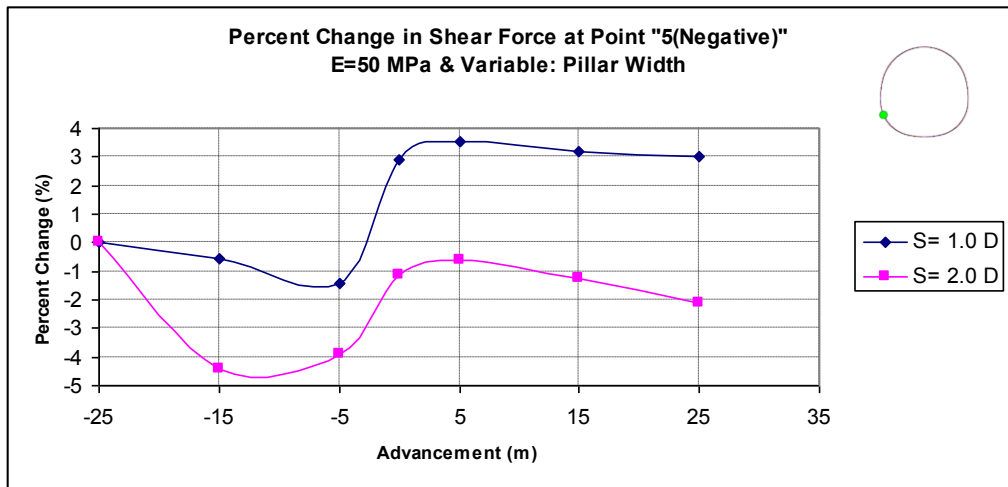


Figure C.44 Percent change in shear force at the left-bottom side of the tunnel

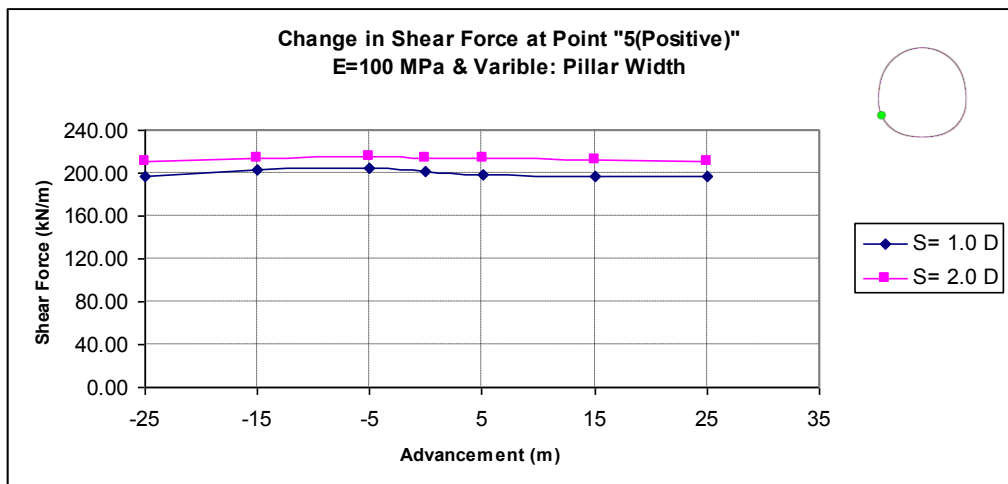


Figure C.45 Shear force values at the left-bottom side of the tunnel

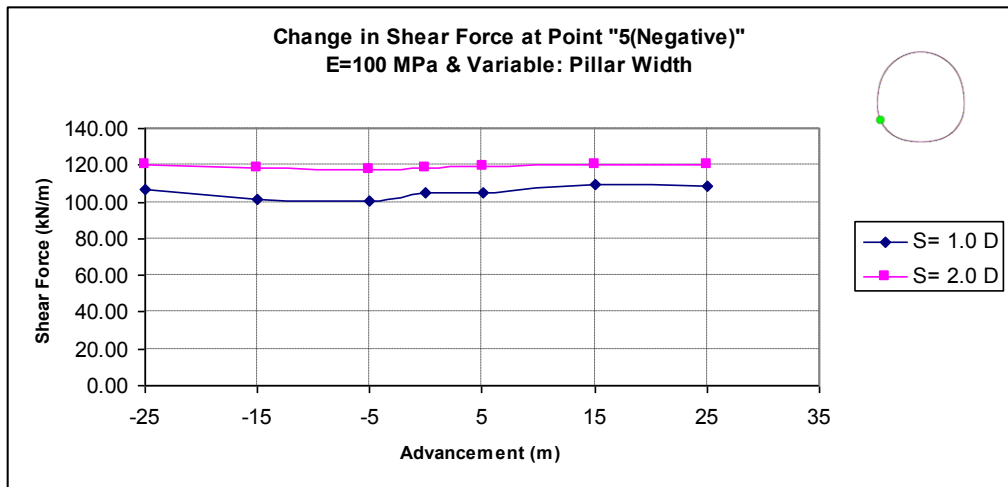


Figure C.46 Shear force values at the left-bottom side of the tunnel

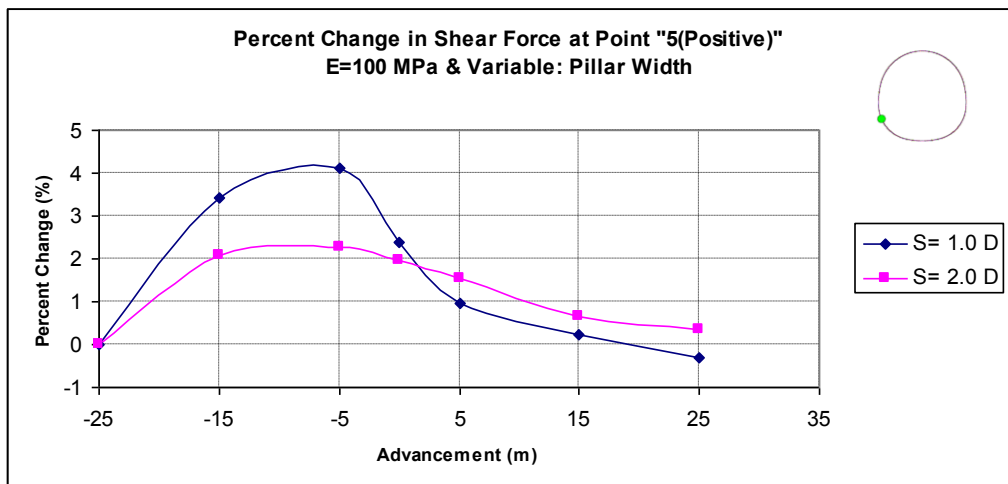


Figure C.47 Percent change in shear force at the left-bottom side of the tunnel

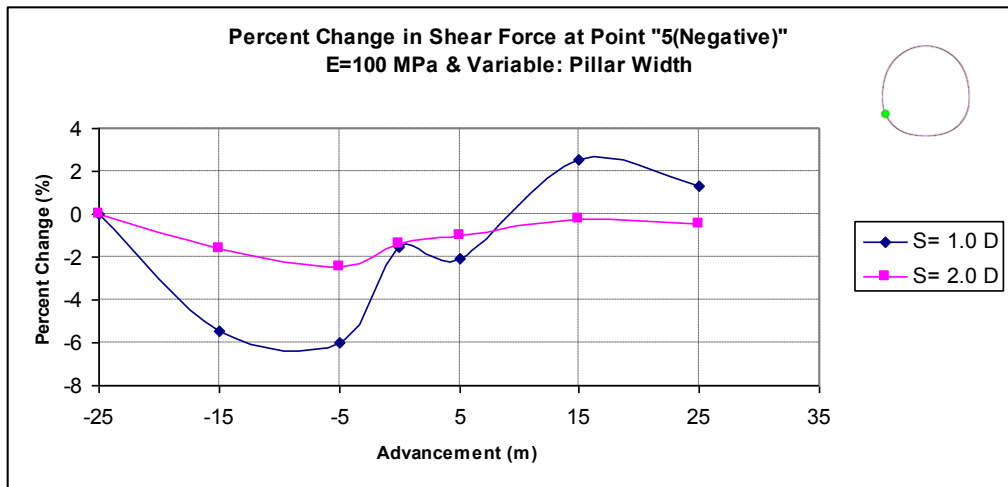


Figure C.48 Percent change in shear force at the left-bottom side of the tunnel

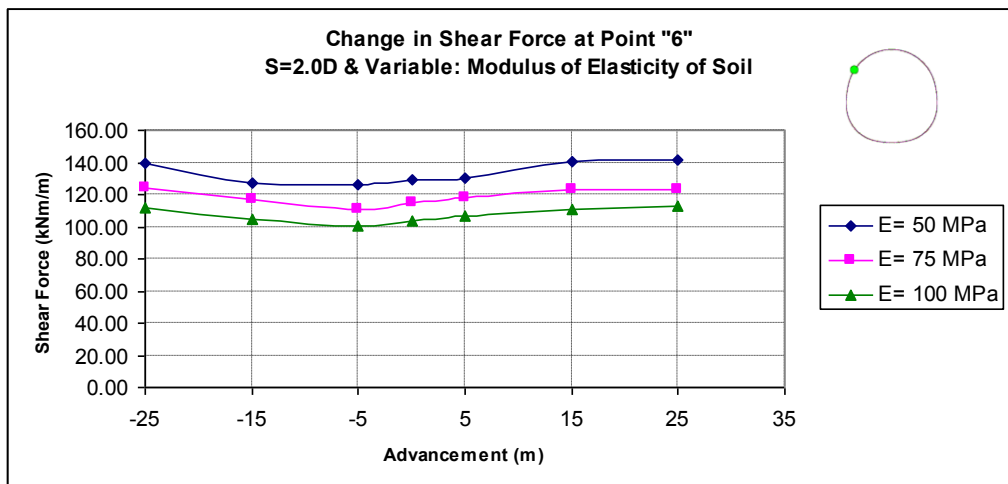


Figure C.49 Shear force values at the left-top side of the tunnel

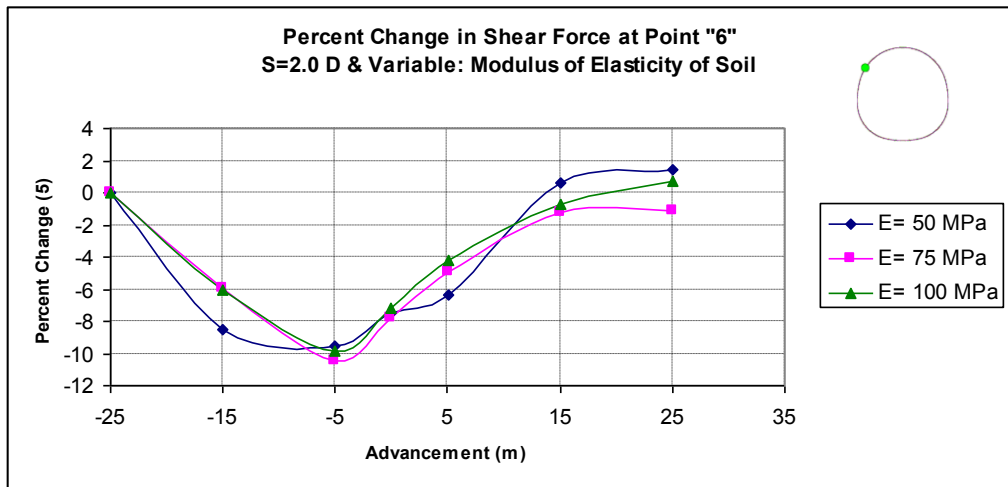


Figure C.50 Percent change in shear force at the left-top side of the tunnel

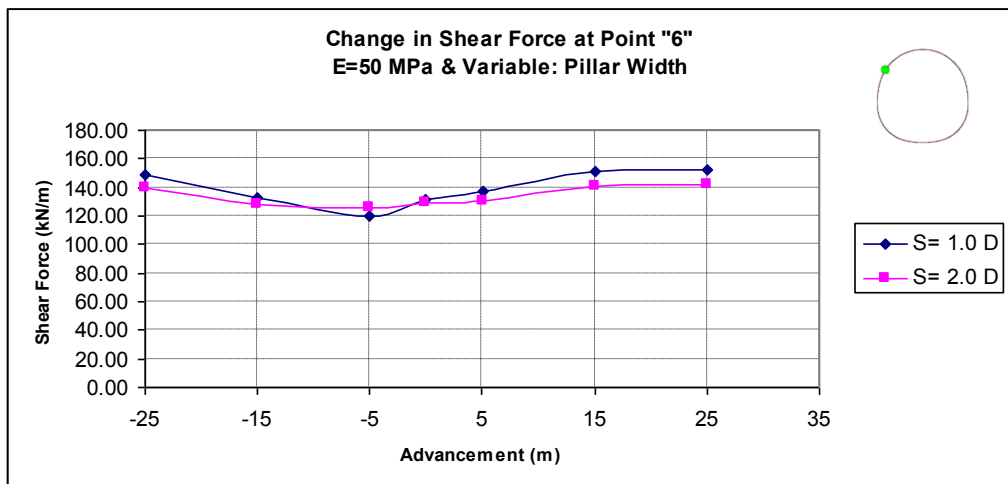


Figure C.51 Shear force values at the left-top side of the tunnel

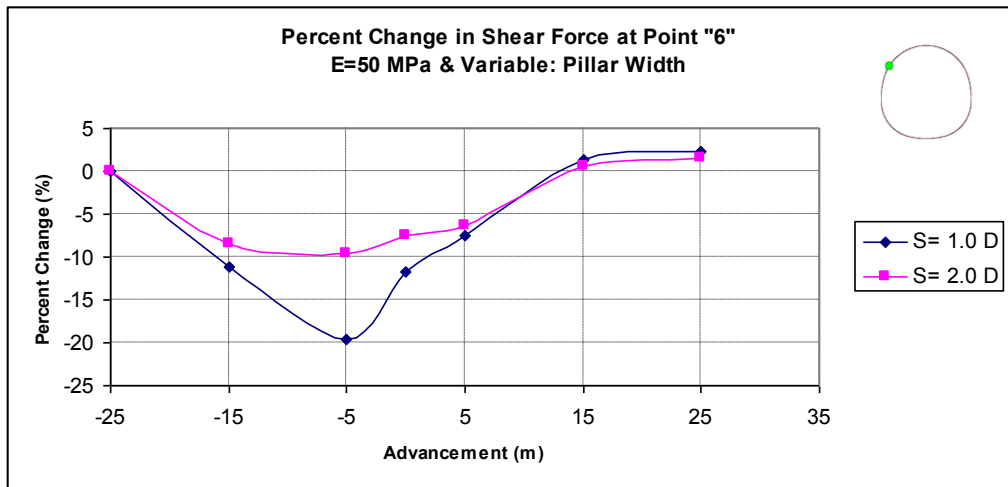


Figure C.52 Percent change in shear force at the left-top side of the tunnel

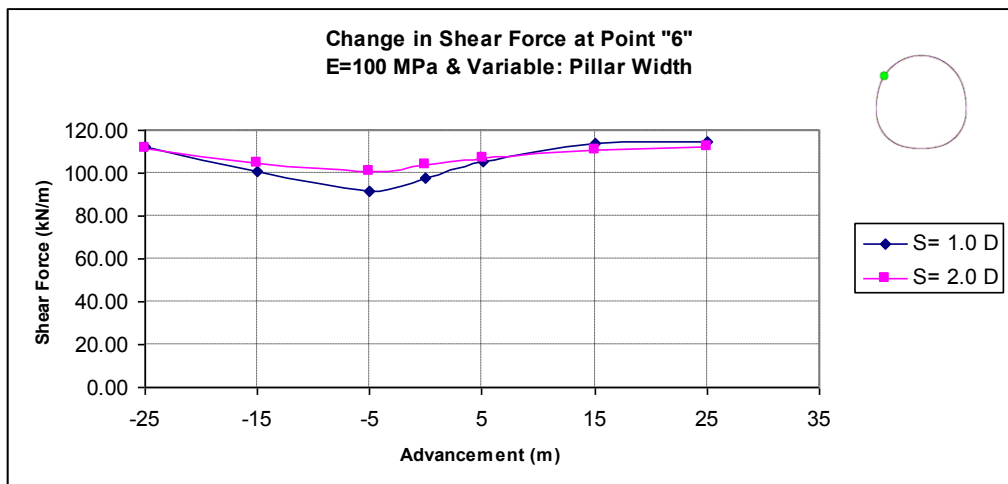


Figure C.53 Shear force values at the left-top side of the tunnel

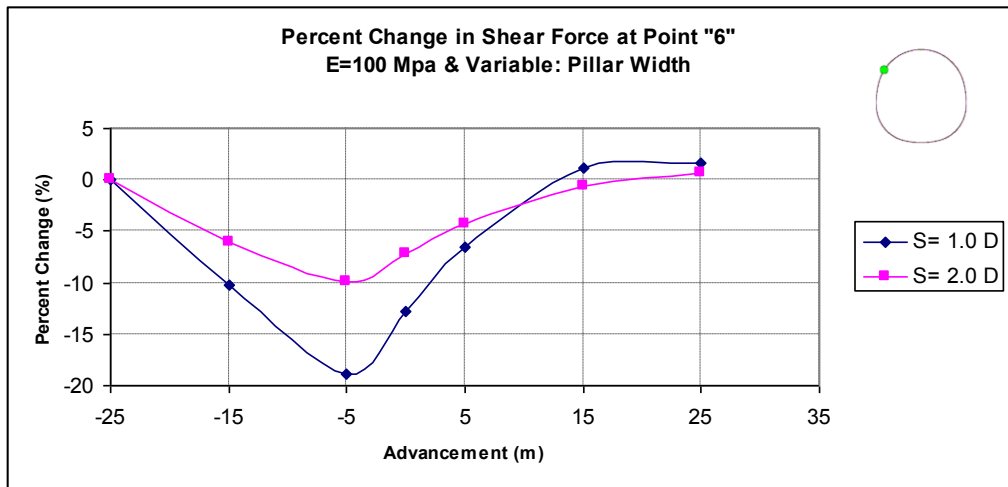


Figure C.54 Percent change in shear force at the left-top side of the tunnel